

8005090362
B

NEDO-24720
Class I
January 1980
DRF-T23-92
TP-517-.0439

GENERAL ELECTRIC
COMPANY PROPRIETARY

MARK III CONFIRMATORY TEST PROGRAM
1/9 AREA SCALE MULTICELL CONDENSATION AND
STRATIFICATION PHENOMENA
TEST SERIES 6003

A. M. Varzaly
K. P. Yu
J. A. Kervinen

Reviewed: *J. E. Torbeck*
J. E. Torbeck, Technical
Leader, Containment Experiments

Reviewed: *Tom R. McIntyre*
T. R. McIntyre, Test Report
Evaluator, Containment Methods

Approved: *D. M. Gluntz*
D. M. Gluntz, Manager
Containment Experiments

Approved: *A. E. Rogers*
A. E. Rogers, Manager
Containment Technology

DISCLAIMER OF RESPONSIBILITY

This document was prepared by or for the General Electric Company. Neither the General Electric Company nor any of the contributors to this document:

- A. Makes any warranty or representation, express or implied, with respect to the accuracy, completeness, or usefulness of the information contained in this document, or that the use of any information disclosed in this document may not infringe privately owned rights; or*
- B. Assumes any responsibility for liability or damage of any kind which may result from the use of any information disclosed in this document.*

CONTENTS

	<u>Page</u>
ABSTRACT	xi
1. INTRODUCTION	1-1
2. SUMMARY	2-1
2.1 Condensation Oscillations	2-1
2.2 Chugging	2-1
2.3 Pool Thermal Stratification	2-2
3. TEST FACILITY DESCRIPTION	3-1
3.1 Pressure Suppression Test Facility	3-1
3.2 Vent System and Suppression Pool	3-2
3.3 Scaling Considerations	3-2
3.3.1 Scaling Effects - Condensation Phenomena	3-3
3.3.2 Scaling Effects - Pool Thermal Stratification	3-5
3.4 Test Instrumentation	3-5
3.5 Test Conditions	3-7
3.6 Test Procedure	3-8
4. DATA ACQUISITION AND REDUCTION	4-1
4.1 Data Acquisition System and Procedure	4-1
4.2 Data Reduction Procedure	4-2
4.2.1 Real-Time Data Processing	4-2
4.2.2 Replay Data Processing	4-3
5. TEST RESULTS AND DISCUSSION	5-1
5.1 Condensation Oscillations	5-1
5.1.1 Pressure - Time Histories	5-3
5.1.2 Repeatability of Pressure Magnitudes	5-4
5.1.3 Multicell Effects on Pressure Magnitudes	5-5
5.1.4 Pressure Oscillation Frequencies	5-6
5.1.5 Conclusions	5-8
5.2 Chugging	5-9
5.2.1 Top Vent Chugging Pressure Response	5-10
5.2.2 Multicell Effects on Top Vent Chugging Pressures	5-11
5.2.3 Weir Wall Chugging Pressure Response	5-12
5.2.4 Multicell Effects on Weir Wall Chugging Pressures	5-13
5.2.5 Drywell Wall Chugging Pressure Response	5-13
5.2.6 Multicell Effects on Drywell Wall Chugging Response	5-14
5.2.7 Containment Wall Chugging Pressure Response	5-15
5.2.8 Multicell Effects on Containment Wall Chugging Response	5-16
5.2.9 Chugging Synchronization	5-16
5.2.10 Chugging Period	5-17
5.2.11 Conclusions	5-18

CONTENTS (Continued)

	<u>Page</u>
5.3 Pool Thermal Stratification	5-18
5.3.1 Introduction	5-18
5.3.2 Data Reduction	5-20
5.3.3 Test Results	5-20
6. REFERENCES	6-1

APPENDICES

A DRYWELL AIR CONTENT MEASUREMENT	A-1
B MEASUREMENT UNCERTAINTIES	B-1
C MULTICELL CCPDDF CALCULATIONS	C-1
D SYSTEM PERFORMANCE	D-1

ILLUSTRATIONS

<u>Figure</u>	<u>Title</u>	<u>Page</u>
3-1	Pressure Suppression Test Facility - Test Series 6003	3-14
3-2	Mark III 1/9-Area Scale Weir and Suppression Pool	3-15
3-3	Steam Generator, Drywell and Vent Duct Real-Time Instrumentation - Test Series 6003	3-16
3-4	Weir Annulus, Vent and Suppression Pool Real-Time Instrumentation - Test Series 6003	3-17
3-5	Top Vent and Basemat Replay Instrumentation - Test Series 6003	3-18
3-6	Weir and Pool Wall Replay Instrumentation - Test Series 6003	3-19
4-1	Data Acquisition System and Processing Block Diagram	4-4
5-1	Drywell Wall, 12.3-ft (3.8-m), Pressure Time Histories, Run 1	5-27
5-2	Drywell Wall, 12.3-ft (3.8-m), Pressure Time Histories, Run 6	5-28
5-3	Drywell Wall, West Cell 12.3-ft (3.8-m), Pressure Short-Term (1.3 sec) Time History, Run 6	5-29
5-4	Drywell Wall, West Cell 13-ft (4-m), Pressure Short-Term (1.3 sec) Time History, Run 6	5-30
5-5	Drywell Wall, West Cell 15.7-ft (4.8-m), Pressure Short-Term (1.3 sec) Time History, Run 6	5-31
5-6	South Weir Wall, 11-ft (3.4-m), Pressure Time Histories, Run 6	5-32
5-7	Containment Wall, 11-ft (3.4-m), Pressure Time Histories, Run 6	5-33
5-8	Drywell Wall, 15.7-ft (4.8-m), Pressure Time Histories, Run 8	5-34
5-9	Drywell Wall, 15.7-ft (4.8-m), Pressure Time Histories, Run 11	5-35

ILLUSTRATIONS (Continued)

Figure	Title	Page
5-10	Drywell Wall, 15.7-ft (4.8-m), Center Cell, Pressure Magnitude Repeatability, Runs 4, 5 and 6	5-36
5-11	Drywell Wall, 15.7-ft (4.8-m), East Cell, Pressure Magnitude Repeatability, Runs 10, 11 and 12	5-37
5-12	Drywell Wall, 15.7-ft (4.8-m), Center Cell, Pressure Magnitude Repeatability, Runs 10, 11 and 12	5-38
5-13	Weir Wall, 11-ft (3.35-m), East Cell, Pressure Magnitude Repeatability, Runs 10, 11 and 12	5-39
5-14	Containment Wall, 2-ft (0.6-m), East Cell, Pressure Magnitude Repeatability, Runs 10, 11 and 12	5-40
5-15	Drywell Wall, 15.7-ft (4.8-m), Pressure Magnitude in RMS versus Time, Run 6	5-41
5-16	Containment Wall, 2-ft (0.6-m), Pressure Magnitude in RMS versus Time, Run 6	5-42
5-17	Drywell Wall, 15.7-ft (4.8-m), Pressure Magnitude in RMS versus Time, Run 11	5-43
5-18	Containment Wall, 2-ft (0.6-m), Pressure Magnitude in RMS versus Time, Run 11	5-44
5-19	Drywell Wall, 14.7-ft (4.3-m), Multicell Average Pressure Magnitudes in RMS versus Time Normalized to Single-Cell Values for 120°F (49°C) Initial Pool Temperature Tests	5-45
5-20	Containment Wall, 2-ft (0.6-m), Multicell Average Pressure Magnitudes in RMS versus Time Normalized to Single-Cell Values for 120°F (49°C) Initial Pool Temperature Tests	5-46
5-21	PSD Plot of Drywell Wall, 15.7-ft (4.8-m), Center-Cell Pressure Signal 11.85 - 14.42 sec, Run 6	5-47
5-22	Drywell Wall, 15.7-ft (4.8 m), East Cell, Dominant Frequencies versus Time for Pressure Data, Runs 10, 11 and 12	5-48
5-23	Drywell Wall, 15.7-ft (4.8-m), Dominant Frequencies versus Time of Pressure Data for One, Two and Three Cell Tests	5-49
5-24	Containment Wall, West Cell, Pressure Amplitude Axial Distribution in Suppression Pool for Different Times, Run 11, 120°F (49°C) Initial Pool Temperature	5-50

ILLUSTRATIONS (Continued)

Figure	Title	Page
5-25	One-Cell Top Vent Chugging Pressure Time History, Run 8	5-51
5-26	One-Cell Top Vent Chugging Pressure Time History, Run 8	5-52
5-27	Three-Cell Top Vent Chugging Pressure Time History, Run 3	5-53
5-28	Complementary Cumulative Probability Density Distribution Function - Multicell Effects on Top Vent Center Chugging Pressures	5-54
5-29	Complementary Cumulative Probability Density Distribution Function - Multicell Effects on Top Vent Exit Chugging Pressures	5-55
5-30	One-Cell Weir Wall Chugging Pressure Time History, Run 8	5-56
5-31	Two-Cell Weir Wall Chugging Pressure Time History, Run 8	5-57
5-32	Three-Cell Weir Wall Chugging Pressure Time History, Run 3	5-58
5-33	Complementary Cumulative Probability Density Distribution Function - Multicell Effects on Weir Wall Chugging Pressures	5-59
5-34	One-Cell Drywell Wall Chugging Pressure Time History, Run 8	5-60
5-35	Two-Cell Drywell Wall Chugging Pressure Time History, Run 8	5-61
5-36	Three-Cell Drywell Wall Chugging Pressure Time History, Run 3	5-62
5-37	Complementary Cumulative Probability Density Distribution Function - Multicell Effects on Drywell Wall Chugging Pressures	5-63
5-38	Complementary Cumulative Probability Density Distribution Function - Multicell Effects on Drywell Wall Chugging Pressures	5-64
5-39	Complementary Cumulative Probability Density Distribution Function - Multicell Effects on Drywell Wall Chugging Pressures	5-65
5-40	Complementary Cumulative Probability Density Distribution Function - Multicell Effects on Drywell Wall Chugging Pressures	5-66

ILLUSTRATIONS (Continued)

Figure	Title	Page
5-41	One-Cell Containment Wall Chugging Pressure Time History, Run 8	5-67
5-42	Two-Cell Containment Wall Chugging Pressure Time History, Run 8	5-68
5-43	Three-Cell Containment Wall Chugging Pressure Time History, Run 3	5-69
5-44	Complementary Cumulative Probability Density Distribution Function - Multicell Effects on Containment Wall Chugging Pressures	5-70
5-45	Complementary Cumulative Probability Density Distribution Function - Multicell Effects on Chugging Synchronization	5-71
5-46	Complementary Cumulative Probability Density Distribution Function - Multicell Effects on Chugging Synchronization	5-72
5-47	Complementary Cumulative Probability Density Distribution Function - Multicell Effects on Chugging Synchronization	5-73
5-48	Complementary Cumulative Probability Density Distribution Function - Multicell Effects on Chugging Period	5-74
5-49	Average Pool Temperature - Time Histories, Run 3, West Cell, X = 2	5-75
5-50	Average Pool Temperature - Time Histories, Run 3, West Cell, X = 4	5-76
5-51	Average Pool Temperature - Time Histories, Run 3, Center Cell, X = 2	5-77
5-52	Average Pool Temperature - Time Histories, Run 3, Center Cell, X = 4	5-78
5-53	Average Pool Temperature - Time Histories, Run 3, East Cell, X = 2	5-79
5-54	Average Pool Temperature - Time Histories, Run 3, East Cell, X = 4	5-80
5-55	Average Pool Temperature - Time Histories, Run 3, Between Center and West Cell, X = 2	5-81
5-56	Vertical Average Pool Temperature - Time History, Run 3	5-82
5-57	Horizontal Average Pool Temperature - Time History, Run 3, X = 2	5-83
5-58	Horizontal Average Pool Temperature - Time History, Run 3, X = 4	5-84

ILLUSTRATIONS (Continued)

Figure	Title	Page
5-59	Three-Cell Pool Temperature Profile, Run 4	5-85
5-60	Three-Cell Pool Temperature Profile, Run 4	5-86
5-61	One- and Two-Cell Pool Temperature Profile, Run 12	5-87
5-62	One- and Two-Cell Pool Temperature Profile, Run 12	5-88
5-63	Pool Temperature Profile Comparison	5-89
5-64	Pool Temperature Profile Comparison	5-90

TABLES

<u>Table</u>	<u>Title</u>	<u>Page</u>
3-1	PSTF Scale Factors	3-9
3-2	Important Parameters - Condensation Phenomena	3-10
3-3	Real-Time Instrumentation	3-11
3-4	Replay Instrumentation	3-12
3-5	Test Matrix	3-13
5-1	Chugging Initiation Mass Flux and Time	5-24
5-2	Chugging Synchronization Based on Top Vent Exit Pressure - Test Series 6003	5-25
5-3	Chugging Period Based on Top Vent Exit Pressure - Test Series 6003	5-26

ABSTRACT

A series of steam blowdown tests were performed to evaluate condensation and stratification phenomena of the Mark III Pressure Suppression Containment System. The tests were conducted in the General Electric Pressure Suppression Test Facility at San Jose. The facility was a nominal 1/130 volumetric simulation of the BWR/6-251 series Mark III containment design. Both the pool and vent system represented a 1/9-area scaled simulation of a 24-degree sector of the Mark III containment, including three pool cells with three 9.06-inch (23.0-cm) inside diameter vents in each cell. The number of pool cells and the initial suppression pool temperature were the test parameters. Particular emphasis was placed on determining the multicell effects on condensation oscillations and chugging loads on the weir wall, vents, and pool walls, and multicell effects on suppression pool thermal response.

1. INTRODUCTION

The Mark III Confirmatory Test Program was initiated in November of 1973 as a confirmation of the analytical models used in design of the Mark III Pressure Suppression System. This was a continuing, multiphase program performed in the Pressure Suppression Test Facility (PSTF) by General Electric's Nuclear Energy Engineering Division in San Jose, California.

The full-scale phase of the Mark III Confirmatory Test Program utilized full-scale 27.5-inch (69.9-cm) inside diameter horizontal vents with a full-size 8-degree sector of the suppression pool. The full-scale tests confirmed the analytical modeling of the vent clearing process with one, two, and three vents, and demonstrated the viability of the horizontal vent pressure suppression concept (see References 1 and 2). Air blowdowns were performed to provide a data base on pool swell and dynamic loads on structures (see Reference 3). Saturated vapor blowdowns were also conducted to evaluate condensation phenomena and associated loads, submerged structure loads, and pool thermal stratification (see Reference 4).

The 1/3-scale phase of the program, conducted using 1/3-area scaled ($1/\sqrt{3}$ linear scaled) 15.875-inch (40.3-cm) inside diameter horizontal vents with an area-scaled 8-degree sector of the suppression pool included both air and steam blowdowns so as to investigate the phenomenon of pool swell, its interaction with flow restrictions above the pool surface, and the impact transient on structure above the pool (see References 5, 6 and 7). Saturated liquid and vapor blowdowns were also conducted to evaluate condensation phenomena and associated loads, and pool thermal stratification (see Reference 8).

The 1/9-area scale multicell experiments completed the final phase of the Mark III Confirmatory Test Program. These tests utilized 1/9-area scaled ($1/3$ -linear scaled) 9.06-inch (23.0-cm) inside diameter horizontal vents with an area-scaled 24-degree sector of the suppression pool. Previous 1/9-area

scaled multicell tests confirmed that one-cell pool swell tests produced loads that are conservative (see Reference 9).

This current series of tests, designated Test Series 6003, was a two part test program started in February 1979, and completed in May 1979. Four shakedown runs and twelve matrix tests were performed in the test series. Test objectives were:

- a. Confirm that single-cell loads due to condensation are conservative when compared to multicell test data.
- b. Study vent interaction and its effects during the condensation phases of the LOCA transient.
- c. Evaluate the multicell effects on pool thermal stratification.

In Part I tests three-cell data was gathered, and in Part II tests one- and two-cell data was gathered. Each covered condensation oscillations, chugging, pool thermal stratification, and system performance.

2. SUMMARY

The following is a summary of principal results obtained from Test Series 6003.

2.1 CONDENSATION OSCILLATIONS

Pressure oscillation magnitudes in the weir and suppression pool characterized by average root-mean-square (rms) values for multicell configuration are less than the single-cell magnitudes at most times of the condensation oscillation (CO) period (see Subsection 5.1.3).

2.2 CHUGGING

- a. The top vent pressures have essentially equal strength for the 1-, 2-, and 3-cell configurations, indicating there were no multicell effects on chugging source pressures (see Subsection 5.2.2).
- b. The weir wall, drywell wall, and containment wall multicell chugging pressures are less than single-cell chugging pressures (see Subsections 5.2.4, 5.2.6, and 5.2.8).
- c. Chugging is generally not synchronized.
- d. As noted in a. above, there are no multicell effects on the phenomena of chugging. However, as expected, pressures measured in a given cell of a multicell system consist of components due to sources both in the given cell and in adjacent cells. Since chugging is asynchronous, the magnitude of chugging pressures measured in a single cell system are bounding to those in a multicell system, but the multicell pressures will be richer in frequency content due to the asynchronous sources located at the adjacent vents (see Subsections 5.2.3, 5.2.5 and 5.2.7).

2.3 POOL THERMAL STRATIFICATION

There are no multicell effects on the suppression pool horizontal and vertical temperature distributions (see Subsection 5.3.4).

3. TEST FACILITY DESCRIPTION

3.1 PRESSURE SUPPRESSION TEST FACILITY

The blowdown runs of Test Series 6003 were performed in the Pressure Suppression Test Facility (PSTF). Figure 3-1 shows a schematic view of the PSTF as configured for these tests. The PSTF includes a large multi-purpose data acquisition system and vessels which simulate the reactor, drywell, and containment volumes. The PSTF reactor and drywell are 1/130, and the containment is 1/135 volumetric scale factor of a 251 series BWR/6 Mark III Containment System (Grand Gulf-1971).

The PSTF reactor simulator is an electrically heated flash boiler having an internal volume of 160-ft³ (4.53-m³). In Test Series 6003, a 10.374-inch i.d. (263.5-mm i.d.) riser tube was installed in the boiler to enable simulation of a saturated vapor blowdown. The riser tube exit position is located on the side of the vessel, near the bottom, and is connected to the 8-inch Schedule 80 (194-mm i.d.) blowdown line which includes a critical flow venturi, double rupture disc assembly, and an 8-inch (203-mm) gate valve. The blowdown line is connected to a 10-inch Schedule 40 (225-mm i.d.) riser and tee which allow steam to be injected near the top of the drywell vessel (see Figure 3-1).

The PSTF drywell is a 10 ft (3-m) diameter cylindrical vessel, 26 ft (7.9 m) high as configured for Test Series 6003. In this configuration the total drywell volume is 2365-ft³ (67-m³). A gas-fired fin tube heater is installed in the drywell to allow the drywell metal to be heated to eliminate surface condensation. The drywell is connected to the vent system inside the pool building with a 6-ft (1.8-m) diameter mitered elbow.

3.2 VENT SYSTEM AND SUPPRESSION POOL

The 1/9-area scale Mark III vent system and suppression pool simulation shown in Figure 3-2 consist of a twenty-four degree segment of the prototype weir annulus and suppression pool with the surface areas appropriately reduced. Both the weir annulus and suppression pool have removable partitions which allow modeling of the system as one three-cell system or as a combined one-cell/two-cell system. This allows comparisons to be made between single-cell and multicell data of the same scale.

The area scale-factor for the flow and surface areas is 1/9-of full scale. The corresponding weir annulus and the suppression pool 1/9 scale total area are 3.74- and 45.98-ft², (0.35- and 4.27-m²), respectively. Each of the three cells has five horizontal vent openings. This allows for testing using full-scale vertical vent spacing or a geometric (1/3 linear) scale vent spacing. For these tests the full-scale 4.5-ft (1.37-m) vent vertical spacing was used. The vents not used during the test are plugged with internally mounted seal plugs. The vents are full-scale length, 5.0-ft (1.52-m), have 1/3-linear scale i.d. of 9.06-in. (230-mm) and are oriented radially outward from the weir annulus to the suppression pool with radial spacing of eight degrees. The radial spacing of the vents within the suppression pool is proportional to scale. However, the radial vent spacing within the weir annulus is less than that which is proportional to scale due to the nongeometric scaling of the vent length.

3.3 SCALING CONSIDERATIONS

The PSTF reactor simulator and drywell were scaled to 1/130 and the suppression pool was scaled to 1/135 of the nominal volumetric scale of a full-scale 251-inch series BWR/6 Mark III Containment System. In the Mark III Confirmatory Test Program the simulated weir annulus and vent flow areas, and the suppression pool surface area are scaled such that the ratio of the simulated area to full-scale area is the same as the ratio of the simulated to full-scale volumes. Volume/area scaling was used to maintain a unity scale factor for flow velocity, mass flux, temperature, pressure, and time. This scaling approach was based on the assumption of one-dimensional flow in the weir

annulus, vents and suppression pool. The scale factors for the surface and flow areas of the various components for the PSTF 1/9-area scale system are given in Table 3-1.

The current tests were performed for investigation of multicell effects on condensation and stratification phenomena. To assure that the phenomena occurring in the PSTF 1/9-area scale tests were not fundamentally different from those which occur in a full scale or prototype system, the parameters expected to influence these phenomena are compared with those for a 251 Mark III system as presented in the following paragraphs.

3.3.1 Scaling Effects - Condensation Phenomena

Parameters affecting the condensation phenomena are given in Table 3-2. The ratio of break area to steam generator volume is given to illustrate that the blowdown flow rate transient was similar in both the PSTF 1/9-scale test system and prototype.

The break area relative to the top vent flow area is an important parameter for condensation phenomena. The proper scaling of this ratio assures the occurrence of prototypical vent mass flux transient in the test system. As indicated in Table 3-2 the prototype and scaled ratios agreed to within 8 percent.

The drywell volume per top vent [active vent(s)] area is an important parameter for condensation phenomena. In the case of CO, proper scaling of this parameter results in correct drywell capacitance relative to heat transfer area of the steam bubbles at the exit of the top vents, and produces an accurate representation of the CO source pressures. In the case of chugging, proper scaling of this parameter determines correct drywell depressurization during each chug which in turn sets the correct weir water level variation and vent reflood/reclearing behavior. The model and prototype drywell volume per top vent area ratios agreed to within 8 percent as given in Table 3-2.

The physical dimensions of the test system are important from the standpoint of condensation bubble size, distance attenuation, and pressure wave travel time. All dimensions were prototypical except for the vent diameter and the horizontal distance between the drywell and containment walls as shown in Table 3-2. In the case of CO, the smaller than prototype vent diameter results in a smaller condensation front and higher CO frequencies than those which may occur in a 251 Mark III system. In the case of chugging, the smaller than prototype vent diameter results in a shorter distance from the source to the measurement point, which would explain the higher chugging pressures and smaller chugging bubble resulting in shorter bubble collapse and rebound times than those in a prototype. The shorter travel distance due to shorter pool length results in less than prototypical attenuation of the pressures at the containment wall. Further, due to nongeometric scaling of the vent length, the radial vent spacing within the weir annulus is smaller than prototypical as indicated in Subsection 3.2. This may result in more synchronized chugging in the PSTF 1/9-area scale system than in the full-scale system.

Based on the comparison of the parameters expected to influence the condensation phenomena, the same phenomena were expected in the 1/9-area scale system as that which occurs in the full-scale system. The dimensional differences affect pressure magnitudes and frequencies and not the condensation phenomena. Thus, the 1/9-area scale test data are applicable for evaluation of multicell effects.

The drywell volume in the combined 1-cell and 2-cell configuration did not appear to affect the condensation phenomena. In the case of CO, all three top vents remained open throughout the CO period, resulting in the same drywell volume per active vent ratio as expected to occur in a prototype and in separate 1-cell and 2-cell systems with appropriate drywell volumes. In the case of chugging, the drywell depressurization rate per multivent cluster of chugs is the same as that expected to occur in a prototype and in separate 1-cell and 2-cell systems.

3.3.2 Scaling Effects - Pool Thermal Stratification

Parameters of importance to pool thermal stratification are the rate and location of energy addition to the pool, and the suppression pool geometry.

As pointed out in Subsection 3.3.1, the blowdown flow rate was scaled to produce prototypical energy addition rate to the pool, i.e., the vent flow enthalpy was full-scale.

The PSTF drywell pressurization was prototypical resulting in correct vent clearing/recovering which resulted in correct time of energy addition through the vents.

The vertical vent spacing and submergence were full-scale providing similar location of energy addition to the pool in both the PSTF and prototype.

The pool geometry was 1/9-area scaled based on a 24-degree sector of the prototype such that the pool mass, surface area, and total energy addition (based on the three top vents) were identical to the 1/3-area scale of an 8-degree sector of the prototype (see Reference 8). In the current tests the pool length was 1/3 scale to maintain 1/9-area scaling of the pool surface which was shorter than the 1/3-area scale system pool length. This mismatch in pool length may result in a different pool heat-up process due to better pool mixing and/or less radial temperature distribution than the 1/3-area scale system (see Reference 8) and prototype. However, the pool thermal stratification data obtained during the 1/9-area scale tests were valuable for evaluation of multi-cell effects, and not intended to be directly applicable to the prototype.

3.4 TEST INSTRUMENTATION

During the 12 blowdown runs of Test Series 6003, 127 instruments were used for collecting data, as described below. In addition, the PSTF process instrumentation was used for monitoring the systems initial conditions.

The instruments for each test consisted of two groups referred to as real-time and replay instrumentation. This instrumentation remained unchanged during Parts I and II of testing. The data collected by the real-time instrumentation were directly recorded by the PSTF Data Acquisition System (DAS). The data acquired by the replay instrumentation were simultaneously recorded by the PSTF DAS and on analog tape recorders for post-test playback at reduced speed through the DAS to increase the data sampling rate. Further details regarding the data acquisition procedure and sampling rates are given in Section 4.

The real-time instruments are given in Table 3-3 and shown in Figures 3-3 and 3-4. They consisted of 9 cavity-type strain gage pressure transducers, 32 conductivity probes (see Reference 5), and 48 1/8-inch (3-mm) o.d. stainless-steel-sheathed iron-constantan (Type J) thermocouples with a grounded tip reduced to 0.093-inch (2-mm).

The real-time instruments were used to collect system performance pressure and temperature data at various locations in the steam generator, blowdown line, and drywell to determine the steam/water interface locations in the weir annulus and the top vents, to acquire pool thermal stratification data, and to determine pool level height throughout the transient.

The replay instruments are given in Table 3-4 and shown in Figures 3-5 and 3-6. They consisted of 1 cavity-type pressure transducer (not shown in the figures), 34 flush-mount thermally insulated strain gage pressure transducers, and 4 variable-capacitance-type accelerometers. The cavity-type transducer was used to measure venturi throat pressure to monitor test start time. Five flush-mount transducers were used to measure the weir wall pressure data and had a range of 100 psi (689 KN/m^2). Six flush-mount transducers were used to measure pressure within the top vents and had a range of 2000 psi (13780 KN/m^2). Eleven flush-mount transducers were used to measure the drywell wall pressure data and had a range of 200 psi and 500 psi (1378 KN/m^2 and 3445 KN/m^2). Twelve flush-mount transducers were used to measure the containment wall and basemat pressure data and had a range of 100 psi (689 KN/m^2). One 100G and three 10G accelerometers were used to measure acceleration of the drywell wall, and containment wall and basemat, respectively.

The PSTF air content in vent flow was monitored utilizing the Steam Air Ratio Sampling System which consisted of a sample exhaust manifold with five sample chambers, and a time sequence controller for sequential sampling. Details regarding the operational procedures, data reduction method, and the results are presented in Appendix A.

An uncertainty analysis of the various instruments used during this test series is given in Appendix B.

3.5 TEST CONDITIONS

Test Series 6003 consisted of 12 blowdown runs grouped into two equal parts. The specific test initial conditions for both Parts I and II, and the common conditions for all blowdown runs are given in Table 3-5.

The test matrix conditions were centered about the Mark III nominal reactor operating conditions with variations specified for cell configuration and initial pool temperature. All tests were performed with top vent submergence of 7.5 ft (2.3 m) and a 2.5-inch (6.4-cm) venturi diameter - representing 100 percent of scaled Design Basis Accident (DBA) - and utilized saturated vapor as a blowdown fluid. The PSTF pool building was closed to allow prototypical containment free-space pressurization. The PSTF drywell vacuum breaker was deactivated throughout the testing to insure minimum air content in the steam flow and maximum chugging pressures.

General environmental conditions and initial test parameters were set within the acceptable limits specified below. These limits were set taking into account generally expected instrument resolutions and possible environmental deviations.

Initial condition tolerances were ± 5 psi (34 KN/m^2) on vessel pressure, $\pm 5^\circ\text{F}$ (2.8°C) on pool water temperature and ± 0.1 -ft (0.03-m) on pool water level.

3.6 TEST PROCEDURE

The standard test procedure was to bring the test facility to the required initial conditions and perform pretest checks to ensure proper configuration of the facility. Then the test instrumentation and the DAS were checked for operability, and the pressure transducers electrically balanced to give a zero voltage offset, and the balanced data taken. The pressure transducers were put on line and on-line data taken. The transducer readings were checked and any abnormalities corrected or noted in the test log book. The blowdown was initiated and blowdown data recorded. Post-test balance data were taken with transducers off line after completion of the blowdown.

Table 3-1
PSTF SCALE FACTORS

<u>Parameter</u>	<u>PSTF^a</u>	<u>Reference 251 Mk III</u>	<u>Scale Factors</u>
Steam Generator Volume	160 ft ³ (4.53 m ³)	2.12 x 10 ⁴ ft (601 m ³)	1/133
Simulated Break Area 2-1/2 inch (6.35 m) Venturi (100% DBA) ^b	0.0341 ft ² (3.17 x 10 ⁻³ m ²)	4.45 ft ² (0.414 m ²)	1/130
Drywell Volume	2365 ft ³ (66.98 m ³)	302500 ft ³ (11591.8 m ³)	1/128
Weir Annulus Area	3.74 ft ² (0.35 m ²)	496.5 ft ² (46.1 m ²)	1/133
Vent Area	4.03 ft ² (0.37 m ²) ^c	556.2 ft ² (51.67 m ²)	1/138
Pool Surface Area	45.98 ft ² (4.27 m ²)	6208 ft ² (57.67 m ²)	1/135
Pool Volume	850 ft ³ (24.1 m ³)	114848 ft ³ (3252.5 m ³)	1/135
Wetwell Air Space Volume	11053 ft ³ (313.02 m ³)	1244000 ft ³ (35280.08 m ³)	1/113

All pressure, temperature, and flow lengths are full scale

^aPSTF vent submergence is variable. All values are based on 7.5-ft (2.3-m) submergence of the top vent [18.5-ft (5.64-m) pool depth]

^bBased on a design basis accident (DBA) of a single main steam line break

^cBased on nine vents

Table 3-2

IMPORTANT PARAMETERS - CONDENSATION PHENOMENA

<u>Parameter</u>	<u>PSTF^a</u>	<u>Reference 251 Mark III</u>
Break Area ^b /Boiler Volume	2.13 x 10 ⁻⁴ 1/ft (6.99 x 10 ⁻⁴ 1/m)	2.10 x 10 ⁻⁴ 1/ft (6.89 x 10 ⁻⁴ 1/m)
Break Area ^b /Vent Area (Top Vents)	0.026	0.024
Drywell Volume/Vent Area (Top Vents)	1765 ft (538 m)	1629 ft (497 m)
Vent Area (top Vents)/Weir Annulus Area	0.36	0.37
Weir Annulus Width	2 ft (0.61 m)	2.12 ft (0.66 m)
Vent Diameter	9.06 inch (23.01 cm)	27.5 inch (69.8 cm)
Vent Length	5.0 ft (1.5 m)	5.0 ft (1.5 m)
Vent Submergence ^a	7.5 ft (2.3 m)	7.5 ft (2.3 m)
Pool Length	6.33 ft (1.93 m)	19 ft (5.8 m)

^aPSTF vent submergence is variable. All values are based on 7.5-ft (2.3-m) top vent submergence

^b100 percent DBA [2.5-inch (6.35-cm) venturi diameter]

Table 3-3
REAL-TIME INSTRUMENTATION

- I. Pressure Transducers
 - 1. Vessel Dome (1)
 - 2. Venturi Throat (1)
 - 3. Drywell Dome (1)
 - 4. Annubar One-Cell Static (1)
 - 5. Annubar One-Cell Differential (1)
 - 6. Annubar Two-Cell Static (1)
 - 7. Annubar Two-Cell Differential (1)
 - 8. Wetwell Air Space (1)
 - 9. Pool Water Level Differential (1)
- II. Thermocouples
 - 1. Vessel Dome (1)
 - 2. Drywell (5)
 - 3. Annubar (1)
 - 4. Weir Annulus (2)
 - 5. Suppression Pool (39)
- III. Conductivity Probes
 - 1. Weir Annulus One-Cell (7)
 - 2. Weir Annulus Two-Cell (7)
 - 3. Top Vents, Top (9)
 - 4. Middle Vents, Top (6)
 - 5. Bottom Vents, Top (3)

Table 3-4
REPLAY INSTRUMENTATION

- I. Pressure Transducers
 - 1. Weir Wall (5)
 - 2. Top Vents, Bottom (6)
 - 3. Drywell Wall (11)
 - 4. Containment Wall (9)
 - 5. Basemat (3)

- II. Accelerometers
 - 1. Drywell Wall (1)
 - 2. Containment Wall (1)
 - 3. Basemat (2)

- III. Miscellaneous Pressure Transducer
 - 1. Venturi Throat Pressure (1)

Table 3-5
TEST MATRIX

<u>Part</u>	<u>Run</u>	<u>Cell Configuration</u>	<u>Initial Pool Temperature</u>	
			<u>°F</u>	<u>(°C)</u>
I	1	3	70	(21)
	2	3	70	(21)
	3	3	70	(21)
	4	3	120	(49)
	5	3	120	(49)
	6	3	120	(49)
II	7	1 & 2	70	(21)
	8	1 & 2	70	(21)
	9	1 & 2	70	(21)
	10	1 & 2	120	(49)
	11	1 & 2	120	(49)
	12	1 & 2	120	(49)

Common Conditions

Vapor Blowdowns	Dip tube installed
Vessel Pressure	1035 psig (7131 KN/m ²)
Vessel Water Volume	60 ft ³ (1.7 m ³)
Drywell Metal Temperature	>300°F (149°C)
Drywell Pressure	Atmospheric
Venturi Diameter	2.5 inch (6.4 cm)
Top Vent Submergence	7.5 ft (2.3 m)

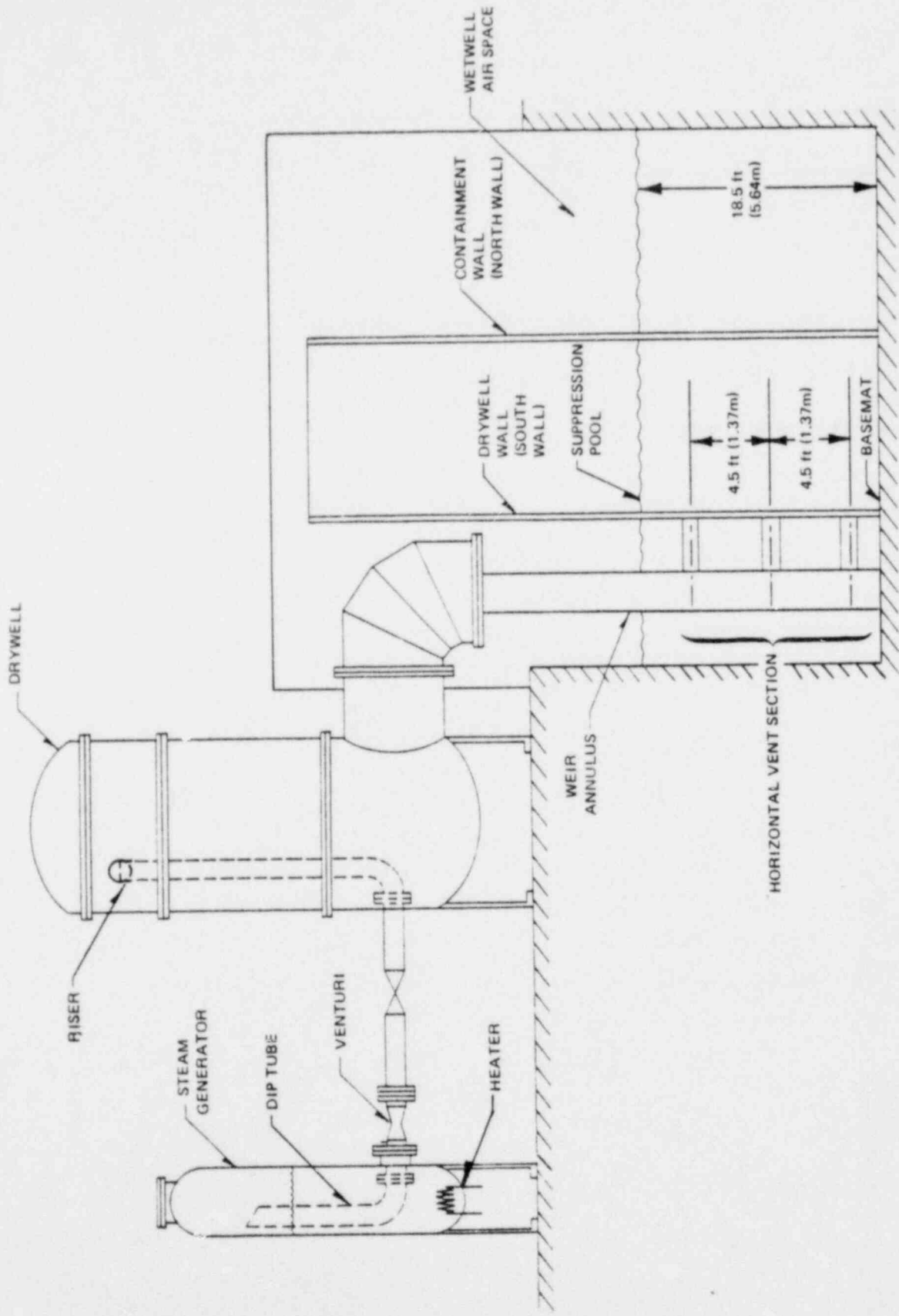


Figure 3-1. Pressure Suppression Test Facility - Test Series 6003

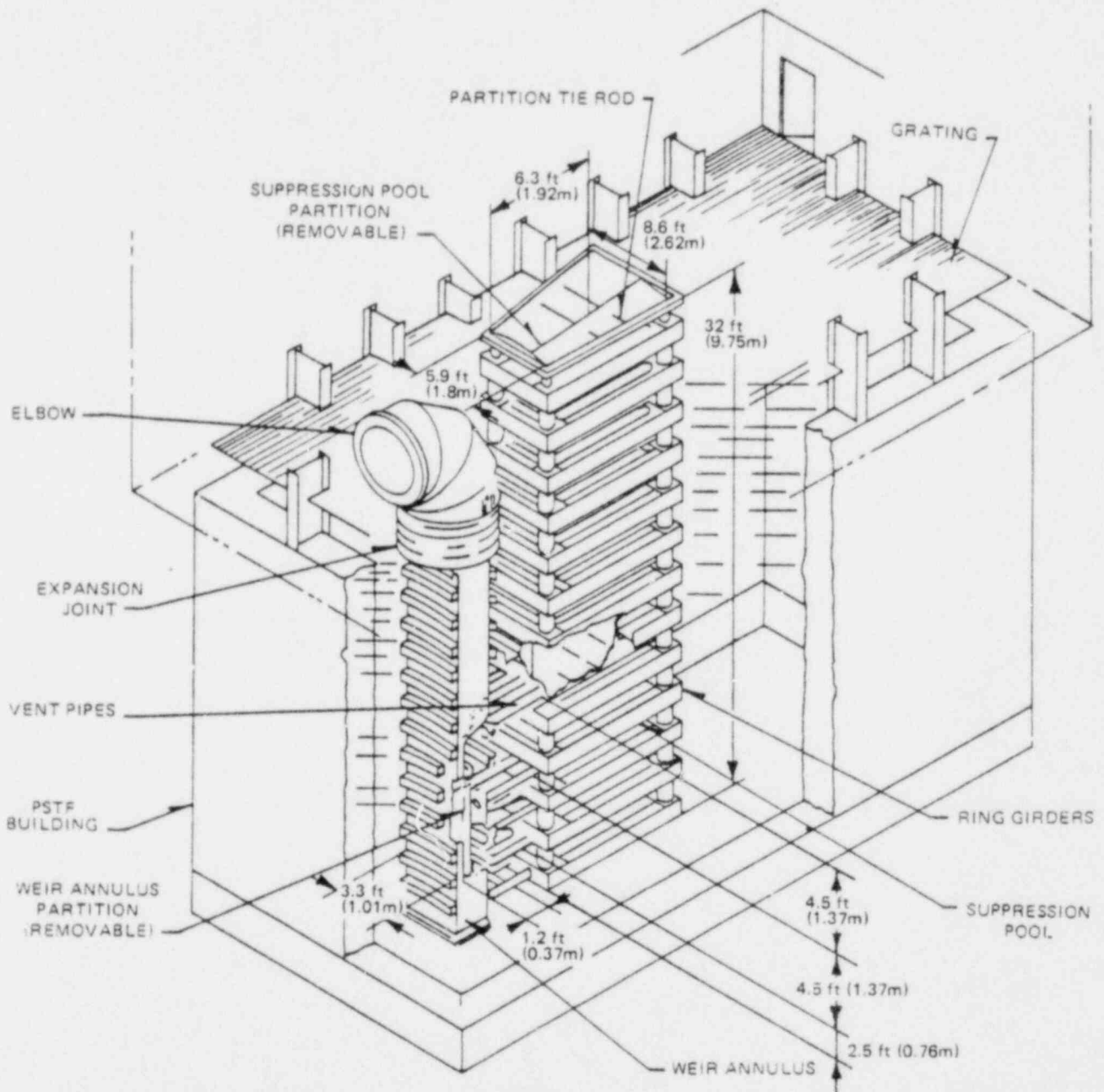


Figure 3-2. Mark III 1/9-Area Scale Weir and Suppression Pool

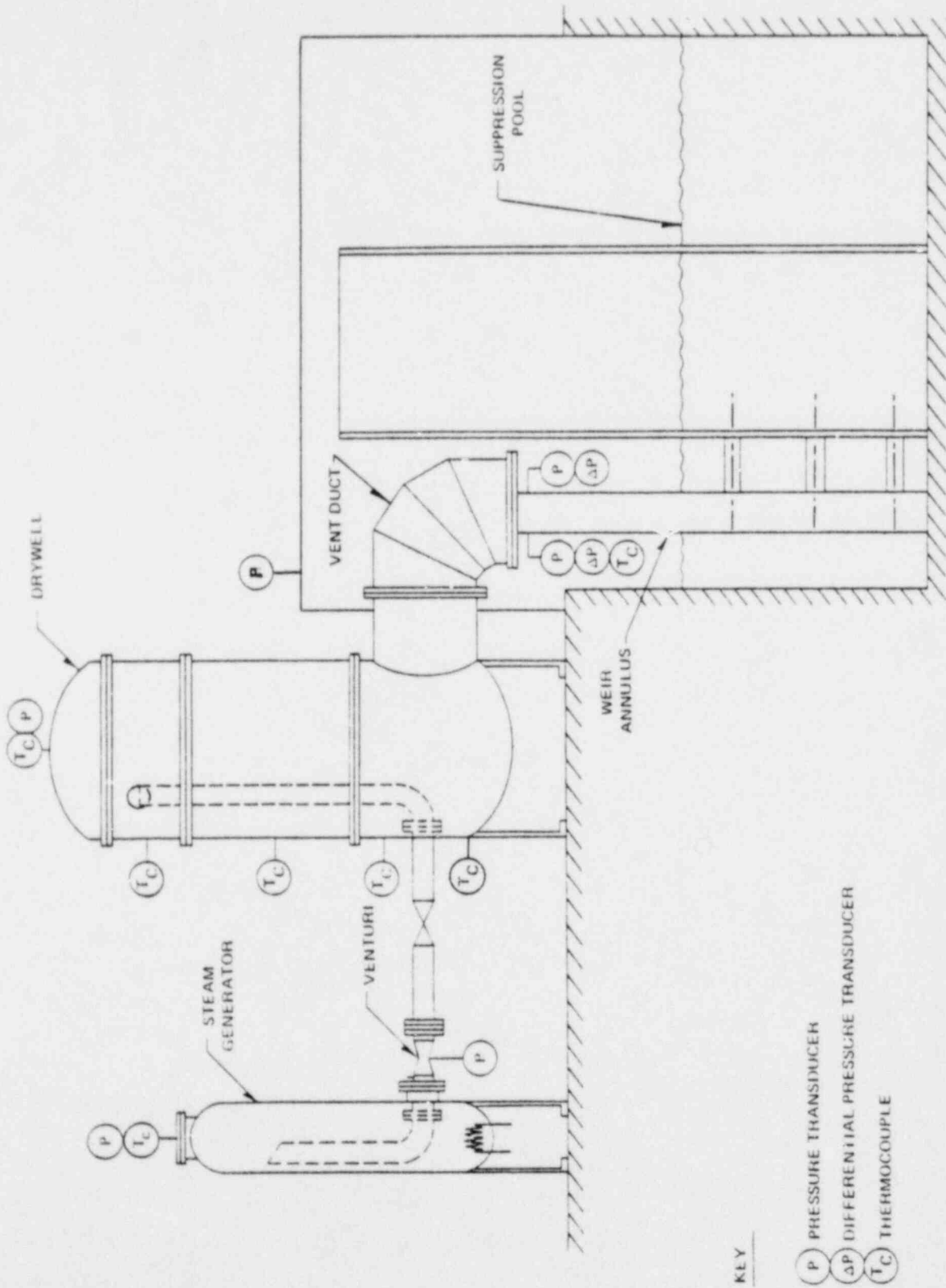


Figure 3-3. Steam Generator, Drywell and Vent Duct Real Time Instrumentation - Test Series 6003

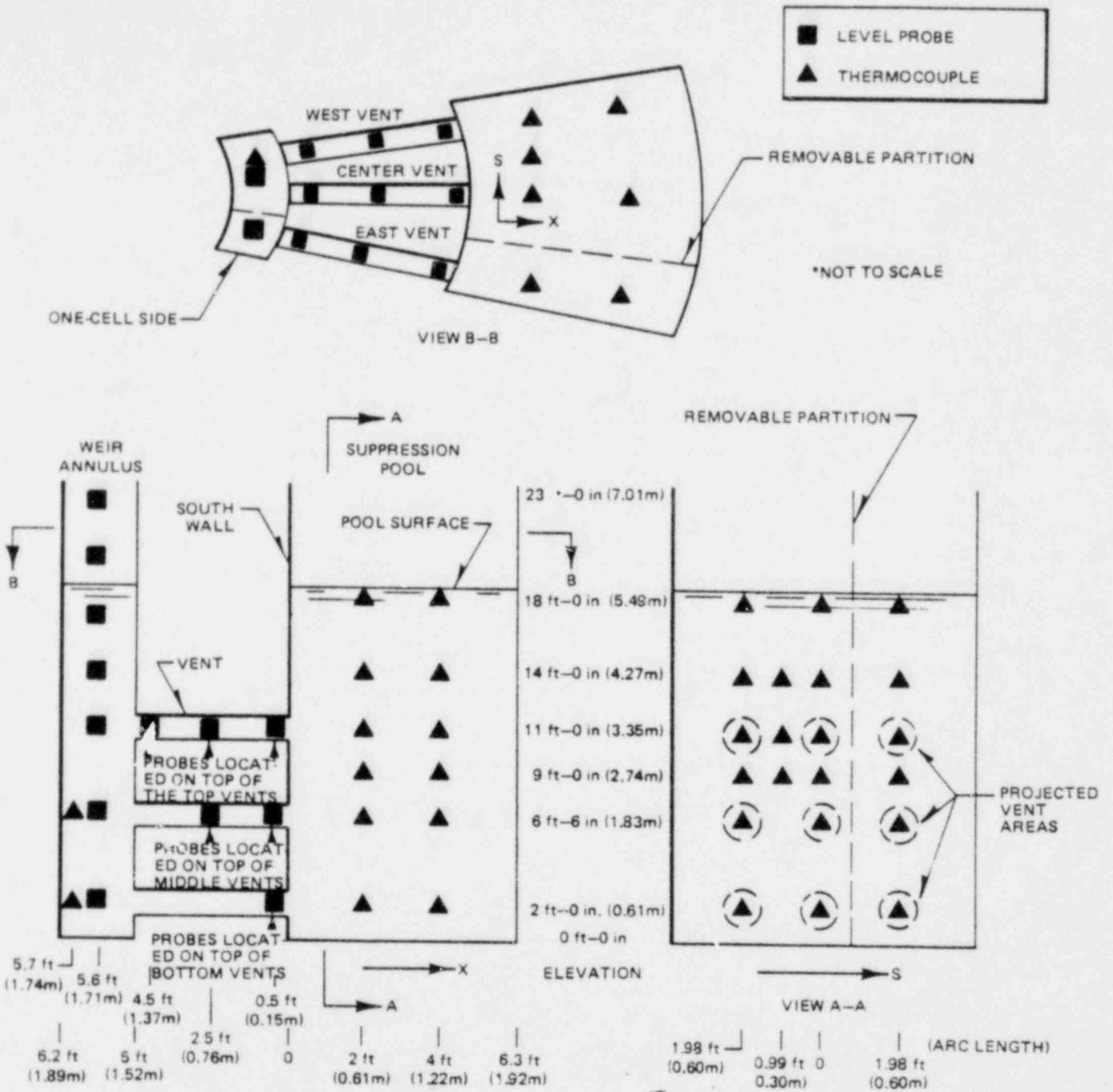


Figure 3-4. Weir Annulus, Vent and Suppression Pool Real Time Instrumentation - Test Series 6003

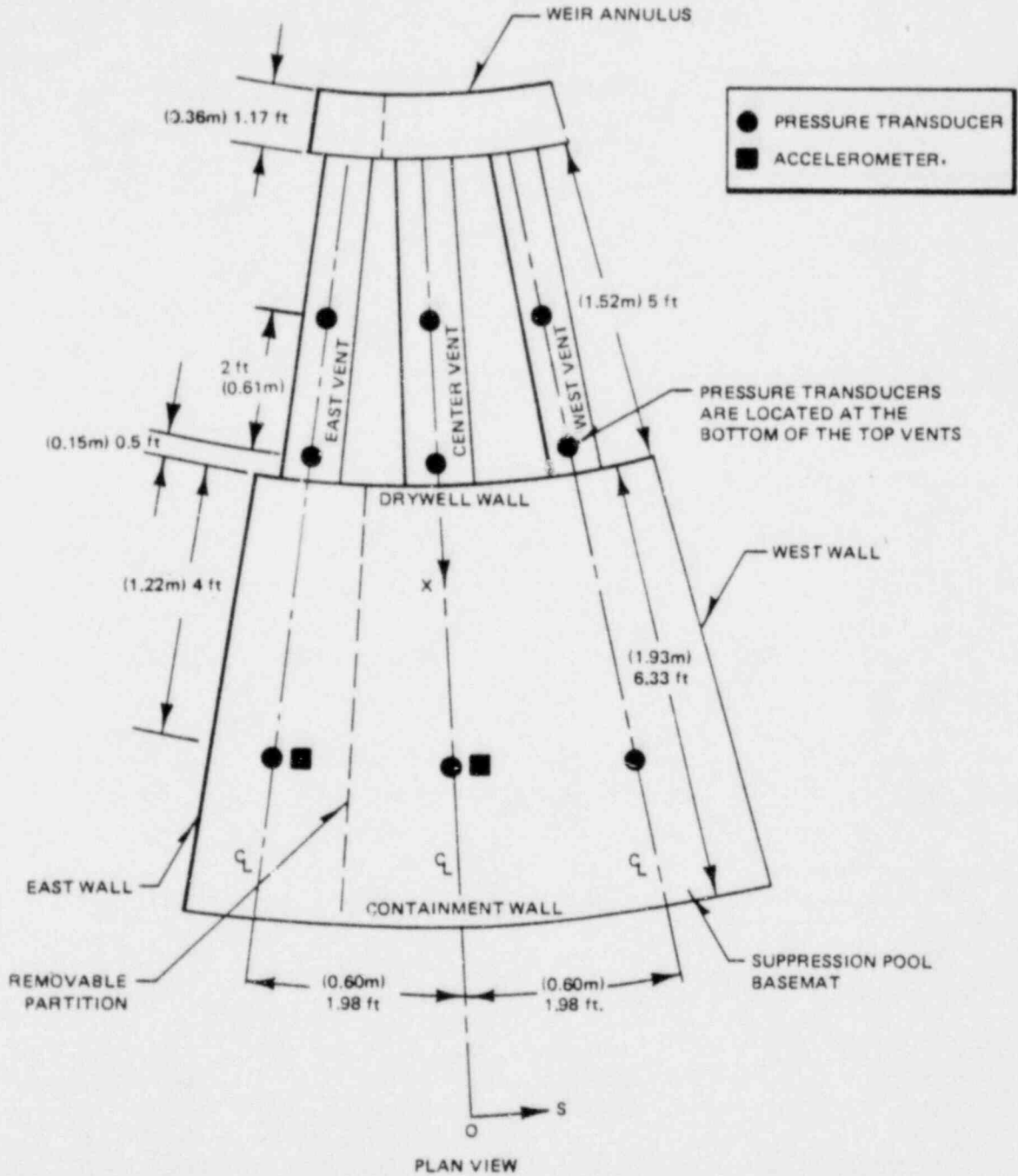


Figure 3-5. Top Vent and Basemat Replay Instrumentation - Test Series 6003

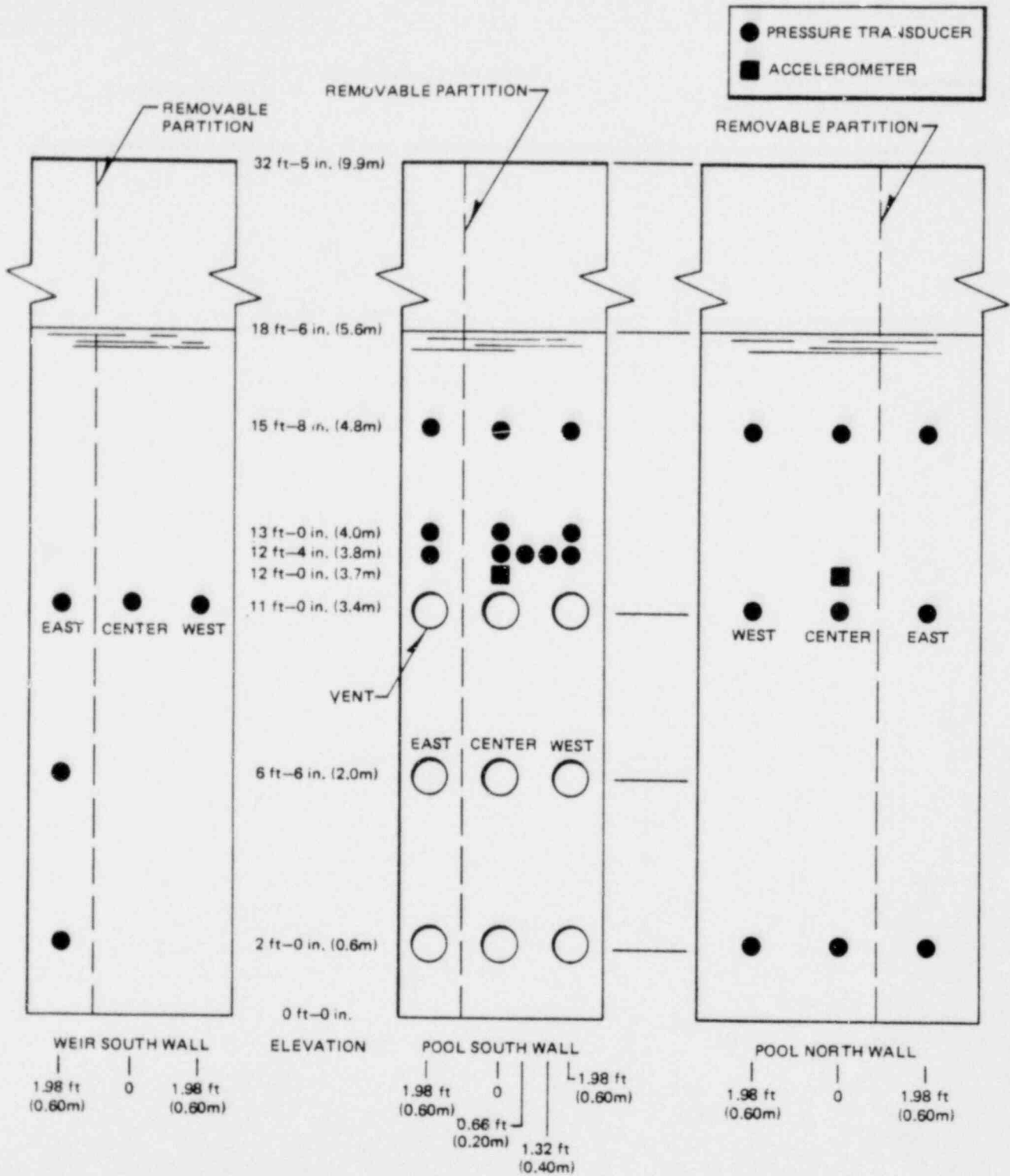


Figure 3-6. Weir and Pool Wall Replay Instrumentation - Test Series 6003

4. DATA ACQUISITION AND REDUCTION

4.1 DATA ACQUISITION SYSTEM AND PROCEDURE

A comprehensive measurement and data acquisition system is provided at the PSTF (see References 1 and 10) and shown schematically in Figure 4-1. The digital portion of the data acquisition system is designed to sample and record data on magnetic tape at a maximum rate of 8000 total measurements per second, with input from a maximum of 128 channels. Data are recorded in blocks of 16 channels, with each block requiring approximately 2.1 ms for a complete scan. This method of recording results in a scan rate which is referred to as the normal scan rate, and its total rate depends on the number of channels being scanned.

During Test Series 6003, 127 instrument channels were scanned during each run. Since all the instruments required a total of eight blocks, the resulting normal scan rate was about 20 ms. This is due to an additional 2 ms delay every 40 blocks when the data are written to the magnetic tape. Since a vast amount of data is generated with the normal scan rate, only the first 100 seconds of the blowdown transient was recorded at high speed, then, the scan rate was reduced to 250 ms. All real-time pressure transducer outputs were passed through low pass, three pole Bessel filters with a cutoff frequency of 30 Hz, prior to digitization. Thermocouples were filtered by a low pass, 10 Hz cutoff frequency L-C network. Conductivity probe outputs were unfiltered.

In addition to the digital data acquisition system, a 28-channel and a 14-channel Honeywell FM analog magnetic tape recorder were used. Utilizing these analog recorders, data was recorded at one tape speed during the test and played back at a lower speed after the test, resulting in an increase of the effective data acquisition rate. This scan rate is referred to as fast scan rate.

The twenty-seven data channels of the Honeywell Model 96, and the thirteen data channels of the Honeywell Model 101 were recorded on analog magnetic tapes at 60 inch/sec (152 cm/sec) during each blowdown, and replayed at 3.75 inch/sec (9 cm/sec). Thus, for a digital scan rate of 5 ms, an effective scan rate of 0.3125 ms resulted for all replay data. The limiting elements of the analog recording system are the low pass Bessel filters used for anti-aliasing. The outputs from the replay instruments measuring pressure, and acceleration were low-pass filtered at 10 kHz before recording on analog tapes so that high frequency components would not be attenuated. On the playback both the 13 and 27 channels were filtered at a low pass cutoff frequency of 100 Hz (effective frequency of 1600 Hz) for all tests.

4.2 DATA REDUCTION PROCEDURE

Data recorded on digital magnetic tape for all runs were processed, printed and plotted using an H-6070 computer system as shown in Figure 4-1. Data were reduced using a general data reduction program. This program reads raw data which are in counts representing millivolts (mV) from the digital magnetic data tape, and converts them to engineering unit (EU) output using transducer calibration data. The EU output data from real-time and replay instruments were processed in two different ways as discussed in the following subsections.

4.2.1 Real-Time Data Processing

The real-time data recorded at normal scan rate were processed in a single pass through the H-6070 computer. After the EU conversion was performed, the data were passed to a user-supplied subroutine for general processing and calculations. Then the outputs from this subroutine were processed by the general data reduction program for printing and plotting the results of the entire run. The data processing included calculations of venturi flow rate from vessel dome and throat pressures, vent duct flow rate from annubar static and differential pressures, time and spatial suppression pool temperature averages from pool thermocouples.

Some of the EU data generated using the general data reduction program were passed to a power spectral density (PSD) analysis program for performing PSD's on the condensation oscillation pressure and acceleration data.

4.2.2 Replay Data Processing

The chugging replay data collected during the two parts of testing were converted to EU using the general data reduction program through the H-6C70 computer. The EU data were then processed in three parts.

First, a scanning program was used to scan the entire blowdown duration to:

- a. pick out the time at which chugging events occurred and print the maximum and minimum of all measured data and their corresponding time for each chug;
- b. calculate and print mean and standard deviation of all measured data for all chugs;
- c. calculate histograms and print the results for each measurement;
- d. summarize and print the order of chugging events and timing between chugs in a multicell configuration; and
- e. plot time histories of selected data channels for all chugs.

Second, data were printed and plotted for all channels of selected individual chugs using the general data reduction program.

Third, a PSD analysis was performed for selected chugs and channels.

The condensation oscillation replay data were converted to EU to be processed by the PSD program and general data reduction program for plotting.

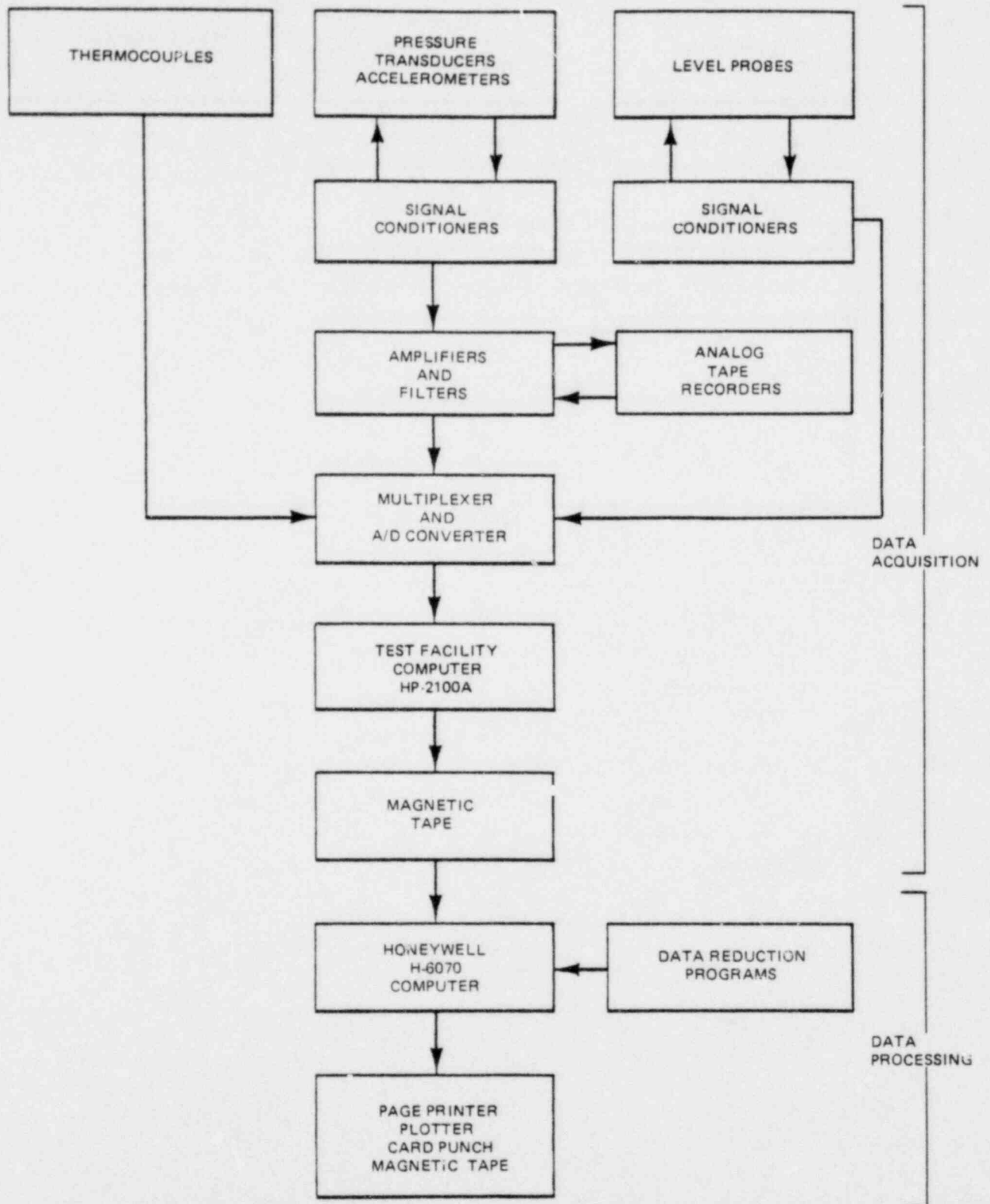


Figure 4-1. Data Acquisition System and Processing Block Diagram

5. TEST RESULTS AND DISCUSSION

Condensation and pool thermal stratification phenomena of the LOCA transient in a 1/9-area scale system were investigated and multicell effects evaluated during Test Series 6003. Each blowdown test covered the pool swell, condensation oscillation, and chugging phases of a LOCA transient. However, the emphasis of the present test program was placed on multicell effects on loads associated with condensation oscillations and chugging measured on the weir wall, in the top vents, and on the suppression pool walls. Multicell effects on pool swell loads for the 1/9-area scale configuration were determined previously during Test Series 6002 and the results documented in Reference 9.

In assessing the repeatability of the system parameters, the system performance was investigated and the results presented in Appendix D. The results of this analysis show that generally the system parameters are repeatable for all runs and that they have not changed with the addition of the partition in the weir annulus and the suppression pool. This provided the basis for direct comparison of the one-cell and two-cell runs with the three-cell runs.

The results from evaluations of the multicell effects on condensation oscillations, chugging, and pool thermal stratification are presented in the following subsections.

5.1 CONDENSATION OSCILLATIONS

After the pool swell phase, the next phase in the pressure suppression process is condensation oscillations (CO).

Flow and pressure oscillations are essentially continuous and reasonably regular in waveform over many cycles.

The vapor flow continues via

the top vents into the suppression pool.

This is the condition associated with chugging and discussed in Subsection 5.2.

Twelve tests were performed with four different initial conditions and pool configurations in Test Series 6003. It will be shown that tests with similar initial pool temperatures and pool configurations are repeatable; i.e., pressure magnitudes and frequencies have similar trends and values. For this reason, only four runs, each associated with one type of initial pool condition and configuration, are emphasized for analyses. These runs are:

<u>Run No.</u>	<u>Test Conditions</u>
1	70°F (21°C) initial pool temperature, 3-cell configuration
6	120°F (49°C) initial pool temperature, 3-cell configuration
8	70°F (21°C) initial pool temperature, 1 and 2 cell configuration
11	120°F (49°C) initial pool temperature, 1 and 2 cell configuration

Note, however, that all runs were included in the data to establish multicell effects on pressure magnitudes.

Pressure magnitudes as a function of time detected by transducers located at the drywell wall, 5.7-ft (4.8-m) elevation and the containment wall, 11.0-ft (3.4-m) elevation are plotted and discussed in Subsection 5.1.1. The repeatability of pressure magnitudes is assessed in Subsection 5.1.2. Multicell multipliers for dynamic pressure amplitudes based on rms values are determined for the drywell and containment walls of the suppression pool in Subsection 5.1.3. In Subsection 5.1.4 time plots of dominant frequencies are presented with discussions emphasizing the observed frequencies at the time of maximum pressure amplitudes.

elevation (see Figure 5-6), for the containment wall at 11.0-ft (3.4-m) elevation (see Figure 5-7), and for the drywell wall at 12.3-ft (3.8-m) elevation (see Figure 5-2). At elevations near the top vent exit elevation, magnitudes are highest at the drywell wall, followed by the containment wall and the weir wall, respectively.

The magnitude of CO pressure oscillations for 70°F (21°C) pool temperature tests and 120°F (49°C) pool temperature tests are shown in Figures 5-8 and 5-9 respectively. The figures give time history plots for transducers located at the 15.7-ft (4.8-m) elevation. Note that pressure magnitudes for the higher pool temperature test (Run 11) are much higher than for the lower pool temperature test (Run 8). This is also evident from pressure histories at the 12.3-ft (3.8-m) elevation, cf, Figures 5-1 and 5-2. For this reason, emphasis is placed on high pool temperature tests in further data analysis; i.e., multi-cell effects, test repeatability, etc.

5.1.2 Repeatability of Pressure Magnitudes

In characterizing the pressure magnitudes, the rms values about the linear trend-removed mean are calculated over a 2.56-second interval. The advantage of using the root-mean-square (rms) values is that they characterize all the data rather than isolated peak-to-peak values taken from histograms. The characterization of CO pressure amplitudes should be based on all the data since the oscillations are continuous with variations in both amplitude and frequency.

In verifying the repeatability of pressure magnitudes for tests at identical initial conditions and cell configuration, the rms values of the drywell wall, 15.7-ft (4.8-m) elevation, center cell of Runs 4, 5 and 6, are plotted and shown in Figure 5-10. The data from run to run show similar temporal trends. Corresponding plots for the 1- and 2-cell tests are given in Figure 5-11 for the single cell, and in Figure 5-12 for the two-cell portion. An estimate of

5.1.1 Pressure Time Histories

Figure 5-1 shows the variations of typical pressure traces of transducers situated 1.3 ft (0.4 m) above the centerline of the last, center, and west bents and on the drywell wall 12.3 ft (3.75 m) elevation. The traces with trend removed*, are from Run 1, a test with 70°F (21°C) initial pool temperature and a 3-cell configuration. The CO pressure oscillations are fairly continuous with small variations in the peak-to-peak amplitudes with time and cell location.

A figure similar to Figure 5-1, but for Run 6 [120°F (40°C)] initial pool temperature and a three-cell configuration, is shown in Figure 5-2. Note that aside from an overall amplitude increase and a longer CO period when compared to Run 1, there are many randomly occurring pressure spikes.

The pressure spikes are believed to be caused by the collapsing of isolated steam bubbles detached from the main CO steam bubble at the vent interface. Figure 5-3 is a 1.3-second time-history plot of the same pressure transducer as shown in Figure 5-1. The signal had been linear trend removed. Note that there is an underpressure prior to the principal spike at indicative of the rapid local acceleration field produced upon bubble collapse. The subsequent overpressure spike is caused by the sharp deceleration of the surrounding water. The magnitude of the spike attenuates rapidly as the distance from the collapse location increases. The proof of this is evident from drywell wall pressures shown in Figure 5-4, 13.0-ft (4.0-m) elevation, and in Figure 5-5, 15.7-ft (4.8-m) elevation. At the 15.7-ft (4.8-m) elevation 4.7 ft (1.4 m) above the centerline of the top vent, no pressure spikes are detected. Because the pressure spikes are localized, they are not indicative of the CO source. Therefore, locations where the pressure reading were affected by the spikes were not used to assess multicell effects.

For comparison of pressure signals at different locations in the facility, time history plots of Run 6 are given for the weir wall at 11.0-ft (3.4-m)

*Using a 200-point rolling average trend removal routine.

the quality of repeatability is the standard deviation of the rms values from similar tests at a given time interval.

Repeatability extends beyond the drywell wall and covers both the weir wall and the containment wall. Figure 5-13 shows the repeatability of rms values calculated from pressure magnitudes from Runs 10, 11, and 12 at the weir wall 11-ft (3.35-m) elevation, east cell. Figure 5-14 shows the repeatability from the same runs at the containment wall 2.0-ft (0.6-m) elevation, east cell. The inference is drawn that this repeatability is sufficiently tight as to allow for valid assessments of multicell effects by an averaging procedure discussed below.

5.1.3 Multicell Effects on Pressure Magnitudes

The drywell wall 15.7-ft (4.78-m) elevation and the containment wall 2.0-ft (0.5-m) elevation pressure transducer signals are used as the data base to investigate the multicell effects on pressure magnitudes during CO. The reason for selecting this specific drywell wall location signal is that the transducer is just far enough away from the vent exit region so that few, if any, random pressure spikes (which are not indicative of the source pressure) are detected. It is also close enough to the vent exit so that the pressure trace will closely reflect the CO source pressure magnitude. The ideal transducer locations for quantifying CO source pressure magnitudes are those in the top vent. However, the high range required to measure chugging pressures peaks in the top vents resulted in an accuracy of ± 0.25 psi (1.72 kN/m²) for the transducers. Since CO pressure magnitudes are close to that range, these transducer readings were not considered to be sufficiently accurate for the CO analysis.

Root-mean-square values of the pressure signal versus time at the drywell wall 15.7-ft (4.78-m) elevation and at the containment wall 2-ft (0.6-m)

elevation for the east, center, and west cells, for Run 6 of the three-cell test, are shown in Figures 5-15 and 5-16, respectively. In general, rms magnitudes for all three cells are similar and the time histories follow similar trends. Similar rms plots for the east cell, the center and west cells are given in Figures 5-17 and 5-18 for Run 11, a one- and two-cell test. The figures show that single cell pressure magnitudes are generally higher than two-cell magnitude.

To quantify multicell effects on pressure magnitudes, rms values calculated from similar rms were averaged as a function of time. By averaging several data points instead of using one point, the level of confidence of the calculated multicell multipliers is increased.

The averaging was performed for rms values at a given time and location in the pool. For the 3-cell tests, the rms values of the east, center, and west cells from the three identical tests were used, a total of 9 values per given time. For the 2-cell average rms, the values of the center and west cells from three identical tests, a total of 6 values, were averaged. Similarly, for the single-cell average rms, the east cell values from these identical tests, a total of 3 points, were averaged. The average values of the 2- and 3-cell tests were divided by the single-cell test value at the same time. The resulting normalized values as a function of time are presented in Figures 5-19 and 5-20.

5.1.4 Pressure Oscillation Frequencies

Frequencies of the CO pressure traces were obtained by performing power spectral analysis (PSD) of the linear trend-removed signal over 2.56-second

time intervals.

The time interval of the PSD analysis is set by the data scan rate (20 milliseconds) and the number of data points per block (128). The desired cutoff frequency, 25 Hz, and the number of data points per block set the frequency resolution. The analyses were performed continuously in time until the start of chugging.

This time period is prior to the excitation of pool acoustics which is discussed later in this subsection.

The dominant frequencies, being the frequency corresponding to the highest power in units of $(\text{psi})^2/\text{Hz}$, are plotted as a function of time for three similar runs in Figure 5-22.

The repeatability of pressure amplitudes was demonstrated in Subsection 5.1.2. Figure 5-22 demonstrates the repeatability of the signal frequencies for runs of similar initial conditions.

Dominant frequencies are independent of cell configuration, as shown in Figure 5-23, where the dominant frequencies of pressure signals at the drywell wall, 15.7-ft (4.8-m) elevation, for single-, two- and three-cell tests are plotted as a function of time. Dominant frequencies from tests of different cell configurations also follow similar temporal trends.

This figure is indicative of dominant frequencies observed throughout the pool.

This dominant frequency is attributed to an acoustic quarter-standing wave in the suppression pool.

To support this hypothesis, the axial distribution of the pressure magnitudes at the containment wall are plotted at different times in Figure 5-24.

The standing wave was probably excited by the condensation pressure oscillations at the vent exit.

While the acoustic speed in water is higher, the presence of steam/air in the water serves to reduce the acoustic speed to this resultant value.

The quantity of air in the pool decreases as a function of time following pool swell, increasing the pool acoustic speed and thereby increasing the frequency. The excitation of pool acoustics is facility unique and therefore is not expected to occur in prototypical Mark III containment systems.

5.1.5 Conclusions

The CO period of higher pool temperature tests lasts longer because the condensation rate at the vent exit interface is lower due to a smaller interface temperature difference.

The repeatability of pressure magnitudes at a given location for runs with similar initial conditions and cell configuration is sufficient to allow valid assessments of multicell effects using rms value averages of similar tests.

The multicell multipliers (i.e., the ratios of three-cell or two-cell pressure amplitudes to single-cell values) are generally below unity for the drywell wall. At the containment wall the multipliers are always below unity. Hence, pressures observed from multicell tests are lower than single-cell tests.

The dominant frequency of the CO pressure signal as characterized by the highest PSD value varies with time.

5.2 CHUGGING

Chugging is defined as low mass flux intermittent condensation. Characteristics of this phenomenon are clearing water from the top vents, formation and collapse of a separate steam bubble in each vent, and reflooding of the top vents. Chugging was observed only in the top vents with the bottom and middle rows of vents remaining flooded throughout this phase of the transient.

These steam mass flux values are based on the total flow area of 1.34 ft^2 (0.12 m^2) for the three top vents. The time and steam mass flux at the onset of chugging for all runs are summarized in Table 5-1.

Chugging pressures varied with each chug. In illustrating the multiple effects a statistical analysis was performed and the results for each cell configuration were compared. This statistical comparison was based on histograms of maximum pressure values chugging events. The histograms were used to generate the complementary cumulative probability density distribution functions (CCPDDF) for all three runs with similar initial conditions. Details regarding the method and procedure used for calculation of CCPDDFs are presented in Appendix C.

The results of the statistical analysis and time history plots of chugging phenomena observed in the top vents, on the weir wall and the pool walls are presented in the following subsections.

5.2.1 Top Vent Chugging Pressure Response

Large magnitude pressure pulse trains of decreasing magnitude and period and increasing base width were observed in the three top vents during both 1- and 2-cell, and 3-cell runs. The collapse and rebound character of the intra-vent chugging signals are similar to that seen in 1/3 and full-scale tests (see References 4 and 8). The pulses appeared to develop acoustic waves which propagated from the point of the bubble collapse inside the top vents toward both the weir wall and the suppression pool.

Further, a comparison of the 1/9-area scale top vent chugging pressure time histories with those observed in the 1/3-area scale (see Reference 8) and the full-scale (see Reference 4) indicates that the same chugging phenomenon occurred in the 1/9-area scale, the 1/3-area scale, and the full-scale.

In illustrating the 1/9-area scale top vents chugging pressure response, typical 1-, 2-, and 3-cell pressure time histories are presented in Figures 5-25 through 5-27 for Runs 3 (3-cell configuration) and 8 (1- and 2-cell configurations). Shown in these figures are top vent pressures measured at the bottom of the vents 2.5 ft (0.76 m) from the vent exit plane (i.e., drywell wall). This measurement location corresponds to the center of the vent length and is also referred to as top vent center pressure. A comparison of these time history plots indicates that the pulse train characteristics of the top vent chugging pressure signal were not affected by different cell configurations.

The top vents chugging pressure magnitudes measured at the center of the vent were higher than those measured near the vent exit at 0.5-ft (0.15-m) away from the drywell wall for both 70 and 120°F (21 and 49°C) initial pool temperatures. This indicates that the bubble collapse location was generally closer to the center of the vent than its exit.

5.2.2 Multicell Effects on Top Vent Chugging Pressures

In assessing the multicell effects on the top vent chugging response and source strength, the one-, two-, and three-cell CCPDDF of the top vent peak center pressure are compared and presented in Figure 5-28. The CCPDDFs (as described in Appendix C) are based on the east vent pressure for one-cell, combination of the center and west vents pressure for two-cell, and combination of the east, center and west vents pressure for three-cell. As shown in this figure, the one-, two-, and three-cell configurations have similar distribution for both 70 and 120°F (21 and 49°C) initial pool temperature indicating that all the three-cell configurations have nearly equal source strengths. The variation observed in the maximum pressure values is considered to be due to the random behavior of the chugging phenomena in terms of the location of the bubble collapse (relative to the pressure transducer) and/or the chugging pressure magnitudes.

The multicell effect on the top vent chugging pressure is further illustrated by CCPDDF of the top vent exit pressure shown in Figure 5-29 for both 70 and 120°F (21 and 49°C) initial pool temperature. These CCPDDFs were determined

by the same method used for the top vent center pressure analysis. A comparison of these CCPDDFs indicates that the one-, two-, and three-cell configurations have similar distribution profiles.

The results presented above illustrate that the one-, two, and three-cell top vent pressures of a essentially equal strengths providing the basis for direct comparison of the pressures measured on the weir wall and the suppression pool walls for investigation of multicell effects on loads as discussed in the following subsections.

5.2.3 Weir Wall Chugging Pressure Response

The weir wall chugging pressure pulses were characterized by small magnitude, short duration pulse trains. Due to timing and similarity between the top vents and weir wall pressure time histories, they appear to be highly attenuated top vents pressure pulses as illustrated in Figures 5-30 through 5-32 for the one-, two-, and three-cell configurations, respectively. Shown in these figures are weir wall pressure response measured at 11-ft (3.35-m) elevation, across from the top vents center line. A comparison of these figures shows that the weir wall pressure time history characteristics of the one-cell are different from the two- and three-cell configurations. The one-cell weir wall pressures are due to the east top vent chugs referred to as "individual vent chugs". The two-cell weir wall pressures are due to the center and/or the west vents chugs, and similarly the three-cell weir wall pressures are due to chugs in the east, center, and/or west top vents referred to as "multi-vent chugs". These weir wall pressure spikes due to chugs occurring in the adjacent vents are indicated in Figures 5-31 and 5-32 for the two- and three-cell configurations.

A comparison of the 1/9-area scale one-cell weir wall chugging pressure time histories with those observed in the 1/3-area scale (see Reference 8) and the full-scale (see Reference 4) indicates that similar single-cell chugging responses occurred in the three differently scaled test systems.

5.2.4 Multicell Effects on Weir Wall Chugging Pressure

In evaluating the multicell effects on the weir wall response a statistical analysis was performed on the individual vent chugs of the east cell for the one-cell configuration on the multivent chugs of the center and west vents for the two-cell configuration, and on the multivent chugs of the east, center, and west vents for the three-cell configuration. This approach was used since the two- and three-cell wall pressures resulted from chugs occurring in one or more of the top vents. These weir wall pressures were then combined for determining the one-, two-, and three-cell CCPDDFs.

The CCPDDFs of the weir wall peak pressures measured at 11-ft (3.35-m) elevation for each cell configuration are presented in Figure 5-33 for both 70 and 120°F (21 and 49°C) initial pool temperature. As shown in this figure, the one-, two-, and three-cell configurations have similar profiles with the one-cell having higher probability than the two- and three-cell at small pressure magnitudes.

This indicates there is enough chugging asynchronization (as discussed in Subsection 5.2.9) to prevent superposition of the two- and three-cell peak pressures resulting in values greater than one-cell values,

5.2.5 Drywell Wall Chugging Pressure Response

The drywell wall (the PSTF south wall) chugging time histories are presented in Figures 5-34 through 5-36 for the one-, two-, and three-cell pressures measured directly above the top vents at 12.3-ft (3.75-m) elevation, respectively. Based on the timing between the top vents and the drywell wall chugging spikes, the drywell wall pressures indicated in these figures appear to be highly attenuated top vent acoustic pressure waves propagating to the suppression pool walls. Similar to the pressures observed on the weir wall (see Subsection 5.2.3), the one-cell drywell wall pressure responses are different from the responses of the two- and three-cell configurations. In

the case of the one-cell configuration, the drywell wall pressures are due to the individual vent chugs occurring in the east top vent. The two-cell drywell wall pressures, however, may result from chugs in either or both the center and west vents. Similarly, the three-cell pressures may result from either one, two, or all three (east, center, and west) vents. The largest magnitude drywell wall pressure spikes are generally measured when the chug occurs in the top vent below the pressure transducer, with the smaller spikes resulting from the chugs occurring in the adjacent vents as illustrated in Figure 5-35, and for the two- and three-cell configurations.

A comparison of the 1/9-area scale one-cell drywell wall chugging pressure time histories with those observed in the 1/3-area scale (see Reference 8) and the full-scale (see Reference 4) indicates that similar single-cell chugging response occurred in all three scales.

5.2.6 Multicell Effects on Drywell Wall Chugging Response

In evaluating the multicell effects on the drywell wall response a statistical analysis was performed on the individual vent chugs of the east cell for the one-cell configuration, on the multivent chugs of the center and west vents for the two-cell configuration, and on the multivent chugs of the east, center, and west vents for the three-cell configuration. This approach was used since the two- and three-cell wall pressures resulted from chugs occurring in one or more of the top vents, as in the case of the weir wall response. These drywell wall pressures were then combined or averaged for determining the one-, two-, and three-cell CCPDDFs and the corresponding load multipliers.

The CCPDDFs of the drywell wall peak pressure measured directly above each top vent at 12.3-ft (3.75-m) elevation for each cell configuration, are presented in Figure 5-37. The one-cell has higher probability of observing pressures at a given value than the two-cell, and the two-cell has higher probability than the three-cell configuration for both initial pool temperatures. This result indicates that the drywell wall pressures decrease with increases in the number of cells.

To further support the conclusion that the one-cell loads are bounding drywell wall pressure loads, the CCPDDFs of the one-, two-, and three-cell configurations at 13.0-ft (3.96-m) elevation are given in Figure 5-38 for 70 and 120°F (21 and 49°C) initial pool temperature. The information given in this figure is similar to the results at 12.3-ft (3.75-m) elevation. Therefore, the one-cell probability is higher than the two-cell, and the two-cell has higher probability than the three-cell.

To investigate superposition of loads on the drywell wall due to synchronized chugs occurring in two adjacent vents, two pressure transducers were located between the center and west vents at 12.3-ft (3.75-m) elevation. These transducers (see Figure 3-6) were 0.7-ft (0.21-m) away (horizontally) from each vent center line and designated as C-Y0.7 and W-Y0.7. The CCPDDFs of the C-Y0.7 for the two- and three-cell configurations are presented in Figure 5-39. The two-cell has higher probability than the three-cell configuration for both 70 and 120°F (21 and 49°C) initial pool temperature. Similarly, the CCPDDFs of W-Y0.7, presented in Figure 5-40, exhibit the same trend of decreasing probability with increasing number of cells. These results indicate that in multicell configurations asynchronisation exists (as is further discussed in Subsection 5.2.9).

5.2.7 Containment Wall Chugging Pressure Response

The containment wall (the PSTF north wall) chugging time histories are presented in Figures 5-41 through 5-43 for the one-, two-, and three-cell pressures measured across the top vents center line at 11-ft (3.35-m) elevation, respectively. The containment wall pressure spikes are due to acoustic pressure waves emanating from the top vents and attenuating upon propagation across the suppression pool. The one-cell containment wall pressures are due to chugs occurring in the east top vent. The two-cell pressures result from chugs occurring in the center and/or west vents, and the three-cell pressures results from chugs occurring in the east, center and/or west vents.

5.2.8 Multicell Effects on Containment Wall Chugging Response

The multicell effects on the containment wall are evaluated by comparing the one-, two-, and three-cell CCPDDFs calculated for every three runs with the same initial conditions based on the individual vent chugs of the east top vent for the one-cell, multivalent chugs of the center and/or west vents for the two-cell, and the east, center, and/or west vents for the three-cell configuration.

The CCPDDFs of the containment wall peak pressure presented in Figure 5-44 are measured across the top vents center line at 11-ft (3.35-m) elevation for each cell configuration at both 70 and 120°F (21 and 49°C) initial pool temperatures. All three cell configurations have similar profiles with one-cell having higher probability than both the two- and three-cell configurations. This indicates that one-cell loads are bounding.

5.2.9 Chugging Asynchronization

The two-cell asynchronization was based on the time interval between the center and west top vents chugs. In the case of the three-cell, the asynchronization was calculated using these three methods (1) as the time difference between the first and second top vent chugs independent of cell position, (2) as the time difference between the second and third top vent chugs independent of cell position, and (3) as the time difference between the center and west top vent chugs independent of time order. The resulting time interval of each method was then used for calculating the corresponding CCPDDFs and averages for both the two- and three-cell configurations. The purpose of this analysis was to investigate multicell effects on chugging asynchronization and to determine whether all chugging events for a given cell configuration were asynchronized as indicated by the weir wall and pool walls multicell pressures relative to single-cell values.

The CCPDDFs of the two- and three-cell configuration are presented in Figures 5-45 through 5-47 for 70 and 120°F (21 and 49°C) initial pool temperature. As shown in these figures both the two- and three-cell configurations have similar profiles indicating the chugging asynchronization was not affected by the increase in the number of cells.

To further support that all chugs were not synchronized, average and standard deviation of chugging time differences are presented in Table 5-2 for each cell configuration.

These results are consistent with those of the weir wall and pool wall loads in that the pressures generally did not superimpose due to chugging asynchronization.

5.2.10 Chugging Period

The chugging period is defined as the time between two consecutive chugs in the case of one-cell configuration, two consecutive cluster of chugs occurring in 1 or 2 vents for the two-cell, and 1, 2, or 3 vents for the three-cell configuration. In evaluating the multicell effects on a chugging period, the corresponding CCPDDFs and averages were calculated for the one-, two-, and three-cell configuration. The results are presented in Figure 5-48 for each cell configuration at both 70 and 120°F (21 and 49°C) initial pool temperatures. All three cell configurations have similar profiles with the one-cell being generally higher than two- and three-cell. Similar results are observed based on the average and standard deviation of chugging period as presented in Table 5-3. Both the two- and three-cell average periods are nearly the same and slightly less than the one-cell average values. On the average chugging is less frequent during the 70°F (21°C) initial pool temperature than during the 120°F (49°C) initial pool temperature. This is similar to the full-scale test results (see Reference 4).

5.2.11 Conclusions

The chugging phenomenon observed in the top vents of the 1/9-area scale system as characterized by pressure pulse trains, appeared to be similar to the phenomenon which occurred in the 1/3-area scale (see Reference 8) and the full-scale (see Reference 4) systems, indicating that the multicell effects seen in this subscale facility are valid for a full-scale system.

The steam bubbles generally collapsed inside the top vents indicating that the resulting top vent pressures were representative of the source strength. A comparison of the top vent peak pressure CCPDDFs of the one-, two-, and three-cell configurations demonstrated that the source strength was not affected by cell configuration. This provided the basis for assessment of the multicell effects by comparing the weir wall and pool wall pressures of all three cell configurations. As illustrated by the results in the above presentation, the multicell weir wall and pool wall chugging pressures were less than the single cell values.

The weir and pool wall chugging pressures were affected by vent interaction due to multicell effects. As was indicated in the pressure time history plots presented above, the pressure spikes measured on the walls of a given cell were also due to chugs occurring in the adjacent cell.

5.3 POOL THERMAL STRATIFICATION

5.3.1 Introduction

Upon initiation of a blowdown, steam and water are forced from the weir annulus region through the vent pipes into the suppression pool. The steam-water mixture heats the suppression pool water as the steam condenses. During the initial phase of blowdown this mixture flows through all vent pipes causing a significant local pool temperature excursion in the region near each vent exit, with the highest and lowest excursion occurring in the top and bottom vents, respectively. As the blowdown progresses, the flow

of steam-water mixture will diminish first in the bottom vents and later in the middle vents, resulting in a diminished mass and energy flow into the lower region of the suppression pool. Beyond this point nearly all of the mass and energy discharged into the suppression pool is through the top vents. Towards the end of the blowdown process a stratified layer is formed with a nearly uniform temperature distribution radially as well as vertically which extends downwards from the pool surface to an elevation slightly below the top vents. Below this elevation the pool temperature decreases nearly linearly with decrease in elevation to the initial pool temperature near the bottom vents. The pool water is stagnant and unaffected by the pressure suppression process below the bottom vents.

The 39 thermocouples used to measure the suppression pool water temperature in these tests were arranged in seven vertical strings within the pool. Six strings contained six thermocouples each located at elevations of 2, 6.5, 9, 11, 14, and 18 ft from the pool basemat. These six strings were radially distributed in the pool so that each cell contained two strings in line with the vent trajectory 2 ft and 4 ft outward from the drywell wall. The seventh string was located on the boundary between the center and west cell, 2 ft out from the drywell wall. This string contained three thermocouples located at elevations 9, 11, and 14 ft from the pool basemat. The following nomenclature was used during these tests:

- X2,X4 - horizontal distances of 2 and 4 ft from the drywell wall, respectively
- 22,26.5,
etc - elevation in feet from basemat
- W,C,E - pool locations west, center and east in line with vent trajectories
- C-W - pool location in the boundary between the center and west cell

5.3.2 Data Reduction

The suppression pool temperatures were plotted as a function of time for each thermocouple location. Figures 5-49 through 5-54 show typical temperature response in the time frame up to 100 seconds after initiation of blowdown for Run 3. In addition, the time average temperature of the vertical string of thermocouples and the time average horizontal temperature at a given elevation at distances of 2 ft (0.6m) and 4 ft (1.2m) from the drywell wall were also plotted as a function of time (see Figures 5-55 through 5-58). To eliminate noise, the temperatures used to generate the above plots were averaged over a time interval of about 2 seconds which corresponds to 100 time steps. Also, to facilitate evaluation of local and regional pool temperatures, all pool temperatures were averaged over a time interval of 25 seconds. Thus, the local pool temperatures averaged were subsequently used to develop plots of pool thermal stratification profiles, investigate multivalent effects on pool bulk temperatures, and evaluate circumferential and radial pool temperature distribution.

5.3.3 Test Results

This is due to the hot air bubble formed in the suppression pool during the pool swell phase of the pressure suppression process. The peak pool temperature, during these excursions, appears to occur randomly in the region of pool top and middle vent trajectories with no dominant preference for a given cell. Generally, the magnitude of peak temperatures are about the same in the top vent and middle vent, but substantially lower in the bottom vent region. These temperatures are of short duration and not important from the standpoint of pool thermal responses.

Thermal mixing in the multicell suppression pool is a turbulent process. Therefore, to make the assessment of multicell effects meaningful, it was necessary to average the local temperatures over a time frame sufficiently large enough to account for this random process. For this reason, a time interval of 25 seconds was selected for the time averaging of the thermocouple outputs. This time the interval divides the blowdown transient into four time zones (0 to 25, 25 to 50, 50 to 75, and 75 to approximately 100 seconds) with each time zone, except the last zone, covering a 25-second time frame. The time frame of the last zone varies slightly from run to run because the data acquisition system was manually started and stopped which resulted in a variation in the termination time.

These time-averaged temperatures were used to generate the suppression pool temperature profiles for the locations of 2 ft (0.6m) and 4 ft (1.2m) from the drywell wall. Figures 5-59 through 5-62 show typical temperature profiles for the 120°F (49°C) initial pool temperature. The typical suppression pool thermal response for the 3-cell test configuration (Run 4) is shown in Figures 5-59 and 5-60. The one-cell/two-cell test configuration (Run 12) is shown in Figure 5-61 and 5-62. These figures show no appreciable difference in the suppression pool thermal response between the two test configurations; in fact, the temperature profiles are nearly identical in character. Furthermore, the magnitude of variation (very small) in thermal response between the west, center, and east cell is about the same for the two test configurations. This indicates there is not any apparent radial or circumferential maldistribution attributable to multicell test configuration. In addition, the radial and circumferential temperature distribution indicates that the thermal energy flow into the suppression pool is equally divided between the vents and that thermal mixing in the upper region (above the top vents) of the pool is extremely good.

Some variation in the suppression pool thermal response, such as vertical temperature distribution and final pool bulk temperature, have been observed in the test results. For example, Runs 7 and 8 were made with a 70°F (21°C) initial pool temperature and the same test configuration (1- and 2-cell configuration). However they resulted in different final pool bulk temperatures. The temperature profiles for these two runs are included in Figures 5-63 and 5-64.

This difference in pool bulk temperature for these runs is evident throughout the blowdown transient.

Because of run-to-run variations in the system performance, such as mass flux and initial pool temperature, a direct comparison of pool thermal stratification between the 3-cell and the 1- and 2-cell test configuration cannot be made. However, acknowledgment of these variations allows a comparison to be made which strongly suggests that thermal stratification is not multicell dependent. Figures 5-63 and 5-64 show a comparison of Runs 7 and 8 to Run 3 (3-cell test configuration) for the 120°F initial pool temperature. Run 3 was selected for this comparison because of the similarity of the mass flux transient and initial pool temperature to Run 8. Note that the mass flux transient in Run 3 is slightly lower (see Systems Performance, Appendix D) than in Run 8, resulting in slightly lower pool temperatures in Run 3. It is clearly evident that the configuration of the pool temperature profile in these test runs is nearly identical, which indicates that thermal mixing is nearly identical in both 1- and 2-cell and 3-cell test configurations. Furthermore, if the mass flux transient in Run 3 and Run 8 had been the same, the pool temperature profiles for these two runs should coincide. Considering the thermocouples that were used to measure pool temperatures have an accuracy of $\pm 2^\circ\text{F}$ ($\pm 1^\circ\text{C}$) and the temperature differences between Run 3 and Run 8 are within this tolerance, it is reasonable to state there is not any appreciable difference in thermal

stratification in these two runs. This strongly suggests that thermal stratification is not multicell dependent.

A direct comparison of multicell effects on thermal stratification can be made between the 1- and 2-cell test configurations, because the mass flow transient and the initial pool temperature in the 1-cell and 2-cell are the same. Figures 5-61 and 5-62 show the temperature profiles in the west, center (2-cell), and east (1-cell) for Run 12 with 120°F (49°C) initial pool temperature.

It is evident (see Figures 5-61 and 5-62) there is not any effect of multicell test configuration on the pool thermal stratification.

Table 5-1
CHUGGING INITIATION MASS FLUX AND TIME

<u>Run Number</u>	<u>Cell Configuration</u>	<u>Initial Pool Temperature</u>		<u>Time (sec)</u>	<u>Steam Mass Flux</u>	
		<u>(°F)</u>	<u>(°C)</u>		<u>(lbm/sec-ft²)</u>	<u>(Kg/sec-m²)</u>
1	3					
2	3					
3	3					
4	3					
5	3					
6	3					
7	1 & 2					
8	1 & 2					
9	1 & 2					
10	1 & 2					
11	1 & 2					
12	1 & 2					

*Proprietary information deleted

Table 5-2
 CHUGGING SYNCHRONIZATION BASED ON TOP VENT EXIT PRESSURE
 TEST SERIES 6003

<u>Run Number</u>	<u>Cell Configuration</u>	<u>Initial Pool Temperature (°F) (°C)</u>	<u>Time Difference Between</u>	<u>Average Time Difference (sec)</u>	<u>Standard Deviation Time Difference (sec)</u>
7, 8, 9	2				
1, 2, 3	3				
1, 2, 3	3				
1, 2, 3	3				
10,11,12	2				
4, 5, 6	3				
4, 5, 6	3				
4, 5, 6	3				

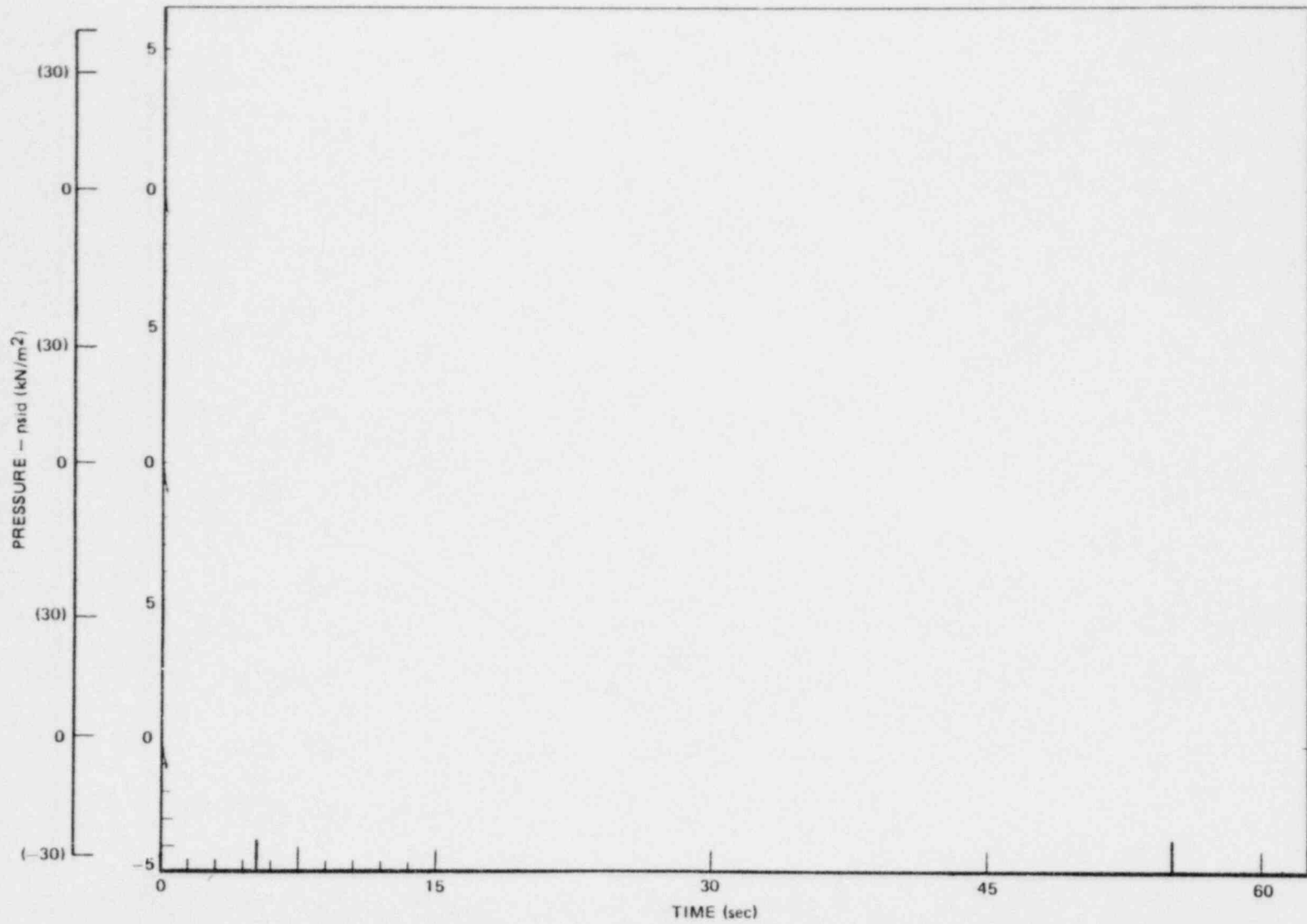
*Proprietary information deleted

Table 5-3
 CHUGGING PERIOD BASED ON TOP VENT EXIT PRESSURE
 TEST SERIES 6003

<u>Run Number</u>	<u>Cell Configuration</u>	<u>Initial Pool Temperature</u> (°F) (°C)		<u>Average Period</u> (sec)	<u>S. Dev. Period</u> (sec)
7, 8, 9	1				
7, 8, 9	2				
1, 2, 3	3				
10,11,12	1				
10,11,12	2				
4, 5, 6	3				

*Proprietary information deleted

5-27



NEDO-24720

Figure 5-1. Drywell Wall, 12.3 ft (3.8 m), Pressure Time Histories, Run 1

*Proprietary information deleted

*

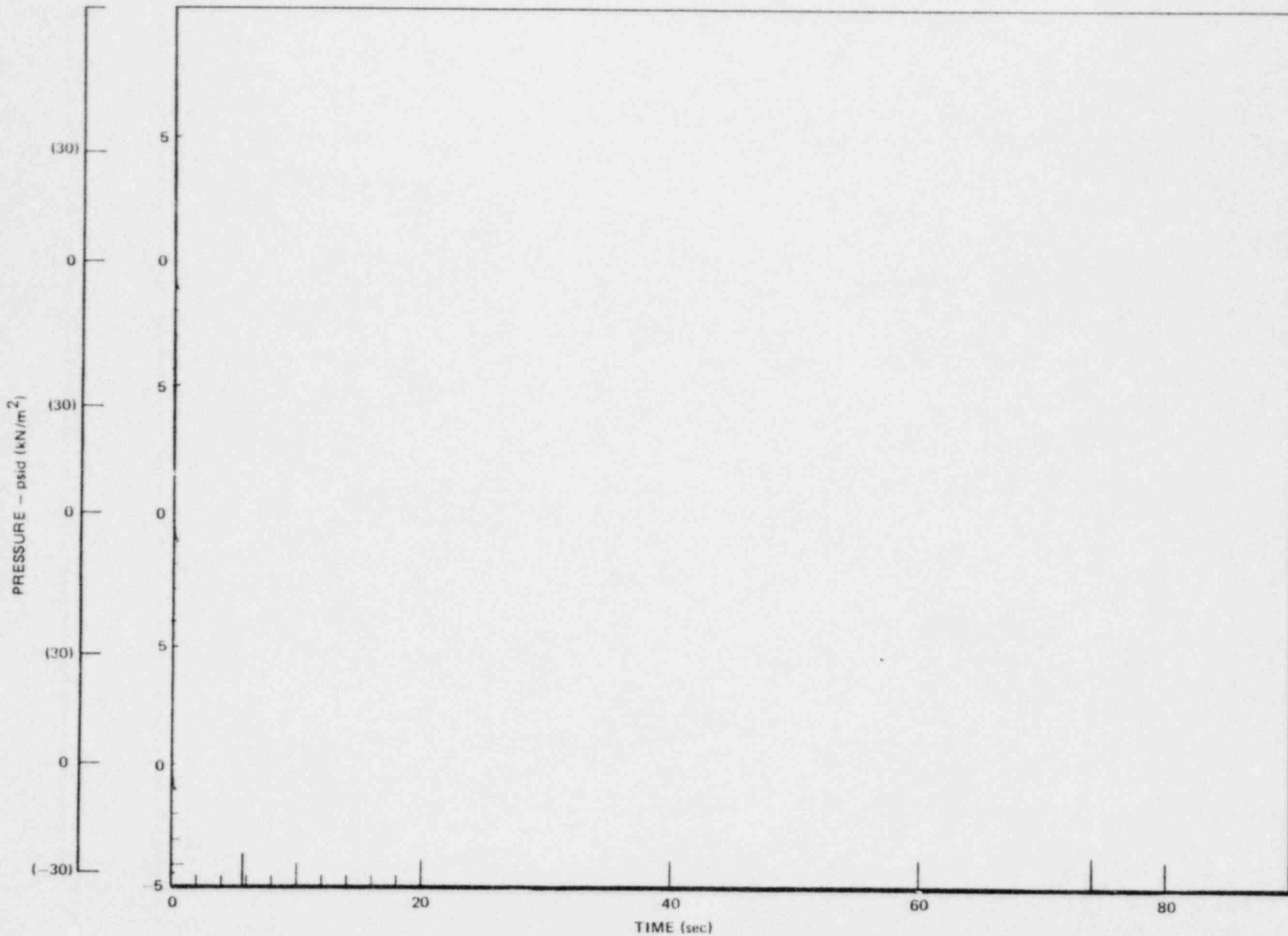


Figure 5-2. Drywell Wall, 12.3 ft (3.8 m), Pressure Time Histories, Run 6

*Proprietary information deleted

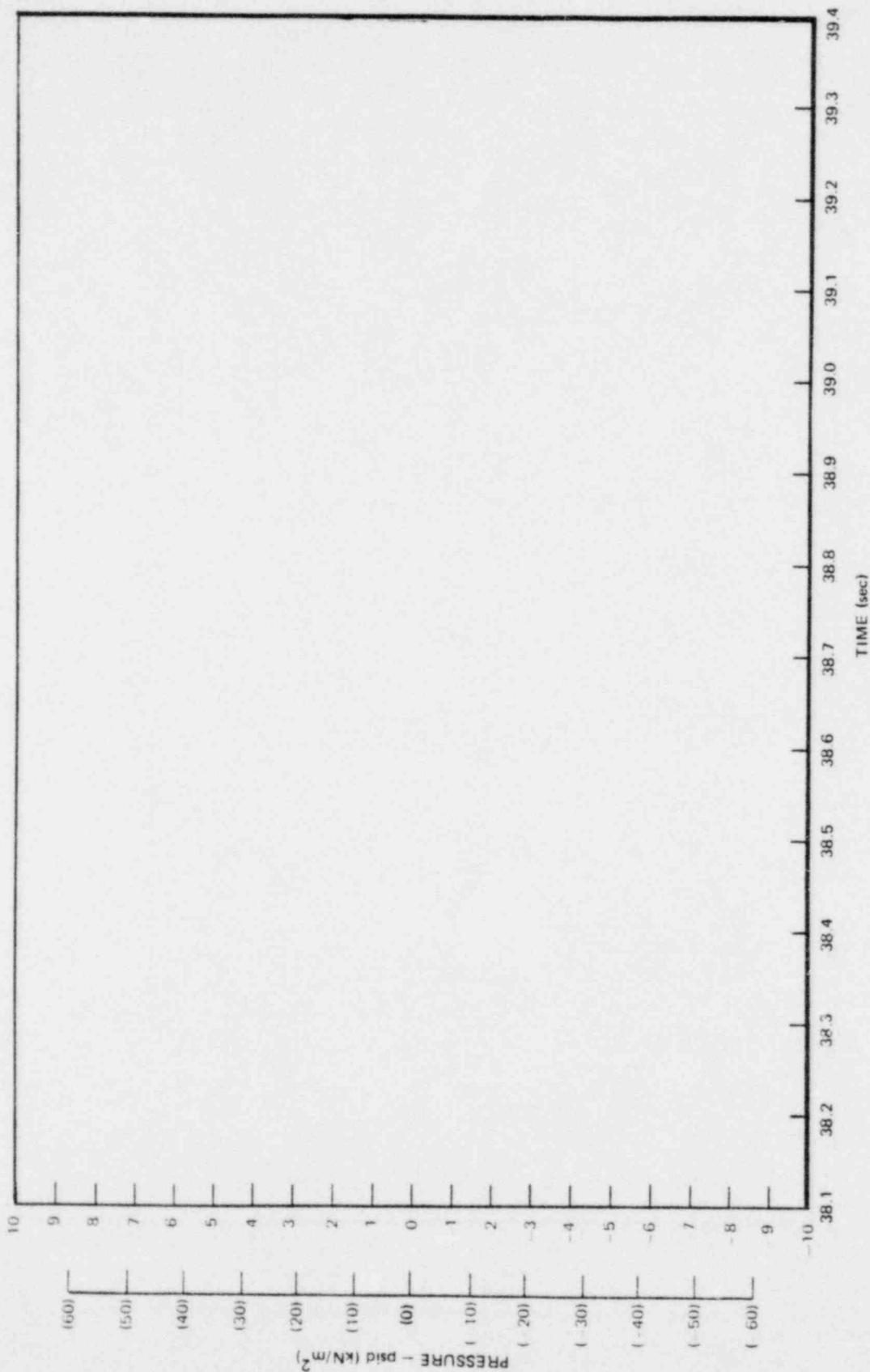


Figure 5-3. Drywell Wall, West Cell, 12.3 ft (3.8 m), Pressure Short-Term (1.3 sec)
Time History, Run 6

*Proprietary information deleted

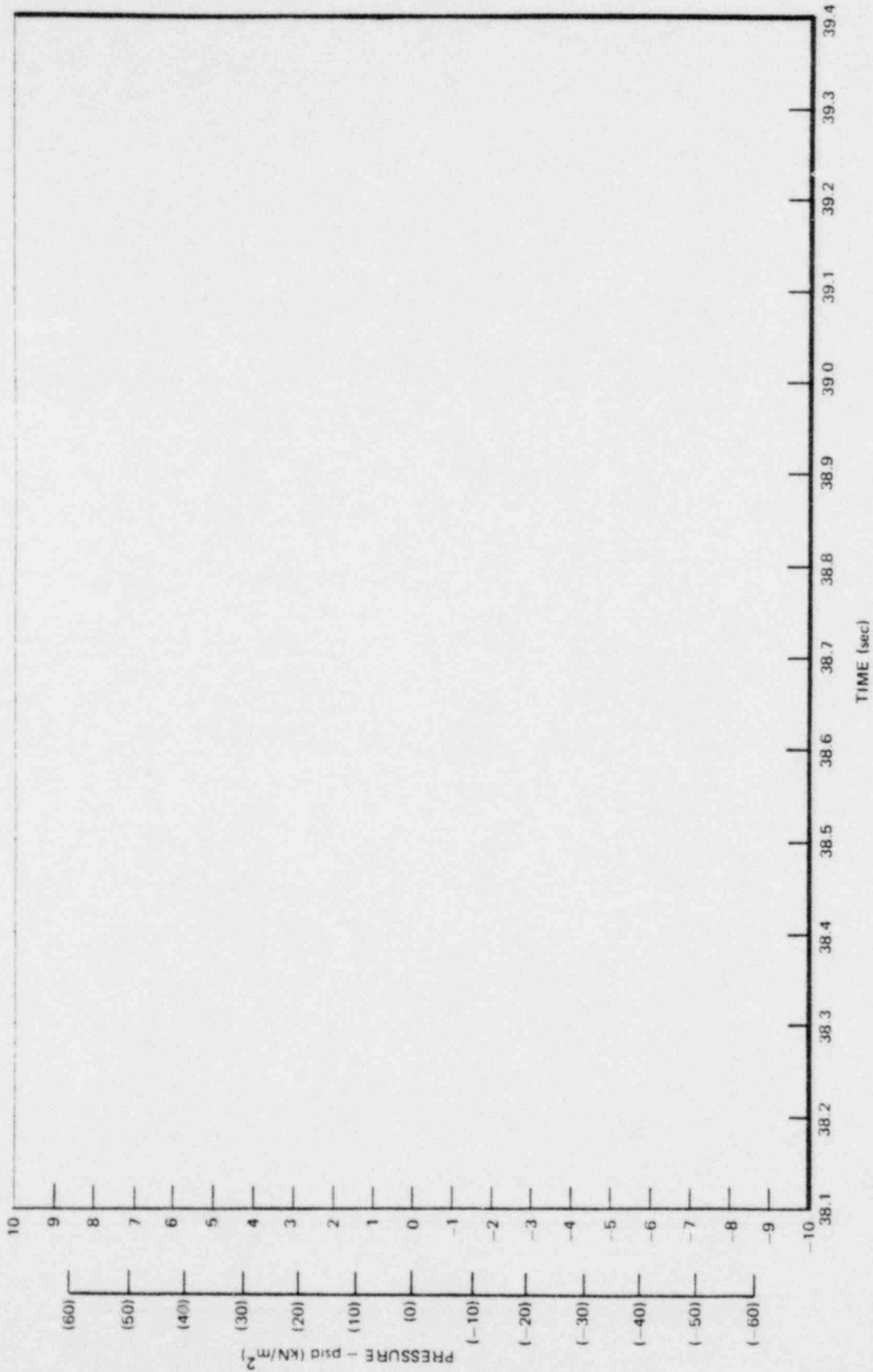


Figure 5-4. Drywell Wall, West Cell, 13 ft (4 m), Pressure Short-Term (1.3 sec) Time History, Run 6

*Proprietary information deleted

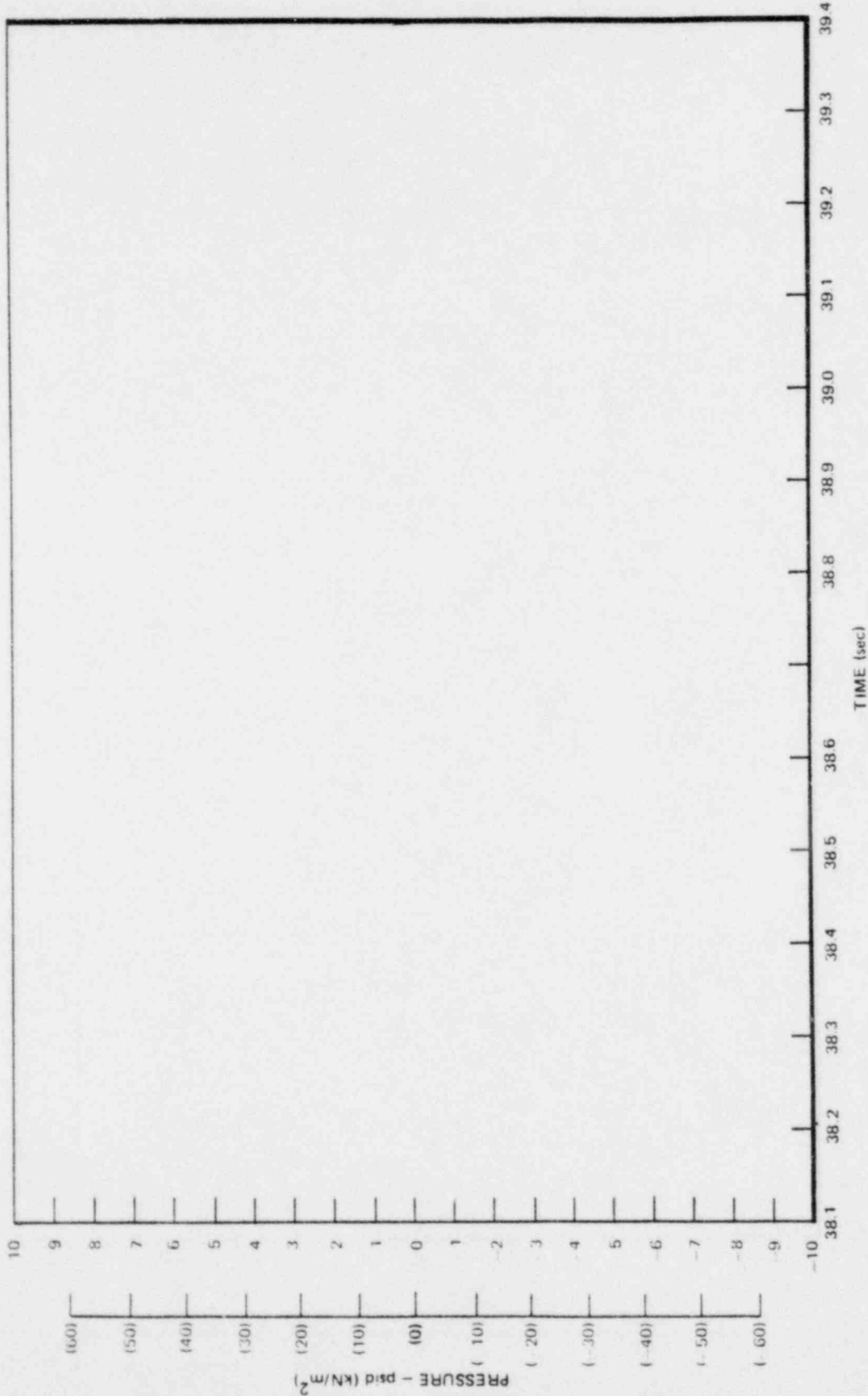


Figure 5-5. Drywell Wall, West Cell, 15.7 ft (4.8 m), Pressure Short-Term (1.3 sec) Time History, Run 6

*Proprietary information deleted

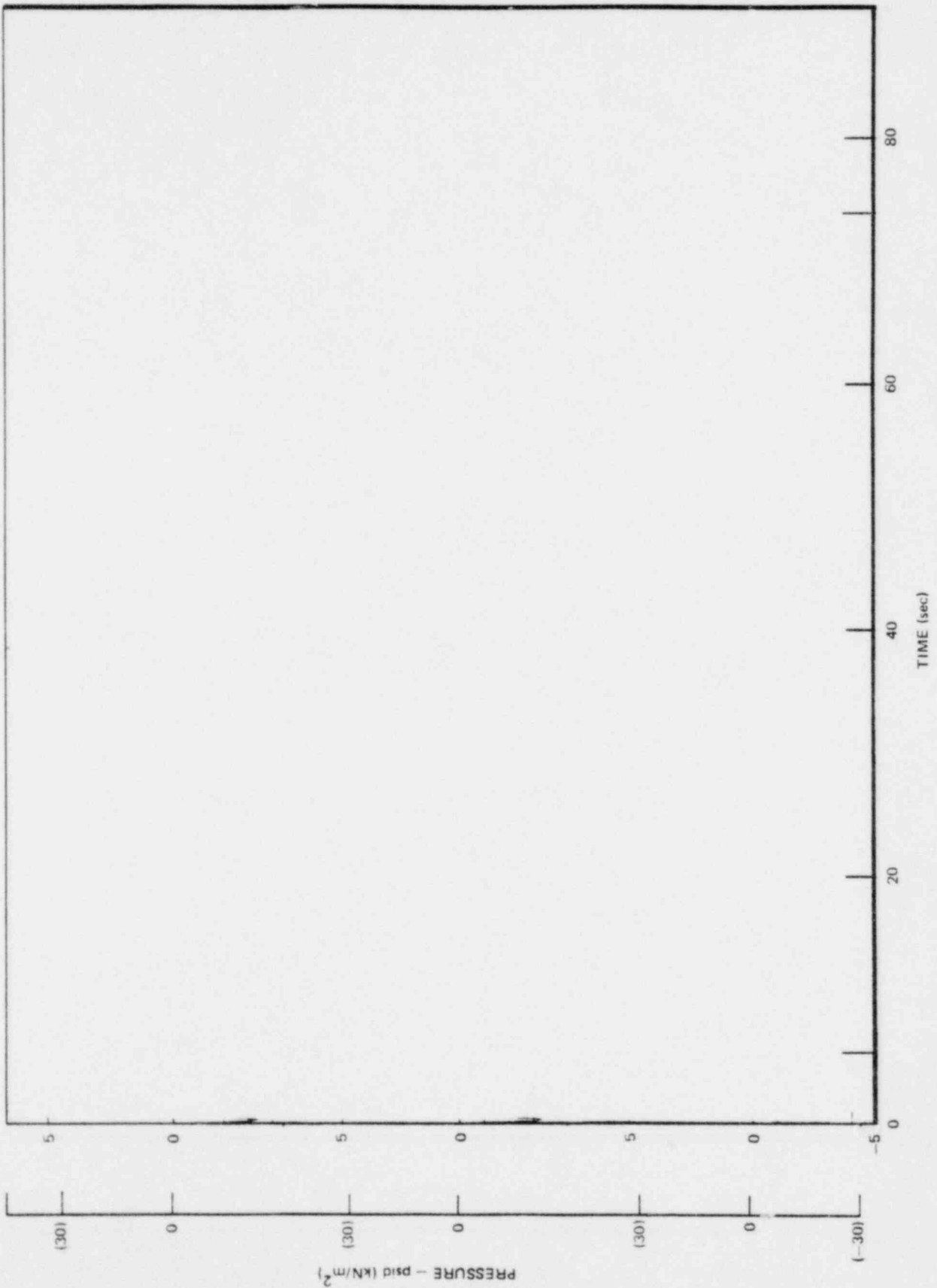
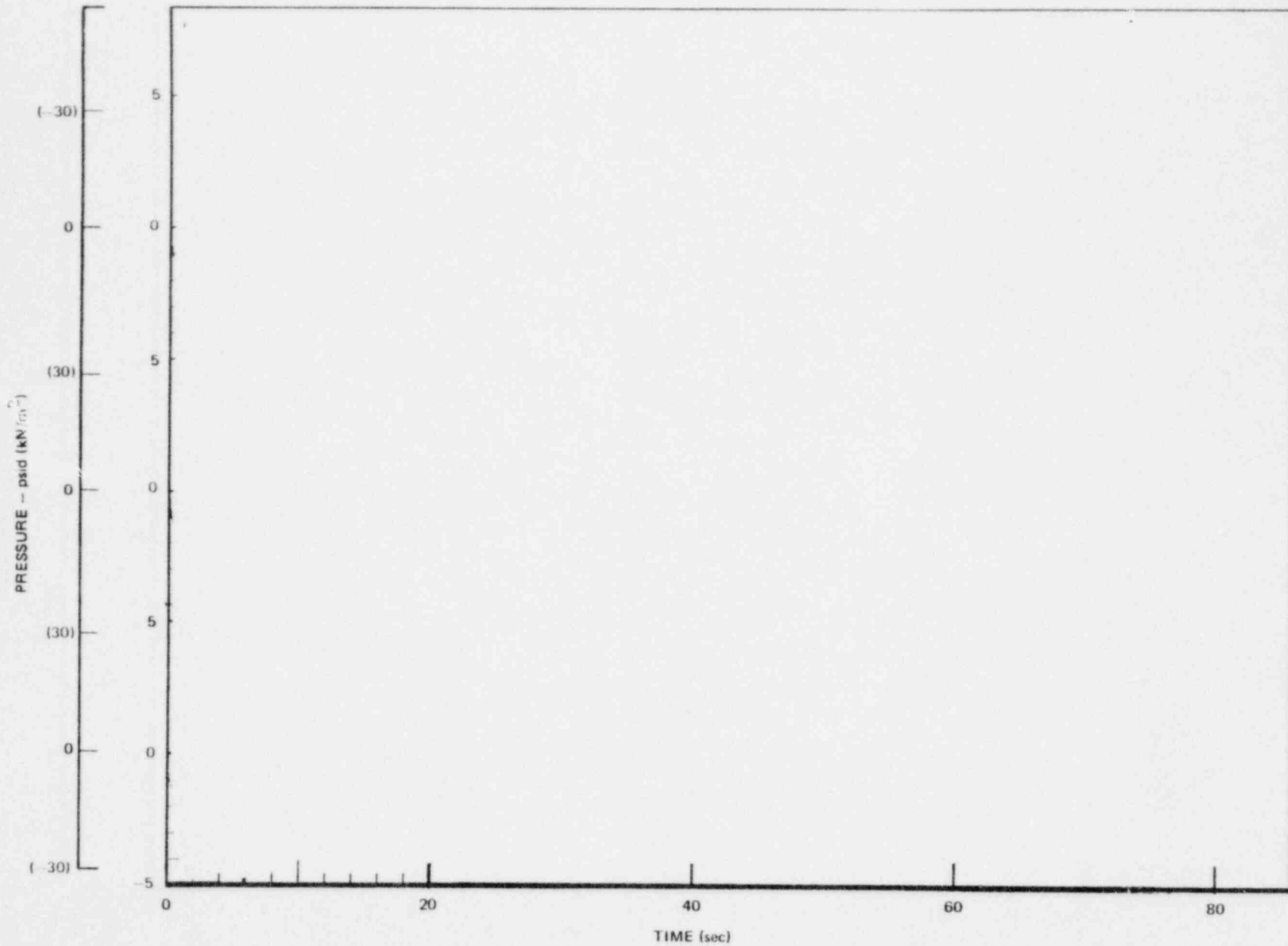


Figure 5-6. South Weir Wall, 11 ft (3.4 m), Pressure Time Histories, Run 6

*Proprietary information deleted

5-33



NEDO-24720

Figure 5-7. Containment Wall, 11 ft (3.4 m), Pressure Time Histories, Run 6

*Proprietary information deleted

*

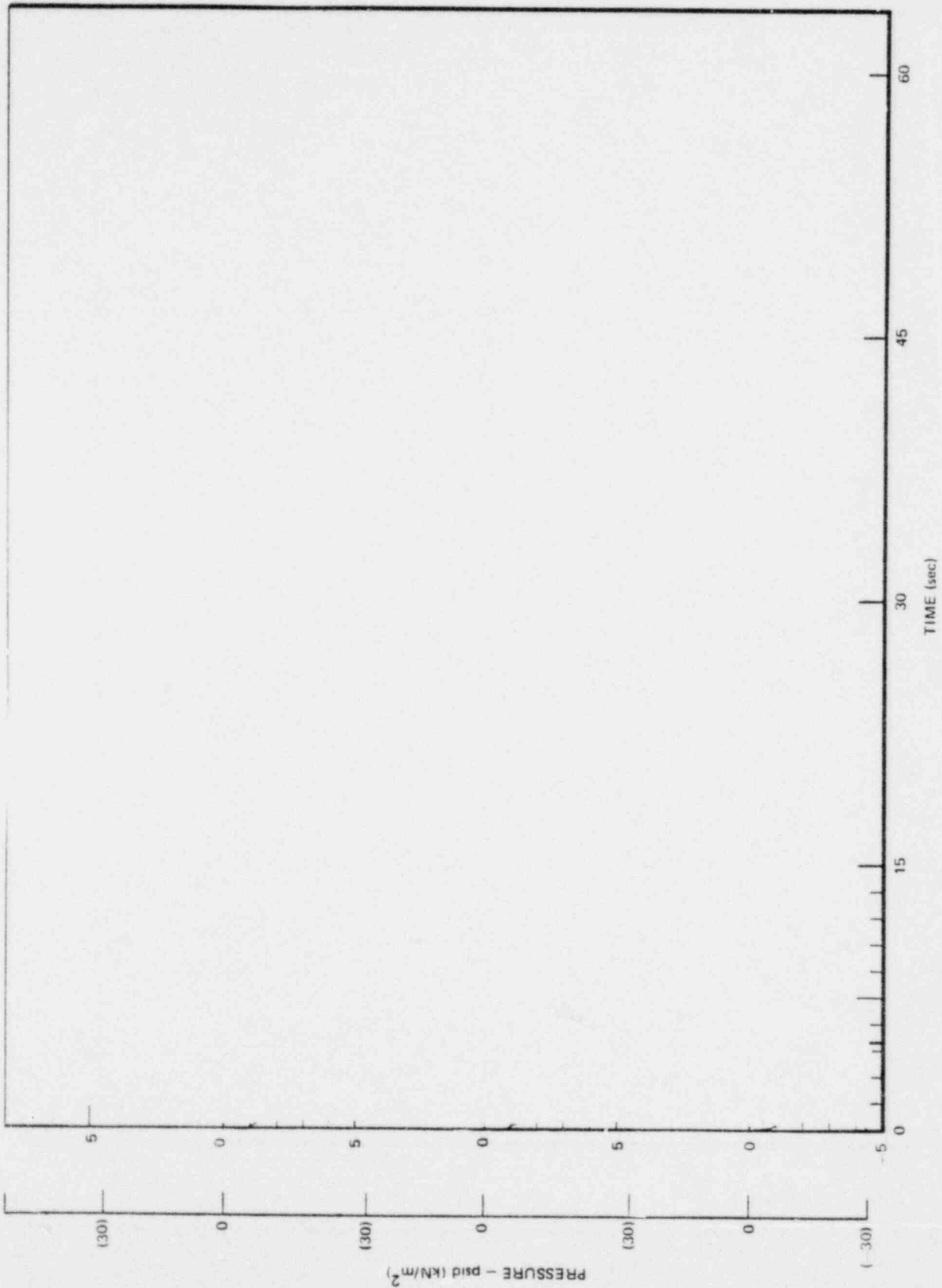


Figure 5-8. Drywell Wall, 15.7 ft (4.8 m), Pressure Time Histories, Run 8

*Proprietary information deleted

*

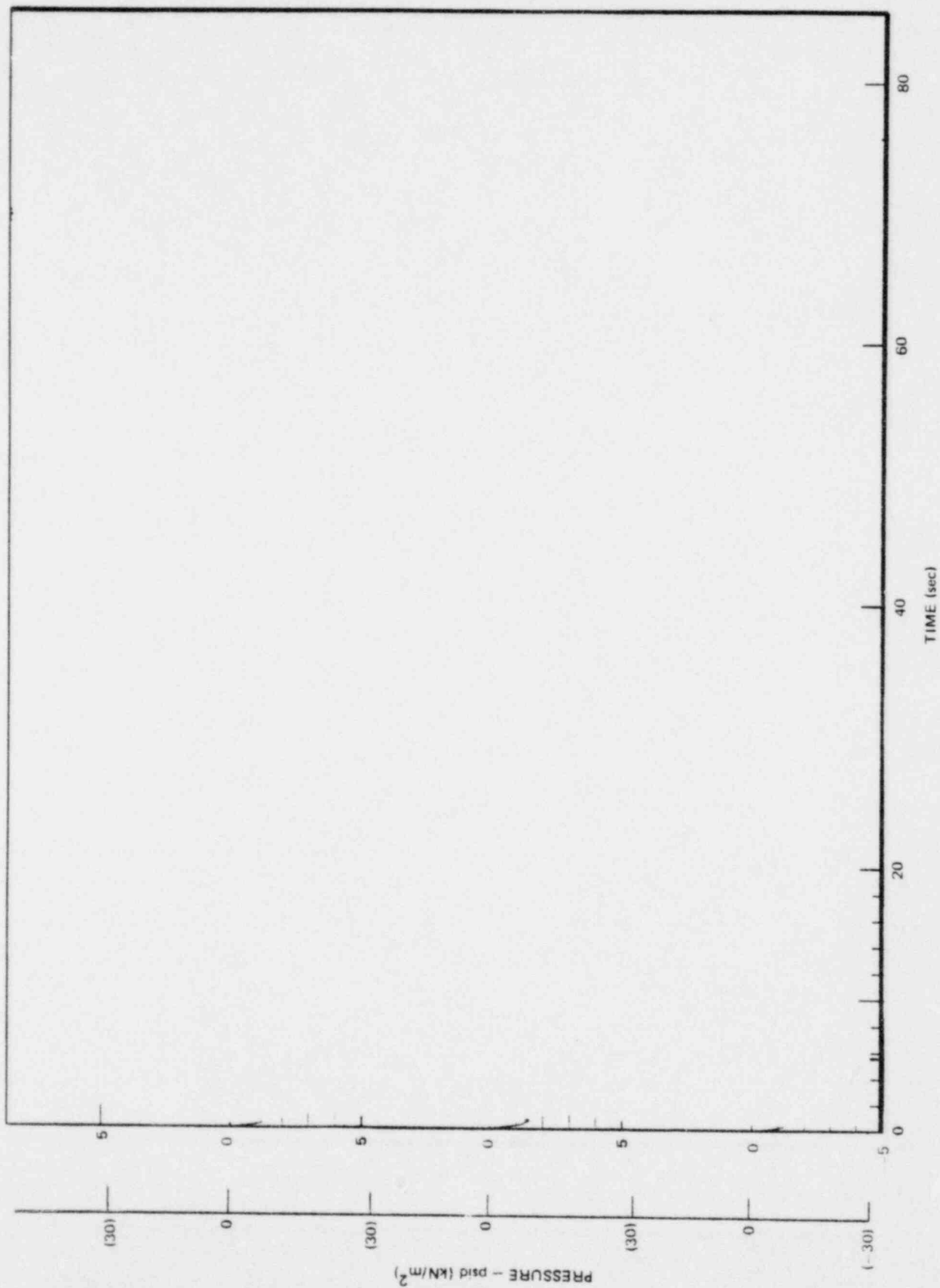
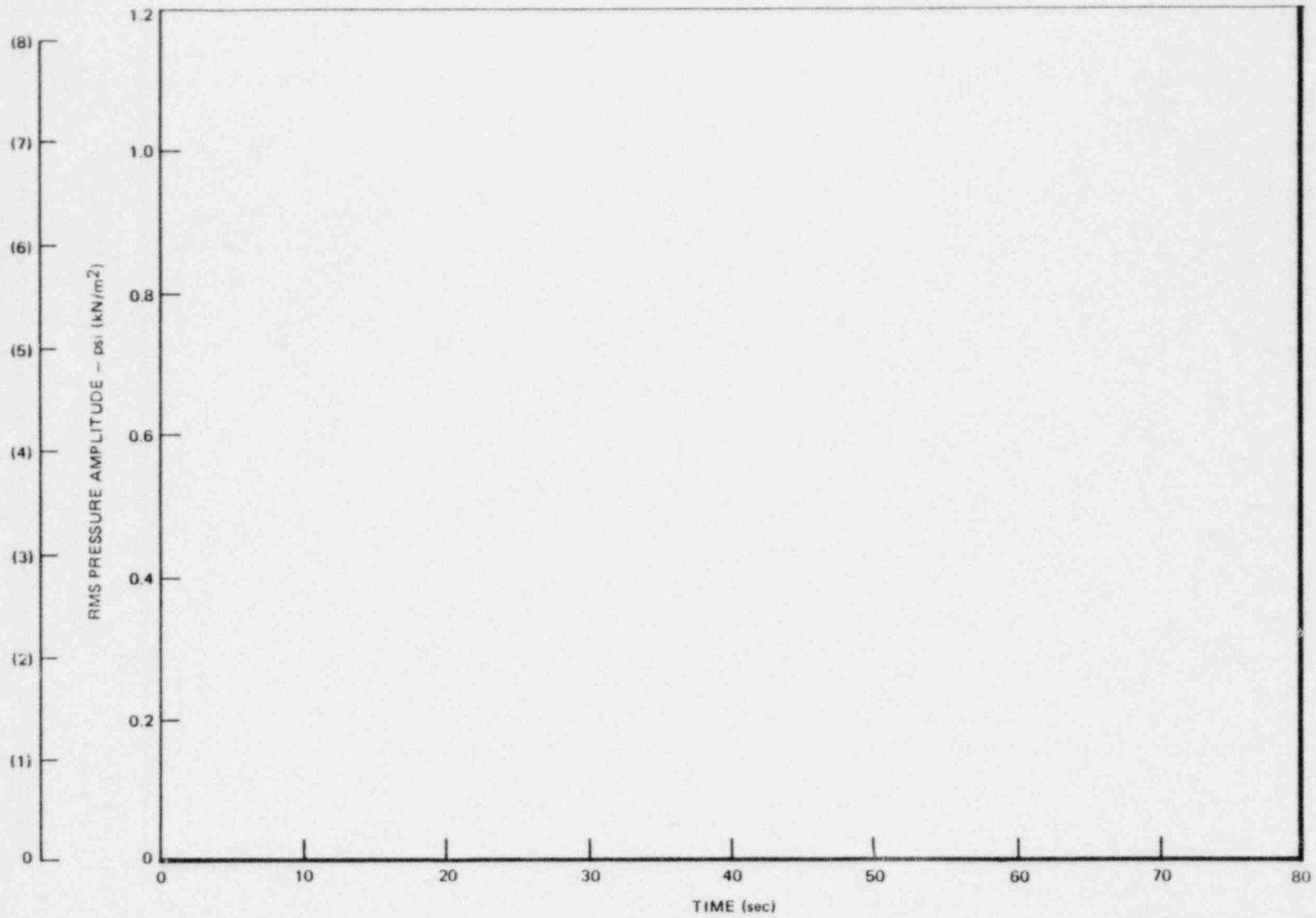


Figure 5-9. Drywell Wall, 15.7 ft (4.8 m), Pressure Time Histories, Run 11

*Proprietary information deleted

5-36



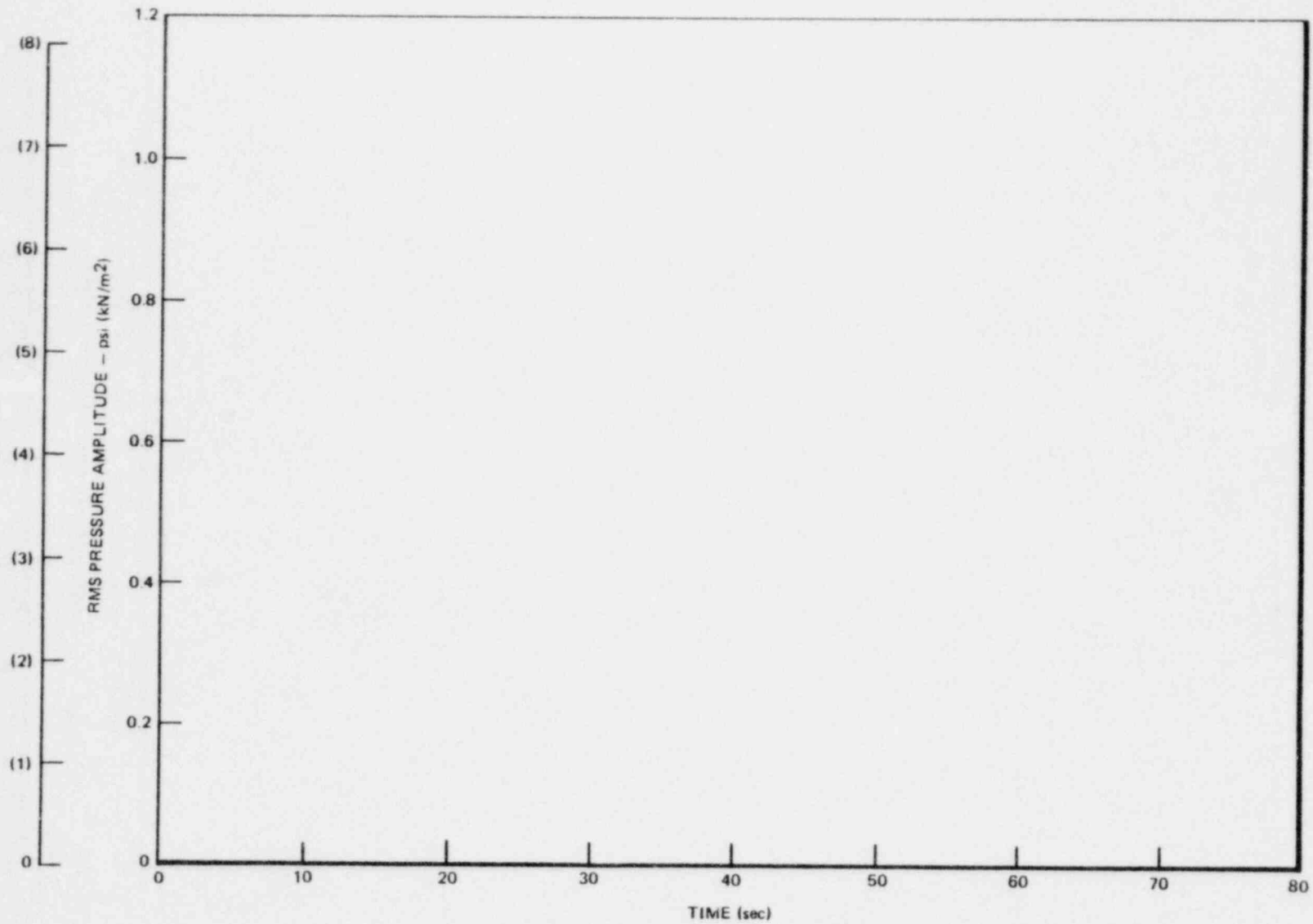
NEDO-24720

Figure 5-10. Drywell Wall, 15.7 ft (4.8 m), Center Cell, Pressure Magnitude Repeatability, Runs 4, 5 and 6

*Proprietary information deleted

*

5-37



NEDO-24720

Figure 5-11. Drywell Wall, 15.7 ft (4.8 m), East Cell, Pressure Magnitude Repeatability, Runs 10, 11 and 12

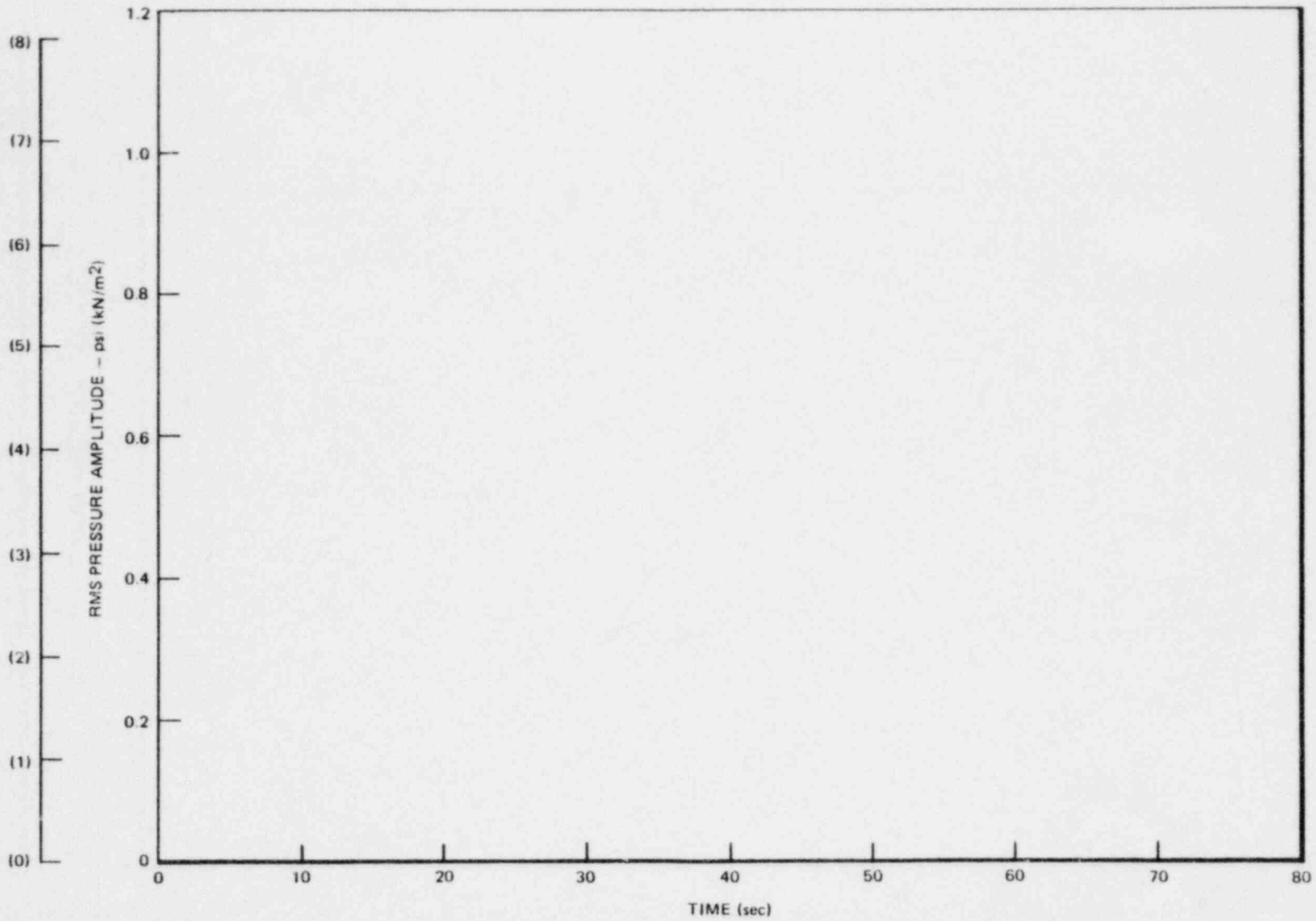


Figure 5-12. Drywell Wall, 15.7 ft (4.8 m), Center Cell, Pressure Magnitude Repeatability, Runs 10, 11 and 12

*Proprietary information deleted

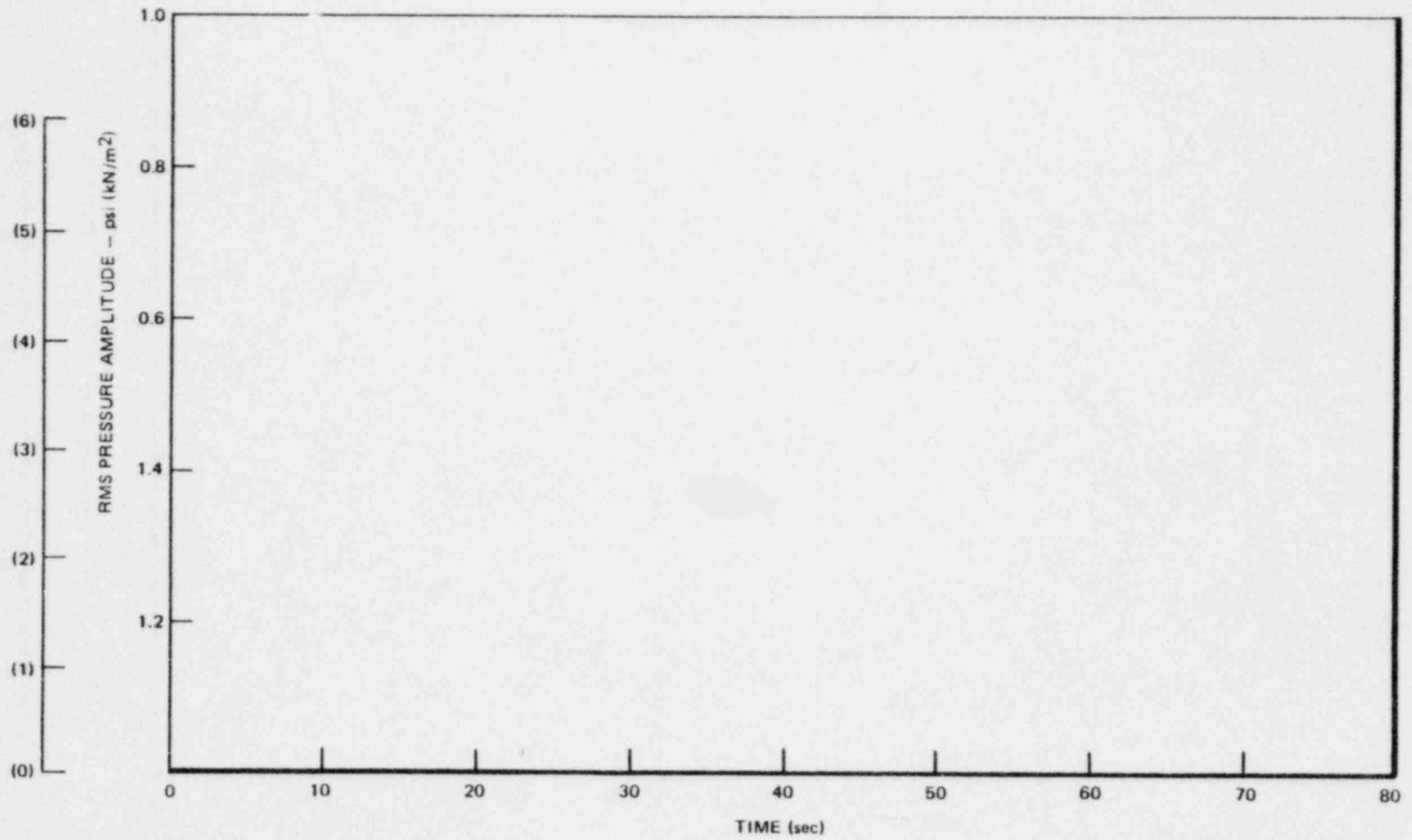
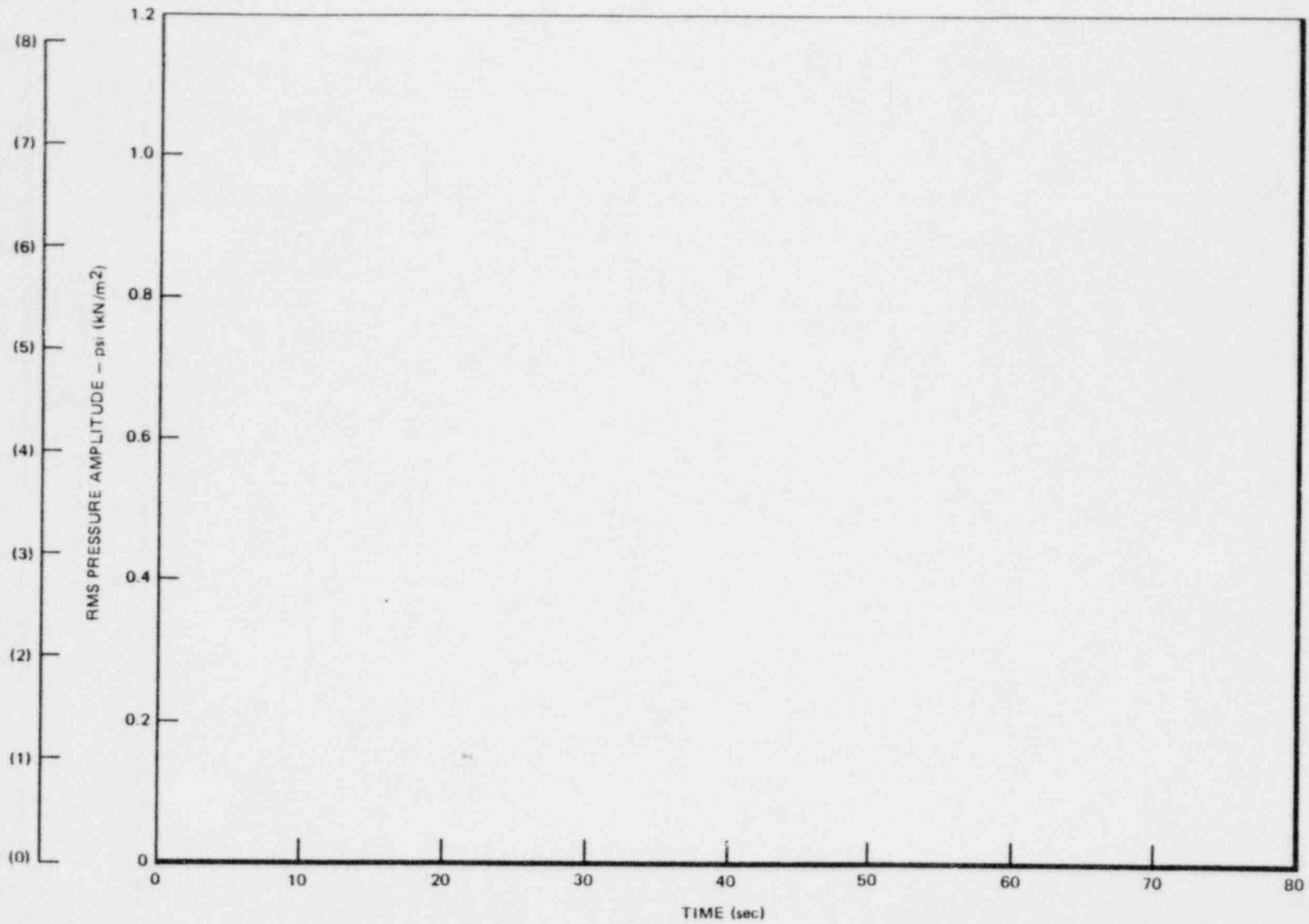


Figure 5-13. Weir Wall, 11 ft (3.35 m), East Cell, Pressure Magnitude Repeatability, Runs 10, 11 and 12

*Proprietary information deleted

5-40



NEDO-24720

Figure 5-14. Containment Wall, 2 ft (0.6 m), East Cell, Pressure Magnitude Repeatability, Runs 10, 11 and 12

*Proprietary information deleted

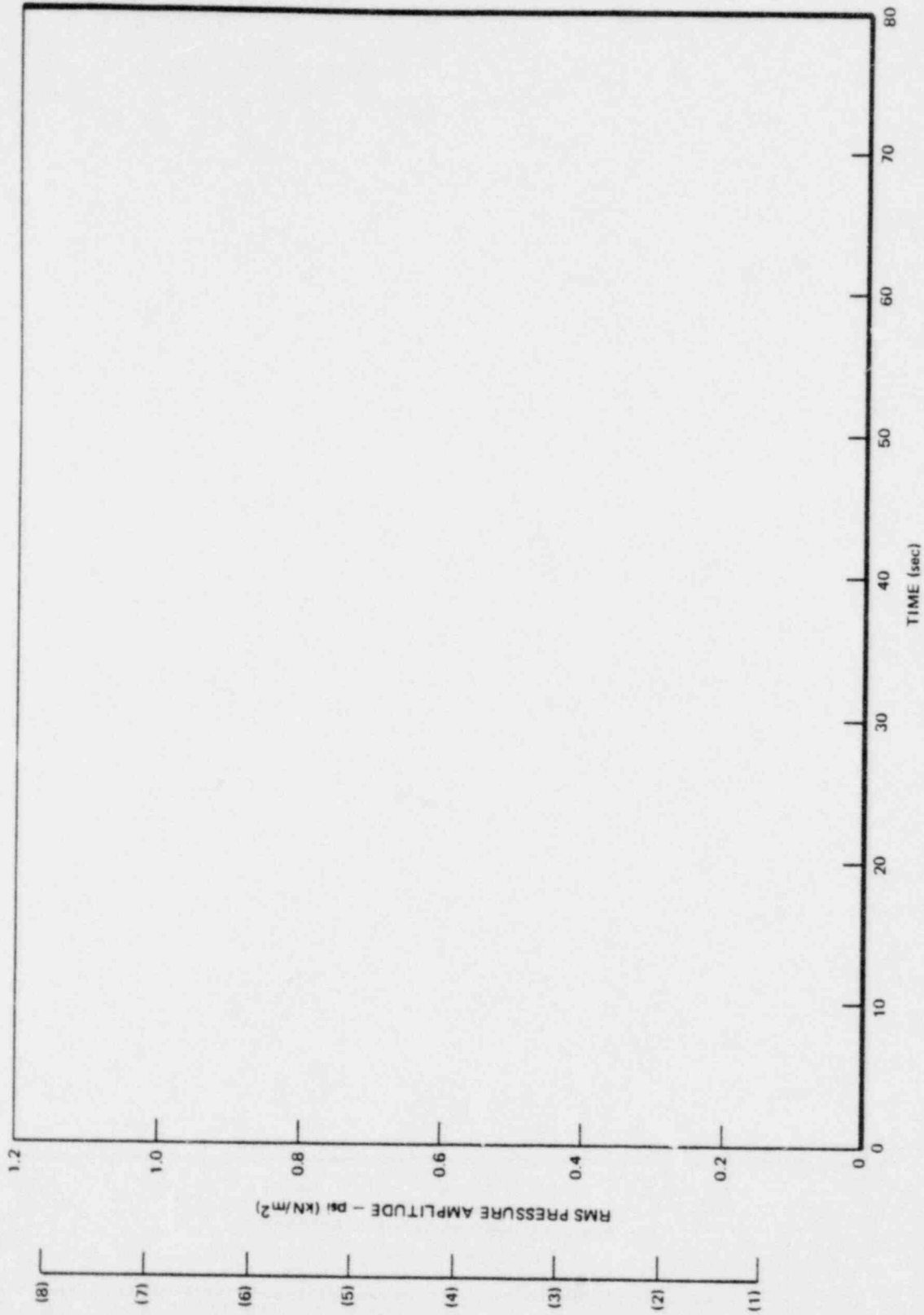


Figure 5-15. Drywell Wall, 15.7 ft (4.8 m), Pressure Magnitude in RMS versus Time, Run 6

*Proprietary information deleted

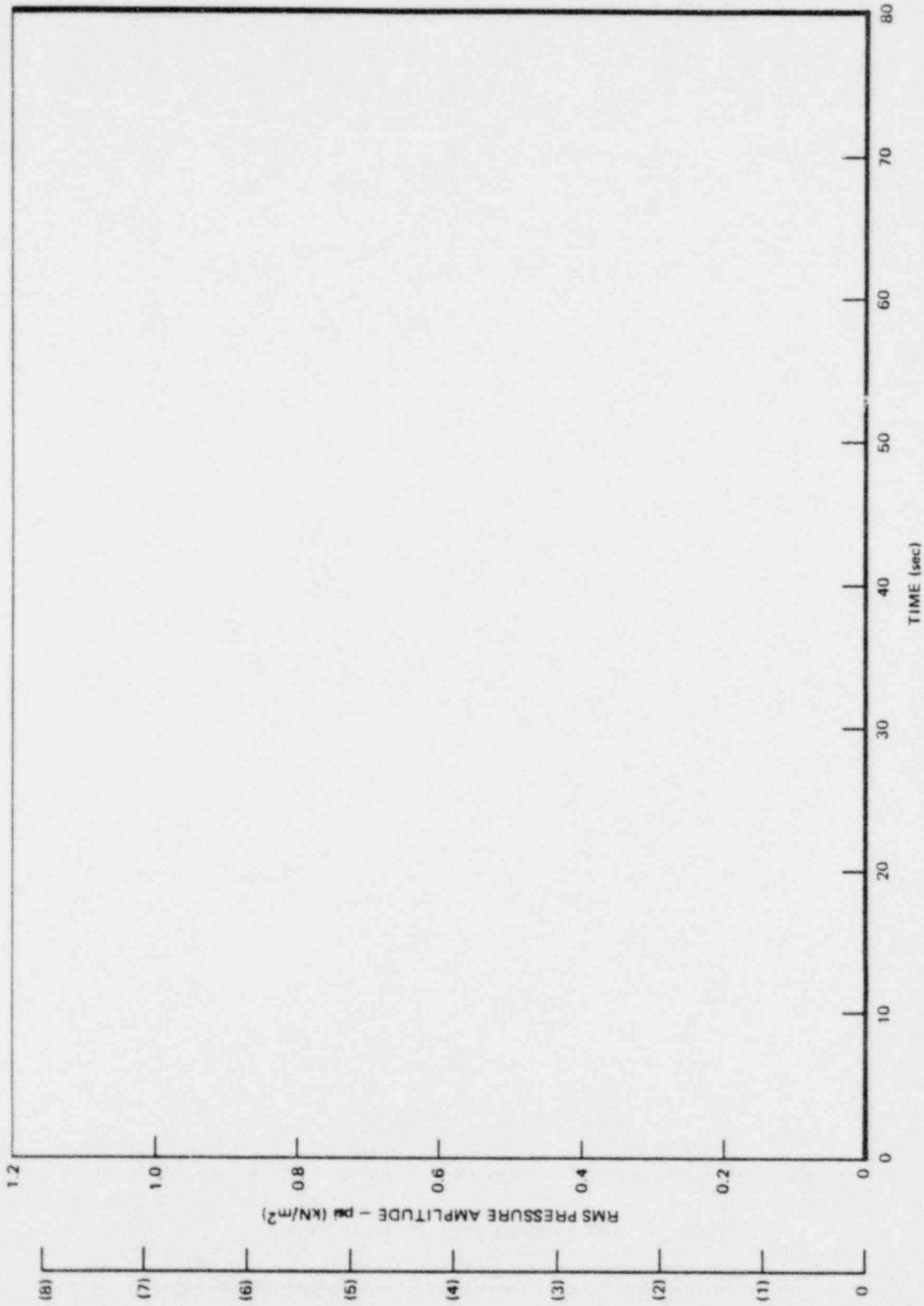
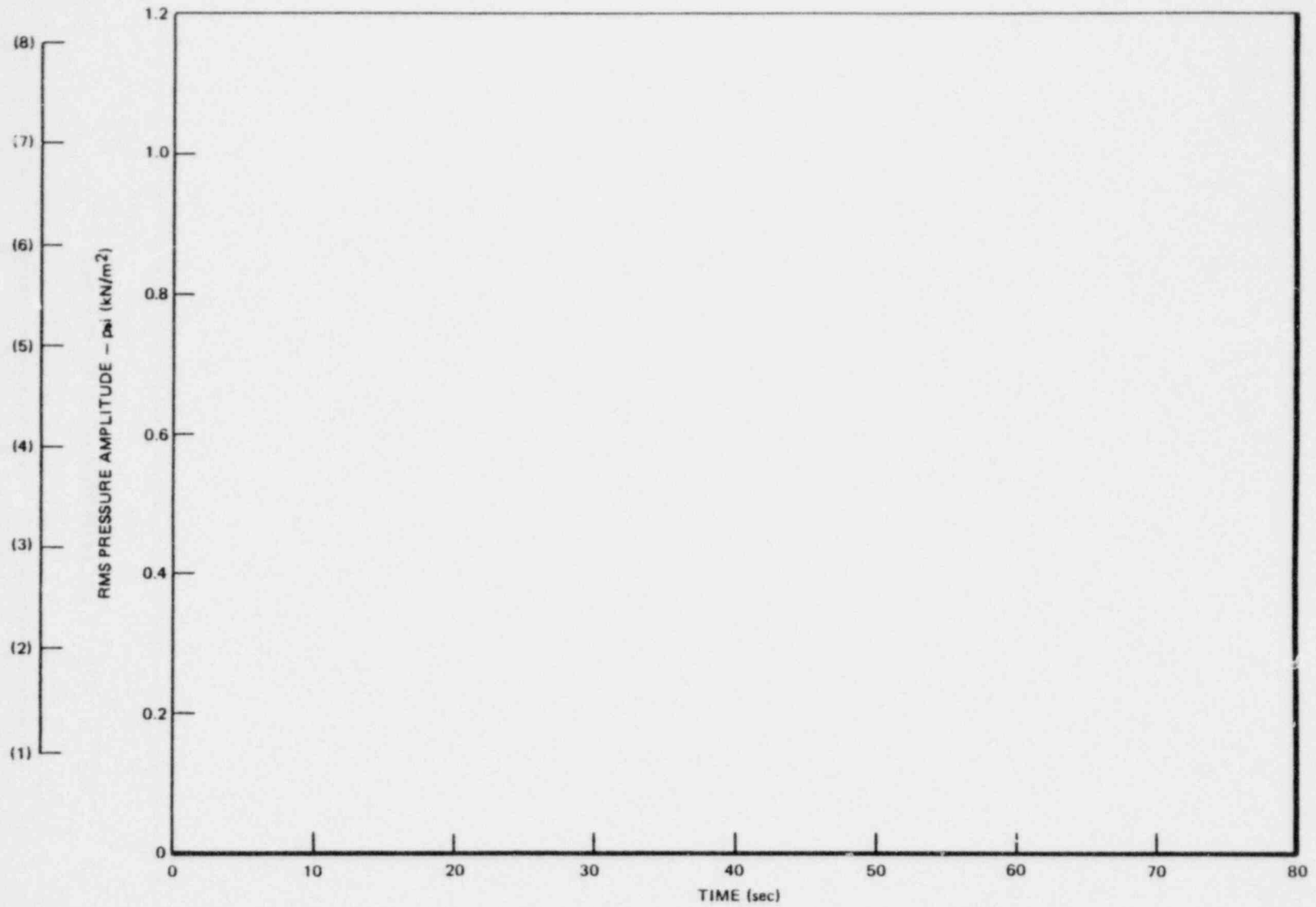


Figure 5-16. Containment Wall, 2 ft (0.6 m), Pressure Magnitude in RMS versus Time, Run 6

*Proprietary information deleted

*

5-43



NEDO-24720

Figure 5-17. Drywell Wall, 15.7 ft (4.8 m), Pressure Magnitude in RMS versus Time, Run 11

*Proprietary information deleted

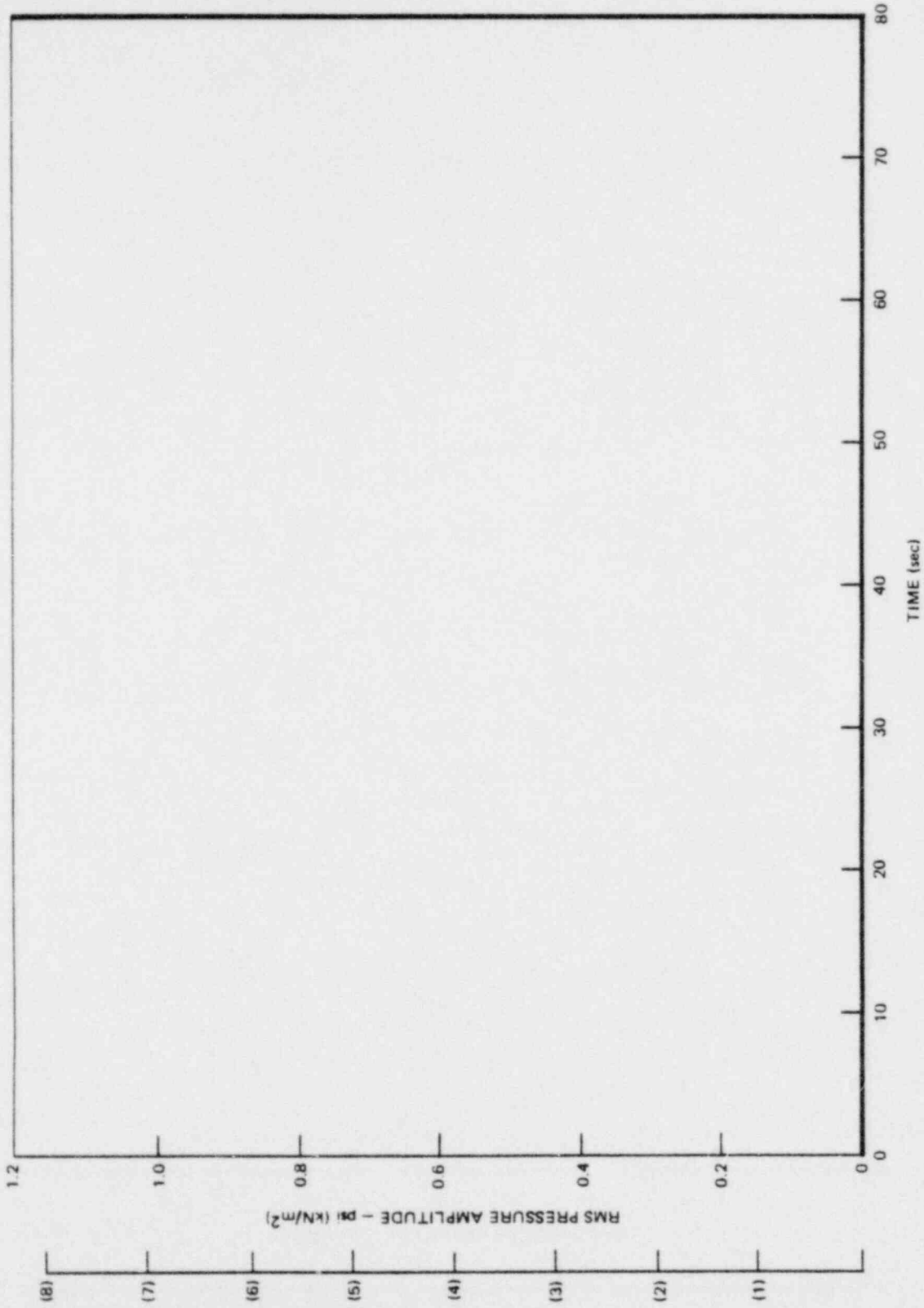
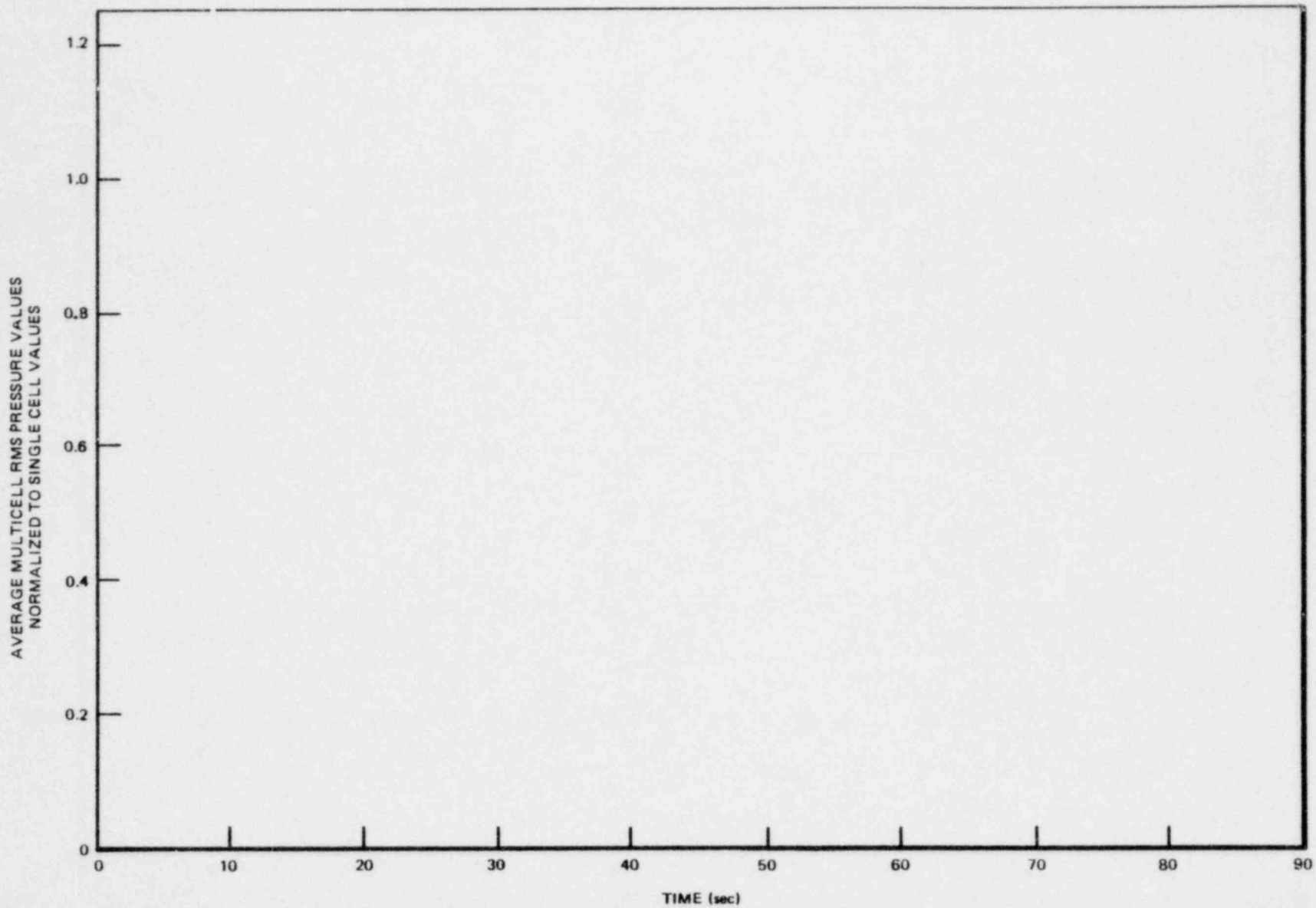


Figure 5-18. Containment Wall, 2 ft (0.6 m), Pressure Magnitude in RMS versus Time, Run 11

*Proprietary information deleted

5-45



NEDO-24720

Figure 5-19. Drywell Wall, 15.7 ft (4.8 m), Multicell Average Pressure Magnitudes in RMS versus Time Normalized to Single Cell Values for 120⁰F (49⁰C) Initial Pool Temperature Tests

*Proprietary information deleted

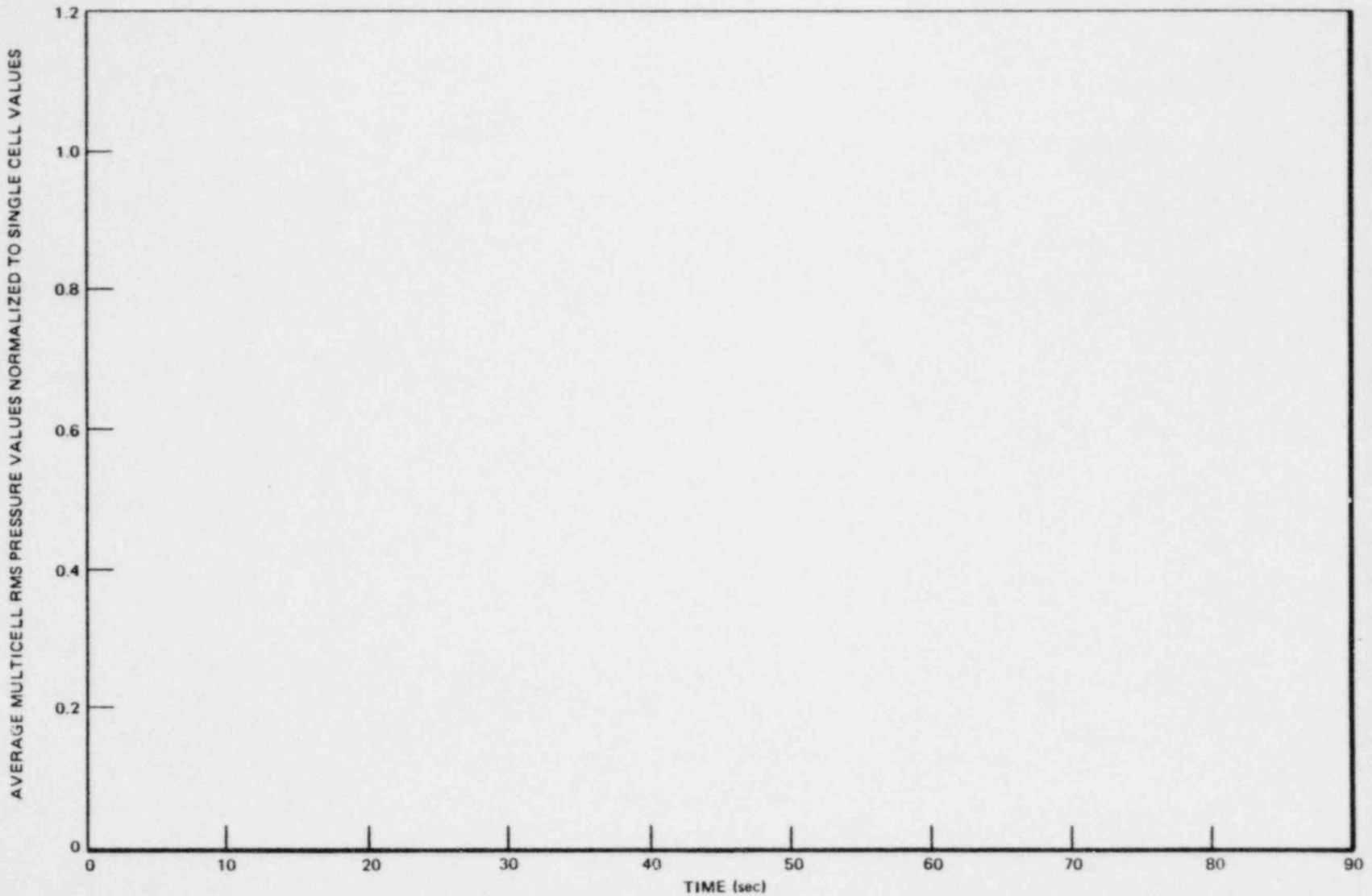
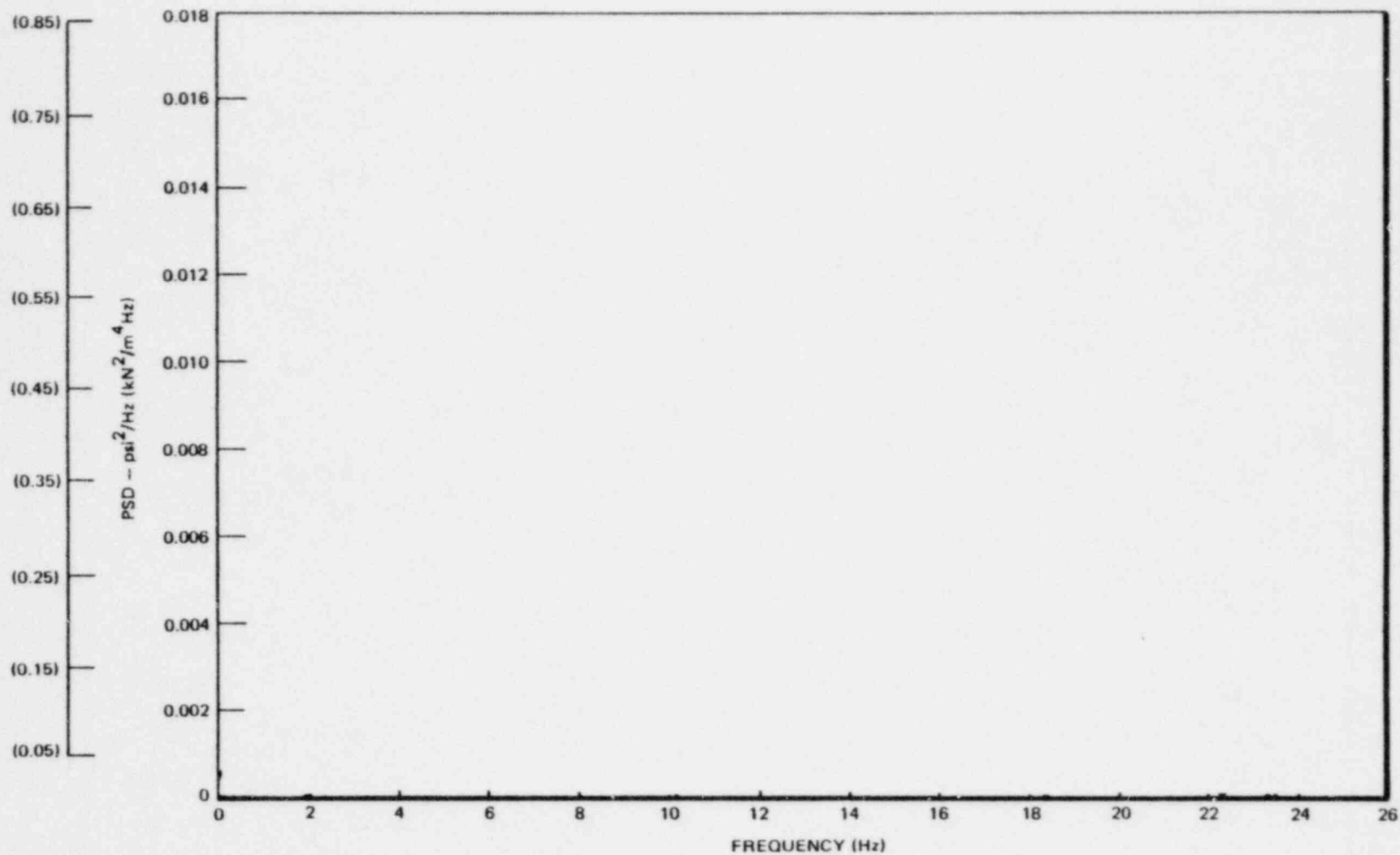


Figure 5-20. Containment Wall, 2 ft (0.6 m), Multicell Average Pressure Magnitudes in RMS versus Time Normalized to Single Cell Values for 120°F (49°C) Initial Pool Temperature Tests

5-47

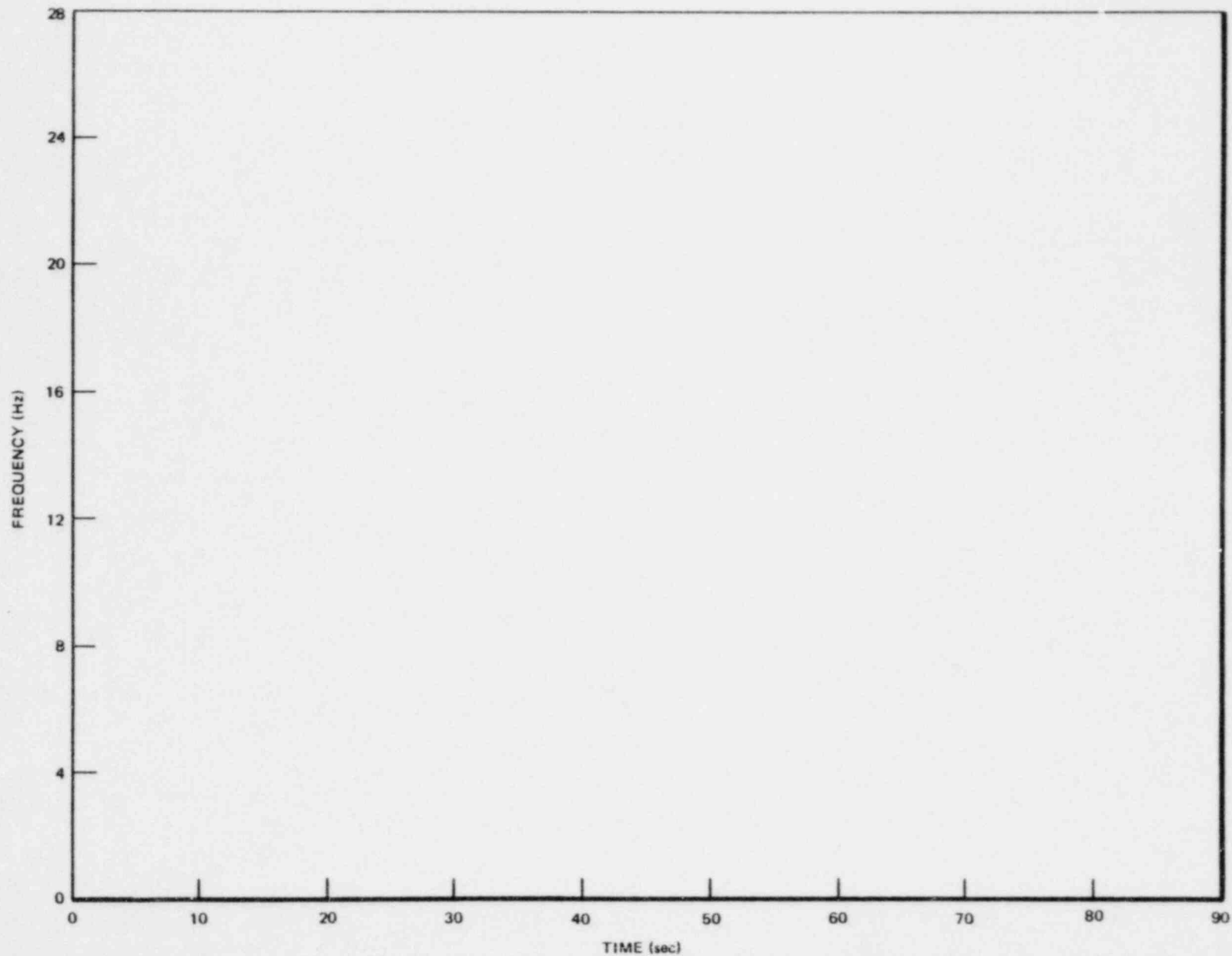


NEDO-24720

Figure 5-21. PSD Plot of Drywell Wall, 15.7 ft (4.8 m), Center Cell Pressure Signal 11.85 ~ 14.42 sec, Run 6

*Proprietary information deleted

5-48



NEDO-24720

Figure 5-22. Drywell Wall, 15.7 ft (4.8 m), East Cell, Dominant Frequencies versus Time for Pressure Data, Runs 10, 11 and 12

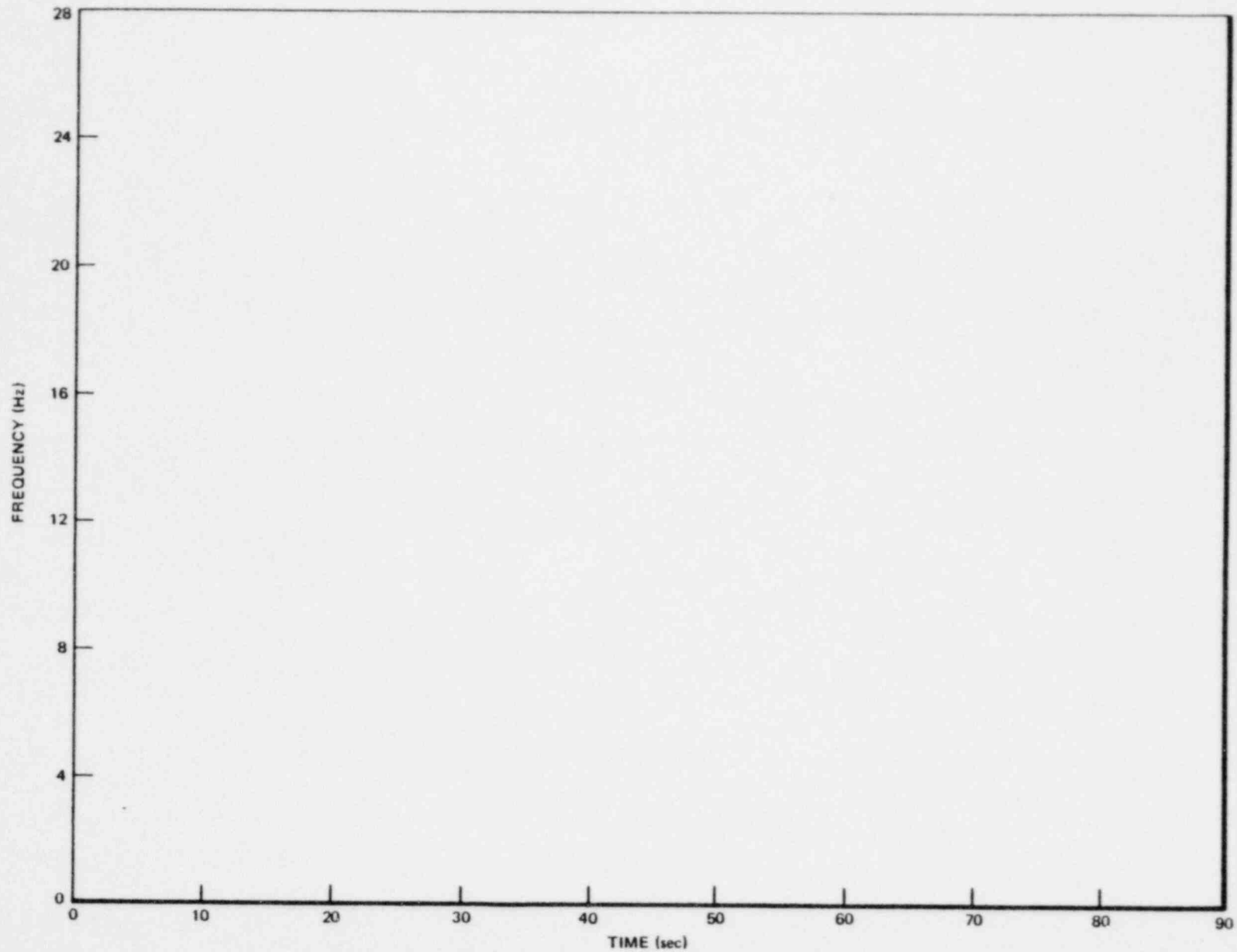


Figure 5-23. Drywell Wall, 15.7 ft (4.8 m), Dominant Frequencies versus Time of Pressure Data for One, Two and Three Cell Tests

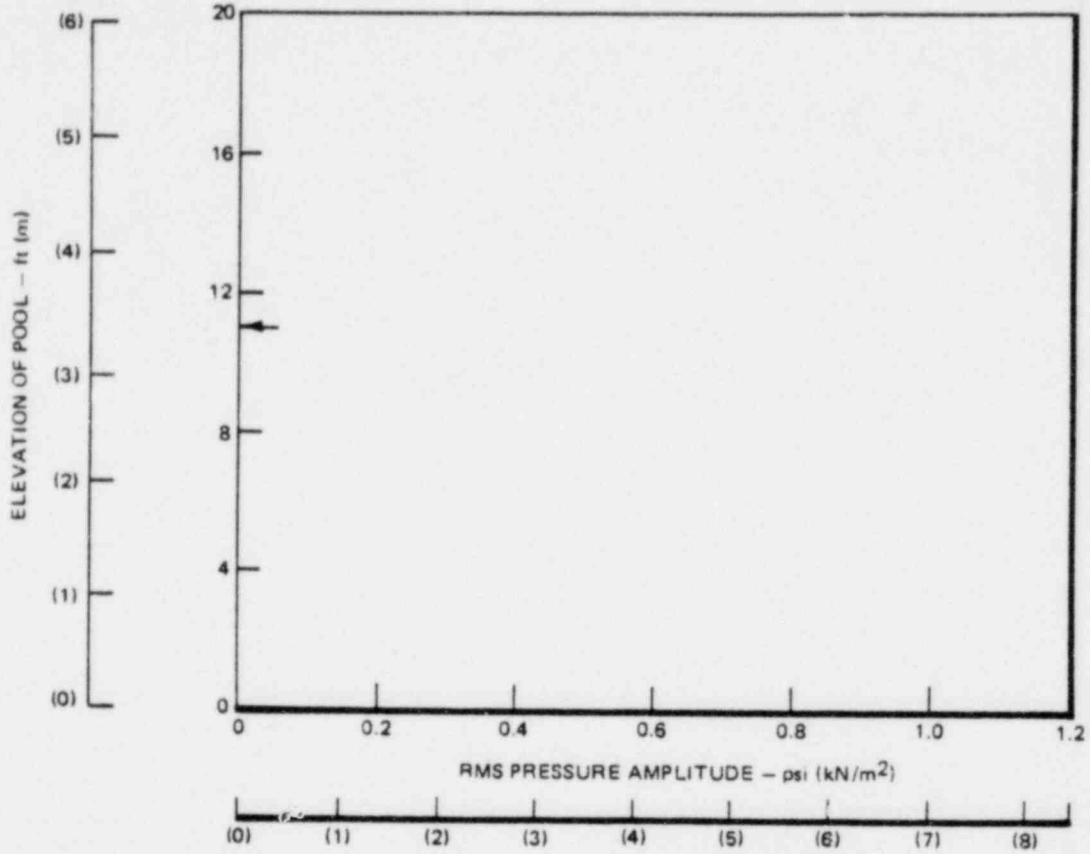
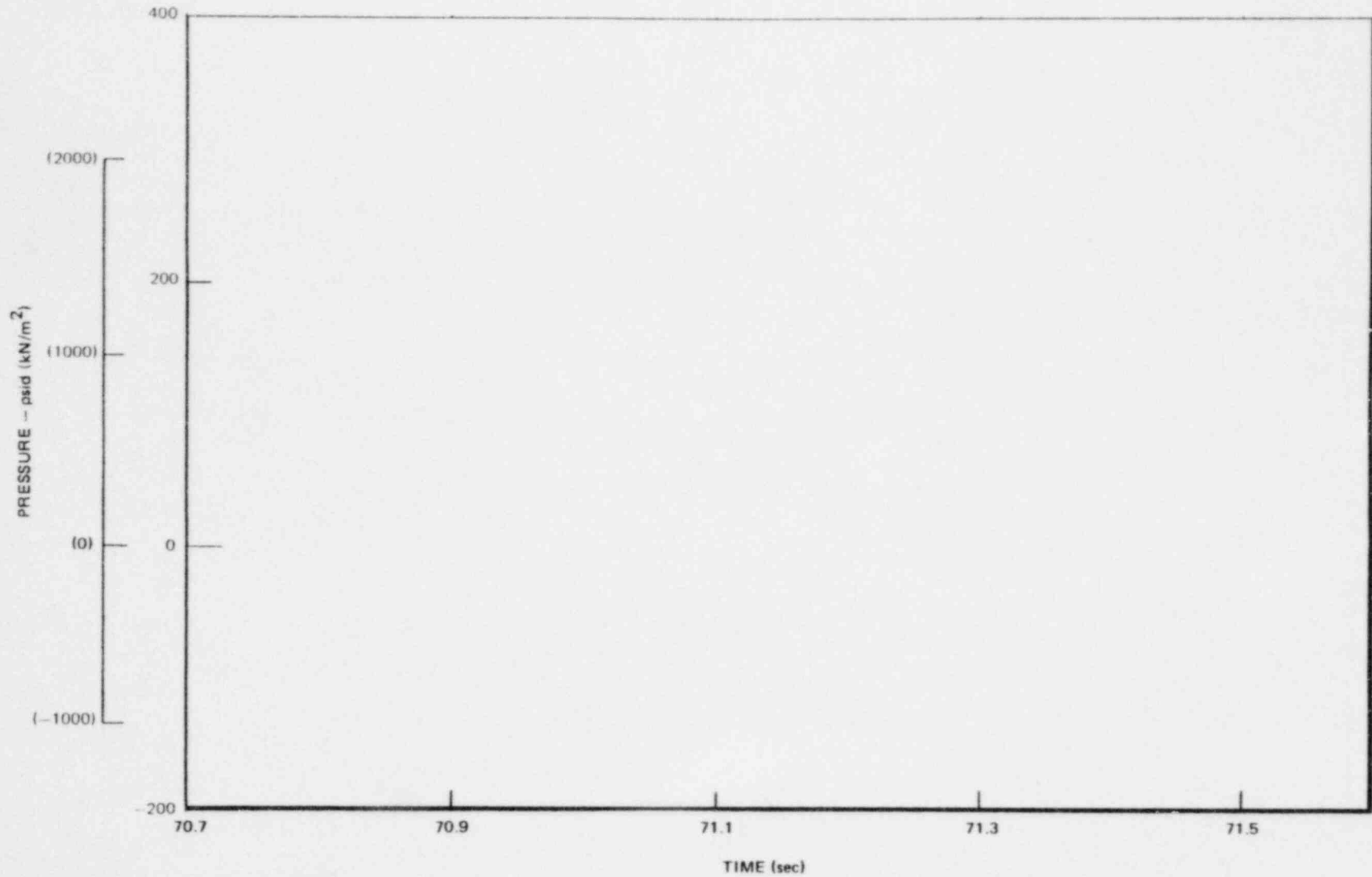


Figure 5-24. Containment Wall, West Cell, Pressure Amplitude Axial Distribution in Suppression Pool for Different Times, Run 11, 120°F (49°C) Initial Pool Temperature

*Proprietary information deleted

5-51



NEDO-24720

Figure 5-25. One-Cell Top Vent Chugging Pressure Time History, Run 8

*Proprietary information deleted

*

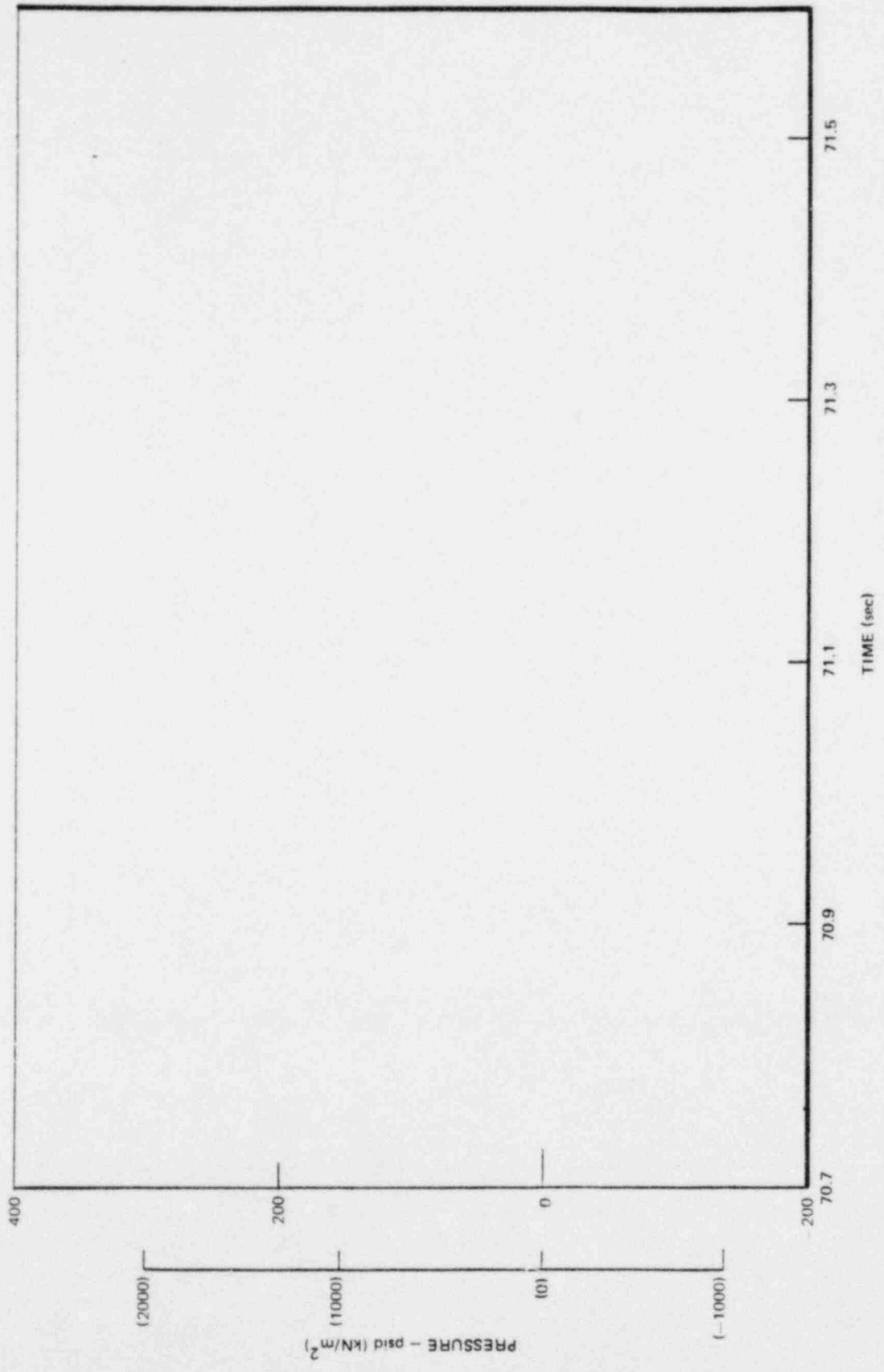


Figure 5-26. Two-Cell Top Vent Chugging Pressure Time History, Run 8

*Proprietary information deleted

*

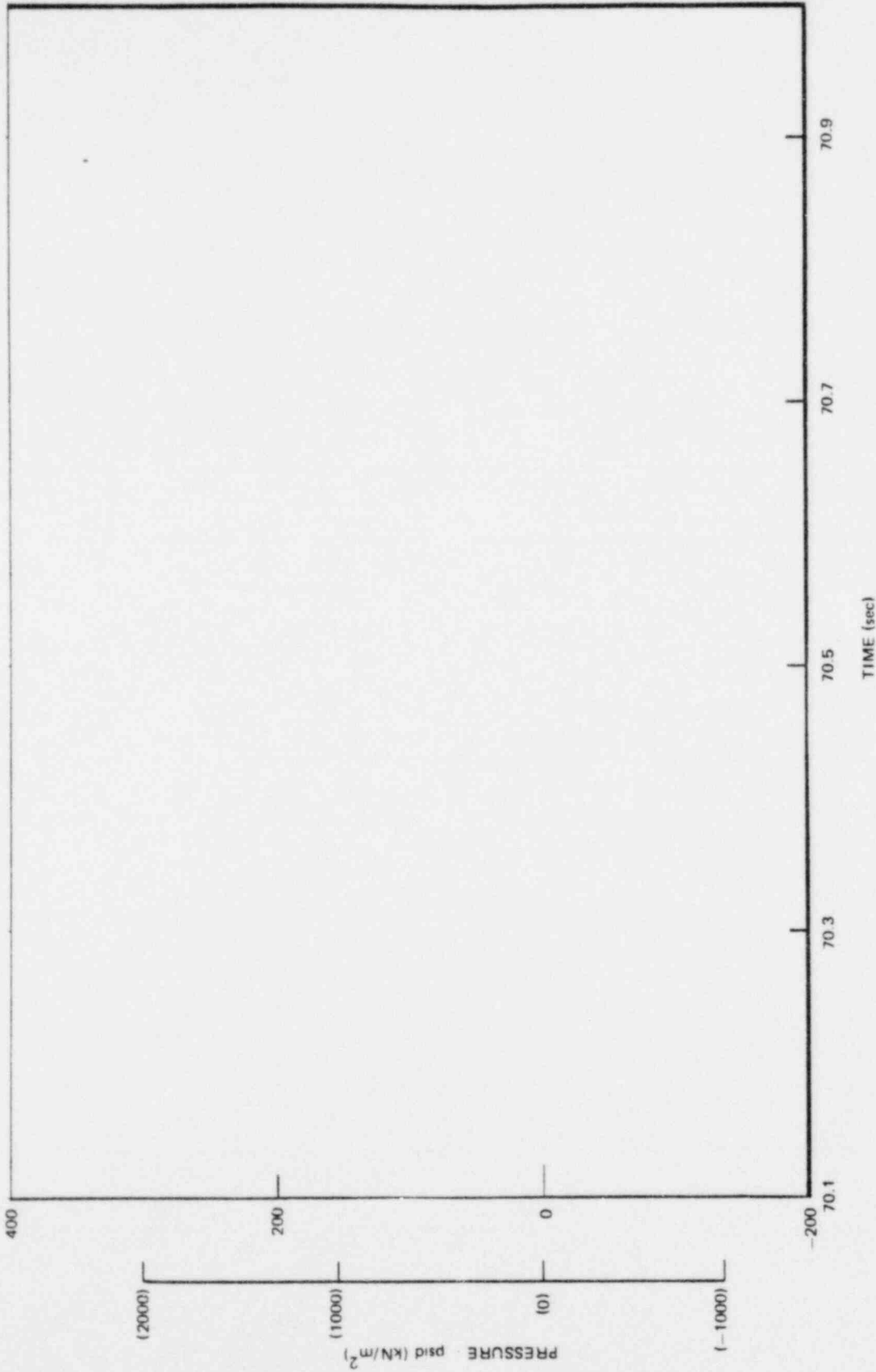


Figure 5-27. Three-Cell Top Vent Chugging Pressure Time History, Run 3

*Proprietary information deleted

*

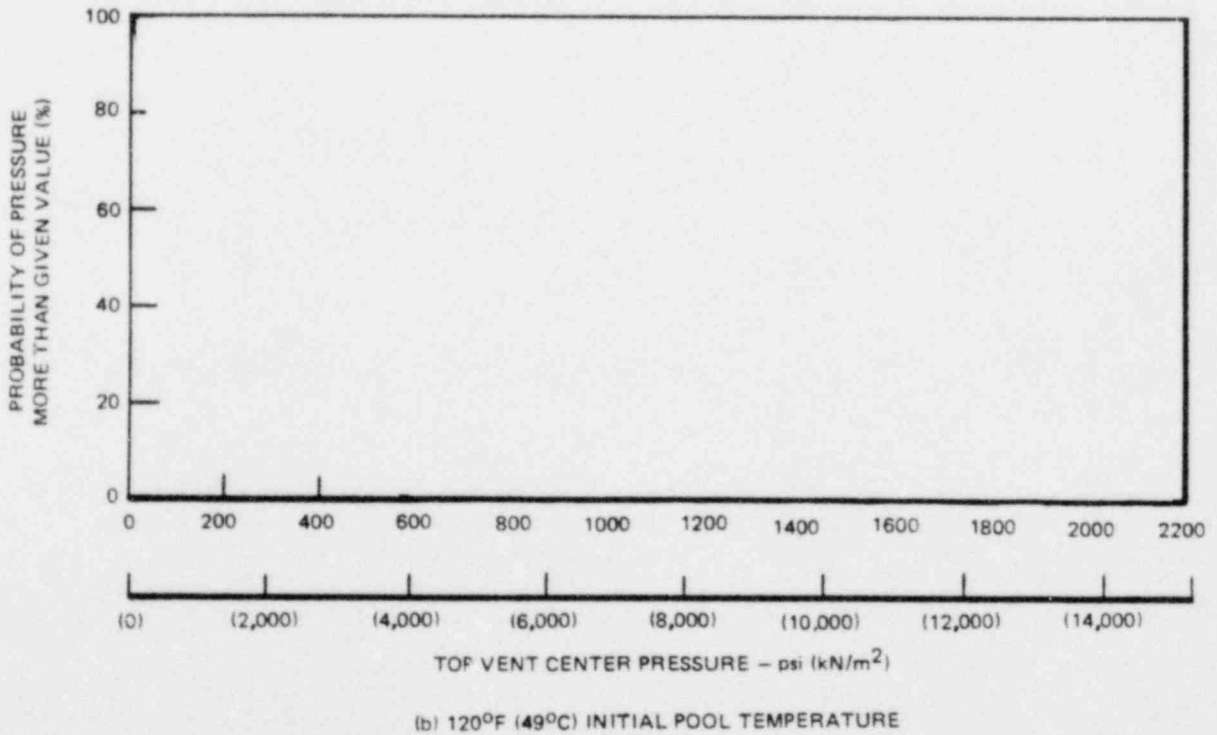
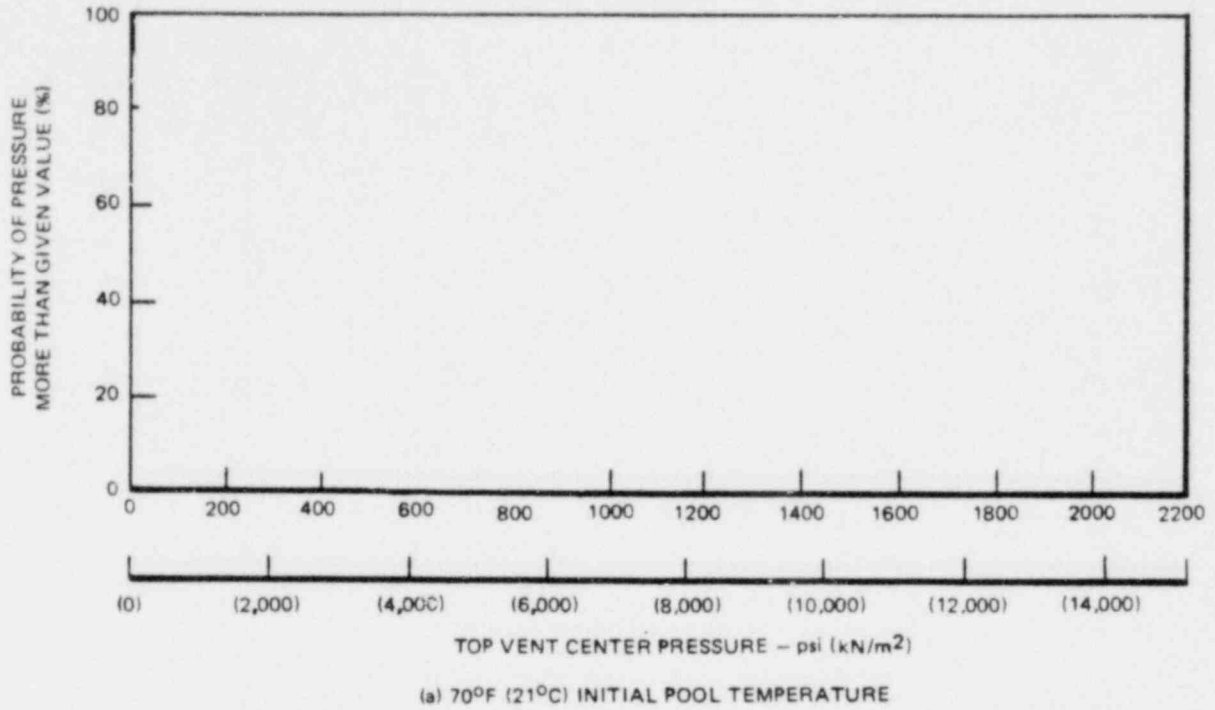
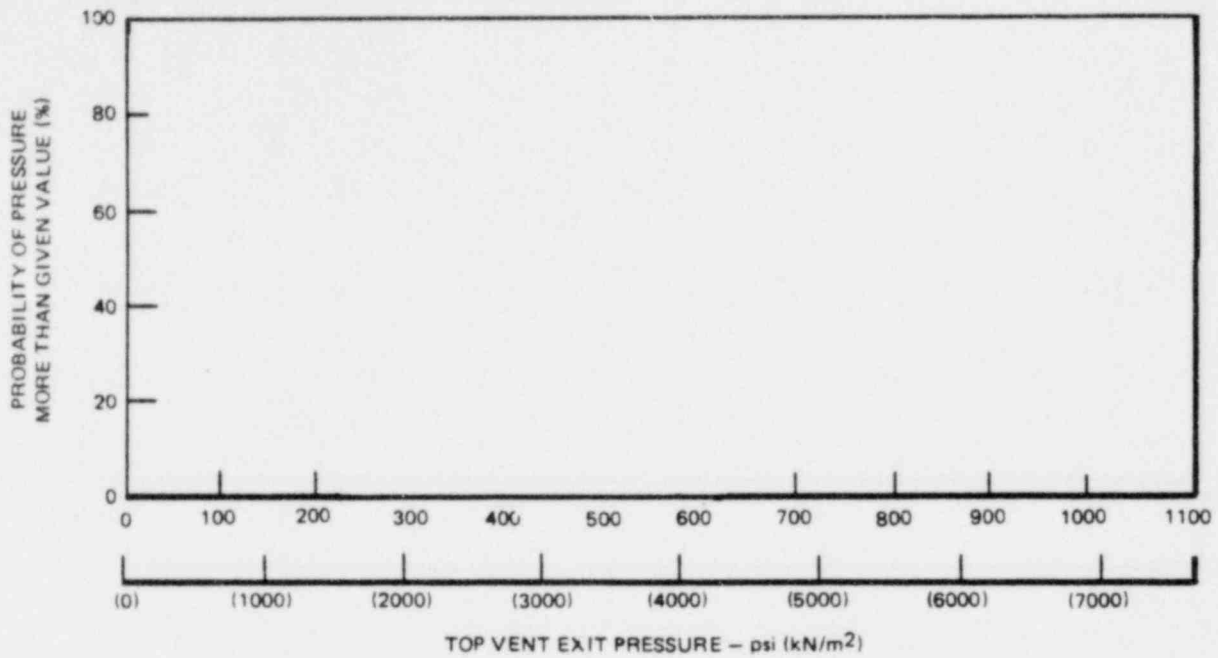
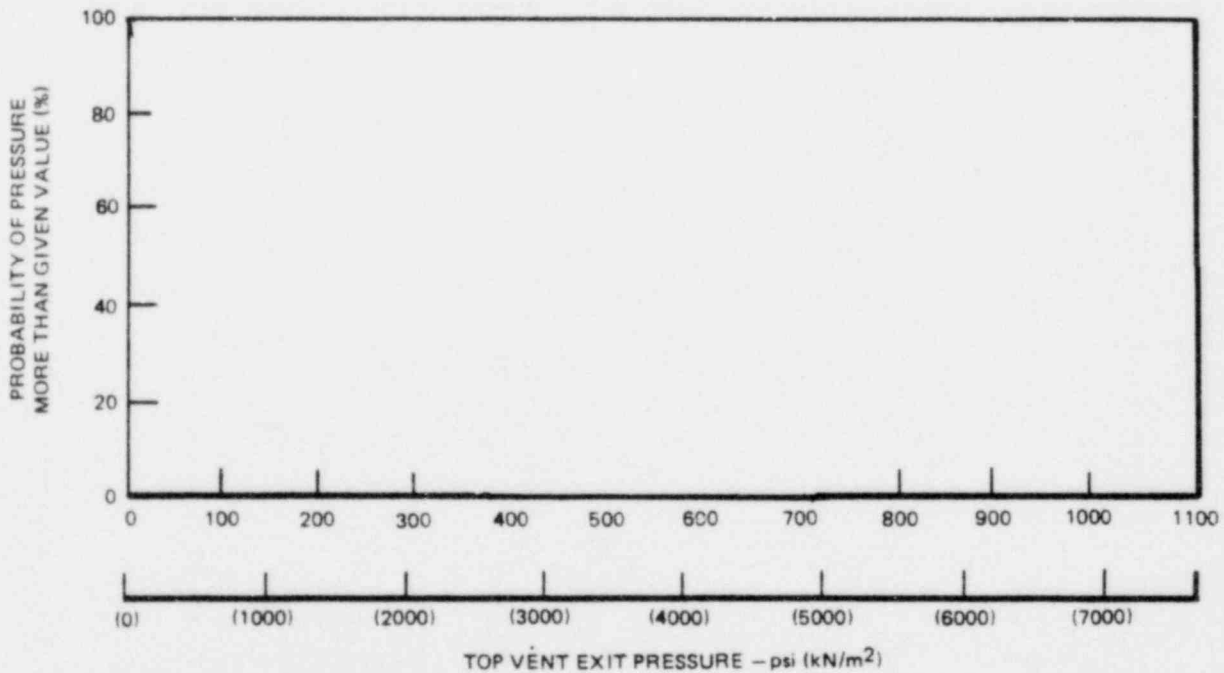


Figure 5-28. Complementary Cumulative Probability Density Distribution Function - Multicell Effects on Top Vent Center Chugging Pressures



(a) 70°F (21°C) INITIAL POOL TEMPERATURE



(b) 120°F (49°C) INITIAL POOL TEMPERATURE

Figure 5-29. Complementary Cumulative Probability Density Distribution Function - Multicell Effects on Top Vent Exit Chugging Pressures

*Proprietary information deleted

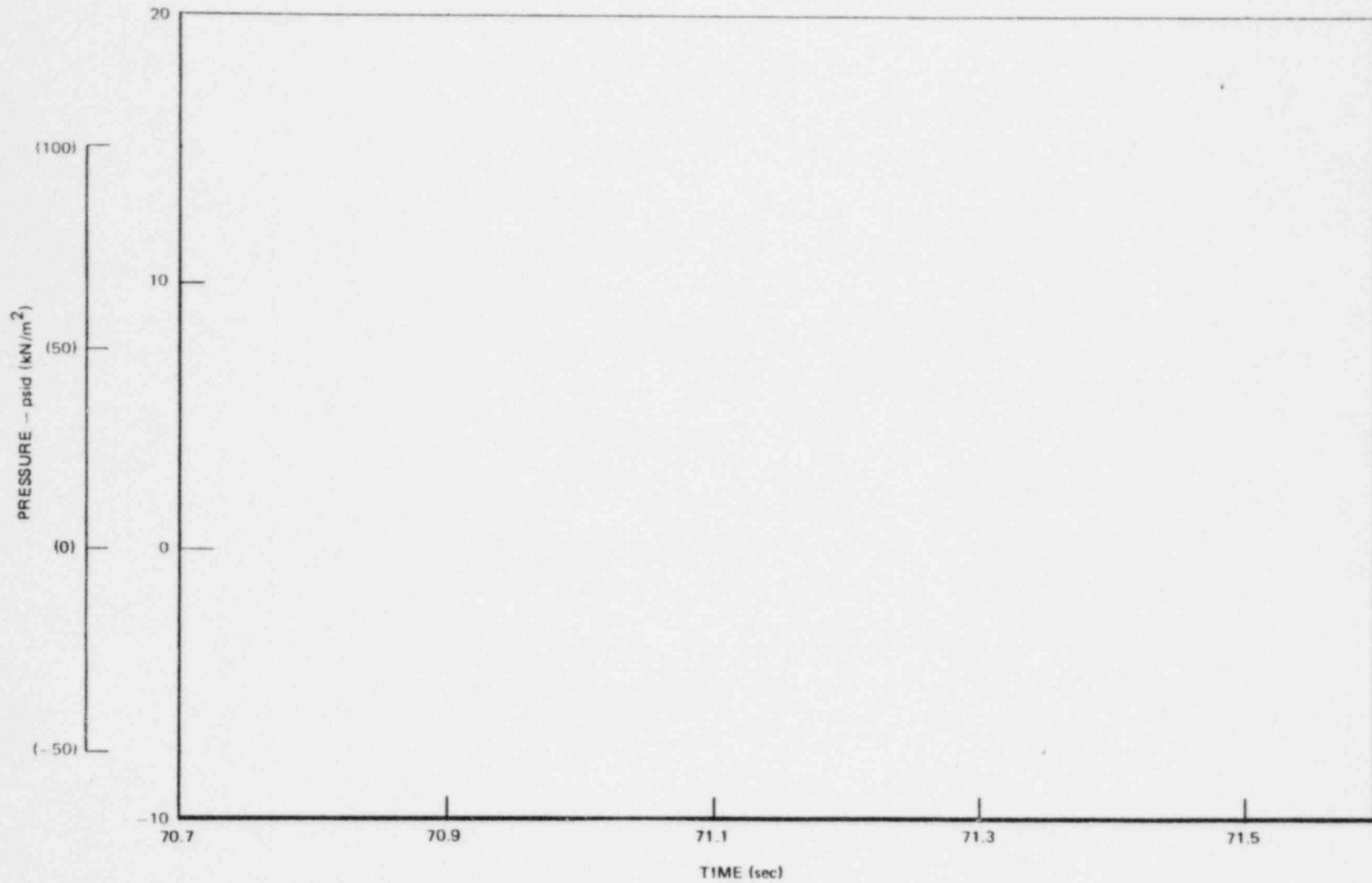


Figure 5-30. One-Cell Weir Wall Chugging Pressure Time History, Run 8

*Proprietary information deleted

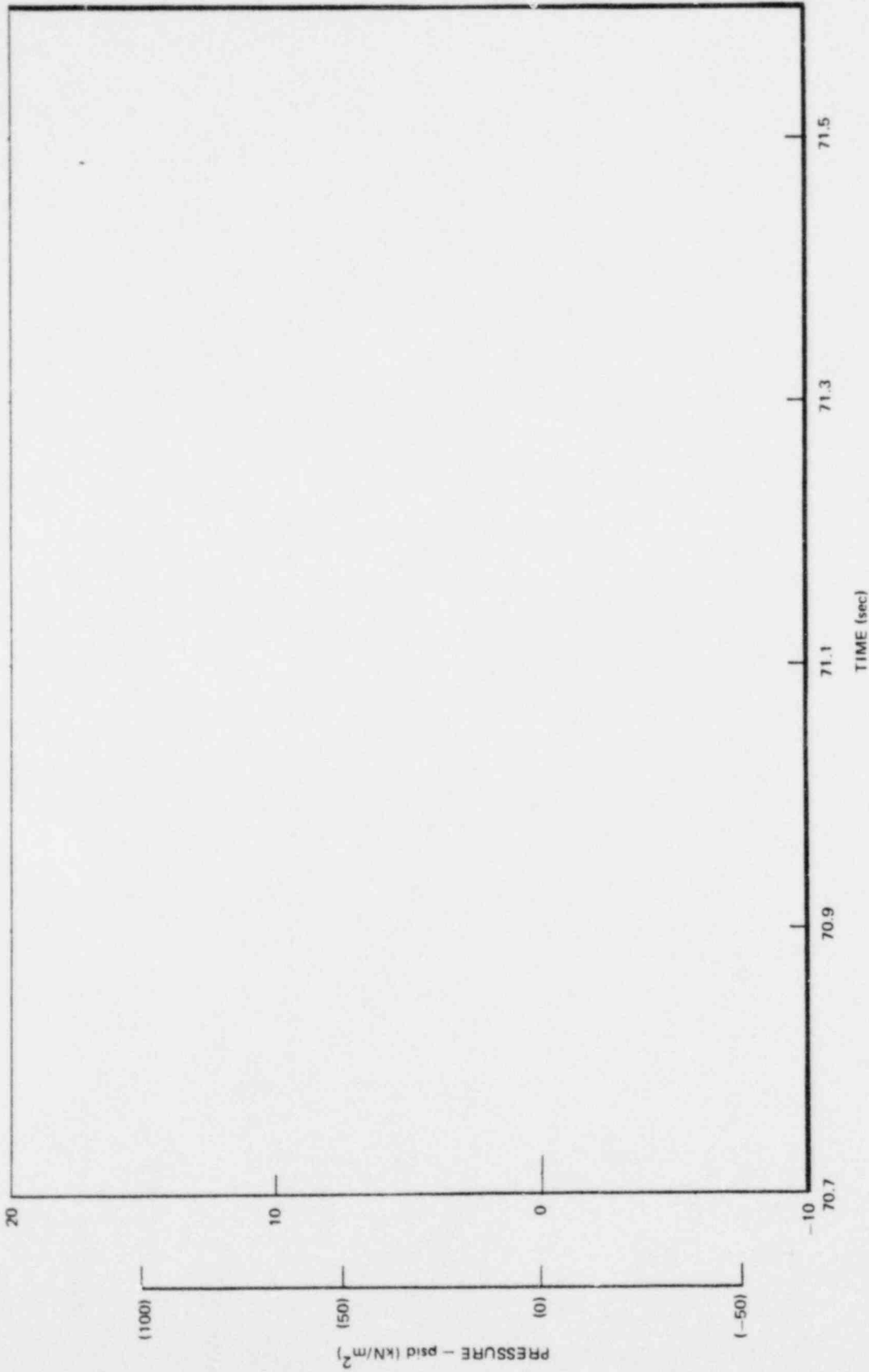


Figure 5-31. Two-Cell Weir Wall Chugging Pressure Time History, Run 8

*Proprietary information deleted

*

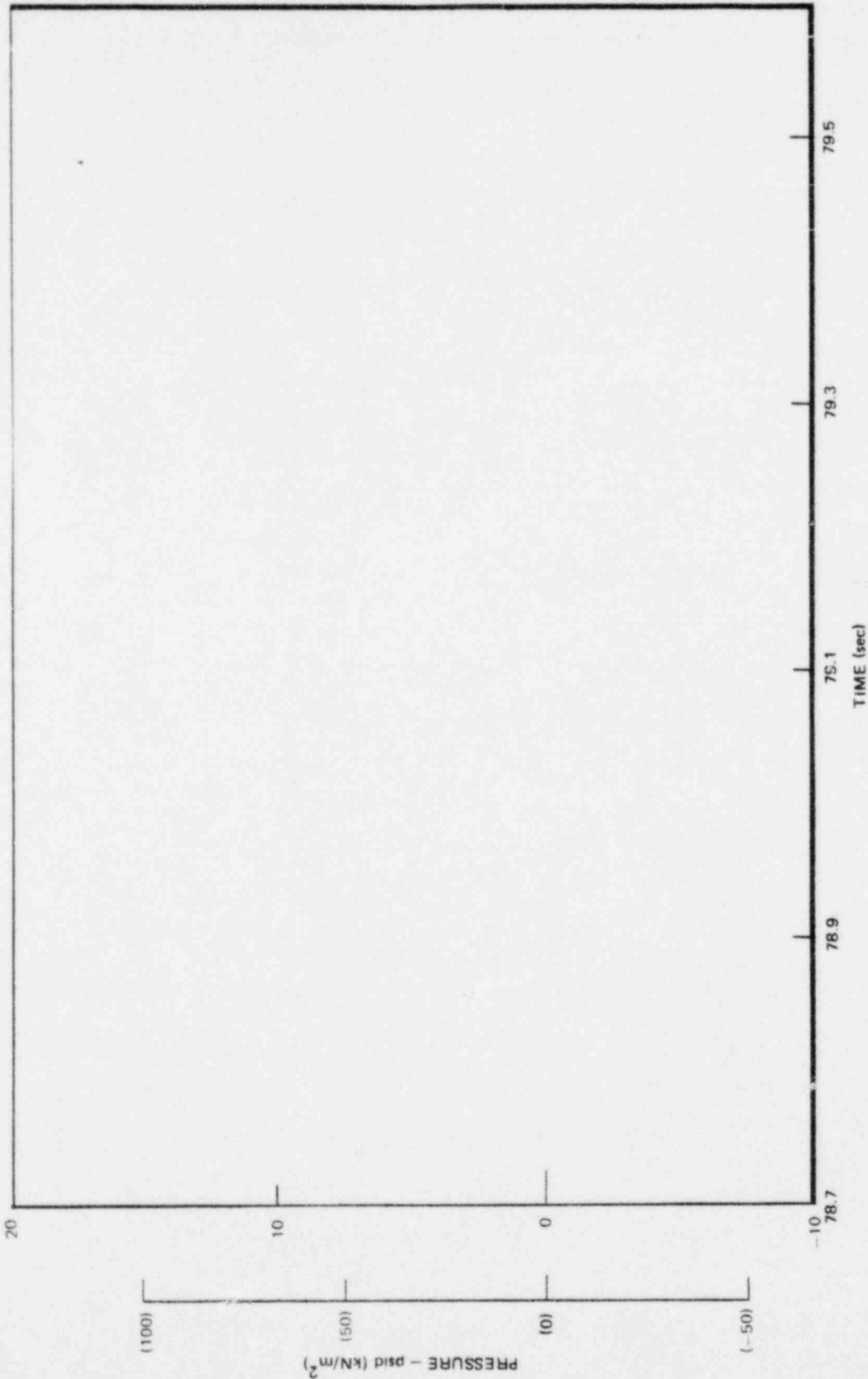
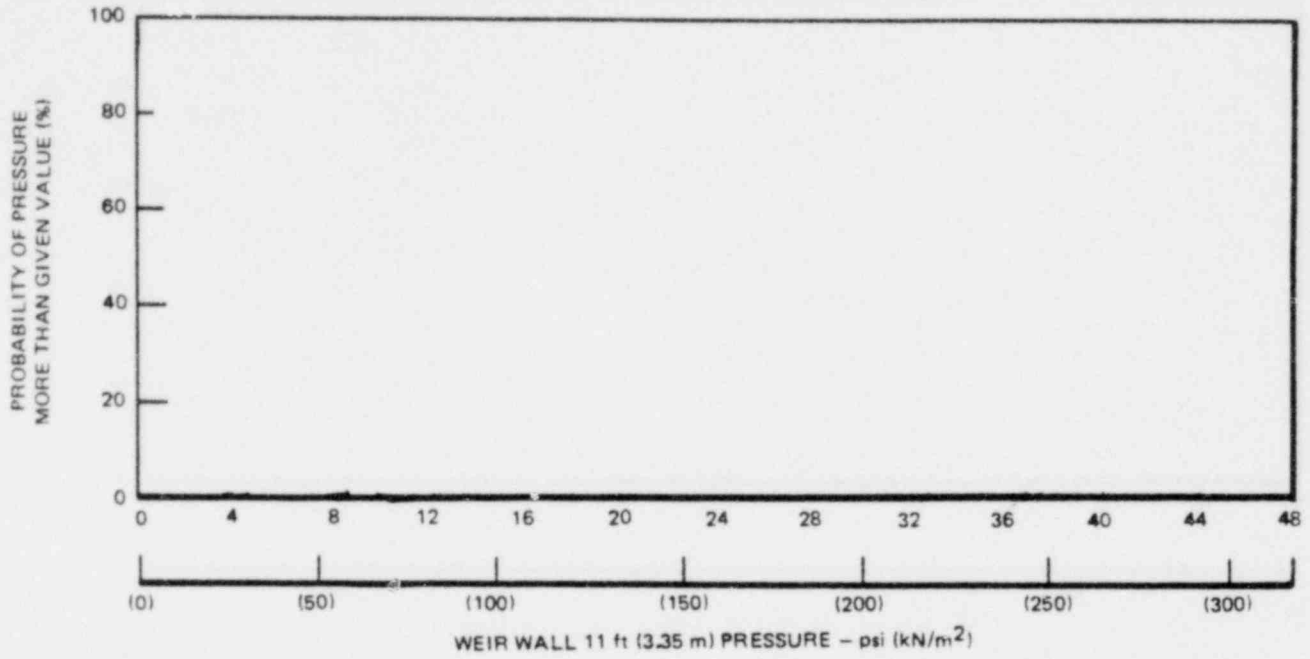


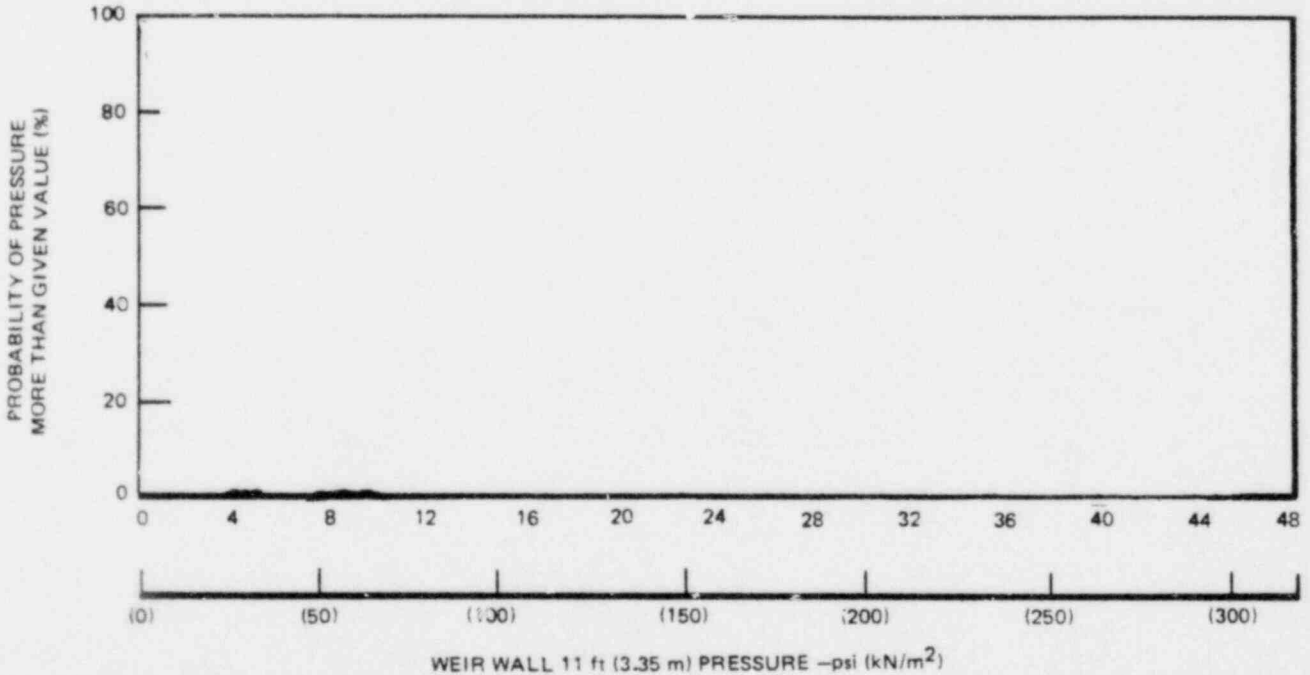
Figure 5-32. Three-Cell Weir Wall Chugging Pressure Time History, Run 3

*Proprietary information deleted

*



(a) 70°F (21°C) INITIAL POOL TEMPERATURE

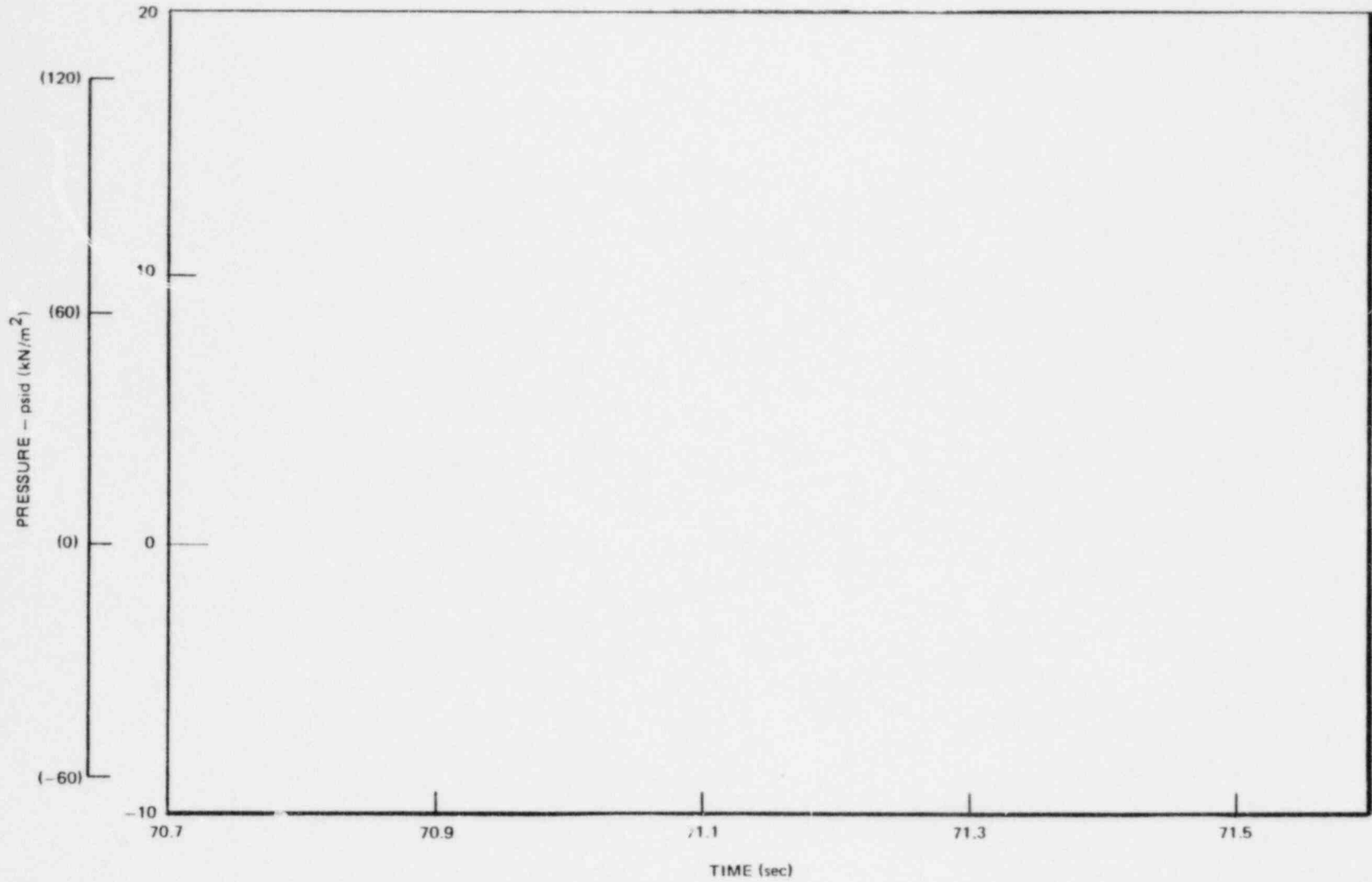


(b) 120°F (49°C) INITIAL POOL TEMPERATURE

Figure 5-33. Complementary Cumulative Probability Density Distribution Function - Multicell Effects on Weir Wall Chugging Pressures

*Proprietary information deleted

5-60



NEDO-24720

Figure 5-34. One-Cell Drywell Wall Chugging Pressure Time History, Run 8

*Proprietary information deleted

*

T9-5

NEDO-24720

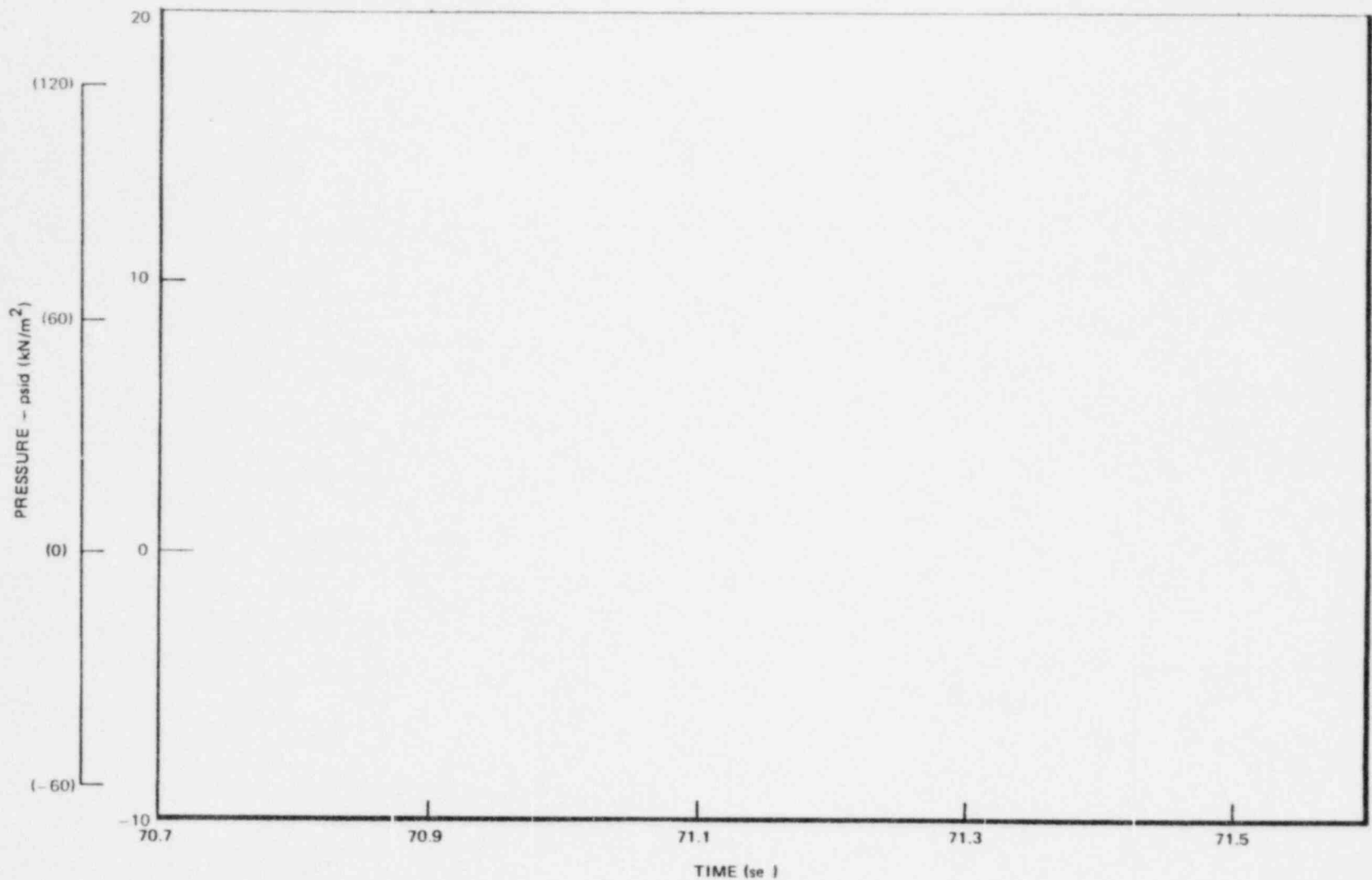
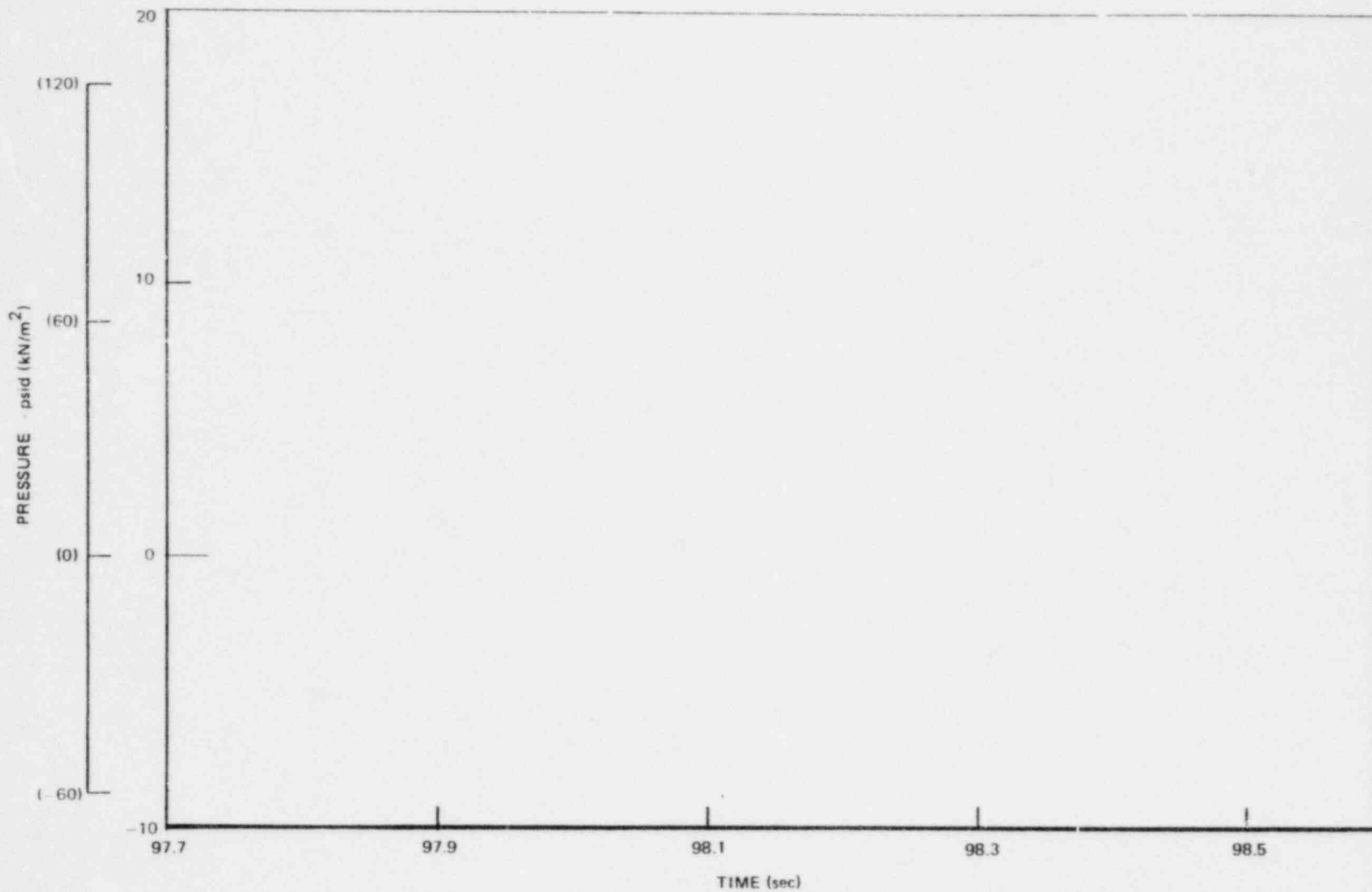


Figure 5-35. Two-Cell Drywell Wall Chugging Pressure Time History, Run 8

*Proprietary information deleted

*

5-62

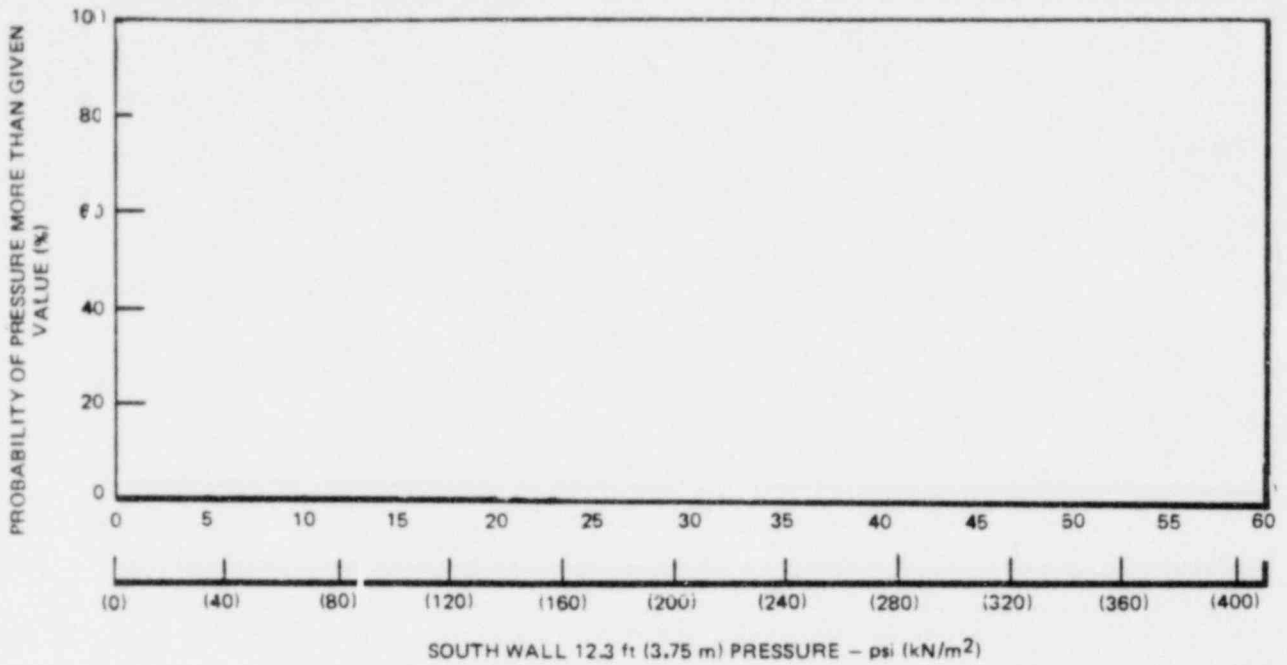


NEDO-24720

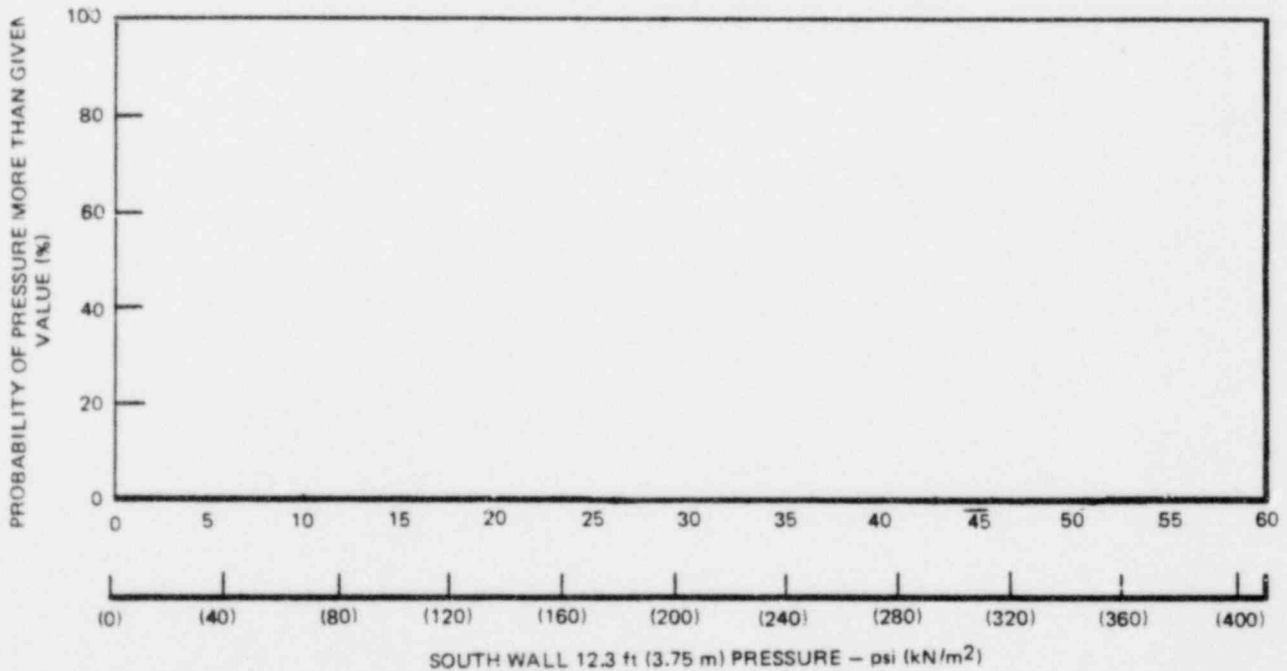
Figure 5-36. Three-Cell Drywell Wall Chugging Pressure Time History, Run 3

*Proprietary information deleted

*



(a) 70°F (21°C) INITIAL POOL TEMPERATURE



(b) 120°F (49°C) INITIAL POOL TEMPERATURE

Figure 5-37. Complementary Cumulative Probability Density Distribution Function - Multicell Effects on Drywell Wall Chugging Pressures

*Proprietary information deleted

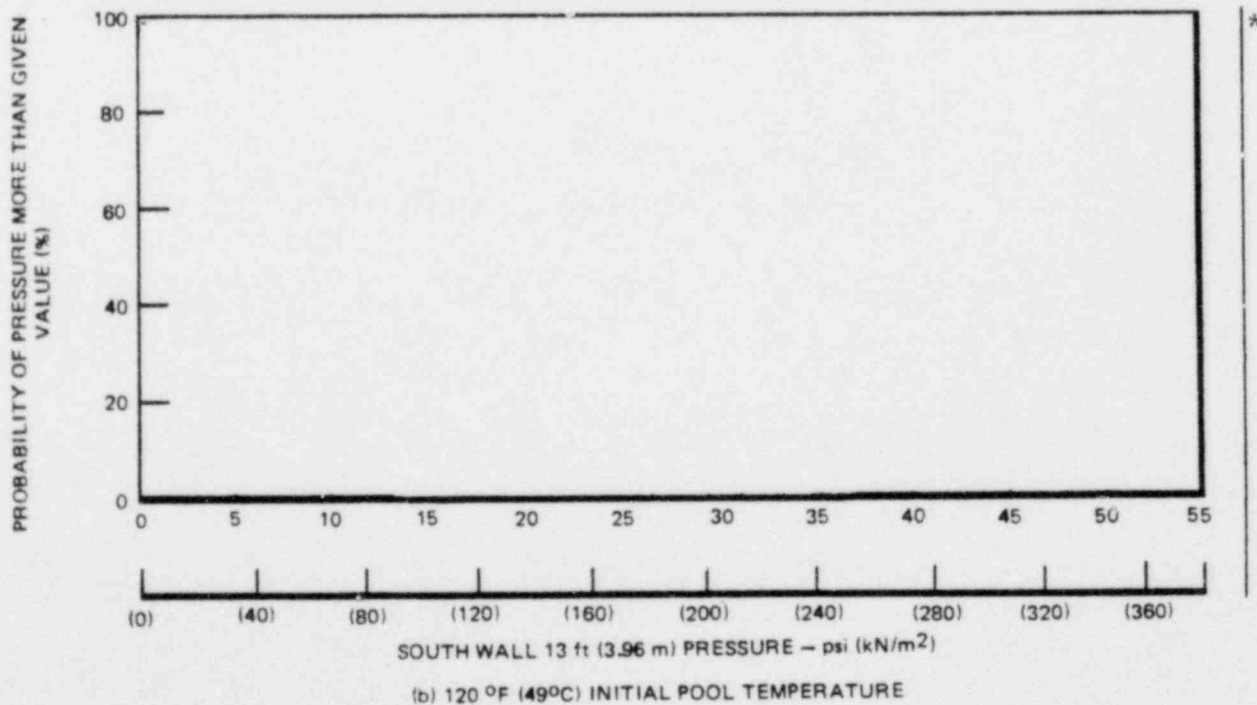
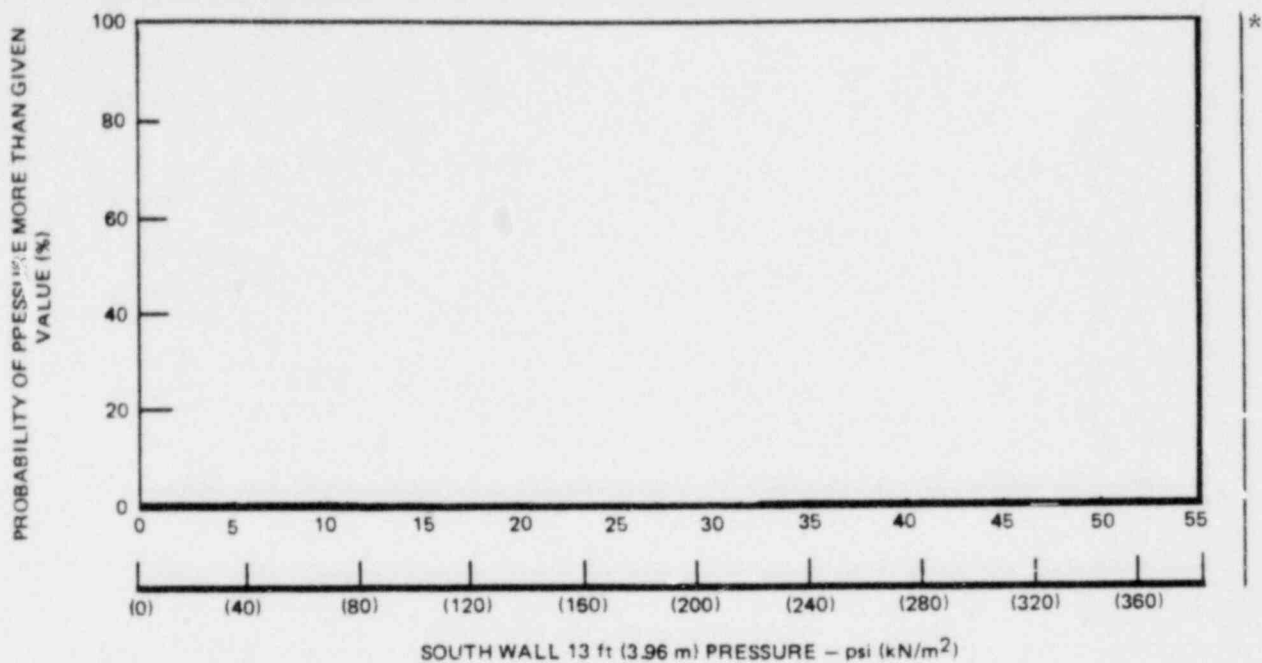
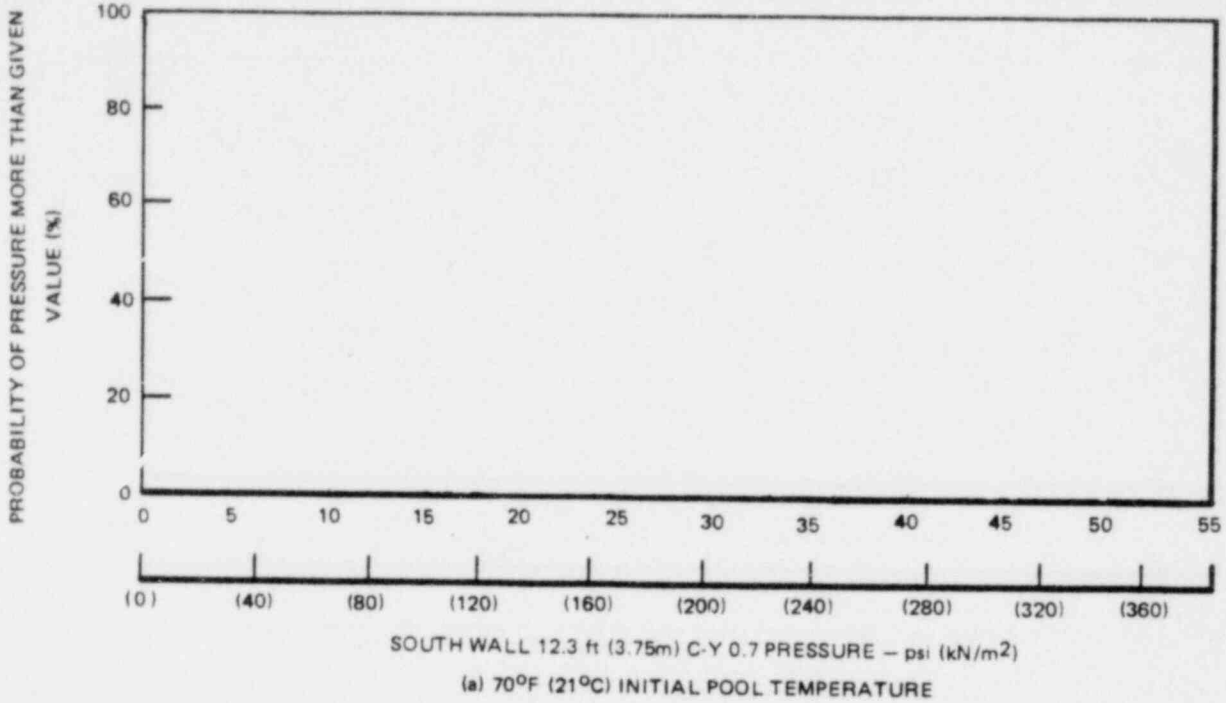
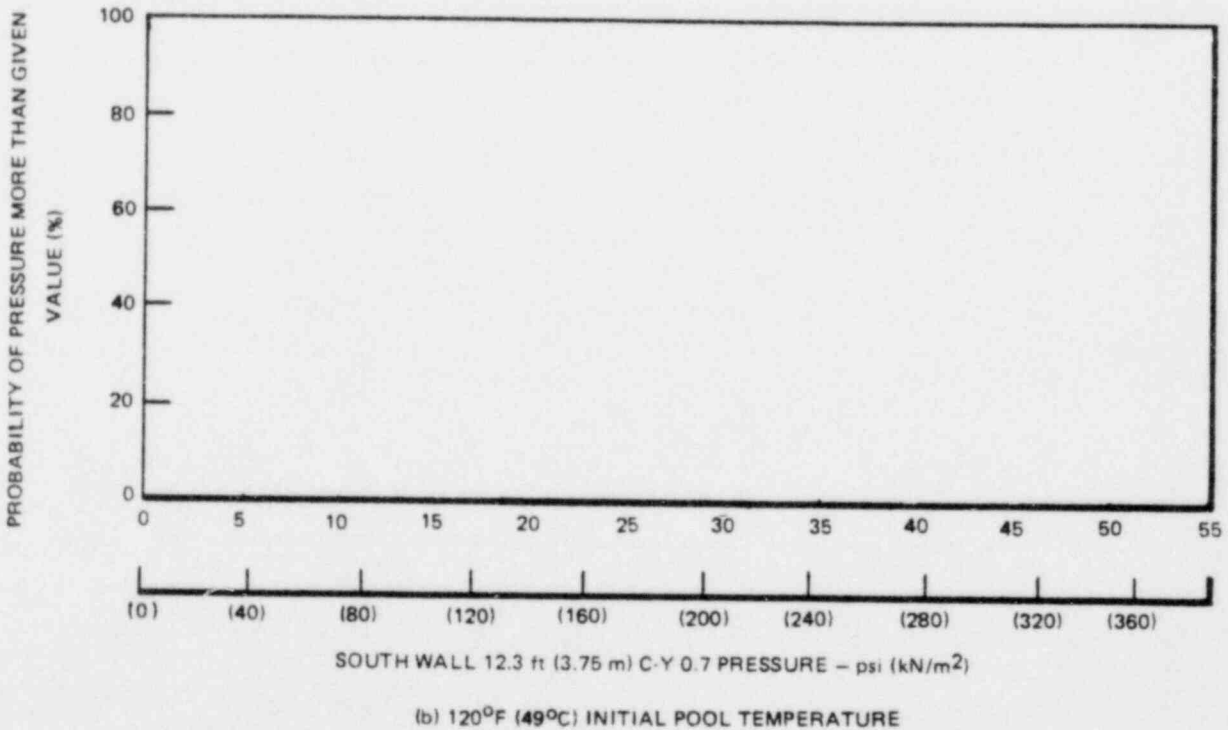


Figure 5-38. Complementary Cumulative Probability Density Distribution Function - Multicell Effects on Drywell Wall Chugging Pressures

*Proprietary information deleted



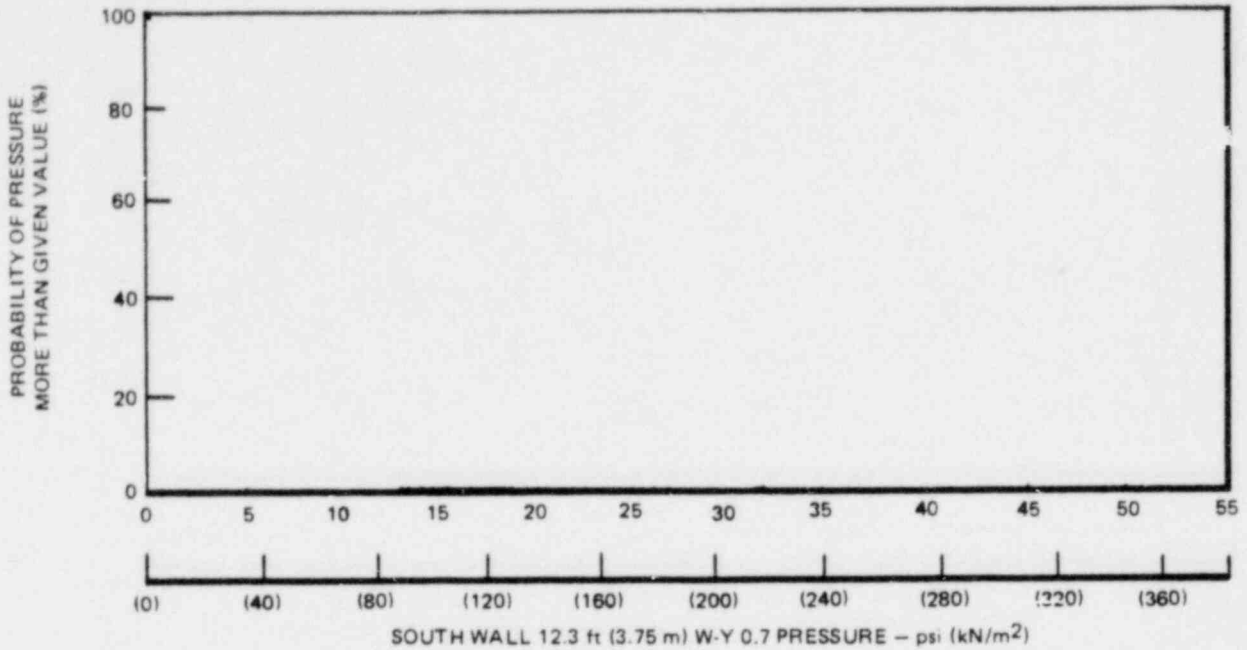
*



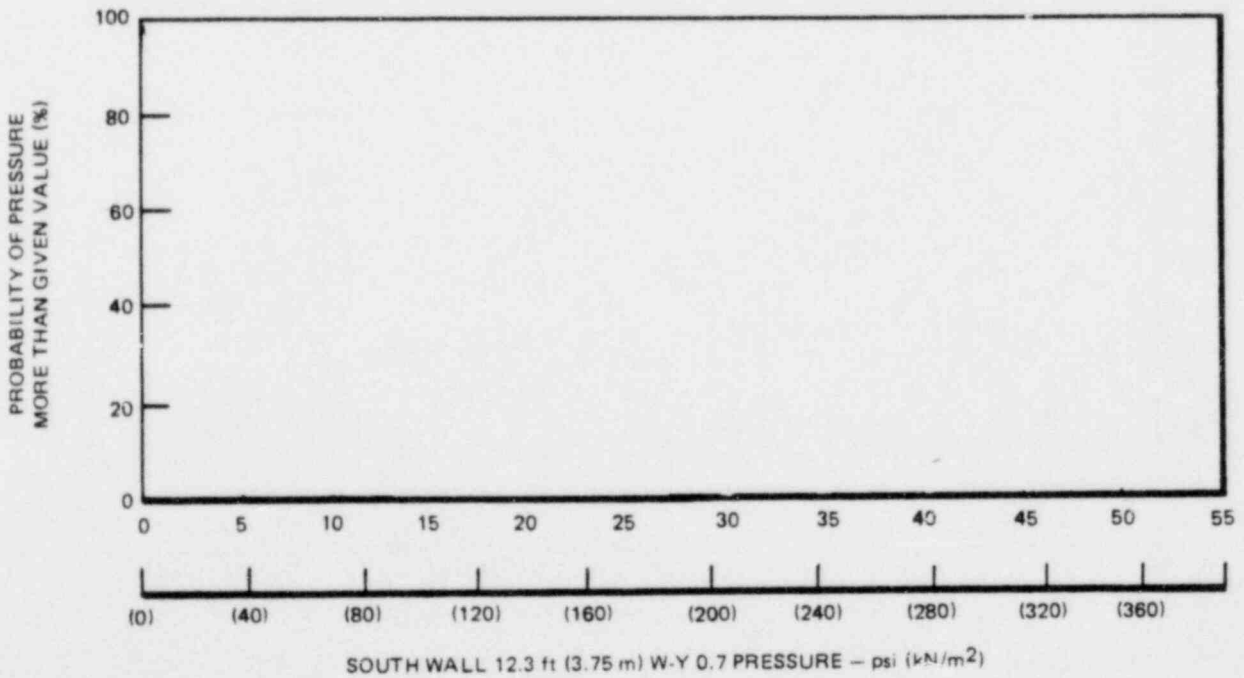
*

Figure 5-39. Complementary Cumulative Probability Density Distribution Function - Multicell Effects on Drywell Wall Chugging Pressures

*Proprietary information deleted



(a) 70°F (21°C) INITIAL POOL TEMPERATURE



(b) 120°F (49°C) INITIAL POOL TEMPERATURE

Figure 5-40. Complementary Cumulative Probability Density Distribution Function - Multicell Effects on Drywell Wall Chugging Pressures

*Proprietary information deleted

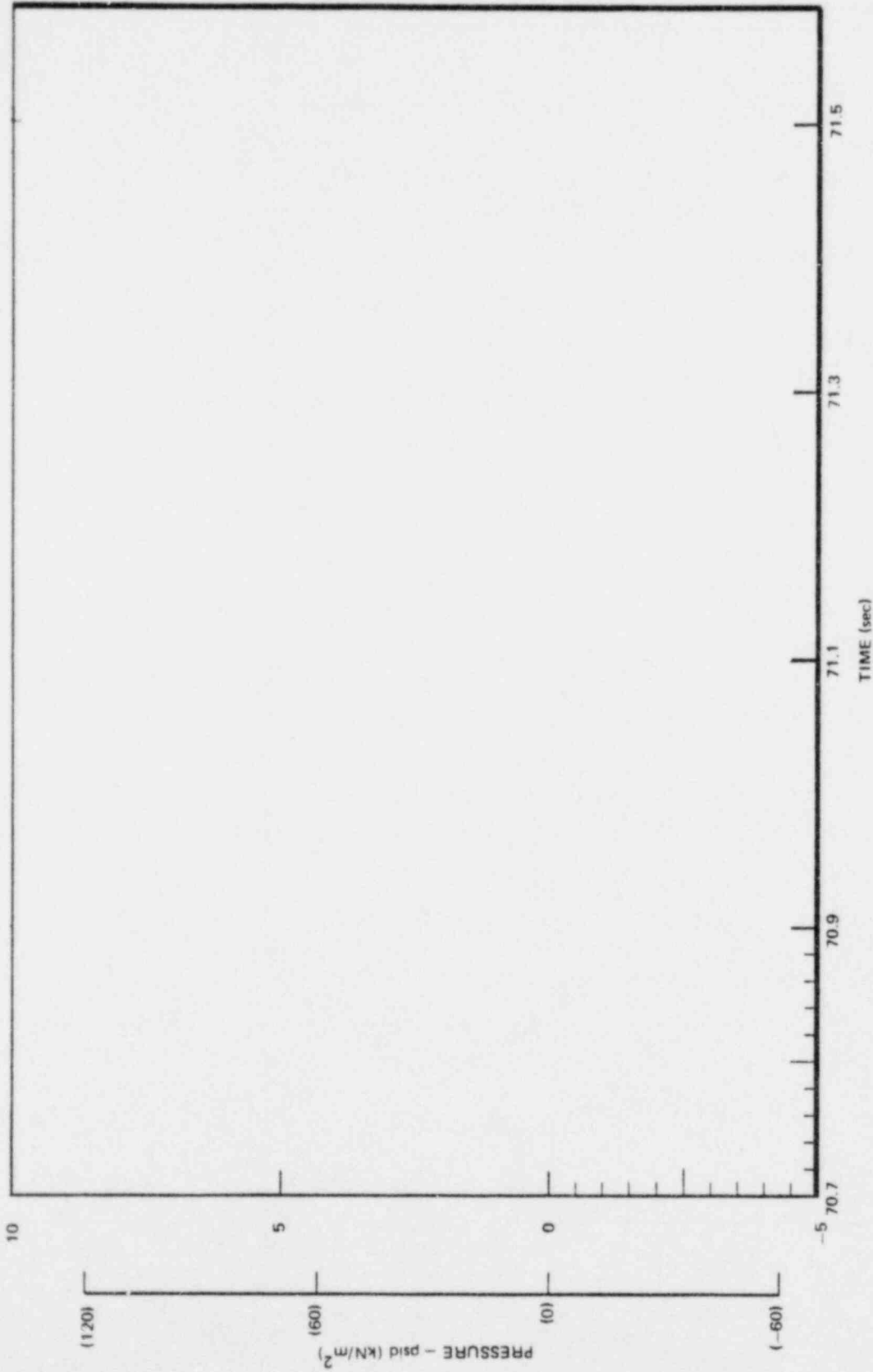


Figure 5-41. One-Cell Containment Wall Chugging Pressure Time History, Run 8

*Proprietary information deleted

*

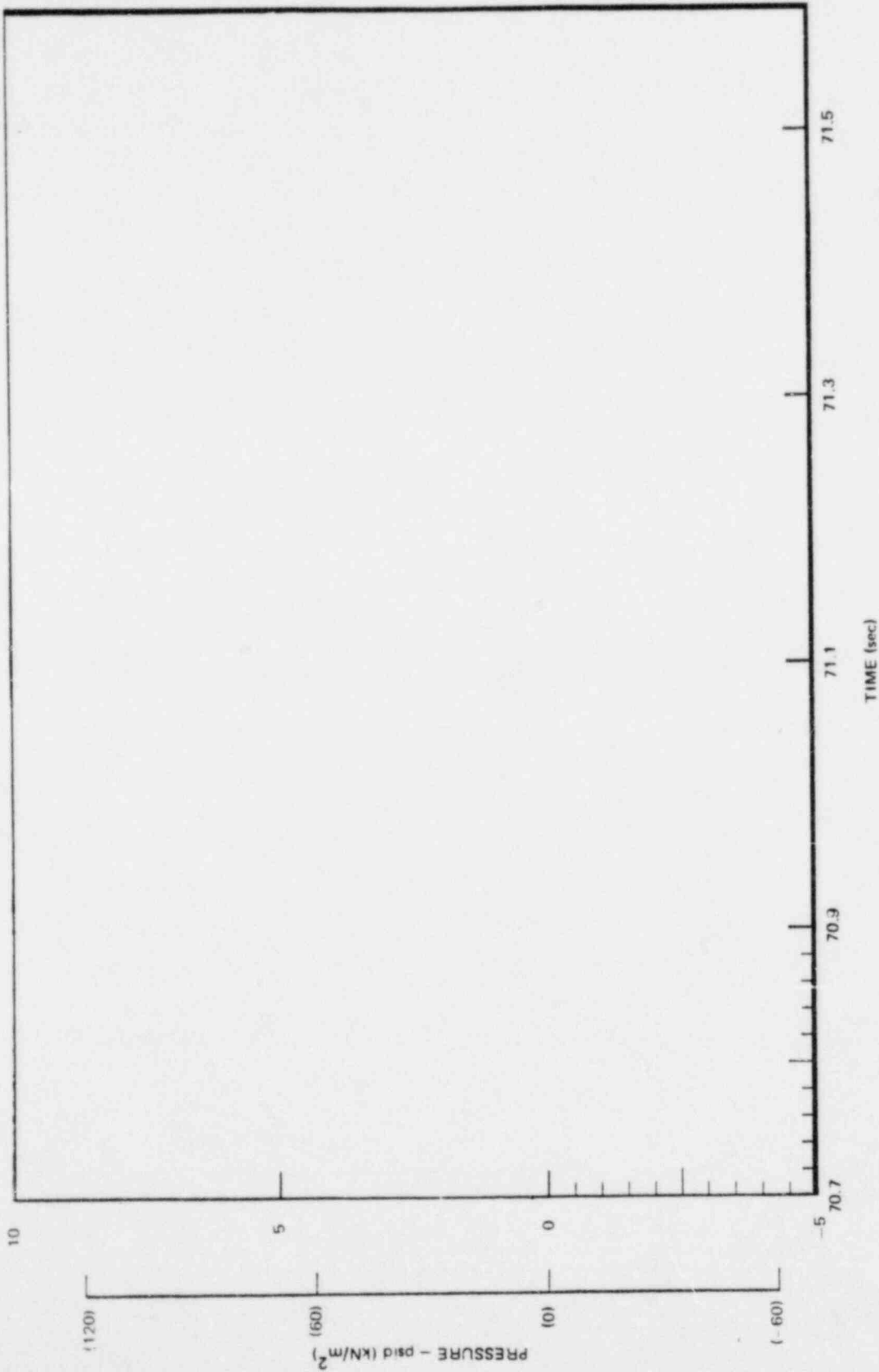
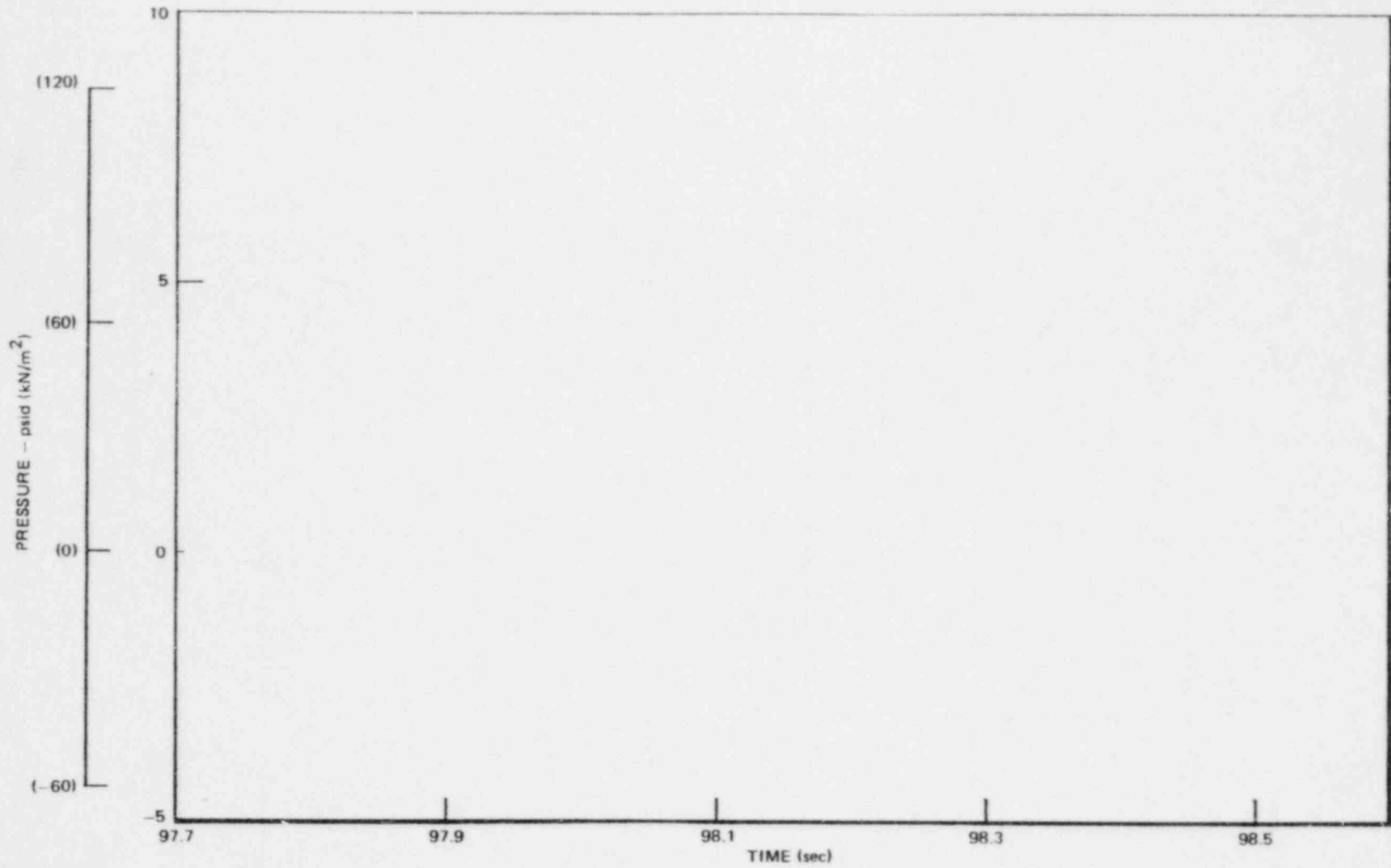


Figure 5-42. Two-Cell Containment Wall Chugging Pressure Time History, Run 8

*Proprietary information deleted

*

5-69

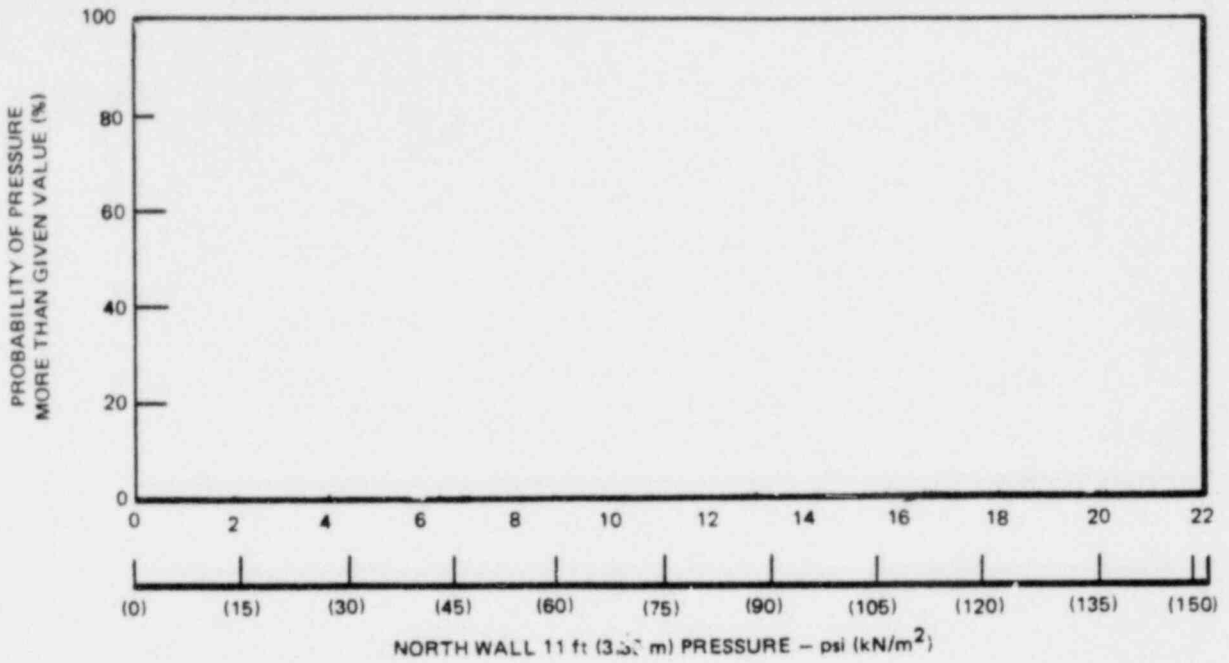


NEDO-24720

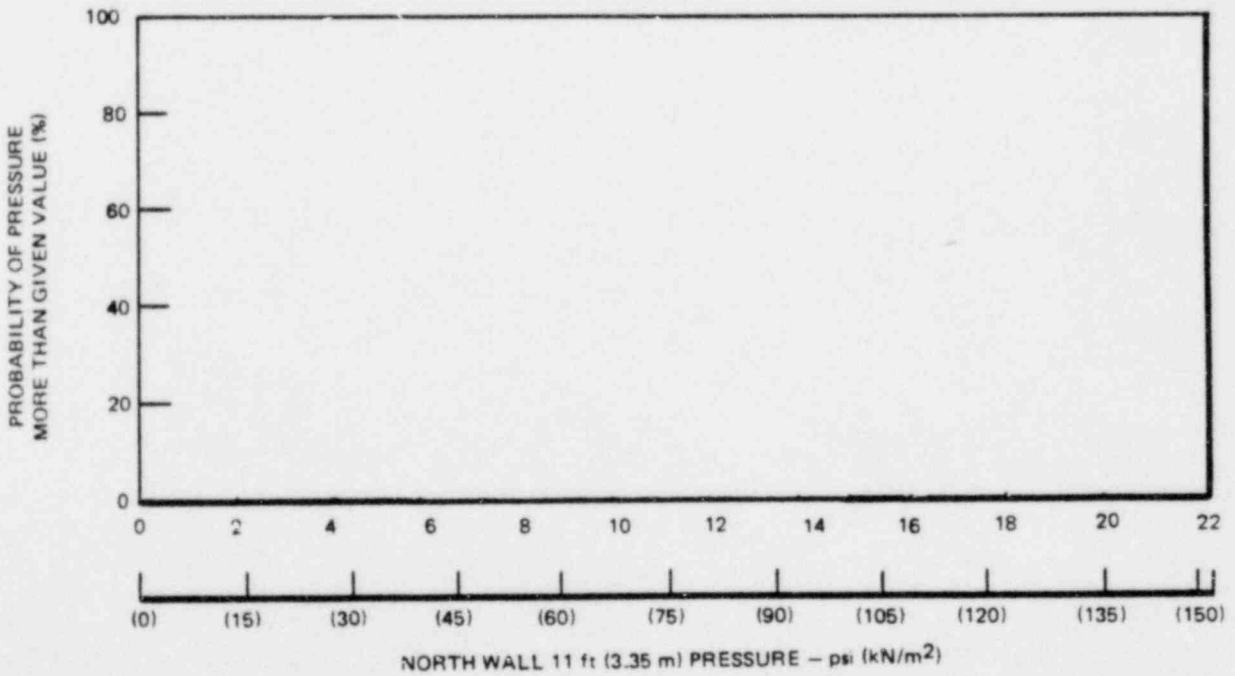
Figure 5-43. Three-Cell Containment Wall Chugging Pressure Time History, Run 3

*Proprietary information deleted

*



(a) 70°F (21°C) INITIAL POOL TEMPERATURE



(b) 120°F (49°C) INITIAL POOL TEMPERATURE

Figure 5-44. Complementary Cumulative Probability Density Distribution Function - Multicell Effects on Containment Wall Chugging Pressures

*Proprietary information deleted

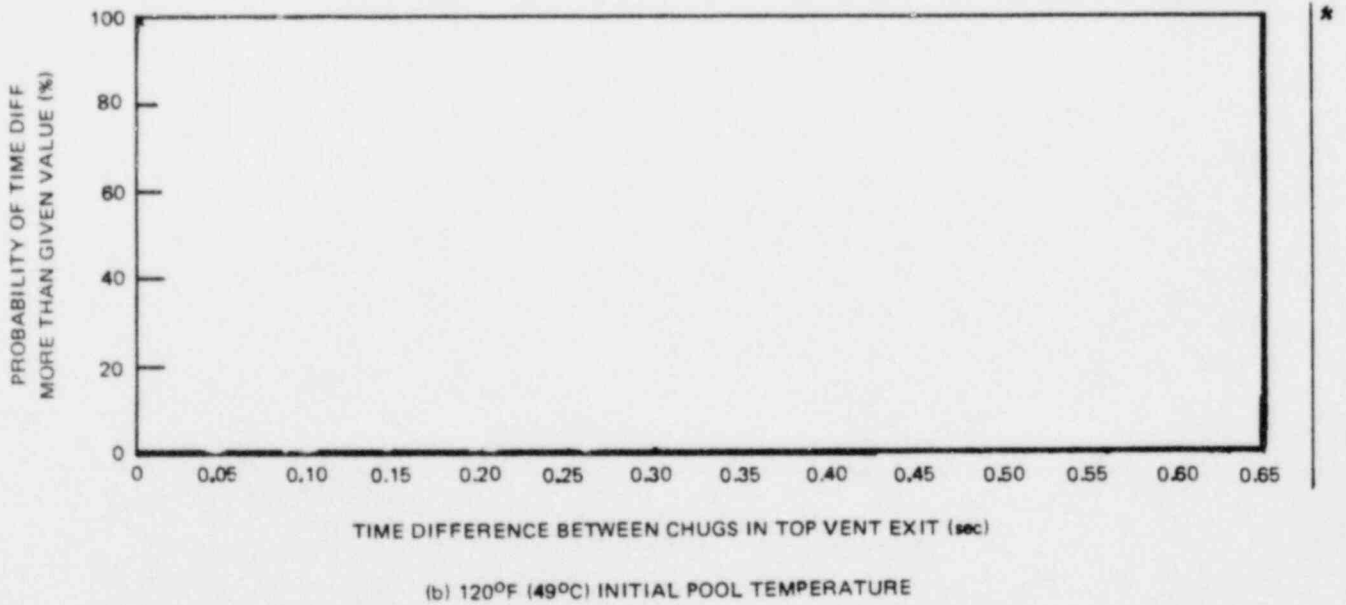
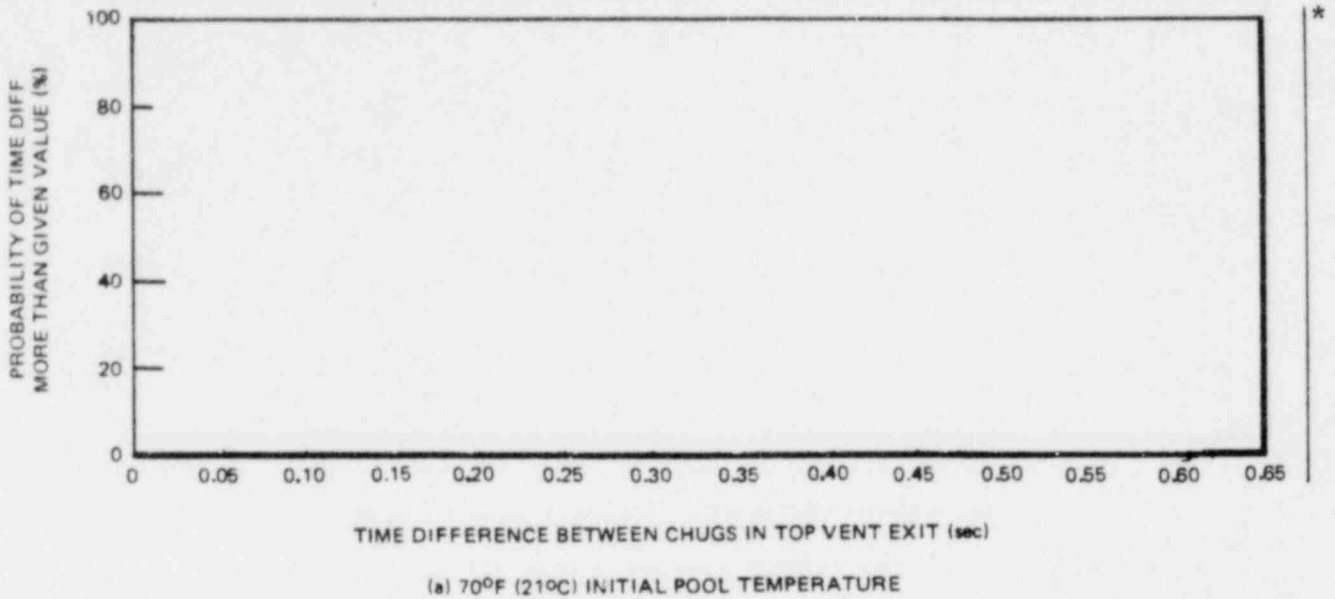


Figure 5-45. Complementary Cumulative Probability Density Distribution Function - Multicell Effects on Chugging Synchronization

*Proprietary information deleted

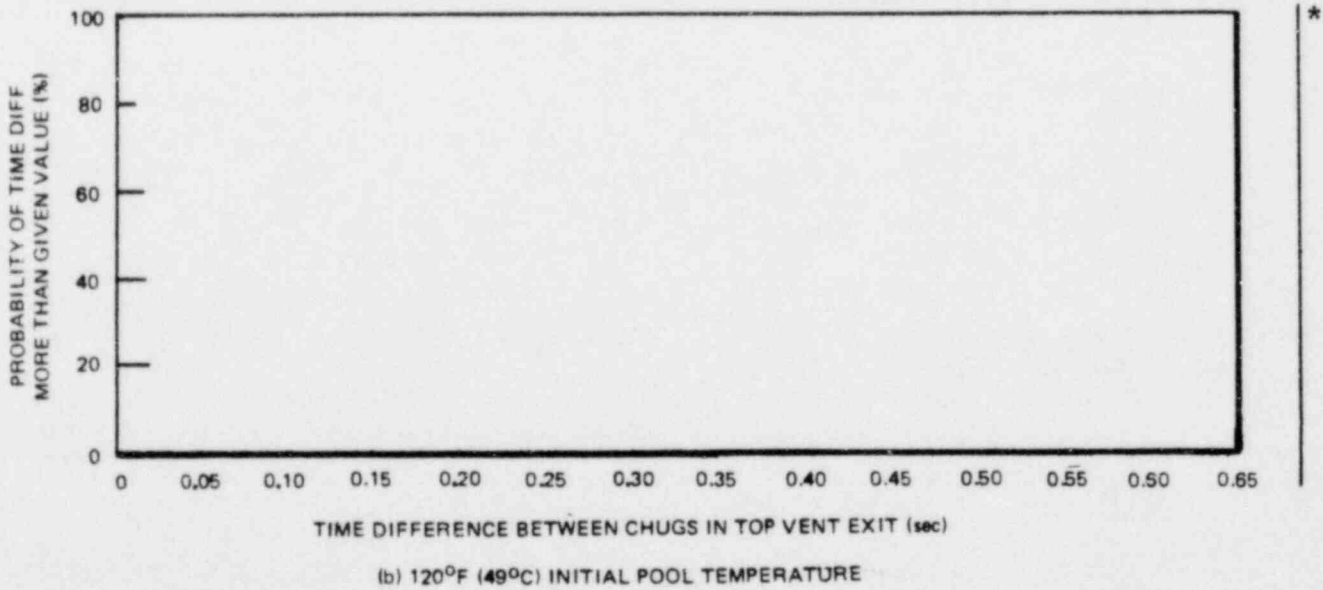
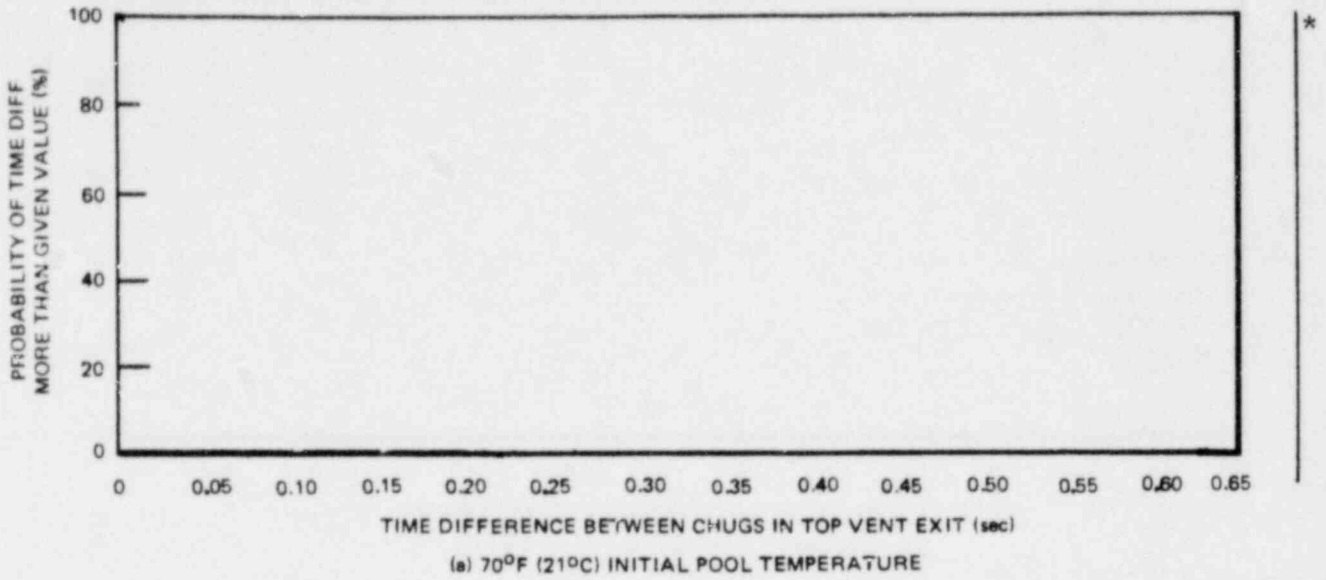


Figure 5-46. Complementary Cumulative Probability Density Distribution Function - Multicell Effects on Chugging Synchronization

*Proprietary information deleted

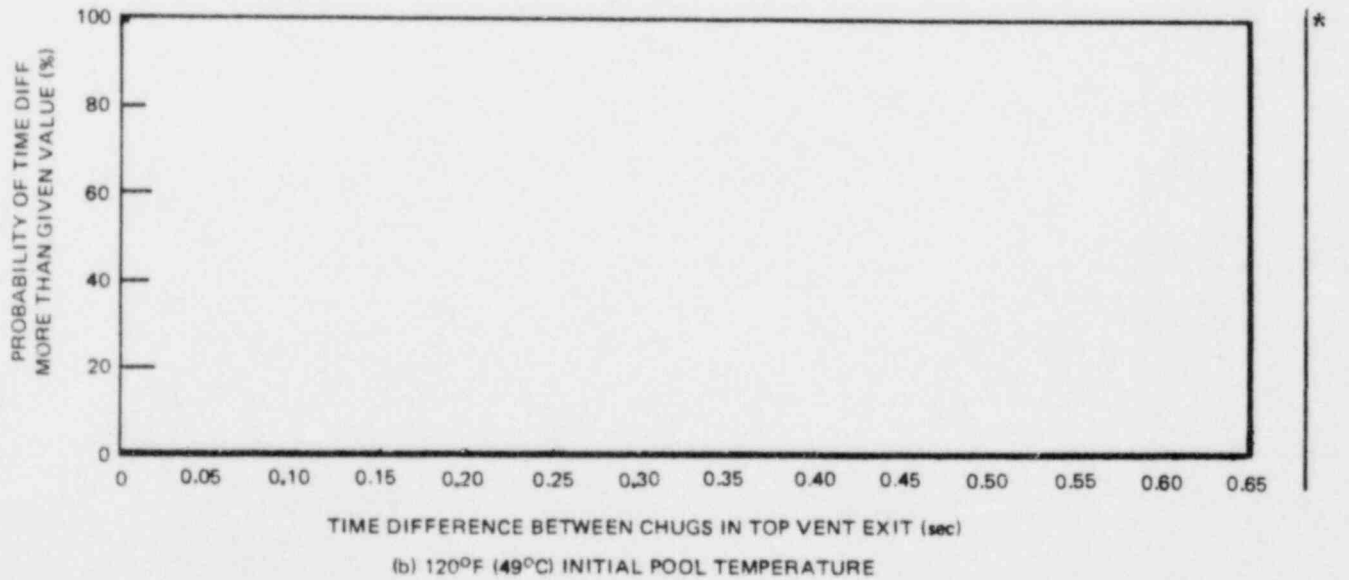
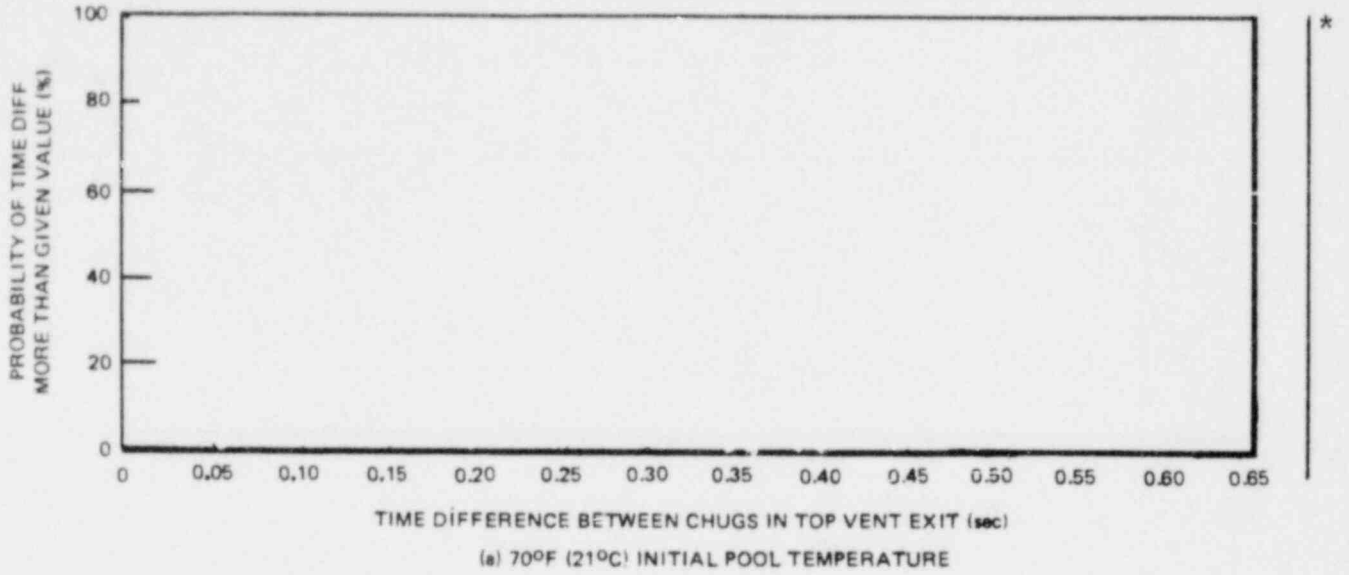
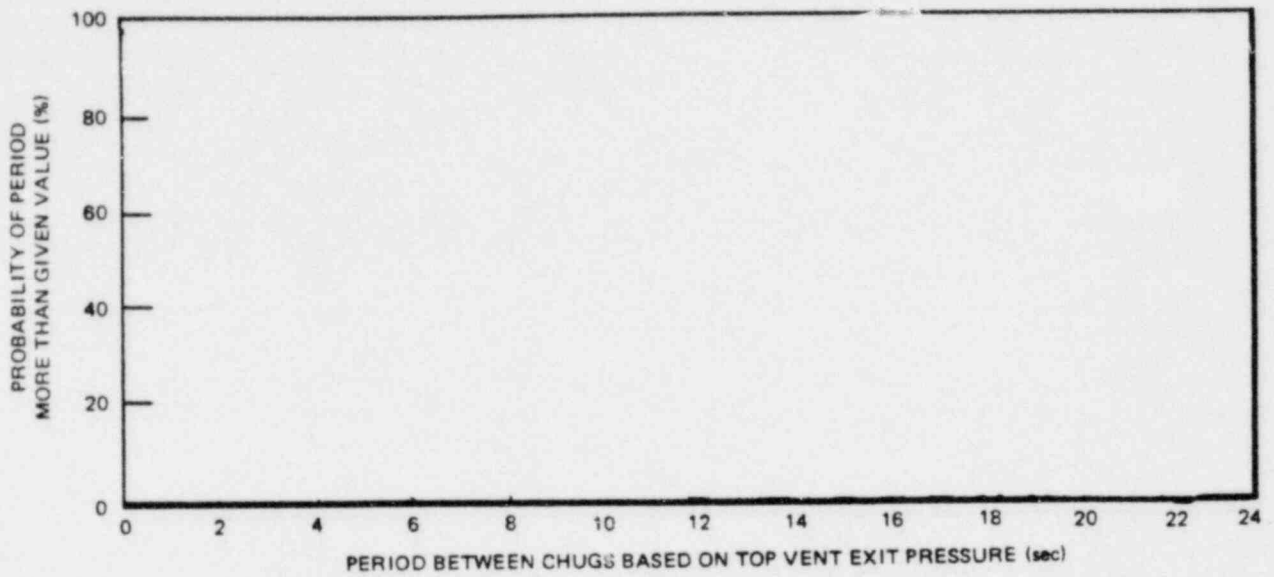
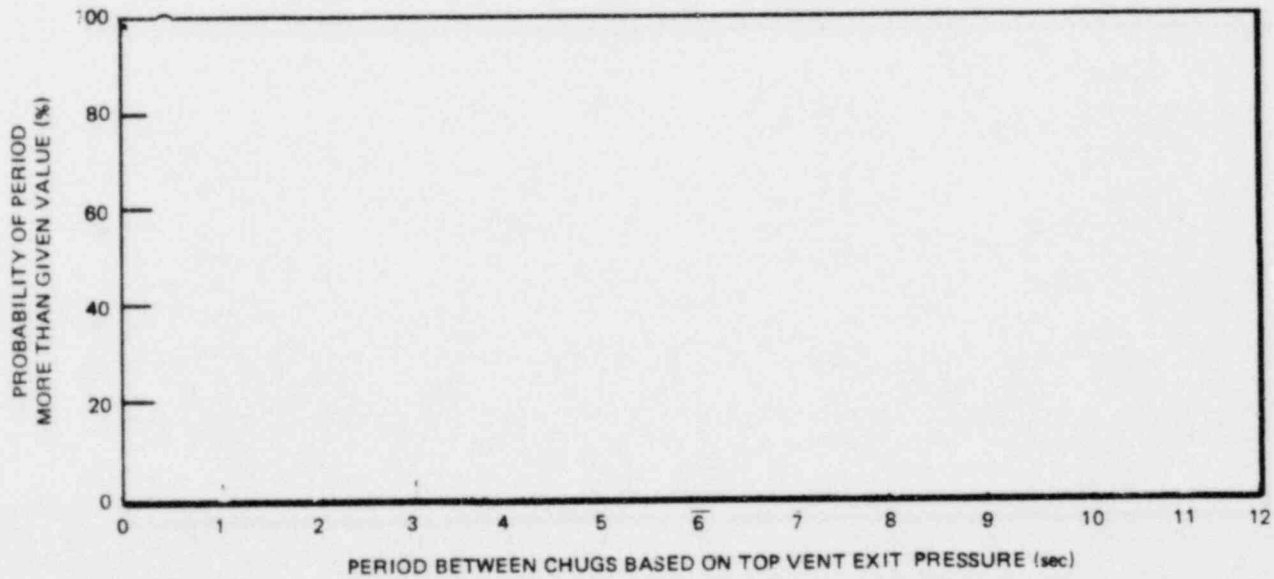


Figure 5-47. Complementary Cumulative Probability Density Distribution Function - Multicell Effects on Chugging Synchronization

*Proprietary information deleted



(a) 70°F (21°C) INITIAL POOL TEMPERATURE



(b) 120°F (49°C) INITIAL POOL TEMPERATURE

Figure 5-48. Complementary Cumulative Probability Density Distribution Function - Multicell Effects on Chugging Period

*Proprietary information deleted

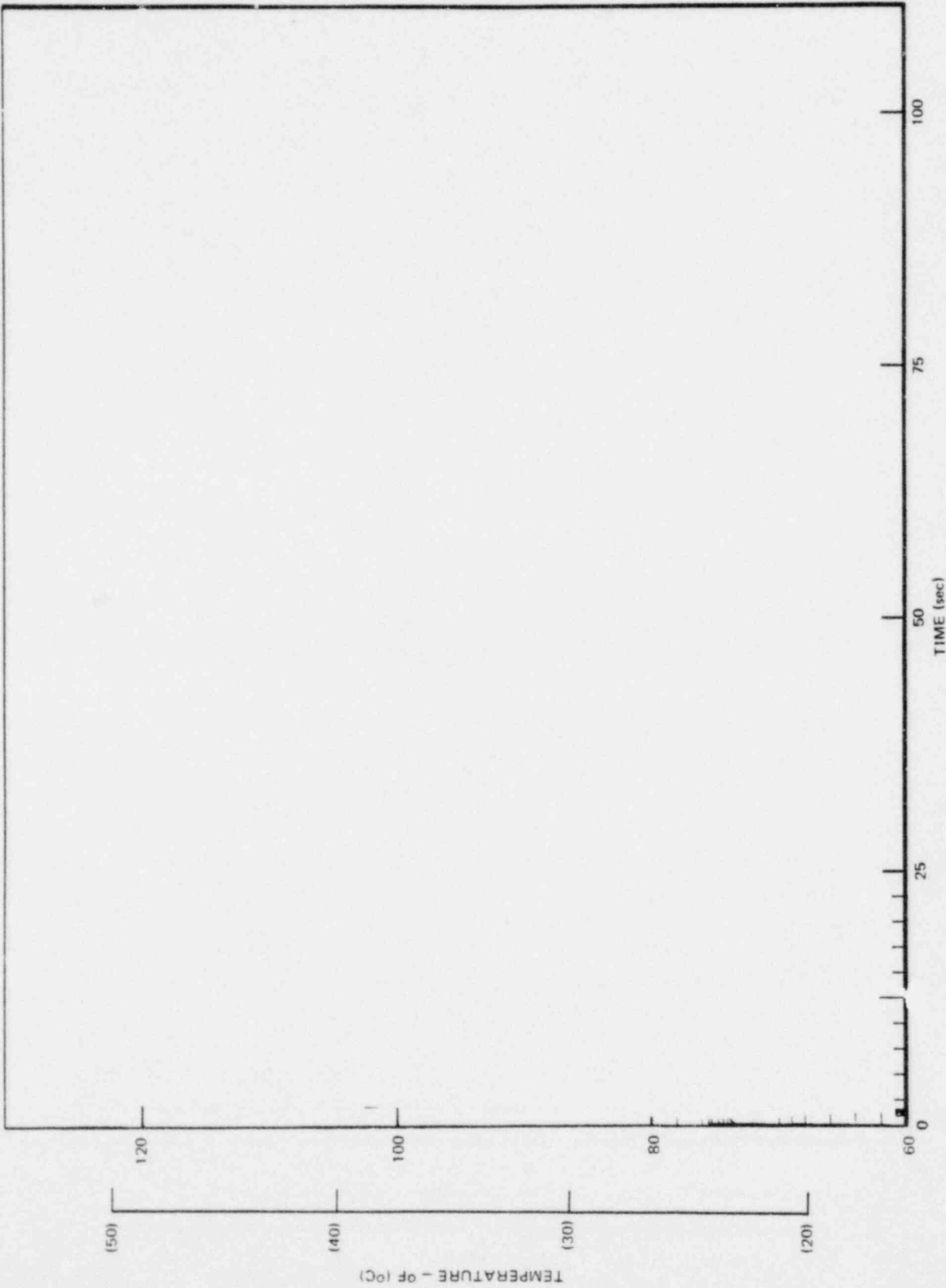


Figure 5-49. Average Pool Temperature - Time Histories, Run 3, West Cell, X = 2

*Proprietary information deleted

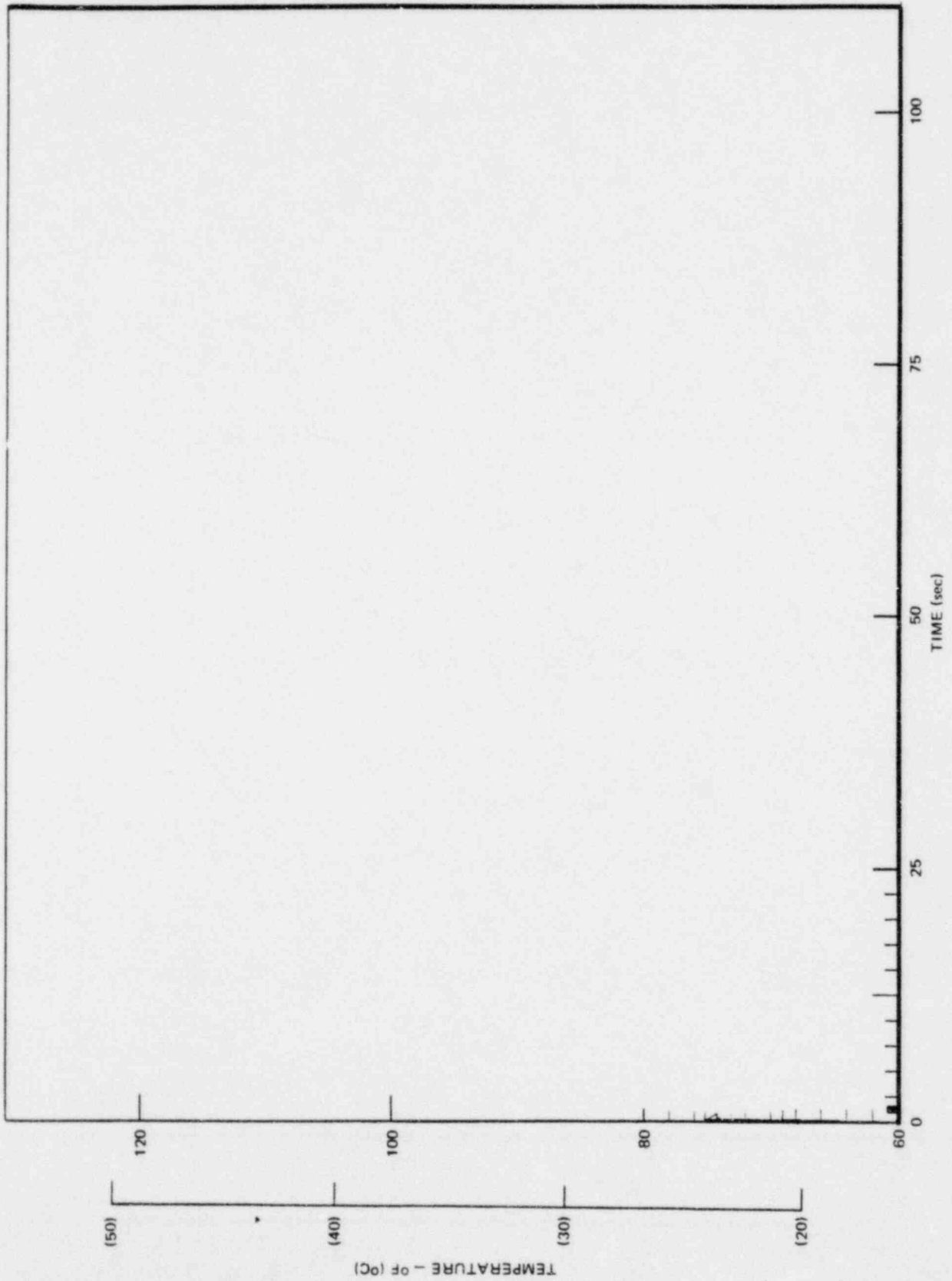


Figure 5-50. Average Pool Temperature - Time Histories, Run 3, West Cell, $\bar{X} = 4$

*Proprietary information deleted

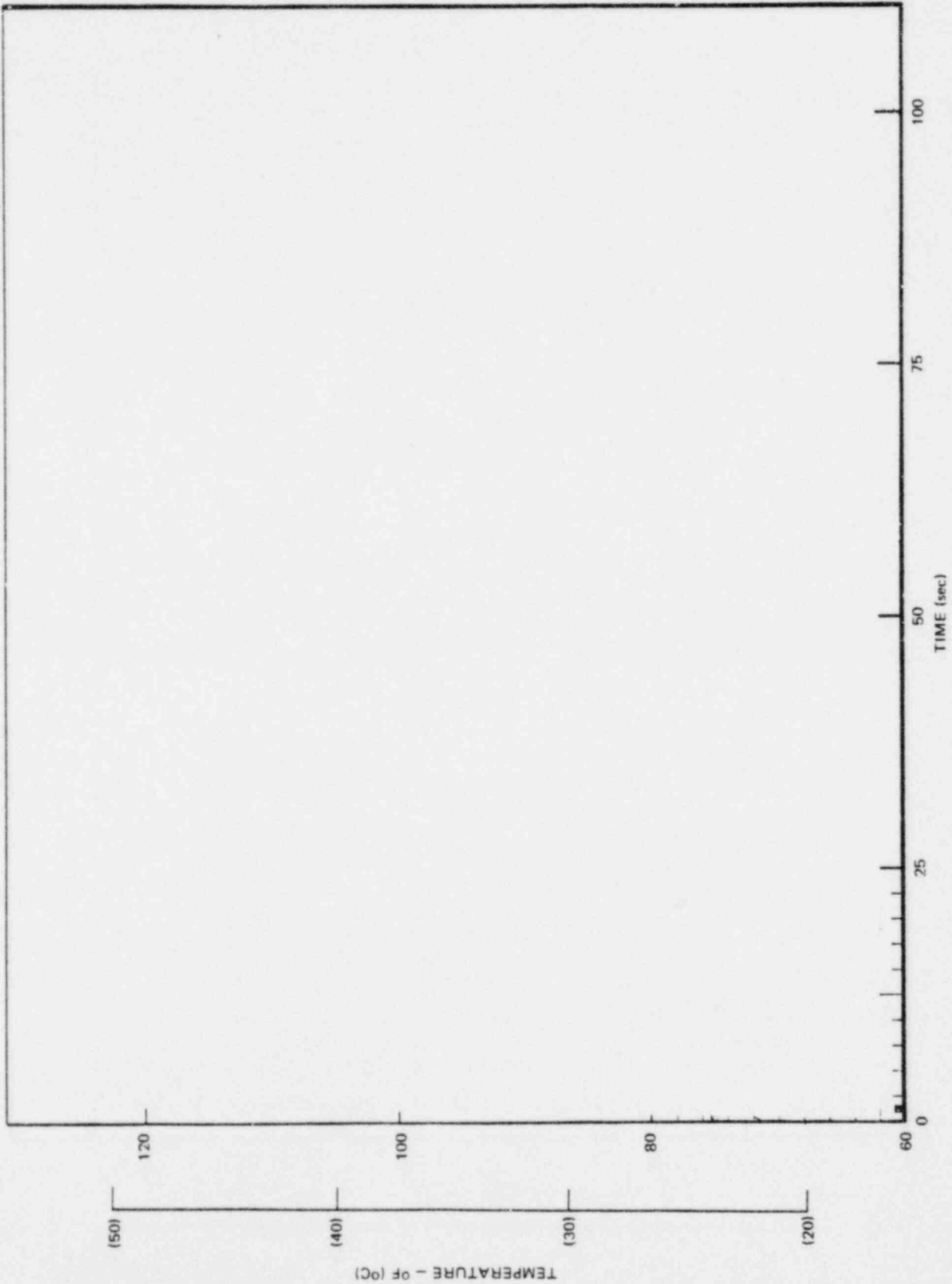


Figure 5-51. Average Pool Temperature - Time Histories, Run 3, Center Cell, X = 2

*Proprietary information deleted

*

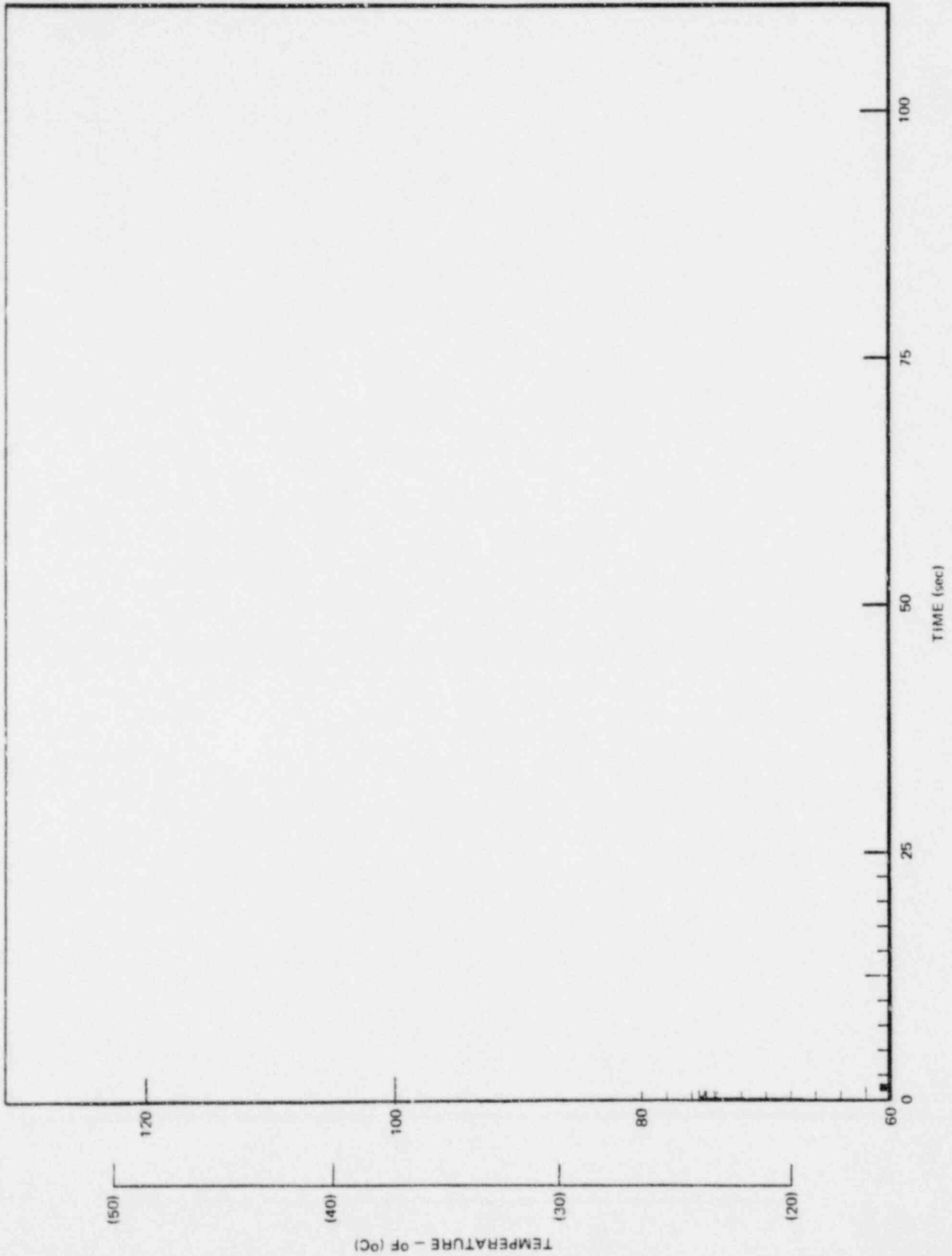


Figure 5-52. Average Pool Temperature-Time Histories, Run 3, Center Cell, X = 4

*Proprietary information deleted

*

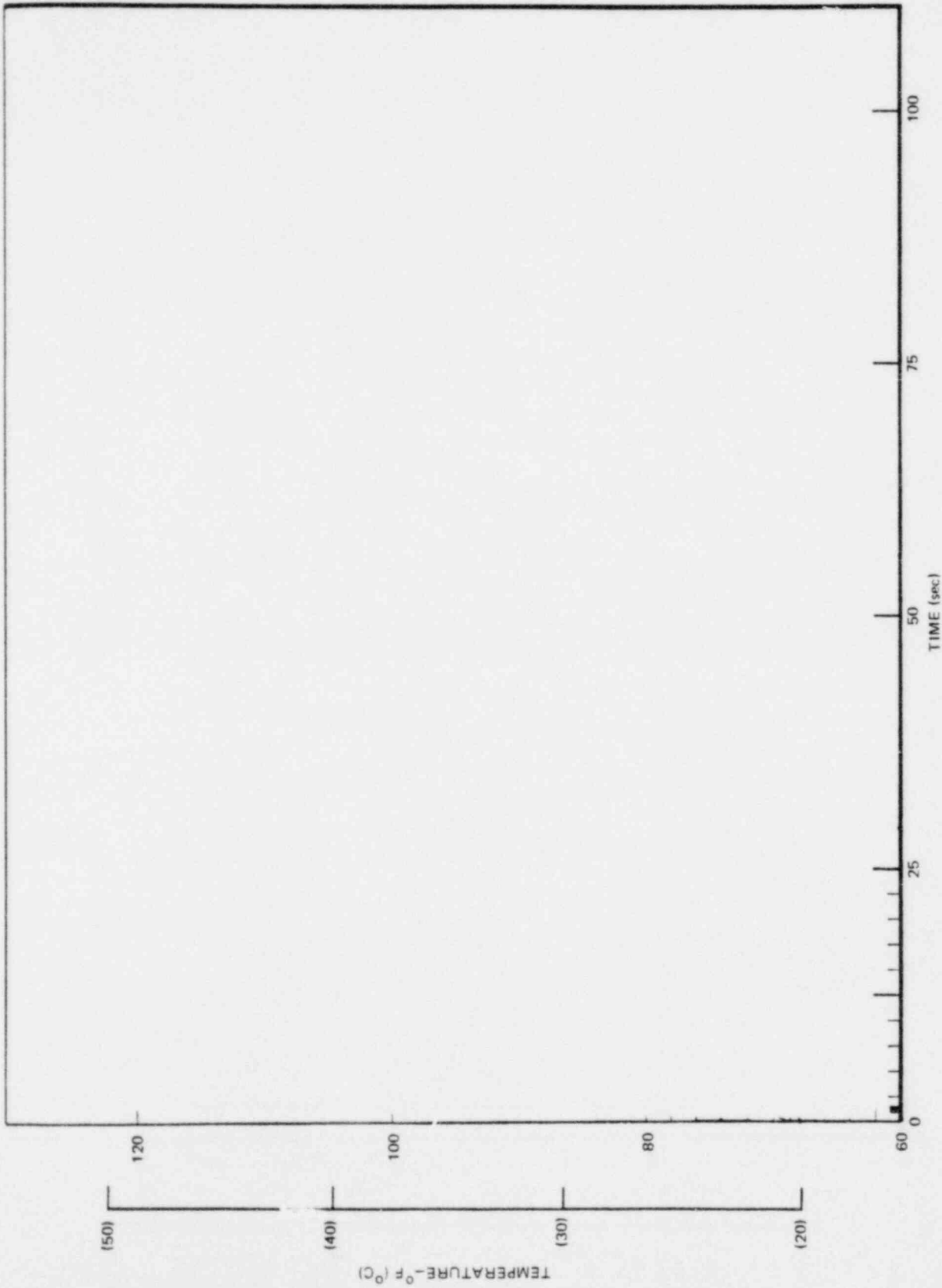


Figure 5-53. Average Pool Temperature-Time Histories, Run 3, East Cell, X = 2

*Proprietary information deleted

*

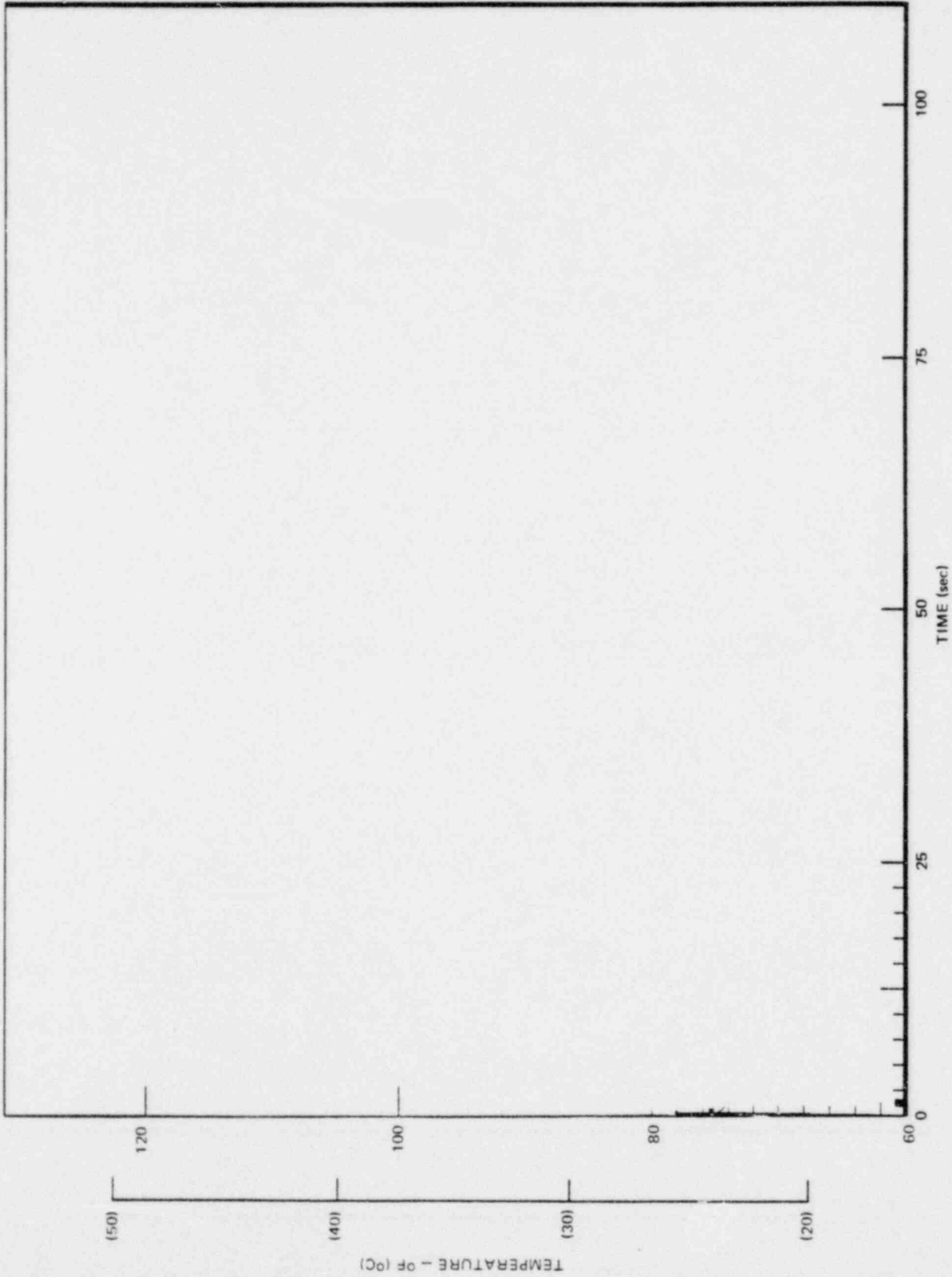
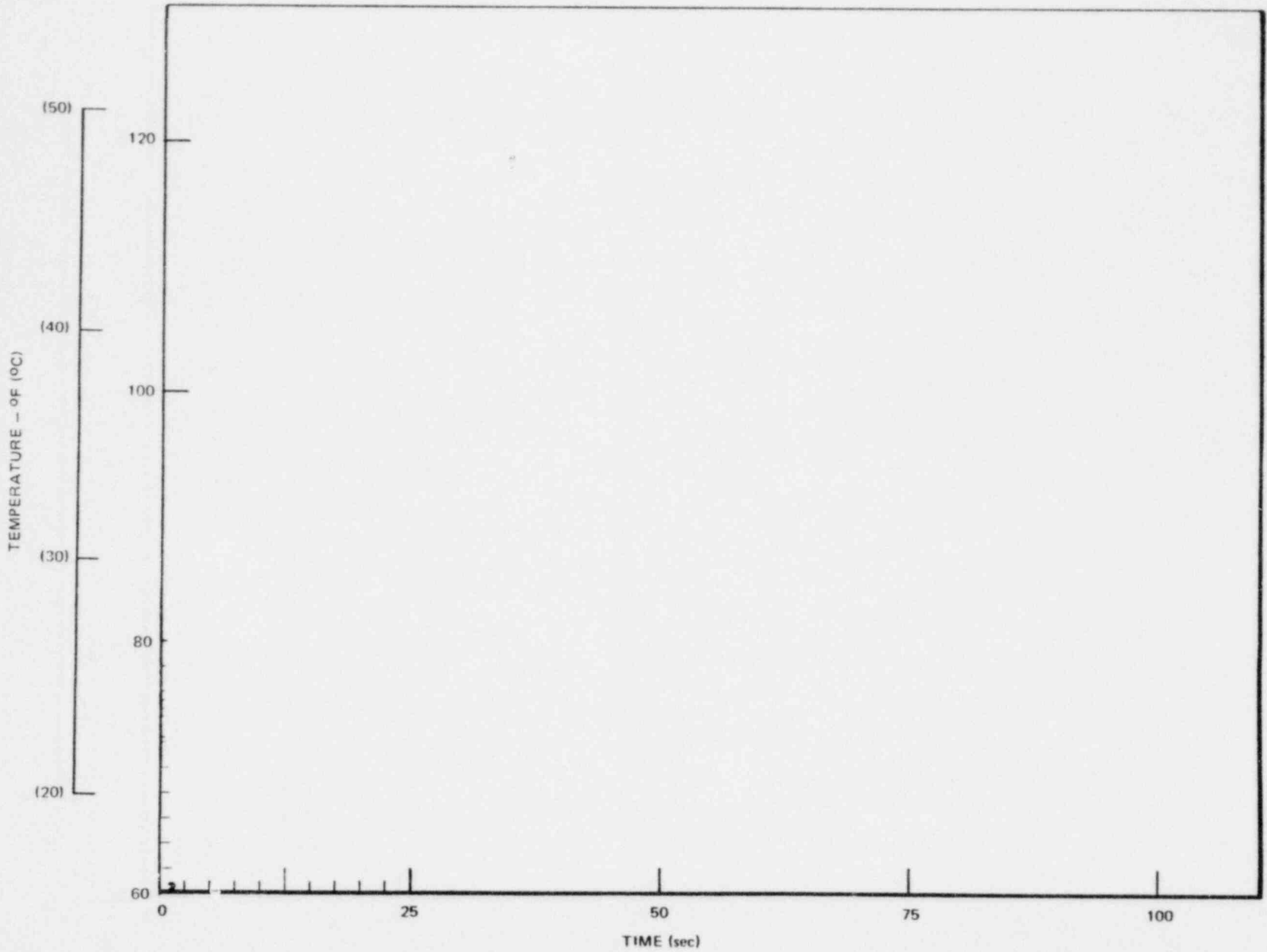


Figure 5-54. Average Pool Temperature-Time Histories, Run 3, East Cell, X = 4

*Proprietary information deleted

5-81



NEDO-24720

Figure 5-55. Average Pool Temperature-Time Histories, Run 3, Between Center and West Cell, X = 2

*Proprietary information deleted

*

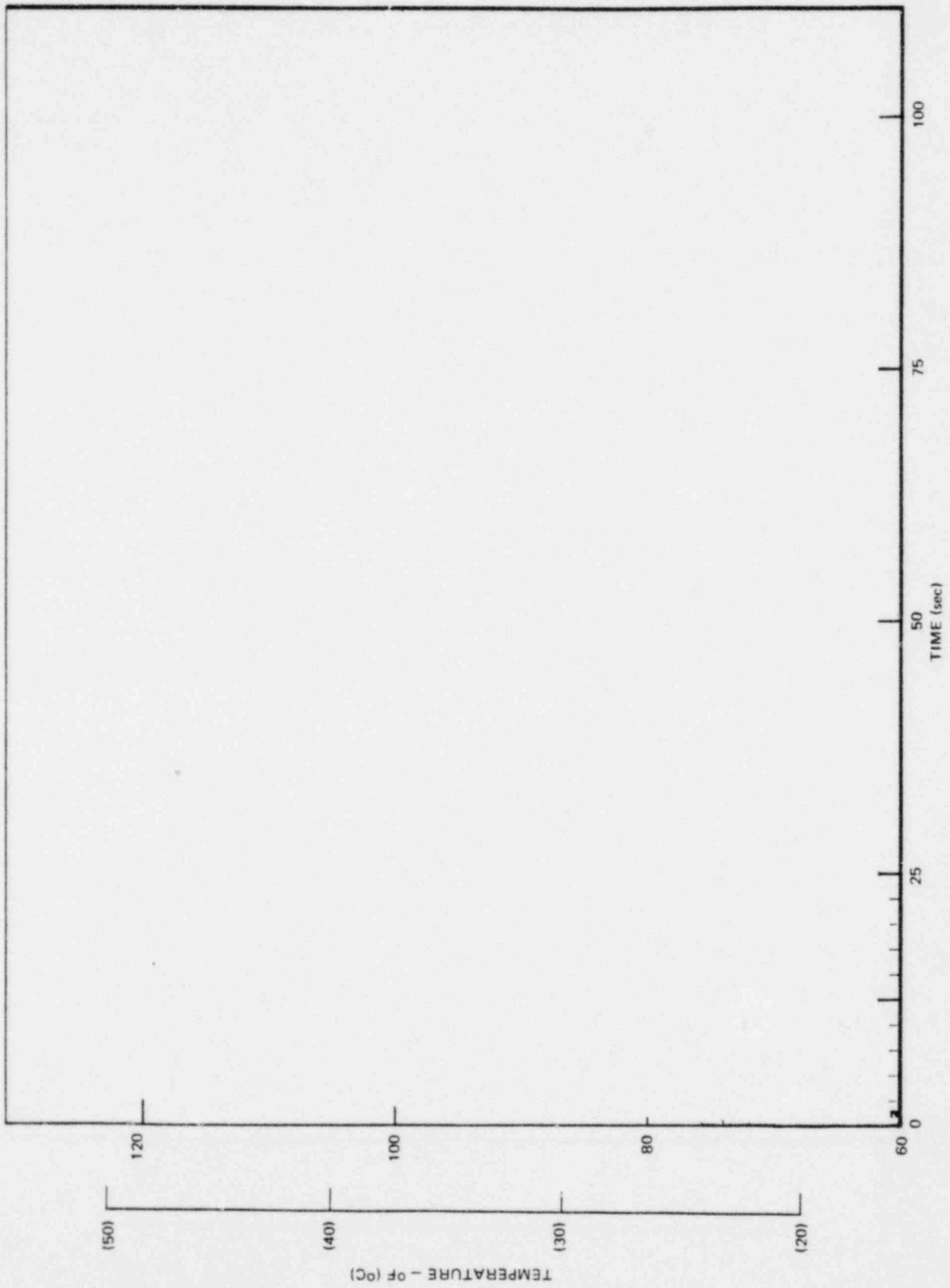


Figure 5-56. Vertical Average Pool Temperature-Time History, Run 3

*Proprietary information deleted

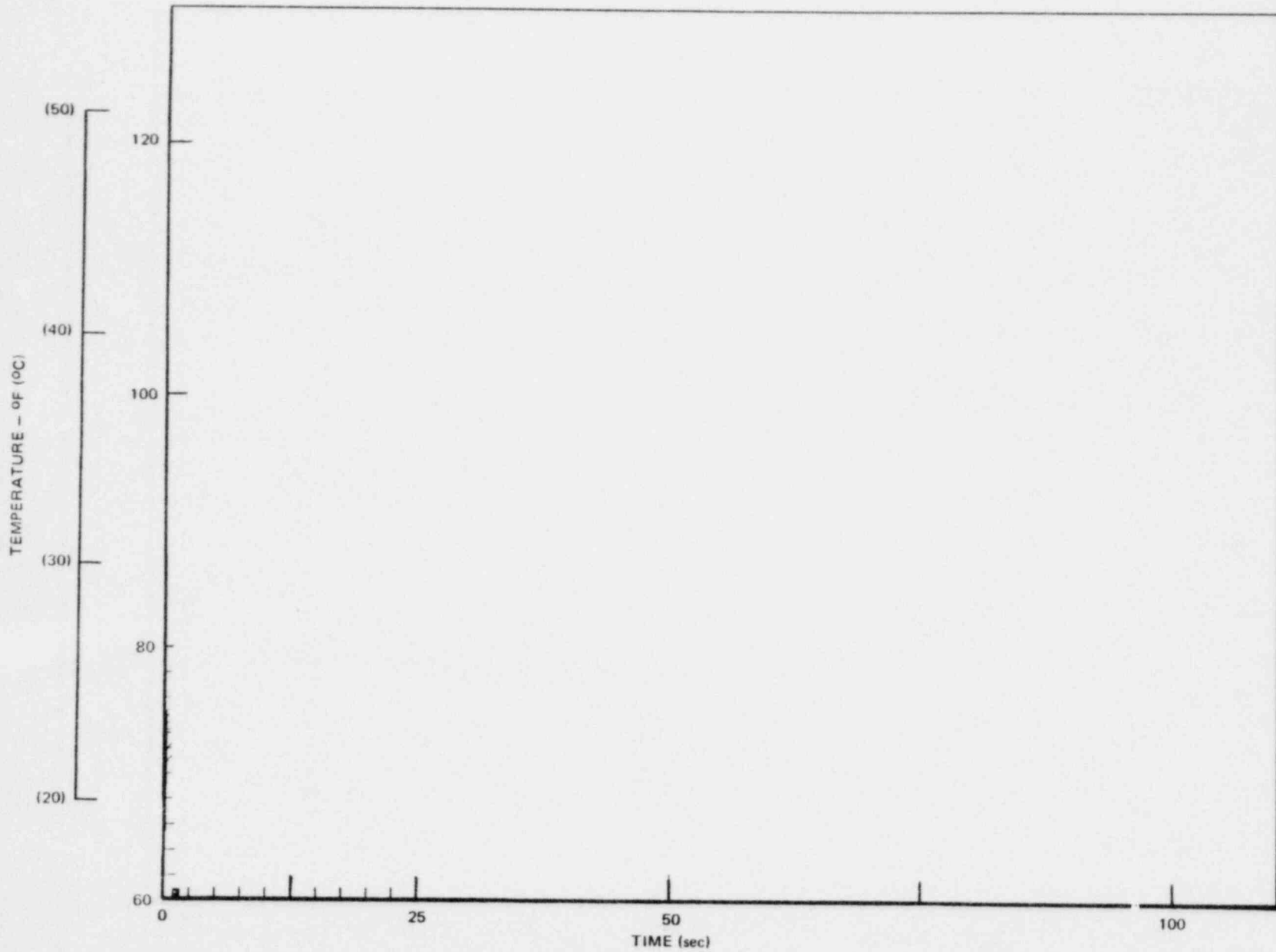
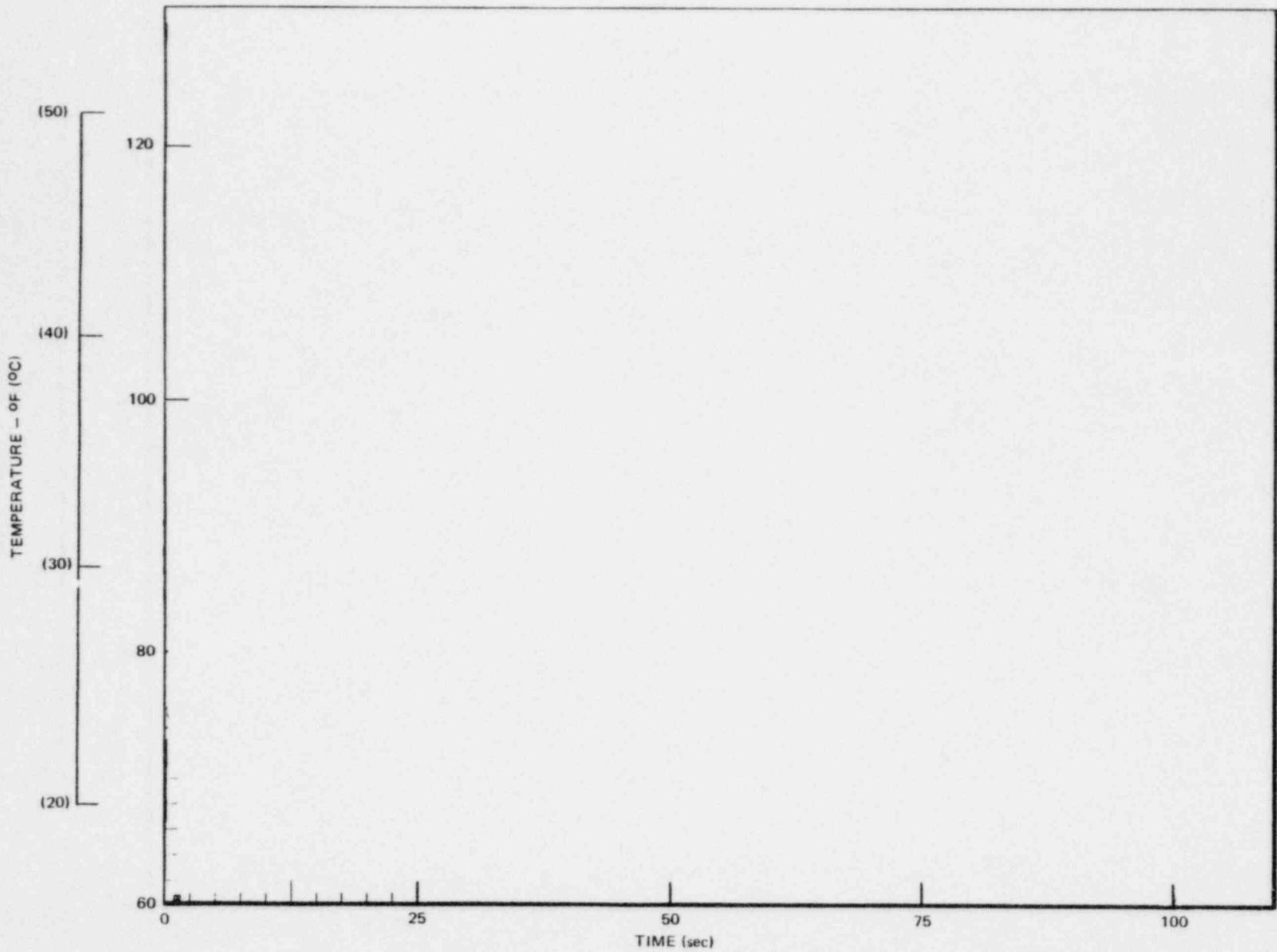


Figure 5-57. Horizontal Average Pool Temperature-Time History, Run 3, X = 2

5-84



NEDO-24720

Figure 5-58. Horizontal Average Pool Temperature-Time History, Run 3, X = 4

*Proprietary information deleted

*

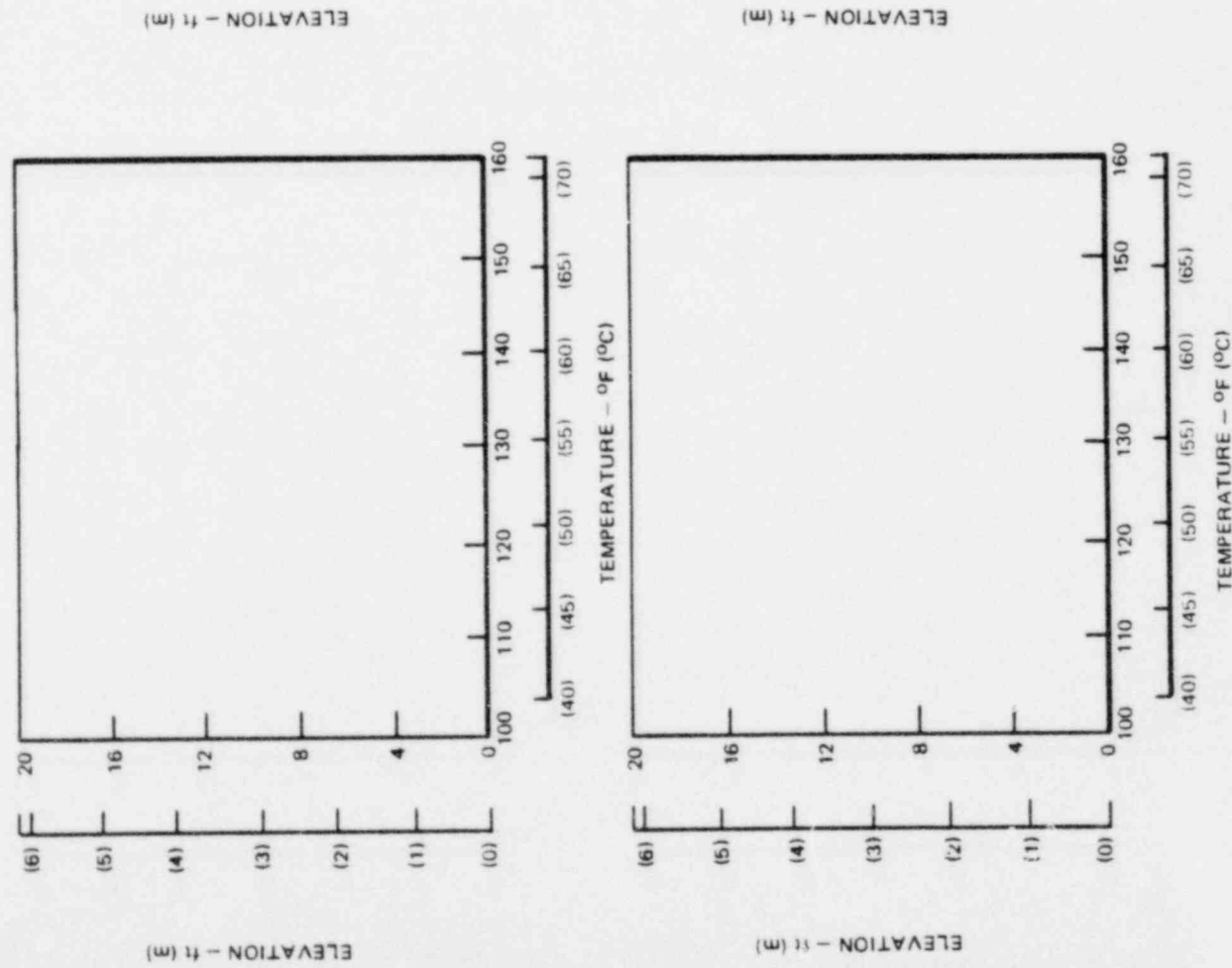
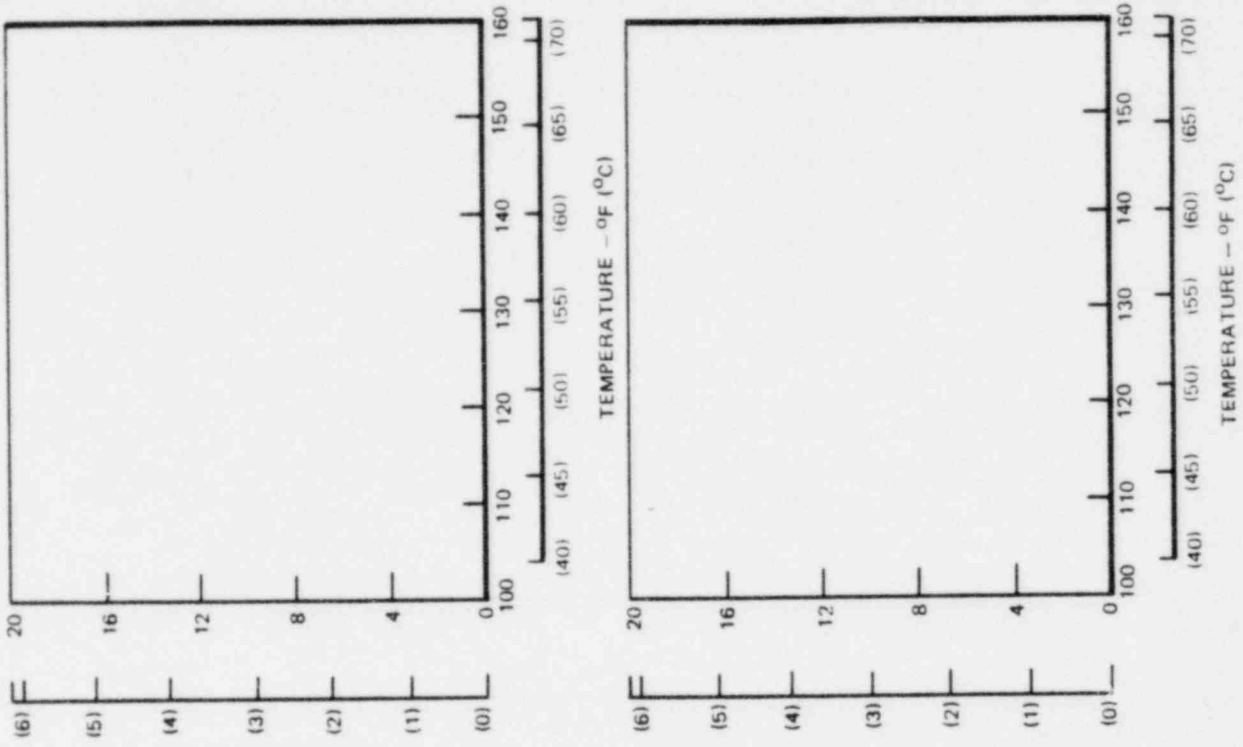


Figure 5-59. Three-Cell Pool Temperature Profile, Run 4

*Proprietary information deleted

*

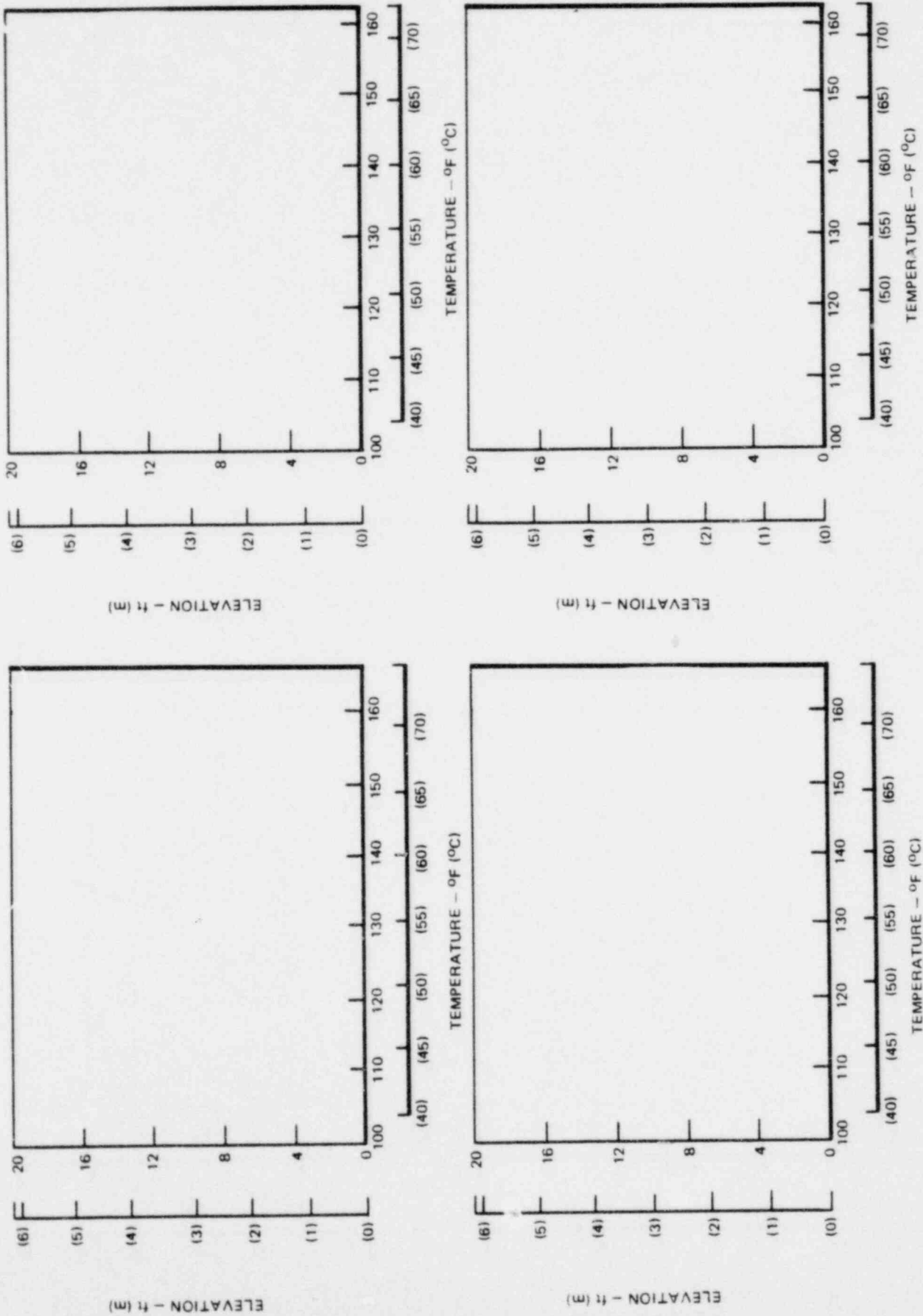


Figure 5-60. Three-Cell Pool Temperature Profile, Run 4

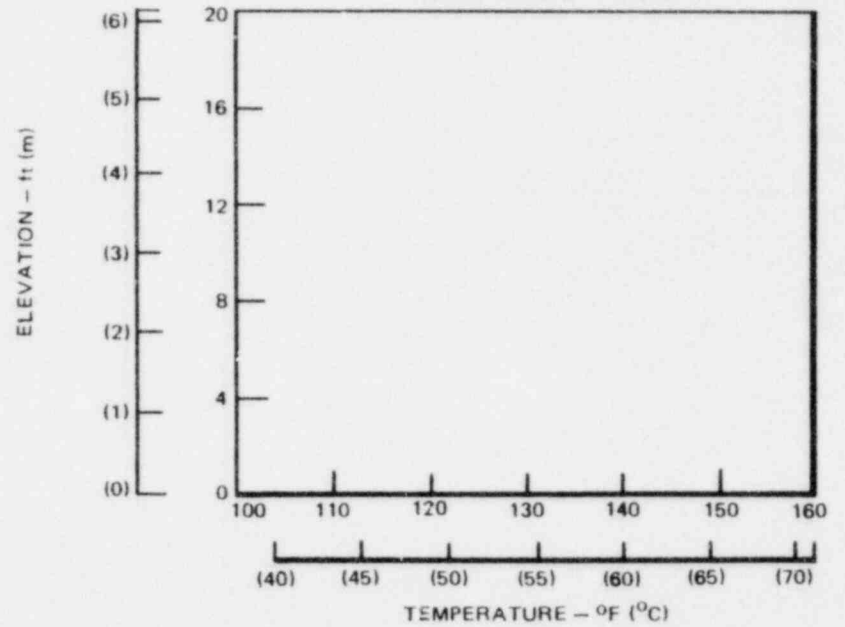
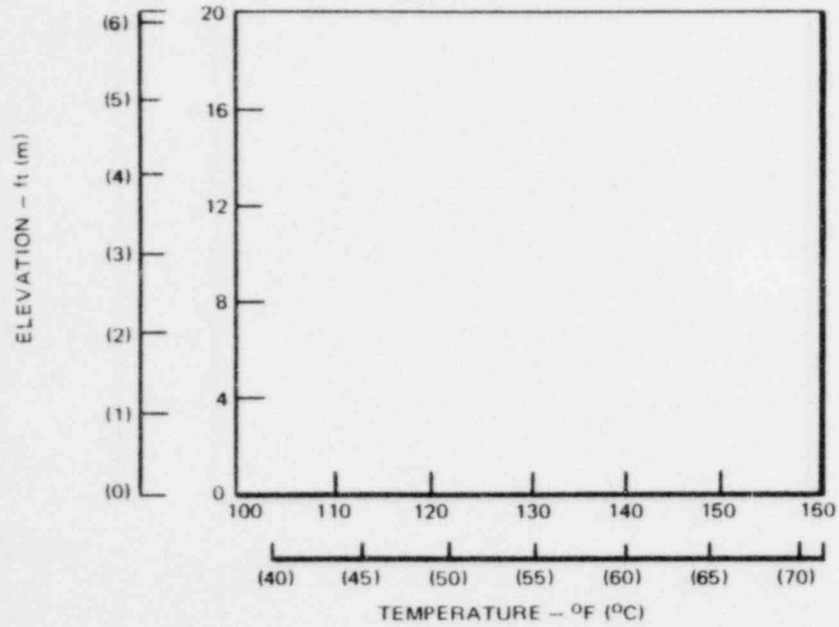
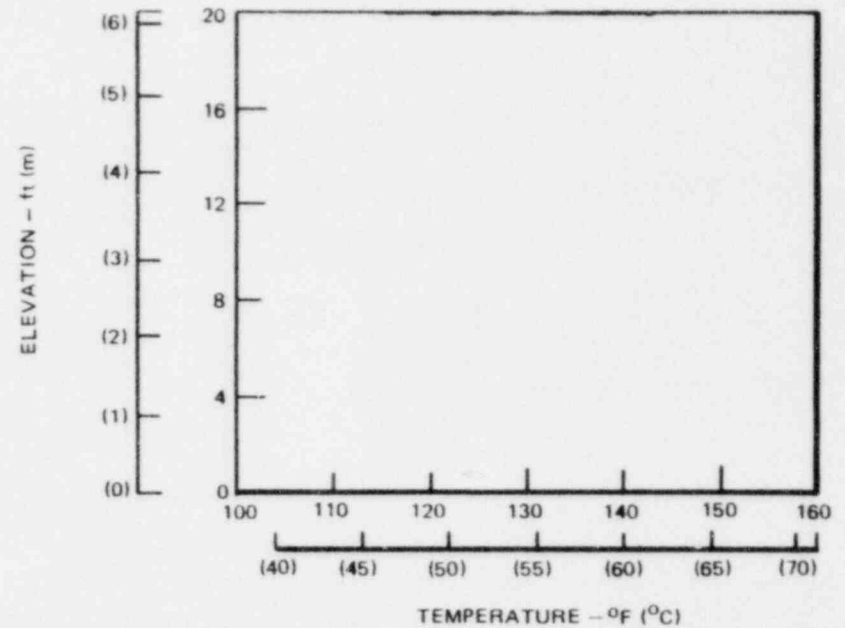
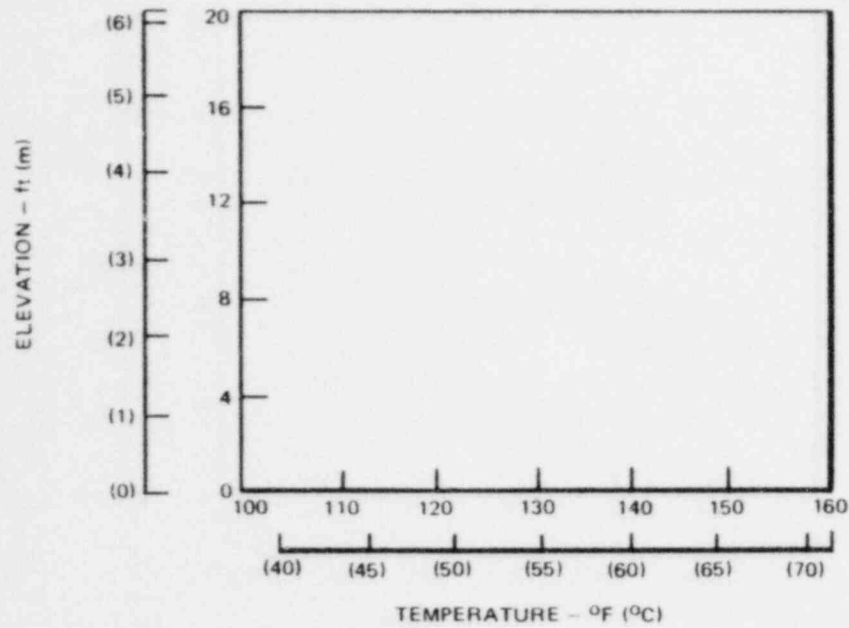


Figure 5-61. One and Two Cell Temperature Profile, Run 12

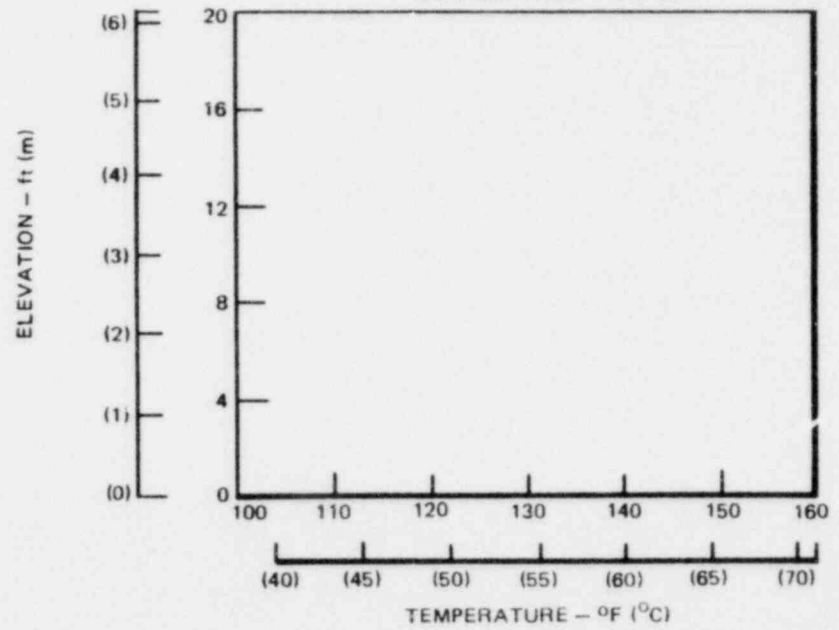
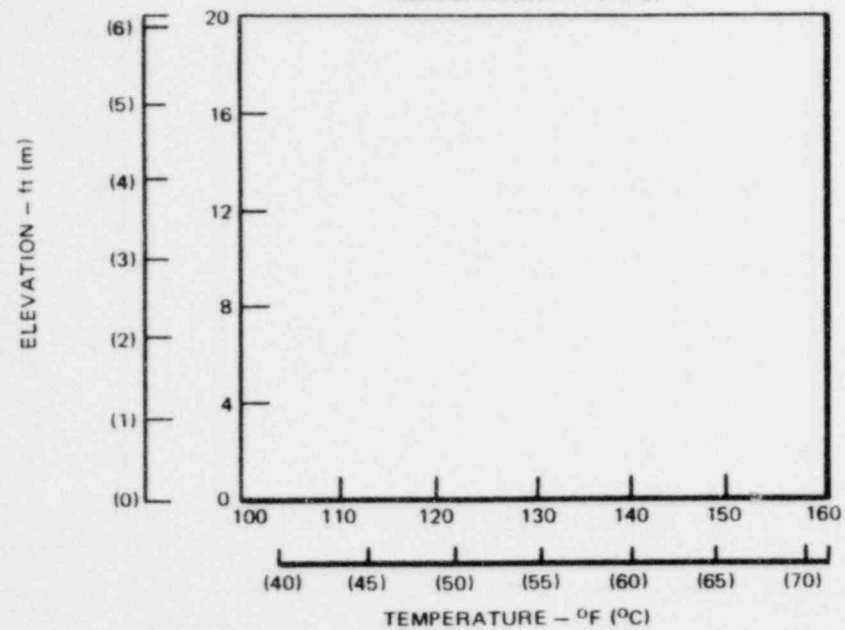
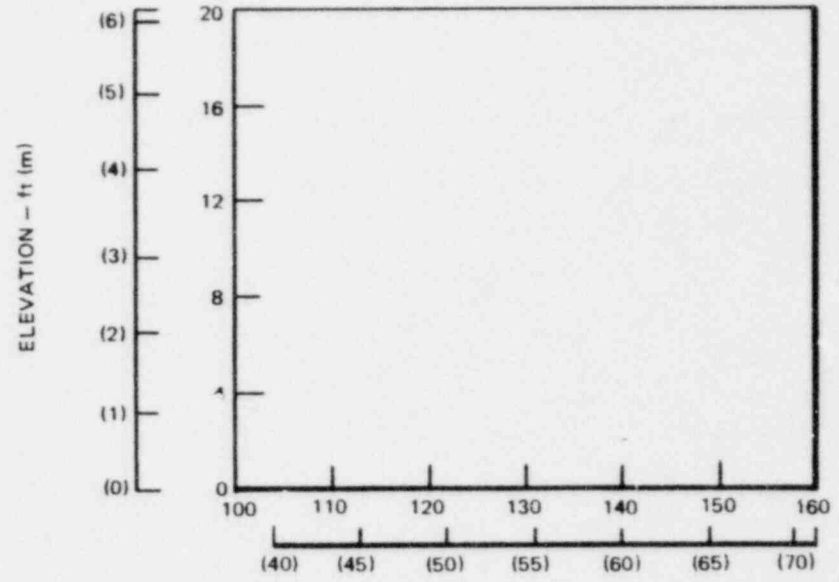
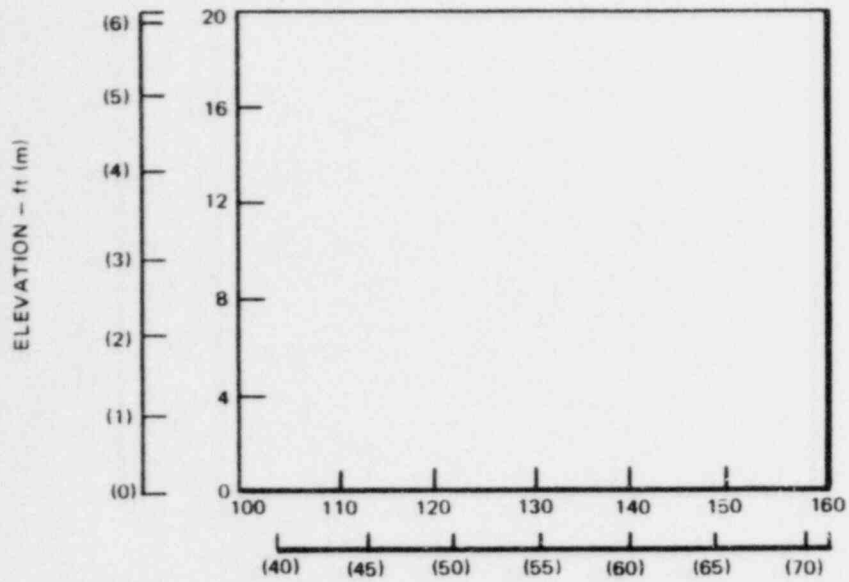


Figure 5-62. One and Two Cell Pool Temperature Profile, Run 12

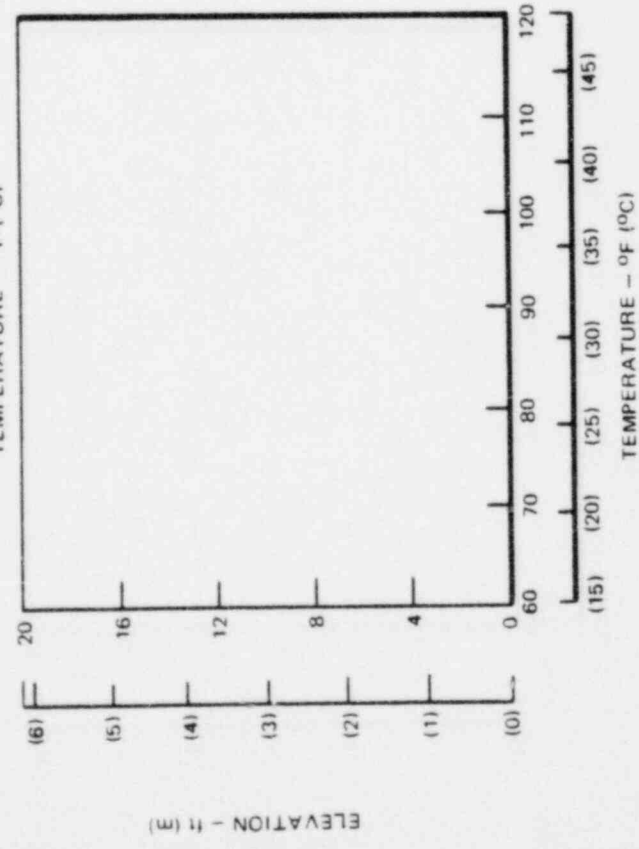
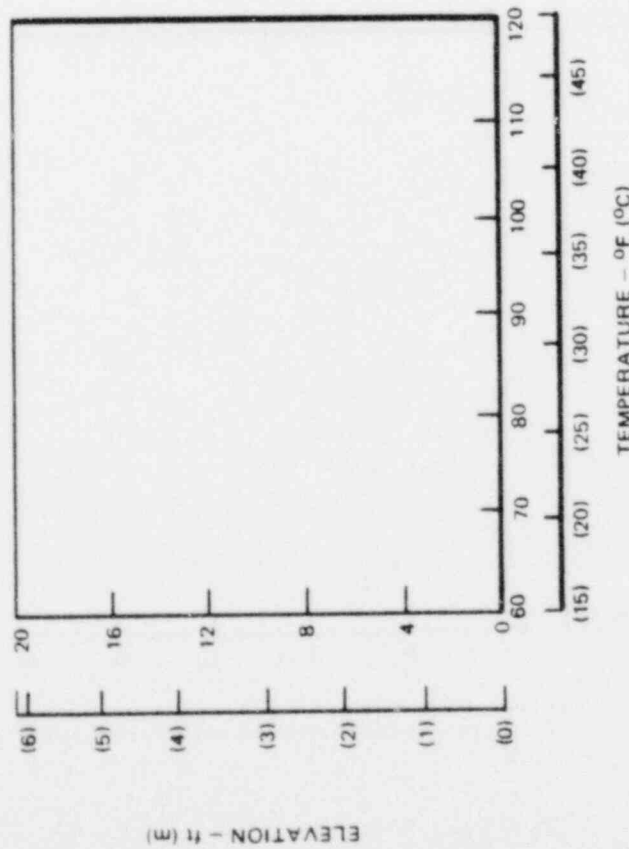
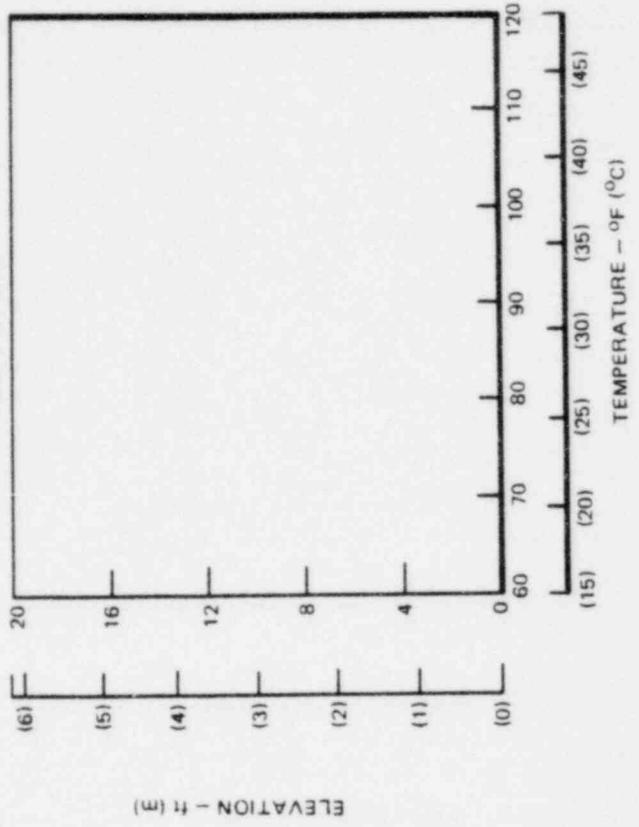
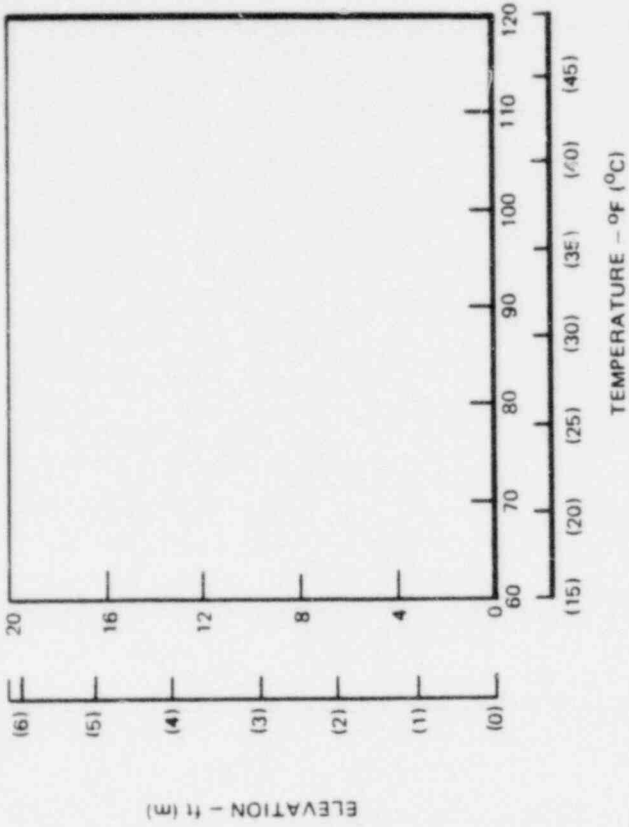


Figure 5-63. Pool Temperature Profile Comparison

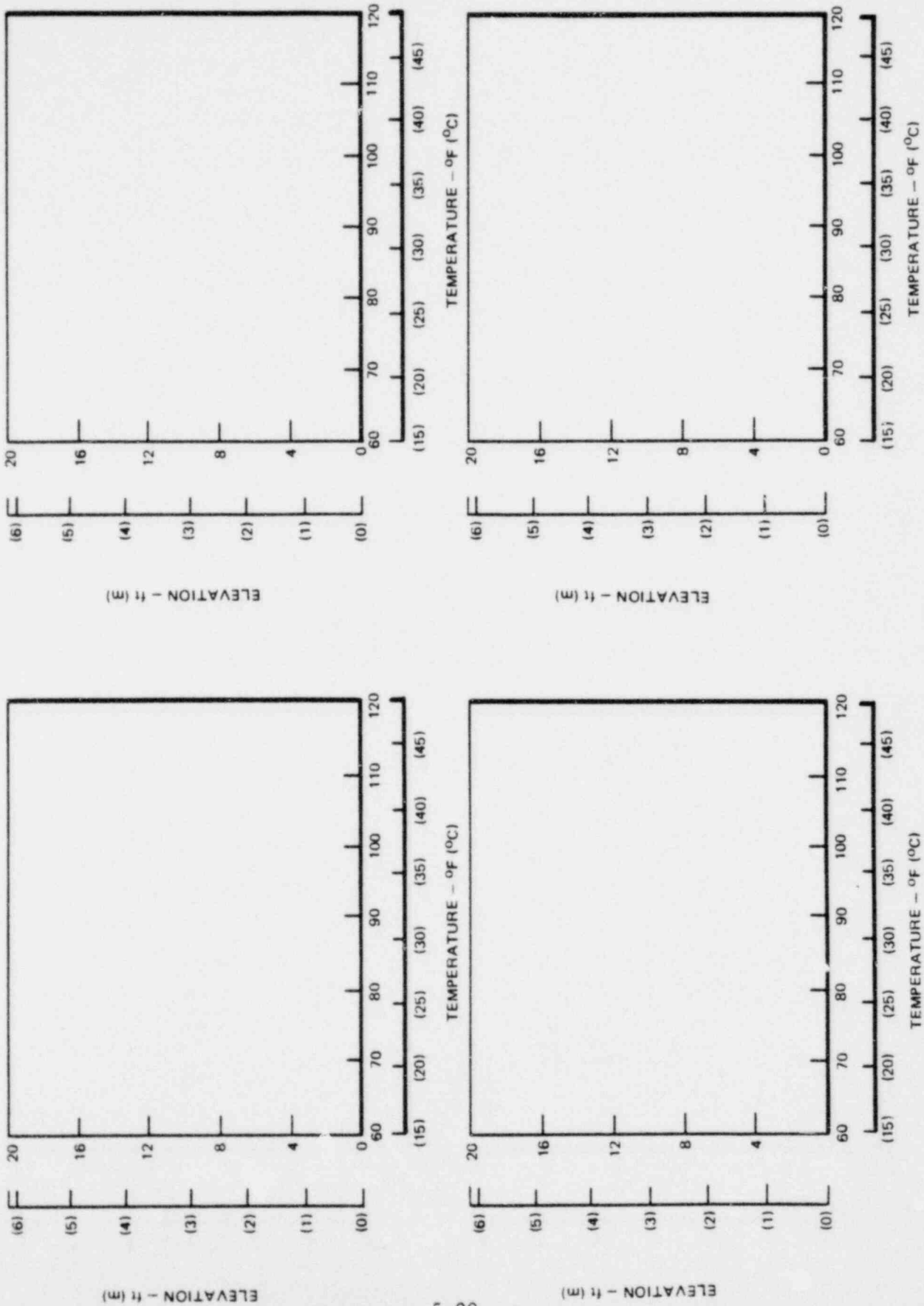


Figure 5-64. Pool Temperature Profile Comparison

6. REFERENCES

1. L. L. Myers, T. R. McIntyre, and R. J. Ernst, "Mark III Confirmatory Test Program, Phase I - Large-Scale Demonstration Test, Test Series 5701 through 5703," NEDM-13377, October 1974.
2. W. J. Bilanin, "The General Electric Mark III Pressure Suppression Containment System Analytical Model," General Electric Co., NEDO-20533, June 1974.
3. T. R. McIntyre and L. L. Myers, *Fifth Quarterly Progress Report: Mark III Confirmatory Test Program*, General Electric Co., NEDO/E-20550, and Supplement 1, Class III, July 1974.
4. A. M. Varzaly, W. A. Grafton, and D. S. Seely, *Mark III Confirmatory Test Program: Full Scale Condensation and Stratification Phenomena, Test Series 5707*," NEDO/E-28153-P, August 1978.
5. R. J. Ernst, T. R. McIntyre, L. L. Myers, and J. E. Torbeck, "Mark III Confirmatory Test Program; One-Third Scale Three-Vent Tests; Test Series 5801 through 5804," General Electric Co., NEDO/E-13407-P, May 1975.
6. T. R. McIntyre, L. L. Myers, J. E. Torbeck, and R. J. Booker, "Mark III Confirmatory Test Program; One-Third Scale Three-Vent Air Tests, Test Series 5806," General Electric Co., NEDO/E-13435-P, October, 1975.
7. T. R. McIntyre, W. J. Bilanin, M. A. Ross, and J. E. Torbeck, "Mark III Confirmatory Test Program; One-Third Scale Pool Swell Impact Tests; Test Series 5805," General Electric Co., NEDO/E-13426-P, August 1975.
8. A. M. Varzaly, W. A. Grafton, H. Chang, and M. K. Mitchell, "Mark III Confirmatory Test Program: $1/\sqrt{3}$ Scale Condensation and Stratification Phenomena, Test Series 5807," General Electric Co., NEDO/E-21596-P, March 1977.
9. R. E. Kingston, "Mark III Confirmatory Test Program $1/9$ Area Scale Multivent Pool Swell Tests (Test Series 6002)," General Electric Co., NEDO/E-24648-P, May 1979.
10. G. W. Burnette, D. W. Danielson, and K. A. Nilsson, *BWR Blowdown Heat Transfer Program Task C-4 Report, Preliminary System Design Description of Two-Loop Test Apparatus - Rev. 1*, General Electric Co., GEAP-13276-1, November 1973.

Appendix A

DRYWELL AIR-CONTENT MEASUREMENTAIR SAMPLING SYSTEM

The Steam-Air Ratio Sampling System consists of a sample exhaust manifold with five sample chambers as shown schematically in Figure A-1, and a time-sequence controller for sequential sampling. The time-sequence controller may be adjusted to vary the time of initiation and duration of sampling for each sample chamber. All sample chambers are evacuated during preparation for a pressure suppression test. The initiation of the pressure suppression process activates the time-sequence controller. The sequence of events starting with the first sample chamber include closing the vacuum isolation valve, opening and closing the steam purge valve, opening the cooling water valve, opening and closing the sampling valve, and closing the cooling water valve. At the completion of the pressure suppression test, the sample chamber isolation valves are manually closed and the sample chamber removed from the sample exhaust manifold. The sample pressure, temperature and volume of condensed vapor are measured and recorded for each sample chamber. Knowing the initial volume of the sample chamber in conjunction with these measurements, the steam-air ratio can be deduced.

TEST PROCEDURE

All air sample measurements in Test Series 6003 were conducted in accordance with the Test Facility Operations "Air Sampler System Operating Procedure" TOPBC Rev. 0. This procedure covers all aspects of air sampling including pretest preparation, operating procedure, and post-test procedure.

DATA REDUCTION AND UNCERTAINTY ANALYSIS

The sample air mass was calculated by assuming behavior as an ideal gas. The initial gas mass (M_{A_1}), which was the residual gas (if any) in the evaluated chamber was calculated from:

$$M_{A_i} = \frac{P_i V}{RT} \quad (A-1)$$

where P_i is the initial evacuated chamber pressure, V the chamber volume, T the gas temperature, and R the gas constant for air. The final gas mass (M_{A_f}) was calculated from

$$M_{A_f} = \frac{V - v_f \cdot M_T}{\left(\frac{RT}{P} - v_f\right)} \quad (A-2)$$

where v_f is the specific volume of the condensate, M_T the total mass in the chamber, V the chamber volume, T the chamber temperature, and P the final chamber pressure. The total mass (M_T) in the chamber (vapor condensate and noncondensable gas) is measured by using a beam balance. Using the desired air mass quantities and the measured total mass quantity, the ratio of air mass to the total mass in the drywell gas sample is calculated from

$$\frac{M_A}{M_T} (\%) = \left(\frac{M_{A_f} - M_{A_i}}{M_T} \right) \times 100 \quad (A-3)$$

Uncertainties in the calculated and measured mass quantities are due to temperature, pressure and mass measurement instrument uncertainties. Additional uncertainties result from inaccuracy in the sample chamber volume determination and from uncertainty in the specific volume of the sub-cooled liquid which is due to uncertainty in the liquid temperature measurement.

The uncertainty analysis conducted for the air sample measurements utilized the "scalar error" formula from the reference* to combine the independent error. The uncertainty dm , in a measured or desired quantity, m , that in a function of n independent variables x_i is calculated from

*S.J. Kline and F.A. McClintock, Uncertainties on Single Sample Experiment, Mech. Engineering, January 1953.

$$dm = \pm \left[\sum_{i=1}^n \left\{ \left(\frac{\partial m}{\partial x_i} \right) dx_i \right\}^2 \right]^{1/2} \quad (A-4)$$

where dx_i represents the known uncertainty in the independent variables x_i . The derivatives $\partial m/\partial x_i$ are obtained from the functional relationship between m and x_i . The magnitudes of uncertainty in the independent variables used for this analysis is tabulated in Table A-1.

TEST RESULTS

The drywell air content was determined at various time intervals from the five sample measurements in each test. The air content, including the uncertainty in the air content, and the sample interval are tabulated in Table A-2 and displayed in Figure A-2. The time scale in this figure represents the average sample time interval from the time of blowdown initiation. Note that Run 4, although tabulated in the above table has been omitted from the above figure because it is considered as bad data.

Evidence shows there is substantial variation in air content from one test run to another, and there are apparent inconsistencies in air content within a test run. Because of the turbulent mixing within the drywell, the vapor-air mixture could be expected to be homogeneous and, therefore, the air content should diminish as the blowdown progresses.

Although this appears to be the case for some of the test runs, it is not a typical trend for at least half the test runs. In these test runs, the air content may be lower in a sample when compared with a sample obtained later

after initiation of blowdown. There is no apparent phenomenological explanation for the above trend; therefore, the only plausible explanation is some form of deficiencies in the air sampling system or possibly insufficient accuracy in the sample measurement or both of the above. It is evident from the uncertainty analysis that the sample variations exceed the calculated uncertainty limits. This suggests that the measured sample variation is not entirely due to measurement inaccuracy.

An analysis was performed to evaluate the effect of the free volume in the sample solenoid valve (valves S-1 to S-5 shown in Figure A-1) on the sample measurement. If the above volume is entirely occupied by compressed stagnant air then an upper limit error would result. A lower limit error will result if the volume is occupied by condensed vapor.

This analysis indicated that the effects of the valve free volume alone does not fully account for the variation in the air sample. In conclusion, the observed variation in the air sample is probably due to a combination of deficiencies in the air sampling system (including sample probe, valving and sample chambers) and measurement inaccuracies.

Table A-1
UNCERTAINTY IN INDEPENDENT VARIABLES

<u>Error Source</u>	<u>Maximum Uncertainty</u>	<u>Data Source</u>
1. Temperature		
2. Pressure		
3. Mass		
4. Total volume		
5. Specific Volume of subcooled liquid		

Note 1.

*Proprietary information deleted

Run No.	<u>Sample 1</u>			<u>Sample 2</u>			Air Cont MA/MT (%)
	Air Content MA/MT (%)	Uncertainty in MA/MT (%)	Air Sample Interval (sec)	Air Content MA/MT (%)	Uncertainty in MA/MT (%)	Air Sample Interval (sec)	
1							
2							
3							
4							
5							
6							
7							
8							
9							
10							
11							
12							

*Proprietary information deleted

le A-2

UREMENT SERIES 6003 TEST

	<u>Sample 3</u>			<u>Sample 4</u>				
ent	Uncertainty	Air	Air	Uncertainty	Air	Air	Uncertainty	Sample
MT	in	Sample	Content	in	Sample	Content	in	Interval
	MA/MT	Interval	MA/MT	MA/MT	Interval	MA/MT	MA/MT	Interval
	(%)	(sec)	(%)	(%)	(sec)	(%)	(%)	(sec)

*

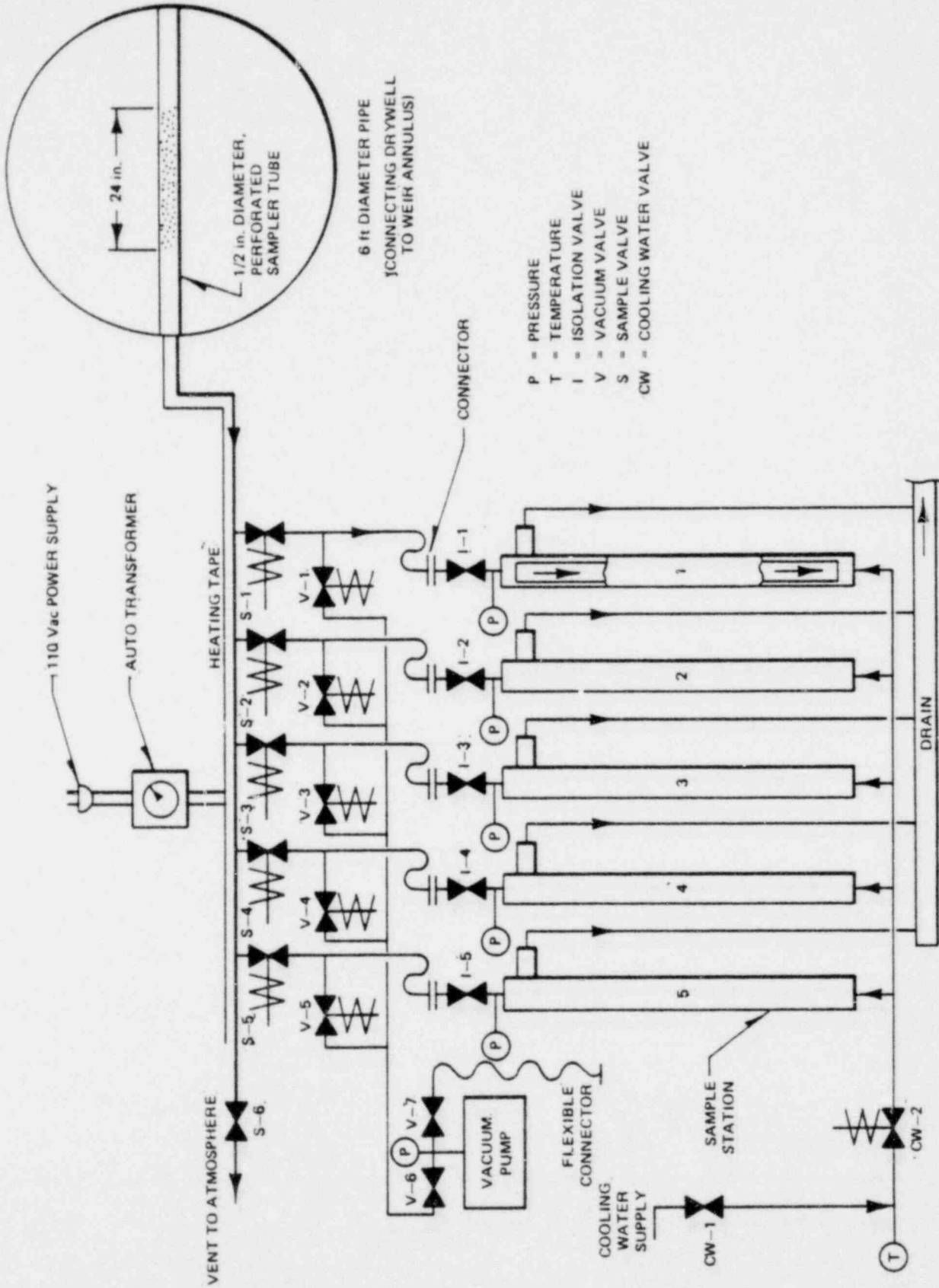


Figure A-1. Steam-Air Ratio Sampler System

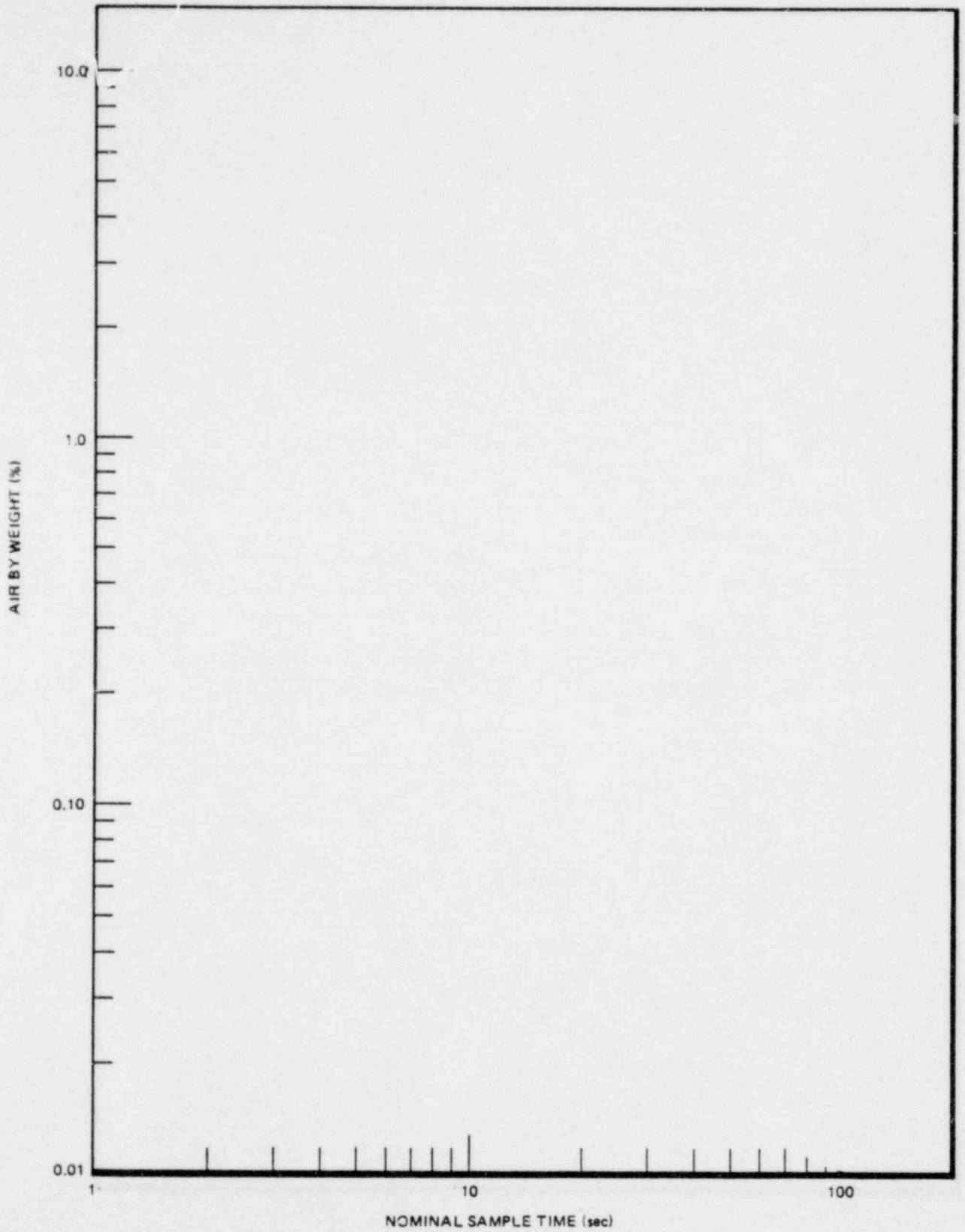


Figure A-2. Measured Air Content, Test Series 6003

*Proprietary information deleted

APPENDIX B
MEASUREMENT UNCERTAINTIES

B.1 INTRODUCTION

The static errors in the prime measurements (e.g., pressure, accelerometer, temperature) are basically due to three sources:

- a. General instrument errors (including thermal errors, hysteresis nonlinearity, repeatability, etc.).
- b. Data acquisition system characteristics (including digitizing, response, signal conditioning, etc.).
- c. Analog record and playback errors (applicable to replay instrumentation only).

To assess the relative magnitude of each of these effects, each prime measurement will be examined on the basis of the applicable error sources. However, common sources pertinent to the measurements, such as data acquisition system characteristics and analog record errors are examined on a generic basis.

The method used to combine independent errors is based on the "scalar error" formula from Reference B-1.* The uncertainty dm is a measured or derived quantity, m is a function of n independent variables, and x is calculated from:

$$dm = \pm \left[\sum_{i=1}^n \left| \left(\frac{\partial m}{\partial x_i} \right) dx_i \right|^2 \right]^{1/2} \quad (B-1)$$

where dx_i represents the known uncertainty in the independent variable x_i . The derivatives $\partial m / \partial x_i$ are obtained from the functional relationship between m and x_i .

*B-1 S.J. Kline and F.A. McClintock, "Uncertainties on Single Sample Experiments," Mechanical Engineering, January 1953.

B.2 DATA ACQUISITION SYSTEM

The test instrumentation measurement system is designed to a target standard of 0.1 percent of full-scale measurement accuracy. The actual measurement accuracy attainable varies with transducer type, calibration reference, signal conditioning used, and whether absolute or relative data are applicable. The best resolution of the system is one part in 4096, or about 0.025 percent of full scale, based on use of the 12-bit (plus sign) analog-to-digital converter.

Several design features were adopted in order to meet the design accuracy objective. First, quality transducers were obtained with characteristics of minimal nonlinearity, hysteresis, zero shift, and temperature sensitivity. The transducers have been carefully bench calibrated using 0.1 percent class pressure gauges and the excitation voltage and transducer output monitored with a 0.01 percent class digital voltmeter.

The signal conditioners for the transducers have individual channel excitation voltage power supplies and use remote voltage sensing (excitation voltage monitored at transducer location rather than instrument panel location). The remote voltage-sensing feature eliminates errors of about 1 percent as a function of cable length. The excitation voltage for each transducer is set at 10 volts using the 0.01 percent digital voltmeter.

Knowledge of the amplifier gain is required to determine the calibration, since the amplifier output is the parameter actually measured during test operation. Amplifier gain accuracy is ± 0.03 percent, and the excitation voltage accuracy is ± 0.05 percent of full scale.

The recording system's analog-to-digital conversion accuracy is about ± 0.01 percent of full scale. Therefore, the signal conditioning and recording contributes only about 0.06 percent of full-scale uncertainty based on Equation B-1.

B.3 ANALOG RECORD/PLAYBACK SYSTEM ERRORS

The analog-replay data acquisition procedures were designed to increase the sampling rate for selected data channels to allow expanded high resolution tracking capability. This procedure includes recording relatively unfiltered data, i.e. cut off set at 10 kHz, on the analog tape system, and replaying the data tape at a reduced tape drive speed back through the real time data acquisition system's amplifiers, filters, and multiplexer/digitizing equipment. In this manner, increased sampling rates are obtainable (final sampling rate employed was 312.5 microseconds per channel).

Information regarding analog record/playback accuracy is available from two sources. The primary and most comprehensive source is the calibration and performance records of the recorder. The second check is by a "common-instrument" correlation using simultaneous test data. This check essentially deals with those certain channels which are available simultaneously on the analog recorder and the real-time digitized output.

The calibration records give the general condition of the tape records for both record and playback operations. However, test-to-test shifts in the calibration of the recorder are sometimes incurred due to varying tape quality, dust accumulation on recorder heads, and operating time and temperature of the recorders. Generally, the test and data replay procedures minimize most of these problems. Furthermore, the large portion of the recorder's playback error is usually in the form of a voltage offset error. This is verified by examination of successive calibration records for the tape recorder units. These records indicate that the full scale voltage error (called the "span" error) is fairly constant and is about 5 percent of the input source signal level. Both data acquisition (digitizing) and data reduction procedures greatly reduce the offset errors in the data, leaving the span of deviation as the primary error source.

B.4 MEASUREMENT UNCERTAINTIES

Errors due to instrument characteristics, including thermal errors, hysteresis and linearity, etc., can be evaluated by utilizing the manufacturer's specification sheets, instrument calibration and performance sheets, and comparison of multiple simultaneous measurements, e.g., pressure and thermocouples. In most cases, however, it will become evident that only one of the three sources of error discussed in Subsection B.1 is usually dominant.

B.4.1 Temperature Measurements

Temperature (thermocouple) measurements were primarily limited by the basic thermocouple instrument accuracies. Generally, all thermocouple calibrations and checks are in place (as-installed) operations. Separate furnace tests are not used partly because of inherent errors involved where the thermal gradient location does not duplicate actual in-service conditions. Therefore, all checks also confirm operation of the reference junction and the computer data acquisition system channels utilized. Standard limits of error for the thermocouple measurements, as published by the Instrument Society of America (ISA), are considered acceptable. Calibration results are generally within the ISA nominal $\pm 4^\circ\text{F}$ ($\pm 2.2^\circ\text{C}$) limits of error quoted for the type J thermocouple used. Uncertainty in areas of highly redundant measurements (as in suppression) is effectively reduced to about $\pm 2^\circ\text{F}$ ($\pm 1.1^\circ\text{C}$). Dynamic response of this instrument in water has been shown to be quite good with a minimum of response lagging (see Reference B-2)*.

B.4.2 Level Measurements

The level (conductivity) probes were utilized to identify liquid/vapor interfaces during the tests. The probes generally have excellent response characteristics. Although the time constant (for 63 percent of final value) for the output is 2 ms, the time when the probe first became wet can be determined within a fraction of a millisecond. The primary uncertainties include location of the probe in the vents or pool, possible misorientation of the electrodes,

*G.W. Burnette, D. W. Danielson, and K.A. Nilsson, "BWR Blowdown Heat Transfer Program Task C-4 Report Preliminary System Design Description of Two-Loop Test Apparatus," GEAP-13276-1, November 1973.

and minimum scan time resolution. The probes were used mainly for vent and even annulus water level observations during the blowdown transient. On this consideration chugging periods, etc., are mainly dependent on the time resolution of the data acquisition system, particularly the size of the incremental time step utilized in the bounding value. The time steps utilized vary from 20 ms for the first 100 seconds of run time to 250 ms thereafter. This is very small compared to the chugging start time or water level oscillation periods.

B.4.3 Pressure Measurements

The two basic types of pressure sensors used were the flush-mount pressure transducer and the differential cavity-type transducer. The most common type sensor used was the flush-mount pressure transducer measurement. The absolute system pressure P is related to the pressure P_m measured by the flush-mount transducer by the expression:

$$P = P_m + P_{a_{tm}} \quad (B-2)$$

where $P_{a_{tm}}$ is the ambient (atmospheric + hydrostatic pressure). Due to the magnitude of the uncertainties involved, the error in the ambient pressure (about 0.1 psia (0.69 KN/m²)) is neglected. The magnitude of the overall uncertainty is not significantly affected by this approximation.

The second type of sensors used were high accuracy, absolute or differential cavity-type transducers utilizing appropriately designed legs. Leg corrections are dynamically calculated based on thermodynamics properties, i.e., leg temperatures and pressures. Errors due to these effects are considered extremely low as compared to the basic measurement errors caused by the data acquisition system and transducer characteristics. The forthcoming measurement evaluations will indicate that the measurement uncertainty is determined primarily by transducer characteristics.

To examine the measurement uncertainties of the transducers, typical properties of both the flush-mount and cavity-type sensors will be applied.

B.4.3.1 Flush Mounts

Weir annulus wall, vents and suppression pool wall pressures were measured by Precise Sensor Transducers, Model 111-3, with operating ranges of 0-100 psi (0-690 KN/m²), 0-200 psi (0-1379 KN/m²), 0-500 psi (0-3447 KN/m²) and 0-2000 psi (0-13,790 KN/m²).

The uncertainties of the test series for each particular transducer model and its calibration range are tabulated in Table B-1, including the function of the transducers. These values are based on either in-house bench calibration tests or manufacturer's data for the instrument.

The recording system's analog-to-digital conversion accuracy is about ± 0.01 percent of full scale. Amplifier gain accuracy is ± 0.03 percent and the excitation voltage accuracy is ± 0.05 percent full scale. Therefore, the signal conditioning and recording contributes only about 0.06 percent of full scale uncertainty. Therefore, most of the overall system uncertainty is contributed by transducer characteristics.

Both the maximum static uncertainties and the representative pressure uncertainties in engineering units, based on the full-scale calibration values, are included in Table B-1. A nominal, or mean, uncertainty for each transducer model is listed also. The nominal uncertainty values are more representative of the errors seen than the maximum values reported with static uncertainties of ± 0.90 to ± 14.46 psi (± 6.22 to ± 99.61 KN/m²).

In conjunction with the basic instrument and data acquisition system error is the analog recording error as discussed in Subsection B.3. The analog recorder's "span error" was about 5 percent for the pressure channels which

contributed most to the overall uncertainty. Therefore, the expected recorder uncertainty is about 2.8 psi (19.3 KN/m²) based on a maximum value of 55 psi (379 KN/m²) for the low-magnitude pressure observed on the containment pool walls. About ± 5 percent of the nominal values observed in the wall pressure measurements should be used as the uncertainty bounds.

The one-time maximum vent pressure value measured was 2051 psi (14131 KN/m²). Using ± 5 percent as the uncertainty, this is equivalent to ± 102.6 psi (706.6 KN/m²) for that measure. However, this is only a one-time reading. Typical vent pressure measurements recorded during the chugging regime of the tests were about 300 psi (2067 KN/m²), a ± 5 percent uncertainty is equivalent to ± 15 psi (103.4 KN/m²) that includes both tape and instrument uncertainties.

B.4.3.2 System Pressure Measurements

Other pressure measurements in the tests included the venturi throat and inlet pressures, the drywell pressure, the pool airspace pressure, and the differential pressure across the pool axially. Different cavity-type transducers were utilized for each measurement. Table B-2 lists the types of transducer, their function and uncertainty. These instruments are designated as real-time instrumentation (see Table 3-3) so the signal conditioning and recording contributes only about 0.06 percent of full-scale uncertainty. Based on Equation B-2, the total maximum uncertainty at full scale is given in the last column of Table B-2.

B.4.4 Acceleration Measurement Uncertainty

Acceleration measurements were recorded on drywell (south) wall, containment (north) wall and the basements using Setra variable capacitance sensors with a 100 g range; and Wilcoxon sensors with a 10 g range. The uncertainties are based on manufacturer's data given in Table B-3.

The maximum measured values for the Setra and Wilcoxon accelerometers were 40 g and 13.5 g, respectively. Based on Equation B-2 and analog record/playback errors (5 percent), the maximum measured value error is ± 2 g for the 100 g

errors (5 percent), the maximum measured value error is ± 2 g for the 100 g Setra sensor and ± 0.8 g for the Wilcoxin sensors.

B.5 SUMMARY OF UNCERTAINTIES

Results of this uncertainty analysis given in Table B-4) for the prime measurements of the test series, are based on maximum measured values.

The uncertainty analysis presented in this appendix does not have an exact statistical analog due basically to the single-sample nature of the data. However, some of the uncertainties utilized in its development (e.g., full-scale percent pressure deviations, etc.) can be shown to bound the 1σ deviations at the 95 percent confidence interval. Therefore, this overall uncertainty analysis would be similar to at least a 1σ error analysis at the 95 percent confidence level.

Table B-1

INSTRUMENT ERRORS FOR WEIR WALL, VENTS, AND POOL WALL PRESSURE MEASUREMENTS
(Precise Sensor Transducer - Model 111-3)

<u>Error Source</u>		<u>Maximum Uncertainty</u>		
A. Thermal Effects (assume a maximum transducer increase of 126°F (70°C))				
B. Repeatability				
C. Combined nonlinearity, hysteresis, and sensitivity				
<u>Transducer Range</u> psi (KN/m ²)	<u>Function</u>	<u>Calibration Range</u> psi (KN/m ²)	<u>Maximum Uncertainty</u> (% FSO)	<u>Nominal Uncertainty</u> (% FSO)
0-100 (0-690)	Weir Wall, North Pool Walls			
0-200 (0-1380)	South Pool Walls			
0-500 (0-3447)	South Pool Walls near vents			
0.2000 (0-13800)	Vents			
D. Total Uncertainties				
<u>Transducer Range</u> (psi (KN/m ²))	<u>Maximum Measured Value</u> psi (KN/m ²)	<u>Maximum Static Uncertainty</u> (% FSO)	<u>Maximum Static Uncertainty</u> psi (KN/m ²) (FSO)	<u>Nominal Static Uncertainty</u> psi (KN/m ²)
0-100 (0-690)				
0-200 (0-1380)				
0-500 (0-3447)				
0-2000 (0-13800)				

*Proprietary information deleted

*

B-9

NEDO-24720

Table B-2
 INSTRUMENT ERRORS FOR SYSTEM PRESSURE MEASUREMENTS

<u>Transducer</u>	<u>Function</u>	<u>Error Source</u>	<u>Magnitude of Uncertainty</u>
Straindyne Sensor	Venturi Throat & Inlet Pressure	Thermal Effects Repeatability	
Genisco Sensor	Annubar Static Pressure	Thermal Effects Repeatability	
Statham Sensor (differential) (static)	Annubar Differential Pressure Pool Level Pool Airspace	Thermal Effects Repeatability	

<u>G. E. Bench Test</u> <u>Sensor</u>	<u>Calibration Range</u> <u>psi (KN/m²)</u>	<u>Linearity & Hysteresis</u> <u>Maximum Uncertainty</u> <u>(% FSO)</u>	<u>Total</u> <u>Maximum Uncertainty</u> <u>psi (KN/m²) F.S.</u>
Straindyne 0-50 psi			
Genisco 0-50 psi			
Statham differential 0-5 psi			
differential & static 0-10 psi			

*Proprietary information deleted

Table B-3

ACCELERATION MEASUREMENT UNCERTAINTIES

<u>Sensor</u>	<u>Error Source</u>	<u>Magnitude of Uncertainty</u>
Setra (0-100 g)	Thermal Sensitivity	
	Nonlinearity	
	Hysteresis	
Wilcoxin (0-10 g)	Thermal Sensitivity	
	Nonlinearity & Hysteresis	

*Proprietary information deleted

Table B-4
SUMMARY OF UNCERTAINTIES

<u>Measurement</u>	<u>Uncertainty</u>
Pool Temperature	
Weir Walls, North Walls in Pool	
South Wall in Pool near Vents	
South Wall in Pool	
Vents (based on typical measured chug values)	
Accelerations	

*Proprietary information deleted

*

Appendix C
MULTICELL CCPDDF CALCULATIONS

C.1 GENERAL APPROACH

The multicell effects were evaluated on a comparison of the CCPDDFs of chugging pressures calculated for the 1-, 2- and 3-cell configurations. The CCPDDFs were calculated on the total number of chugs at each cell configuration as determined by the following approach. This approach consisted of a three-step inclusion of all chugs to form a single large data base at each cell configuration.

First, all chugs of each run over the entire duration of the chugging phase in the transient were considered for calculating CCPDDFs. This procedure increased the statistical data base and established justification on the basis that the chugging peak pressures did not follow any particular trend with respect to time, as illustrated in Figures C-1 and C-2. Shown in these figures are the top vent chugging pressure CCPDDF calculated over two equal parts of the chugging duration for 70°F (21°C) initial pool temperature Runs 2 and 8, and 120°F (49°C) initial pool temperature Runs 5 and 11.

Second, all the chugs which occurred in each cell were included for all three runs with the same initial condition. This resulted in a combined data base of chugs for the east, center, and west cells. This approach was based on the repeatability observed among runs with similar initial conditions as shown by CCPDDF of the top vent chugging pressure for Runs 1 through 12 in Figures C-3 and C-4.

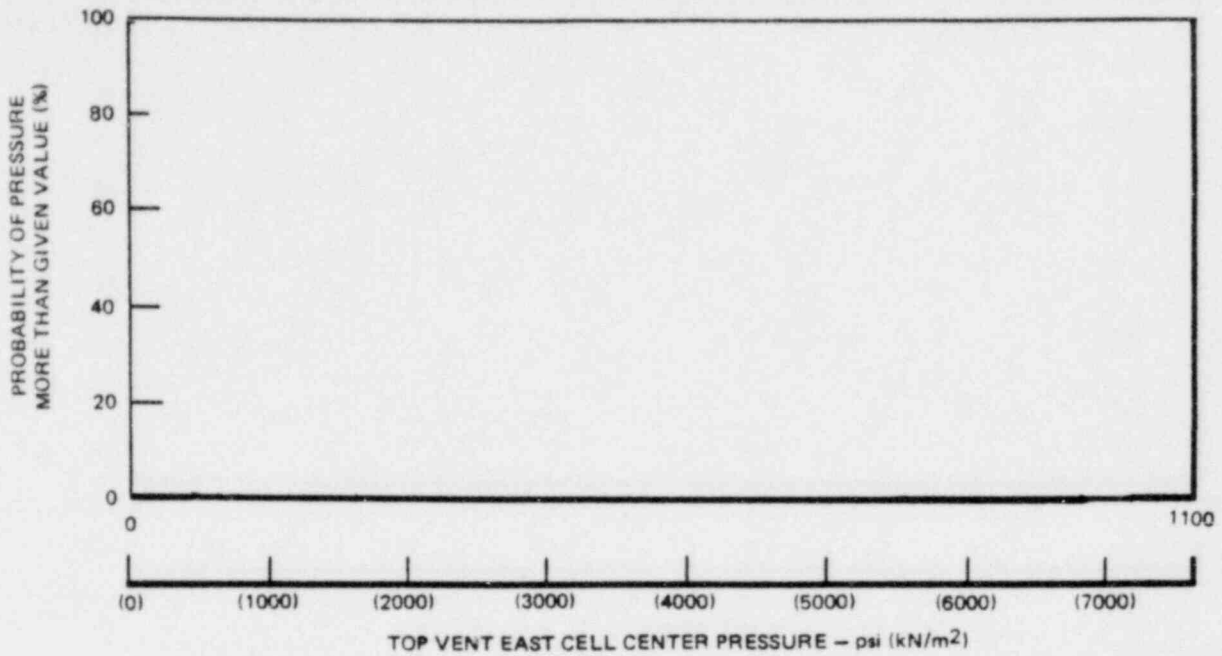
Third, the total number of chugs for the center and west, or east center and west cells were added for establishing the 2- or 3-cell chug data base, respectively. This final combination was based on an unbiased distribution of chugging pressures in each of the vents in a 2- or 3-cell system as shown in Figures C-5 and C-6. CCPDDF of the top vent center and west cell pressure for combined 1- and 2-cell runs, and east center and west cell pressure for combined 3-cell runs at 70 and 120°F (21 and 49°C) initial pool temperature are presented in these figures.

C.2 CCPDDF OF TOP VENT

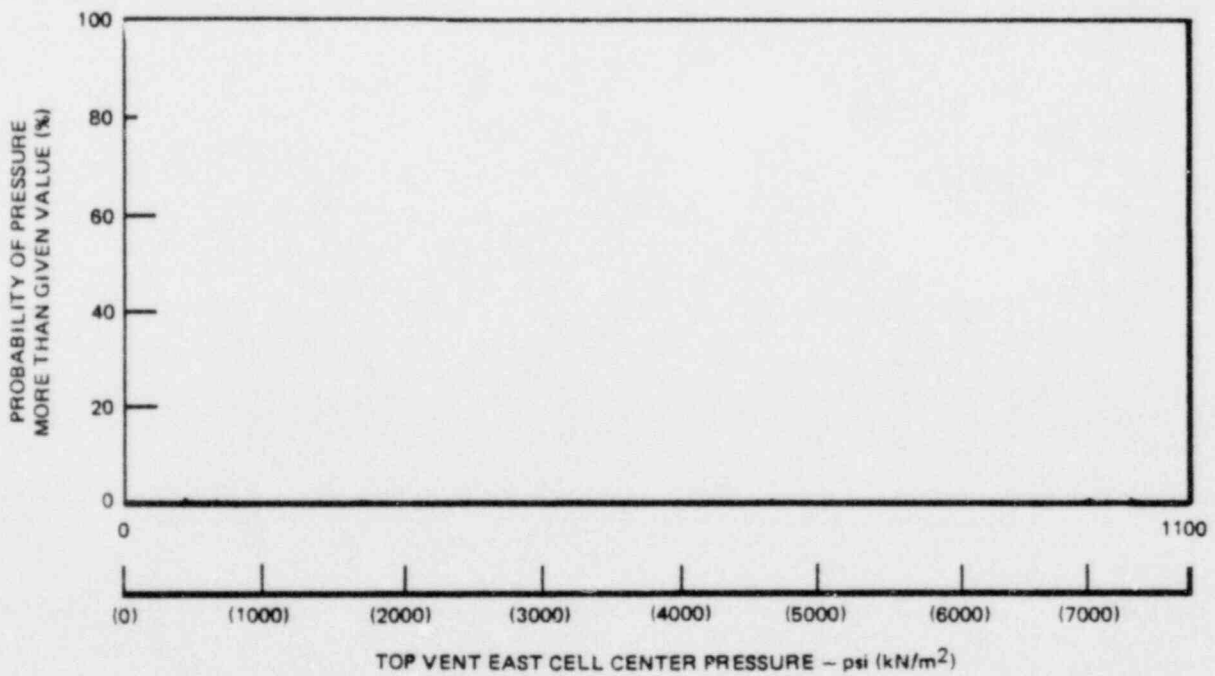
The top vent chug data bases used in calculating the top vent for 1, 2 and 3-cell CCPDDFs were determined based on individual chugs occurring in each top vent. Thus, in a 3-cell configuration there were three different numbers of chugs each corresponding to chugging events in east, center, and west vents, and in a 2-cell system there were two different numbers of chugs each resulting from chugs in the center and west vents. This method of individual vent chugs was used only in the case of the statistical analysis performed for the top vents to illustrate that the source strength resulting from the steam bubble collapses inside the top vents were the same for the 1-, 2- and 3-cell configurations. This supported the direct comparisons of the weir wall and pool walls peak pressures resulting from individual and multivent chugs to assess the multicell effects.

C.3 CCPDDF OF WEIR WALL AND POOL WALLS

The weir wall and pool walls chug data bases used in determining the CCPDDFs were calculated for the 1-cell configuration based on the individual vent chugs of the east cell, for the 2-cell based on the multivent chugs of the center and west vents, and for the 3-cell based on the multivent chugs of the east, center, and west vents. This approach was utilized because the 2- and 3-cell wall pressures resulted from chugs occurring in one or more of the top vents.



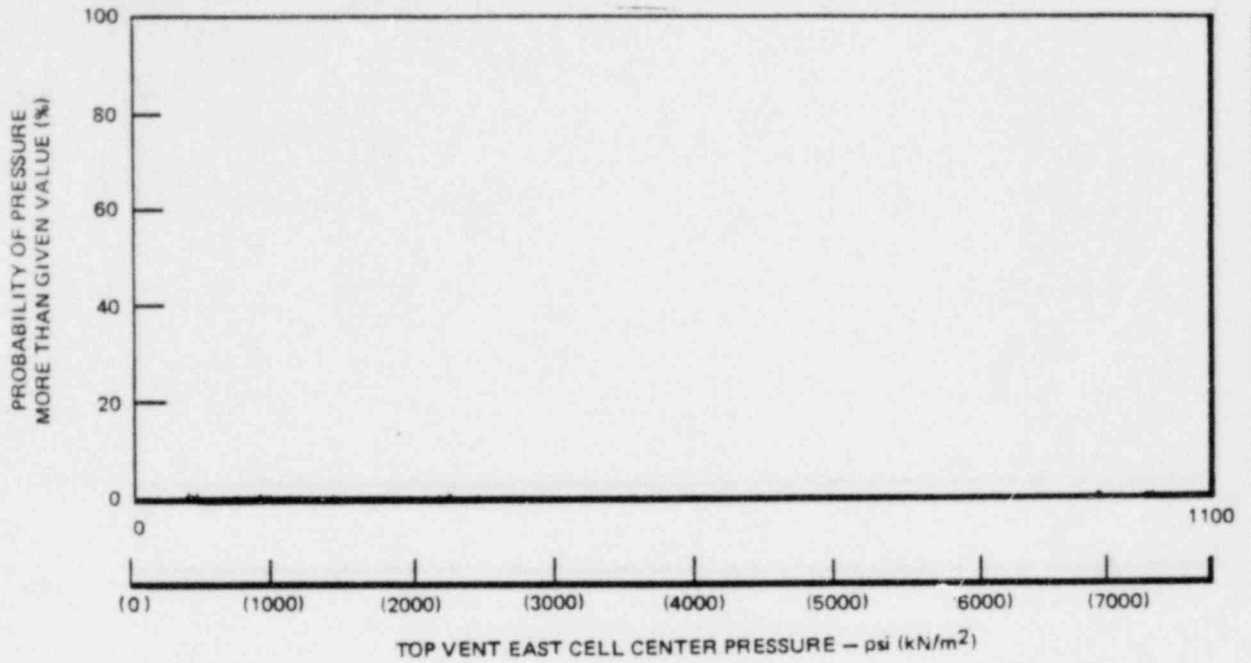
(a) RUN 2, 3-CELL CONFIGURATION



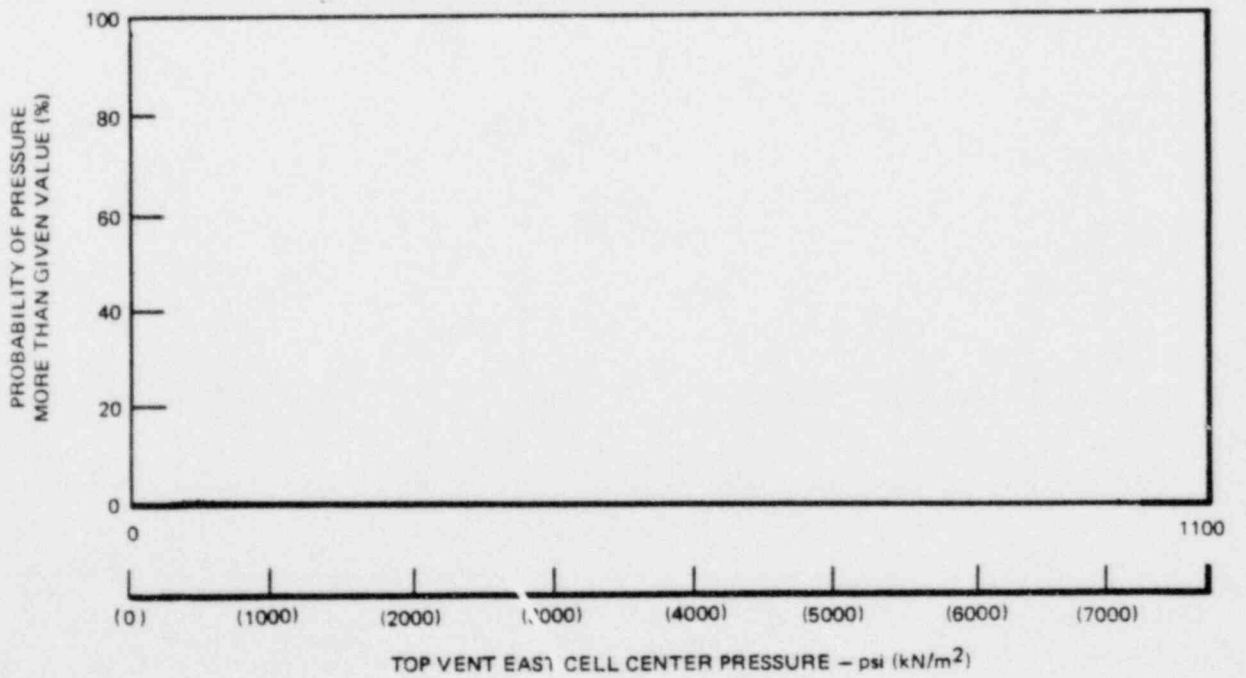
(b) RUN 8, 1 AND 2-CELL CONFIGURATION

Figure C-1. Complimentary Cumulative Probability Density Distribution Function-Time of Chugging Effect on Top Vent Pressure at 70°F (21°C) Initial Pool Temperature

*Proprietary information deleted

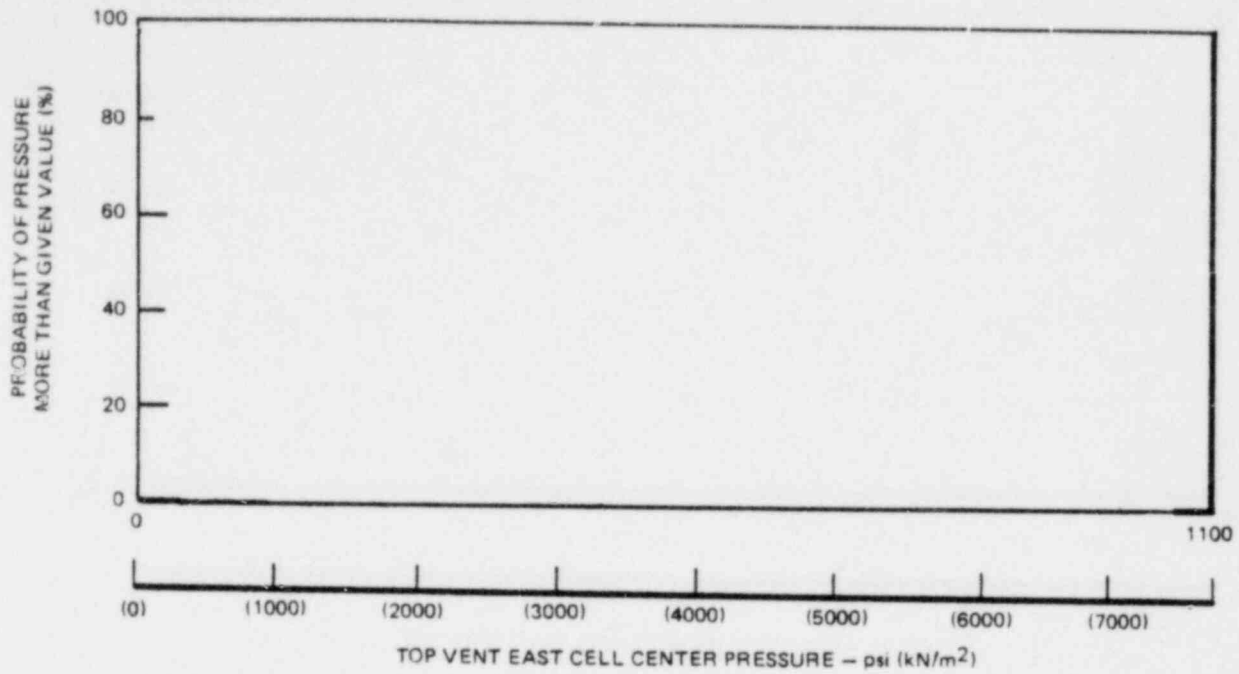


(a) RUN 5, 3-CELL CONFIGURATION

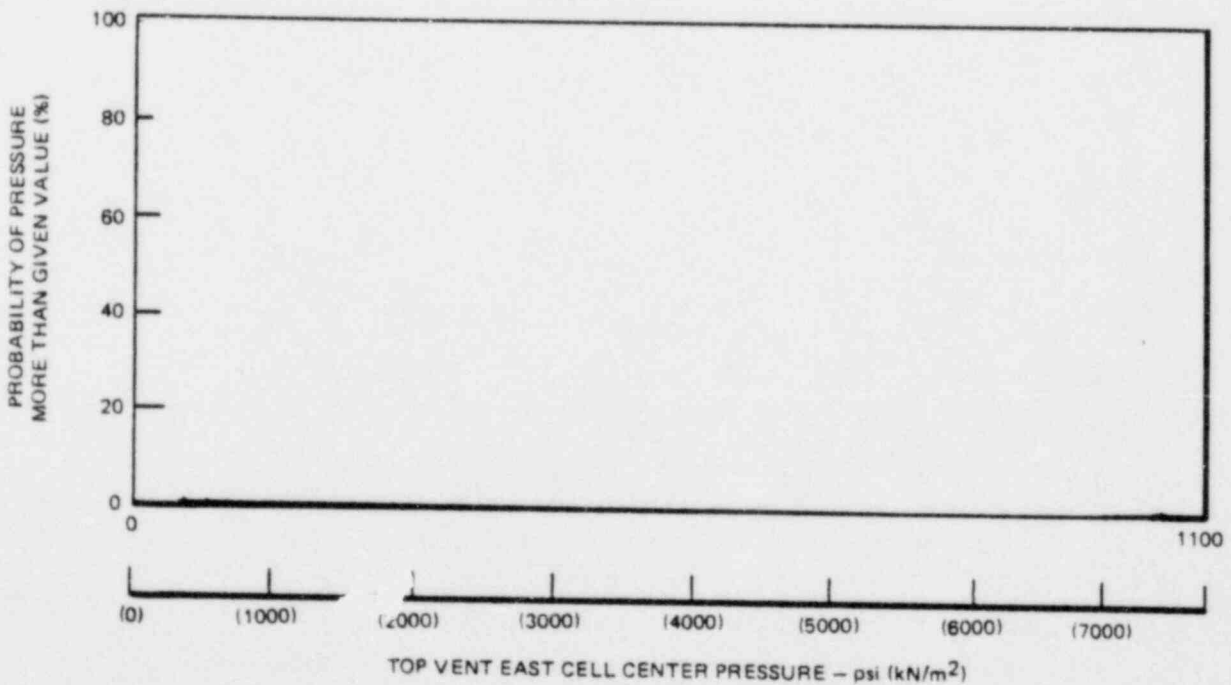


(b) RUN 11, 1 AND 2-CELL CONFIGURATION

Figure C-2. Complimentary Cumulative Probability Density Distribution Function-Time of Chugging Effect on Top Vent Pressure at 120°F (49°C) Initial Pool Temperature

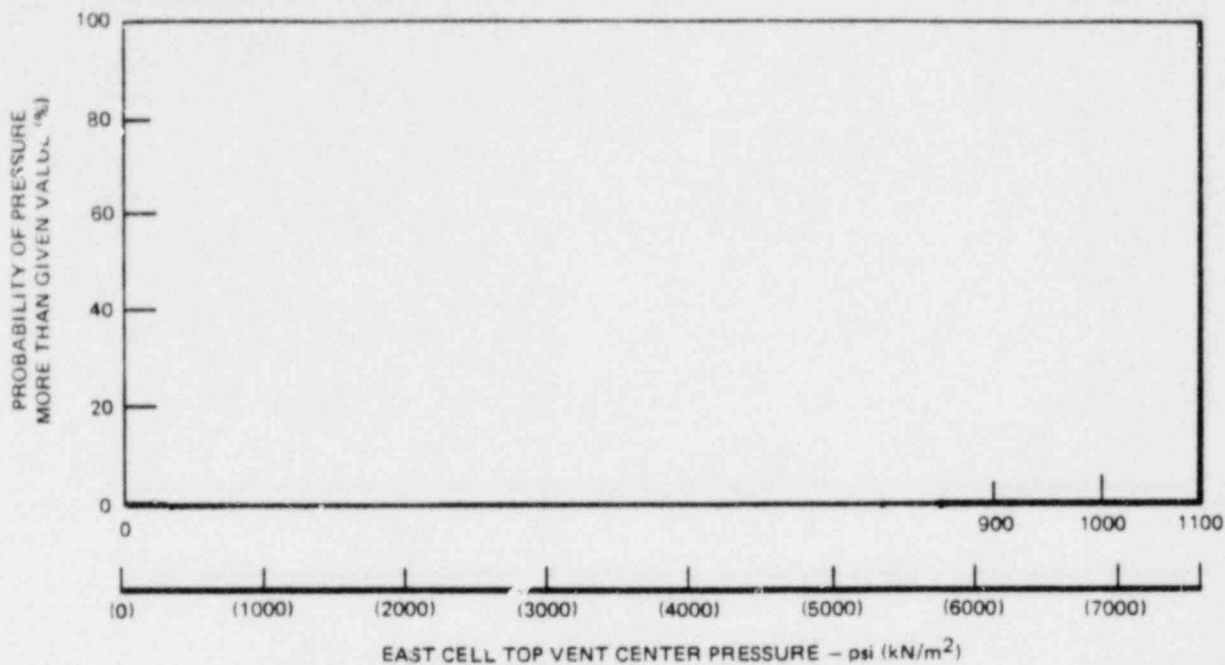


(a) 3-CELL CONFIGURATION

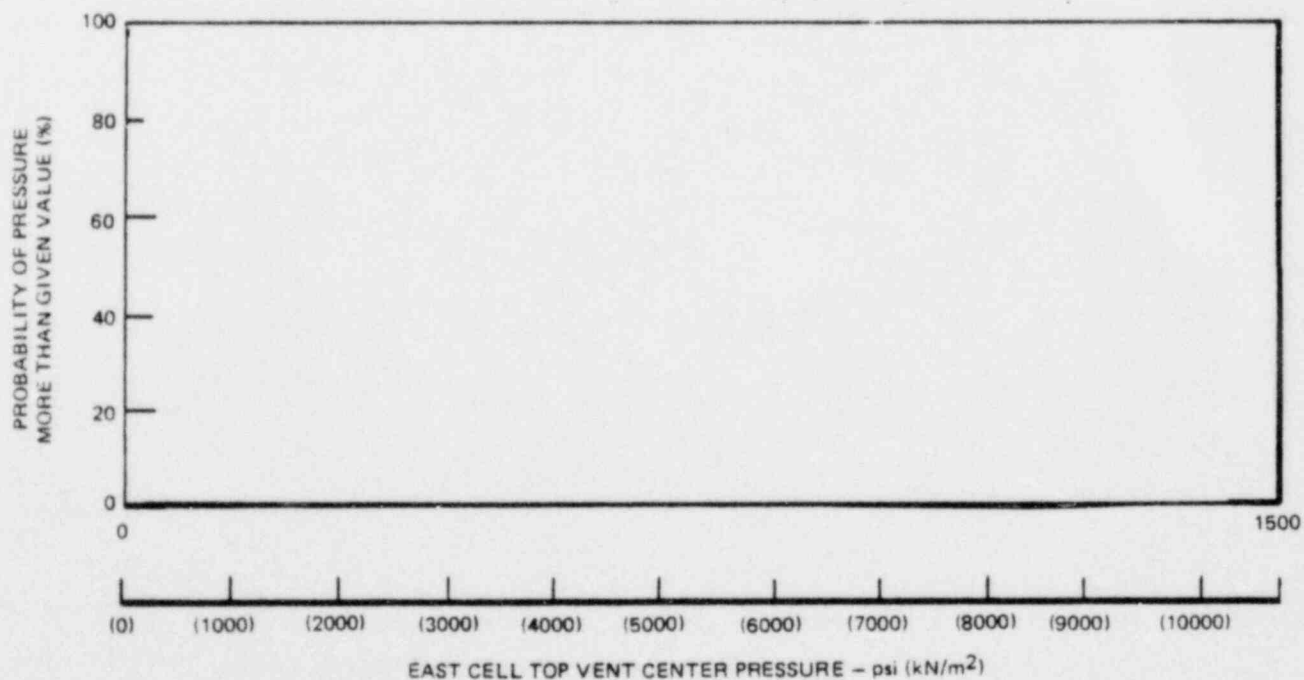


(b) 1 AND 2-CELL CONFIGURATION

Figure C-3. Complimentary Cumulative Probability Density Distribution Function-Repeatability of Top Vent Chugging Pressure at 70° (21°C) Initial Pool Temperature

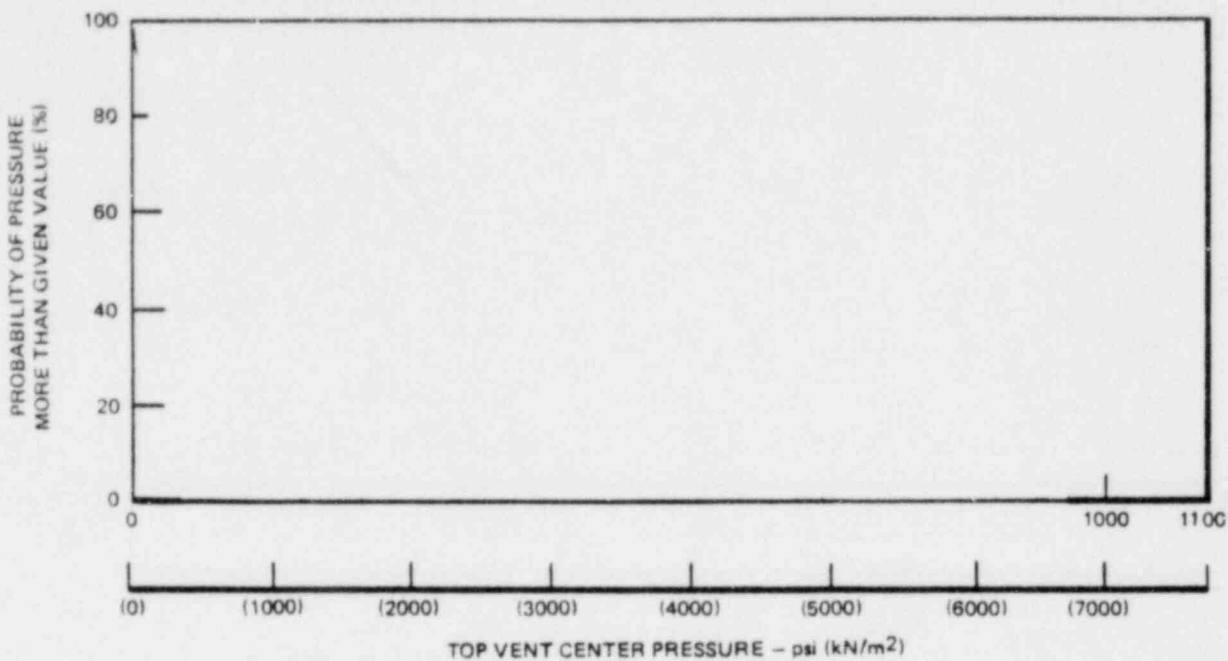


(a) 3-CELL CONFIGURATION

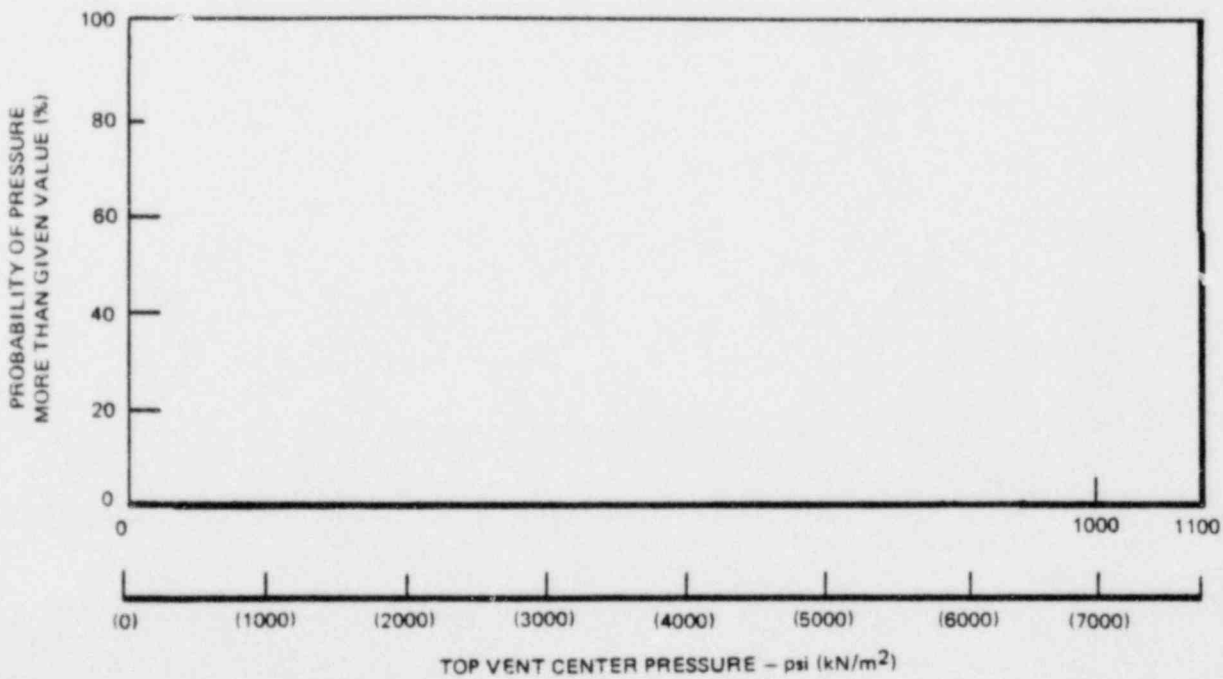


(b) 1 AND 2-CELL CONFIGURATION

Figure C-4. Complimentary Cumulative Probability Density Distribution Function-Repeatibility of Top Vent Chugging Pressure at 120°F (49°C) Initial Pool Temperature

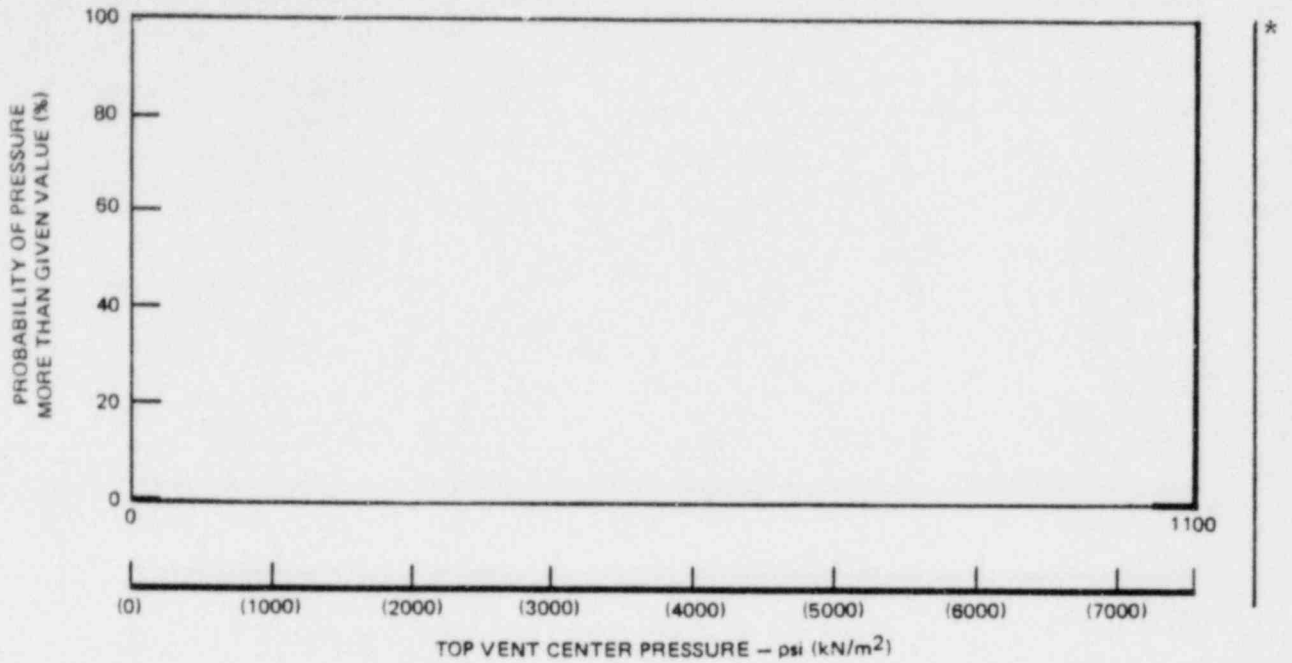


(a) RUNS 1, 2, 3; 3-CELL CONFIGURATION

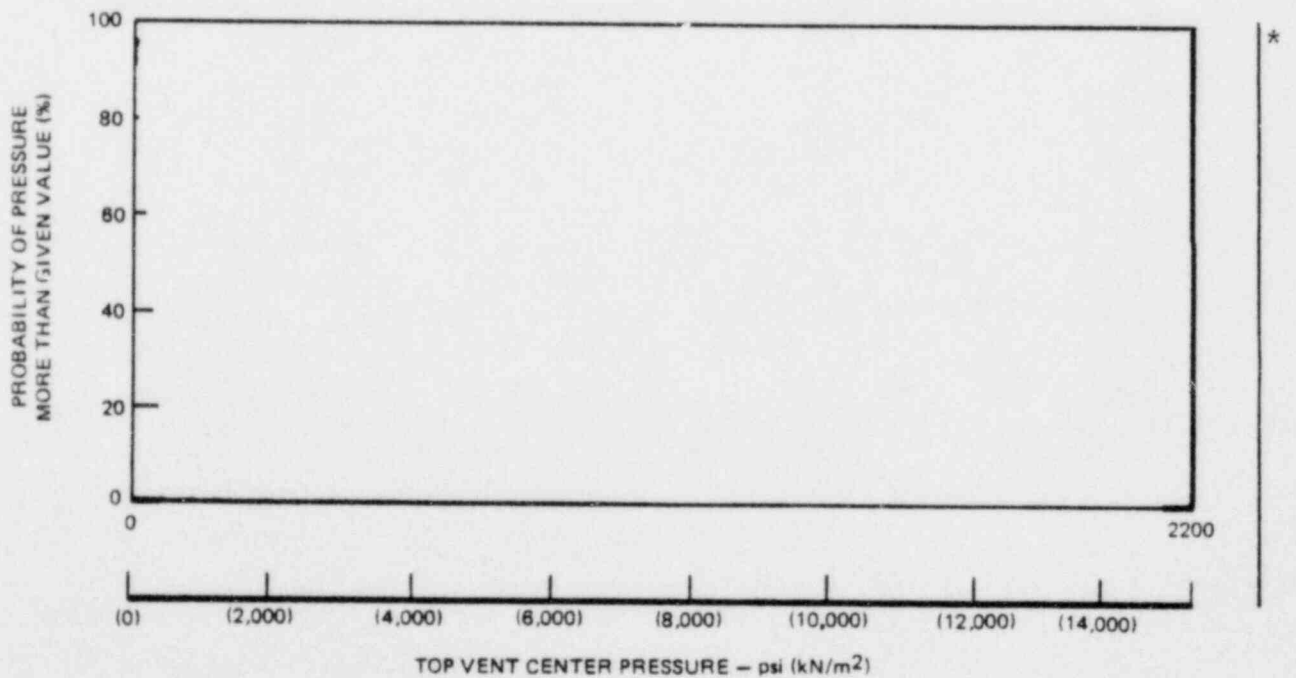


(b) RUNS 7, 8, 9; 1 AND 2-CELL CONFIGURATION

Figure C-5. Complimentary Cumulative Probability Density Distribution Function-Comparison of Individual Top Vent Chugging Pressures at 70°F (21°C) Initial Pool Temperature



(a) RUN 4, 5, 6: 3-CELL CONFIGURATION



(b) RUN 10, 11, 12: 1 AND 2-CELL CONFIGURATION

Figure C-6. Complimentary Cumulative Probability Density Distribution Function-Comparison of Individual Top Vent Chugging Pressures at 120°F (49°C) Initial Pool Temperature

*Proprietary information deleted

Appendix D
SYSTEMS PERFORMANCE

This appendix contains an evaluation of system response variations to determine if any bias favoring either the 1-2 cell test configurations or the 3-cell test configuration was present that would lead to circumstances where a comparison of 3-cell configuration test results could not be made with the 1-2 cell test configuration results. The two parameters investigated are the venturi flow transient and the drywell pressure transient.

The venturi flow and drywell pressure transients were examined at time intervals of 5, 10, 20, 40, 60 and 80 seconds after blowdown initiation. A mean value of flow and drywell pressure was calculated on the basis of all 12 test runs. A comparison of the venturi flow and drywell pressure transient for each run, at the specified time intervals was made using the mean value.

In this comparison the difference between the mean flow rate and the flow rate in any given run was determined by

$$\% \text{ Difference} = \left(\frac{\text{Mean Flow} - \text{Flow in Given Run}}{\text{Mean Flow}} \right) \times 100$$

and was similarly determined for the drywell pressure transient. The differences in the venturi flow transient and the drywell pressure transient have been tabulated in Tables D-1 and D-2, respectively.

In comparing the flow transient (see Table D-1) it is apparent that the run-to-run variation in flow with respect to the mean flow occurs randomly, i.e., there is no apparent correlation with the initial pool temperature or the test configuration. Also, when comparing a set of three runs in the 3-cell configuration and 1-2 cell configurations with 70°F (21°C) initial pool temperature, the average variation in both sets of data is apparently about the same. Similarly, sets of three runs in all configuration with 120°F (49°C) initial pool temperature, show no apparent difference in the average variation of the flow rates.

The magnitude of difference in the flow transient in comparison with the mean flow varies from run to run. The greatest overall difference is evident between Run 7 with the lowest (-22.1 percent) flow transient, and Run 8 with the highest (+7.52 percent) flow transient. However, the greatest difference (+7.86 percent) in the flow transient occurs towards the end of the transient in Run 1. These bounding values establish the limits in the repeatability of the flow transients in Test Series 6003. Therefore, in this series of tests the flow transient can be characterized as repeatable within a tolerance of -22.1 percent to +7.86 percent.

In comparing the drywell pressure transient (see Table D-2) it is apparent that the magnitude of variation in the drywell pressure transient with respect to the mean also varies randomly from run to run. However, a definite correlation is evident which appears to be due to the initial pool temperature. The higher drywell pressure transients appear to favor the 120°F (49°C) in initial pool temperature test runs, while the lower drywell pressure transients favor the 70°F (21°C) initial pool temperature test runs. However, there isn't any apparent bias towards one test configuration when compared with the other, with respect to the same initial pool temperature. Furthermore, the average variation in the magnitude of the drywell pressure transient is about the same in both test configurations. The greatest variation in the drywell pressure transient is evident between Run 2 with the lowest (-6.53 percent) and Run 4 with the highest (+5.46 percent) drywell pressure transient, with respect to the mean. Note that the variation in drywell pressure transient beyond 40 seconds after initiation of blowdown is meaningless, because the drywell pressure is significantly effected by the onset of chugging, as illustrated in Figure D-1. Because of the bounding values of these two runs, the drywell pressure transient can be characterized as repeatable, within a tolerance of 6.53 percent to +5.46 percent. A comparison of the system response between the 1-2 cell and 3-cell test configuration was also made by comparing the average mass flux and drywell pressure transient for the set of three runs in the 1-2 cell test configuration to the set of three runs in the 3-cell test configuration, with the same initial pool temperature. The average mass flux and drywell pressure, including the calculated difference between the 1-2 cell

and 3-cell transient, is tabulated in Table D-3. This comparison shows good agreement of the blowdown transient between the 1-2 cell and 3-cell test configuration.

The following conclusions can be drawn from the above observations:

- a. There is not any apparent propensity in the system response that can be attributed to difference in geometry between the 3-cell configuration and the 1-2 cell configurations.
- b.
- c.
- d.
- e.

Table D-1

BLOWDOWN VENTURI FLOW TRANSIENT COMPARISON

		<u>3-Cell Test Configuration</u>											
		<u>70°F (21°C) Initial Pool Temperature</u>						<u>120°F (49°C) Initial Pool Temperature</u>					
		Run 1		Run 2		Run 3		Run 4		Run 5		Run 6	
Time (sec)	"Mean" All Test Runs	Mass Flow	% Diff	Mass Flow	% Diff	Mass Flow	% Diff	Mass Flow	% Diff	Mass Flow	% Diff	Mass Flow	% Diff
5	52.15												
10	38.05												
20	21.28												
40	9.369												
60	5.449												
80	3.675												
		<u>1 and 2 Cell Test Configuration</u>											
		<u>70°F (21°C) Initial Pool Temperature</u>						<u>120°F (49°C) Initial Pool Temperature</u>					
		Run 7		Run 8		Run 9		Run 10		Run 11		Run 12	
Time (sec)	"Mean" All Test Runs	Mass Flow	% Diff	Mass Flow	% Diff	Mass Flow	% Diff	Mass Flow	% Diff	Mass Flow	% Diff	Mass Flow	% Diff
5	52.15												
10	38.05												
20	21.28												
40	9.369												
60	5.449												
80	3.675												

*Proprietary information deleted

*

Table D-2

BLOWDOWN DRYWELL PRESSURE TRANSIENT COMPARISON

		<u>3-Cell Test Configuration</u>											
Pressure (psia)		<u>70°F (21°C) Initial Pool Temperature</u>						<u>120°F (49°C) Initial Pool Temperature</u>					
"Mean"		Run 1		Run 2		Run 3		Run 4		Run 5		Run 6	
All		%		%		%		%		%		%	
Time (sec)	Test Runs	Press	Diff	Press	Diff	Press	Diff	Press	Diff	Press	Diff	Press	Diff
5	23.27												
10	22.20												
20	21.23												
40	20.08												

		<u>1 and 2 Cell Test Configuration</u>											
Pressure (psia)		<u>70°F (21°C) Initial Pool Temperature</u>						<u>120°F (49°C) Initial Pool Temperature</u>					
"Mean"		Run 7		Run 8		Run 9		Run 10		Run 11		Run 12	
All		%		%		%		%		%		%	
Time (sec)	Test Runs	Press	Diff	Press	Diff	Press	Diff	Press	Diff	Press	Diff	Press	Diff
5	23.27												
10	22.20												
20	21.23												
40	20.08												

D-5

NEDO-24720

*Proprietary information deleted

*

Table D-3

BLOWDOWN TRANSIENT COMPARISON BASED ON AVERAGE FLOW AND DRYWELL PRESSURE TRANSIENT

TIME (sec)	INITIAL POOL TEMPERATURE							
	70°F (21°C)				120°F (49°C)			
	Runs 1-3		Runs 7-9		Runs 4-6		Runs 10-12	
	\dot{m} (lbm/sec)	P_{DW} (psia)	\dot{m} (lbm/sec)	P_{DW} (psia)	\dot{m} (lbm/sec)	P_{DW} (psia)	\dot{m} (lbm/sec)	P_{DW} (psia)
5								
10								
20								
40								
60								
80								

D-6

NEDO-24720

*Proprietary information deleted

*

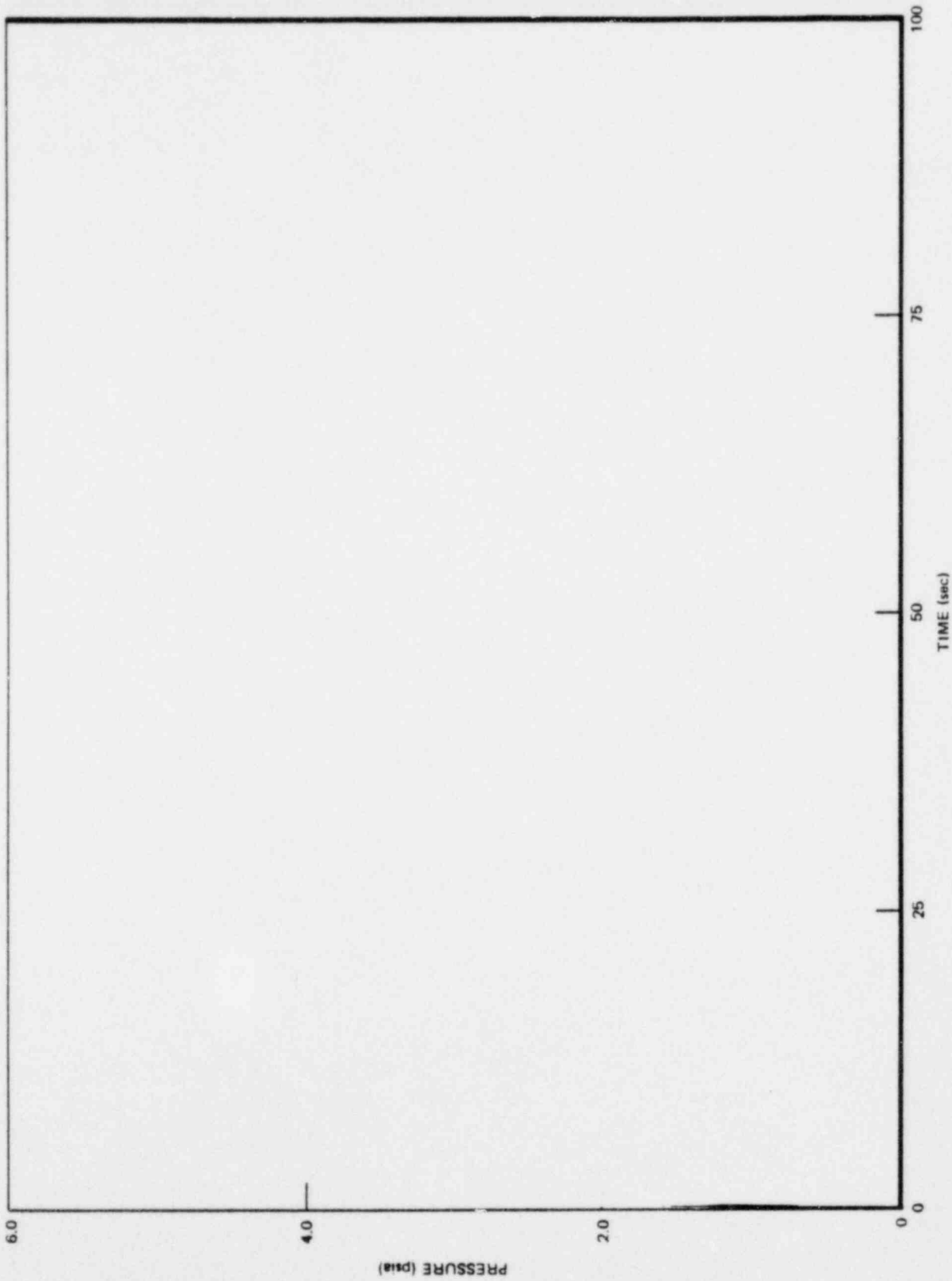


Figure D-1. Drywell Pressure Transient, Run 7

*Proprietary information deleted

DISTRIBUTION

<u>Name</u>	<u>M/C</u>
W. G. Gang (3)	392
L. S. Gifford	Bethesda Mail Pouch
D. M. Gluntz	584
F. E. Hatch	904
L. H. Larson (21)	395
R. L. Lebre (3)	392
A. J. Levine	682
R. C. Mitchell (3)	392
H. D. Powell (4)	392
R. F. Pratt	094
J. F. Quirk	682
R. M. Schuster	892
R. M. Schuster (18)	892
A. R. Smith (4)	392
L. J. Sobon (3)	905
L. J. Sobon (25)	905
W. H. Summers (2)	392
F. Weinzimmer (3)	392
Mark III Containment Design File	113
K. P. Yu	584